UNIVERSITY OF ALBERTA

DEVELOPMENT OF A COMPUTERIZED SASW TECHNIQUE

BY

KOFI O. ADDO

©

A THESIS

SUBMITTED TO THE FACULTY OF GRADUATE STUDIES AND RESEARCH
IN PARTIAL FULFILMENT OF THE REQUIREMENTS FOR THE DEGREE OF
DOCTOR OF PHILOSOPHY
IN
GEOTECHNICAL ENGINEERING

DEPARTMENT OF CIVIL ENGINEERING

EDMONTON, ALBERTA

FALL 1992

National Library of Canada
Canadian Theses Service
Ottawa, Canada
K1A 0N4

Bibliothèque nationale du Canada
Service des thèses canadiennes

The author has granted an irrevocable non-exclusive licence allowing the National Library of Canada to reproduce, loan, distribute or sell copies of his/her thesis by any means and in any form or format, making this thesis available to interested persons.

The author retains ownership of the copyright in his/her thesis. Neither the thesis nor substantial extracts from it may be printed or otherwise reproduced without his/her permission.

L'auteur a accordé une licence irrévocable et non exclusive permettant à la Bibliothèque nationale du Canada de reproduire, prêter, distribuer ou vendre des copies de sa thèse de quelque manière et sous quelque forme que ce soit pour mettre des exemplaires de cette thèse à la disposition des personnes intéressées.

L'auteur conserve la propriété du droit d'auteur qui protège sa thèse. Ni la thèse ni des extraits substantiels de celle-ci ne doivent être imprimés ou autrement reproduits sans son autorisation.

ISBN 0-315-77154-2

Canadä

UNIVERSITY OF ALBERTA

RELEASE FORM

NAME OF AUTHOR	*Kofi O. Addo*
TITLE OF THESIS	*Development of a computerized SASW technique.*
DEGREE	*Doctor of Philosophy*
YEAR DEGREE GRANTED	*1992*

Permission is hereby granted to THE UNIVERSITY OF ALBERTA LIBRARY to reproduce single copies of this thesis and to lend or sell such copies for private, scholarly or scientific research purposes only.

The author reserves all other publication and other rights in association with the copyright in the thesis, and except as hereinbefore provided neither the thesis nor any substantial portion thereof may be printed or otherwise reproduced without in any material form whatever without the author's prior written permission.

214 Central Road,
Morden, Surrey,
SM4 5RQ.
U.K.

DATED June, 1992

UNIVERSITY OF ALBERTA

FACULTY OF GRADUATE STUDIES AND RESEARCH

The undersigned certify that they have read, and recommend to the Faculty of Graduate Studies and Research for acceptance, a thesis entitled Development of a Computerized SASW Technique submitted by Kofi O. Addo in partial fulfillment of the requirements for the degree of Doctor of Philosophy.

PK Robertson

P. K. Robertson

N. R. Morgenstern

J. D. Scott

J. D. Scott

K O Anderson

K. O. Anderson

E. Nyland

(for) K. H. Stokoe (III)

Date June 1992

To my brother Charles
and
in ever-loving memory of my parents and brother Felix

ABSTRACT

DEVELOPMENT OF A COMPUTERIZED SASW TECHNIQUE

The Spectral Analysis of Surface Waves (SASW) is an in-situ test for determining the variation of shear wave velocity (or shear modulus) with depth for soil, rock and road and runway structures. The parameters measured from the test can also be used in the design of machine foundations, assessment of liquefiability, evaluation of static and dynamic compaction, assessment of ground softening, evaluation of the integrity of underground mine walls and roofs and as an indication of the relative magnitudes of directional in-situ stress levels. Unlike most in-situ tests, the derivation of material parameters is based on a well-accepted theory (that of elastodynamics) and does not use empirical correlations. The most attractive advantage of the SASW test is that it is non-destructive as well as non-intrusive. Shear wave velocity profiles up to about 30 metres deep can be determined in a relatively short time from the surface without drilling. The SASW test is based on the theory of surface wave dispersion in a multi-layered medium. According to this theory, surface waves of different wavelengths travel at different velocities in such a medium. The reason is that the different wavelengths propagate at different depths, which in a layered medium, have different properties and hence different velocities. The variation of velocity with wavelength is called dispersion and a graph that shows this variation is called a dispersion curve.

The current SASW test procedure is to collect surface wave data with a spectrum analyzer and later transfer the data to a microcomputer attached to the analyzer for further analysis. This interpretation analysis involves computing an in-situ dispersion curve and

iteratively seeking a layered medium whose dispersion curve matches the measured in-situ curve. This process is called forward modelling and current computer programs for this process require users to make the necessary structural changes in the initially assumed layered medium until the in-situ curve is matched. Thus users must be familiar with surface wave dispersion theory in order to know what structural parameters to adjust, whether to decrease or increase the magnitudes and if so by how much.

The new instrumentation system developed in this research eliminates the requirement of a spectrum analyzer by programming the attached microcomputer to acquire and analyze surface wave data. This new system reduces the number of equipment pieces to be conveyed to site, substantially reduces the financial cost of SASW equipment, speeds up interpretation analyses (since file transfer times are saved) and enables the determination of the in-situ dispersion curve in the field. The forward modelling process has also been automated and therefore does not require user intervention. This enables less experienced personnel to man the operation of the system. The forward modelling algorithm has been theoretically verified with benchmarks, gratefully provided by Professor Stokoe of the University of Texas at Austin.

For experimental evaluation and verification, the new system has been used to determine the shear wave velocity profiles of ten different sites in western Canada. In general, the results were in good agreement with independent results obtained at the same sites with the seismic cone penetrometer, an in-situ tool that is well accepted by the geotechnical community.

ACKNOWLEDGEMENT

I would like to express my gratitude to my supervising professors, Drs. Peter K. Robertson, Norbert R. Morgenstern, J.D. Scott, K.O. Anderson and E. Nyland for their advice, correction and guidance during the research.

The encouragement, support, and direction offered by Dr N.R. Morgenstern and especially Dr. P.K. Robertson during the early and difficult stages of research is greatly appreciated. Dr. E. Nyland was very helpful in my studies on the theory of surface wave dispersion.

While at the University of Alberta, I had the opportunity to work with Dr. J.D. Scott in other areas of research. His devotion and dedication to research was exemplary and a challenge.

I would also like to thank Roy Gitzel and Dale Lathe of the Electronics section of the Civil Engineering Department for their involvement and commitment during the stages of computer programming and equipment development. My gratitude also goes to the technical and administrative staff of the Geotechnical section of the Department - Gerry Cyre, Steve Gamble, Christine Hereygers, Sharon Mayan and Jay Khajuria.

The assistance of fellow graduate students Flavio Kuwajima and David Das are greatly appreciated. Finally, I would like to thank my wife Sylvia, for the patience and encouragement throughout this research.

The independent seismic CPT results at all the test sites were provided by ConeTec Investigations Ltd. of Vancouver, who also gave field assistance during SASW testing in British Columbia.

The benchmarks provided by Professors Ken Stokoe of the University of Texas at Austin are appreciated.

This research was funded from a grant by the Natural Science and Engineering Council of Canada.

TABLE OF CONTENTS

Release Form

Dedication

Abstract

Acknowledgment

List of Tables

List of Figures

List of Symbols

CHAPTER 1

INTRODUCTION....1

1.1 ELASTIC WAVES....1

1.1.1 Scope....1

1.1.2 Types of Elastic Waves....1

1.1.2.1 Body Waves....4

1.1.2.2 Surface Waves....9

1.1.3 Rayleigh Wave Formulation....10

1.1.4 Properties of Rayleigh Waves....14

1.2 IN-SITU WAVE PROPAGATION METHODS....16

1.2.1 Scope....16

1.2.2 Intrusive Methods....17

1.2.3 Non-Intrusive Methods....19

1.2.3.1 Seismic Refraction Method....20

1.2.3.2 Seismic Reflection Method....22

1.2.3.3 Steady-State Vibration Method....25

1.2.3.4 Spectral Analysis of Surface Waves (SASW)................28
1.3 Geotechnical Applications of Surface Wave Measurements........................30
1.4 Objectives and Outline of Research..36

CHAPTER 2

SIGNAL ACQUISITION AND ANALYSIS 49
2.0 Introduction..49
2.1. Signal Acquisition..49
2.1.1 Sampling Rate..50
2.1.2 Number of Samples..53
2.1.3 Filtering..54
2.1.4 Averaging...56
2.1.5 Windowing...57
2.2 Signal Analysis...58
2.2.1 Frequency Domain Transformation..59
2.2.1.1 The fast Fourier Transform. 60
2.3 Spectral Analysis..63
2.3.1 Determination of Phase Velocity..64
2.3.2 Signal Quality...68
2.4 Determination of in-situ Dispersion Curve..70
2.5 A Computerized SASW System 73
2.6 Program SASW-DA..74

CHAPTER 3

FORWARD MODELLING 88
3.1 Introduction...88
3.2 Historical Background..89
3.3 Forward Modelling..91

3.3.1 Rayleigh Wave Dispersion Function....92
3.3.2 Love Wave Dispersion Function....95
3.4 Solution by Propagator Matrix Method....97
3.5 Matching Dispersion Curves....106
3.5.1 The simplex algorithm....107
3.6 Program SASW-FM....110
CHAPTER 4
EQUIPMENT DEVELOPMENT AND FIELD TESTING....117
4.1 Introduction....117
4.2 Equipment Development....117
4.2.1 Energy Sources....117
4.2.2 Receivers....119
4.2.3 Source-Receiver Configuration and Coupling....122
4.2.4 Receiver Coupling....124
4.2.5 Signal Acquisition and Recording....125
4.2.6. Equipment Assembly....127
4.3 Site Selection....127
4.4 Field Procedure....128
CHAPTER 5
ANALYSIS AND DISCUSSION OF RESULTS....141
5.0 Introduction....141
5.1. University LRT Station....142
5.2. NAIT Experimental Test Site, Edmonton, Alberta....145
5.3. Richmond Dykes at Blundell Road, Richmond, B.C....146
5.4. Richmond Dykes at Francis Road, Richmond, B.C....147
5.5. Richmond Dykes at Chatham

Road, Richmond, B.C. 148
5.6. Sea Island Site, Vancouver, B.C. 149
5.7. Burnaby Site, Burnaby, B.C. 149
5.8. Annacis Site, Annacis Island, B.C. 150
5.9. Delta Site, Delta, B.C. 151
5.10. Matsqui Site 151
5.11 Summary 152

CHAPTER 6

CONCLUSIONS AND RECOMMENDATIONS 179
6.1 Summary 179
6.2 Conclusions 180
6.3 Recommendations 181

BIBLIOGRAPHY 183

APPENDICES

I. SASW-DA Program Sequence 196
II. SASW-FM 222
II.1 SAMPLE INPUT 223
II.2 SAMPLE OUTPUT 224
II.3 BENCHMARK SOLUTIONS 225
III. CPT Results at University LRT Station 230
IV. CPT Results at NAIT Experimental Site. 233
V. CPT Results at Richmond Dykes (Blundell Road) 236
VI. CPT Results at Richmond Dykes (Francis Road) 245
VII. CPT Results at Richmond Dykes (Chatham Road) 250
VIII. CPT Results at Sea Island Site 254

IX. CPT Results at Burnaby Site....258

X. CPT Results at Annacis Site....263

XI. CPT Results at Delta Site....265

XII. Becker Hammer Results at Matsqui Site....270

LIST OF TABLES

Table 3.1. Time Estimates for Rayleigh Wave Dispersion Computations......................116

Table 4.1 Characteristics of Geophones Used in Research...140

Table 5.1. Measures of Fit between Theoretical and Experimental Dispersion Curves...178

LIST OF FIGURES

Figure 1.1 Elastic Wave Motion (After Bolt, 1976) 38

Figure 1.2 Dependence of Rayleigh Wave Velocity 0n Poisson's Ratio. 39

Figure 1.3. Idealized Model for Deriving Rayleigh Wave Equation 39

Figure 1.4 Particle Displacements in a Rayleigh Wavefield 40

Figure 1.5 Schematic representation of intrusive in-situ wave propagation methods. 41

Figure1.6 Schematic Layout of Downhole Seismic Cone Penetration Test 42

Figure 1.7 Seismic Refraction Method 42

Figure 1.8 Traveltime Curves for Direct, Reflected and Refracted Waves - 43

Figure 1.9 Principles of the Seismic Reflection Method 43

Figure 1.10 Steady-State Vibration Method 44

Figure 1.11 The University of Texas SASW System 44

Figure 1.12 Variation of normalized shear modulus with shear strain 45

Figure 1.13 Measurement of Damping from Wave Propagation Tests 45

Figure 1.14 Shear wave velocity profiles of sites with previous exposure to liquefaction (Redrawn after Stokoe et al, 1987). 46

Figure 1.15. Effect of Rolling on Rayleigh and Love Wave Dispersion Curves 46

Figure 1.16 Effect of Dynamic Compaction on Rayleigh Wave Dispersion 47

Figure 1.17 Effect of softening on Love wave dispersion 47

Figure 1.18 Following the effects of base softening by water (II) and gradual recovery by draining (III) on Rayleigh wave dispersion 48

Figure 1.19 Stratification of a Pavement Structure by Surface Waves 48

Figure 2.1. Schematics of SASW Testing Without A Spectrum Analyzer 78

Figure 2.2 . The Phenomenon of Aliasing 78

Figure 2.3 . Types of Filters 79

Figure 2.4 Characteristics of a Butterworth filter. 79

Figure 2.5 Characteristics of a Chebyschev filter. 80

Figure 2.6 Characteristics of a Cauer Filter. 80

Figure 2.7 Characteristics of a Bessel Filter. 81

Figure 2.8 Noise Reduction by Signal Averaging (After Ramirez, 1985)....82

Figure 2.9 Time-Frequency Domain Transformation (After Ramirez, 1985)....83

Figure 2.10 Determination of Phase Lag from Cross-Spectrum....84

Figure 2.11 Typical variation of cross-spectrum phase with frequency. 84

Figure 2.12 Typical variation of coherence with frequency. 85

Figure 2.13. SASW Instrumentation System....85

Figure 2.14 Flow Chart of the program SASW-DA. 86

Figure 2.15 The Front Panel of program SWAGE-DA. 87

Figure 3.1. The Homogeneous Layer Model....114

Figure 3.2. The Simplex Algorithm....115

Figure 4.1 Schematics of Signal Receivers....132

Figure 4.2 Types of SASW Source-Receiver Set-Up. 133

Figure 4.3 The Circuit Diagram of the ICU....134

Figure 4.4. University of Alberta SASW System....135

Figure 4.5a. Location of University of Alberta LRT Station (Edmonton Site)....136

Figure 4.5a. Location of NAIT Experimental Site (Edmonton Site)....137

Figure 4.6a. Location of Matsqui Site....138

Figure 4.6b. Location of Selected Sites in British Columbia....139

Figure 5.1a. Dispersion Curves at University LRT Station....155

Figure 5.1b. Shear Wave Velocity Profile at University LRT Station....156

Figure 5.1c. Dispersion Curve from Four-Array Receiver. 157

Figure 5.2a. Dispersion Curves at NAIT Experimental Site....158

Figure 5.2b. Shear Wave Velocity Profile at NAIT Experimental Site. 159

Figure 5.3a. Dispersion Curves at Richmond Dykes (Blundell Road)..........160

Figure 5.3b. Shear Wave Velocity Profile at Richmond Dykes (Blundell Road)..........161

Figure 5.4a. Dispersion Curves at Richmond Dykes (Chatham Road)..........162

Figure 5.4b. Shear Wave Velocity Profile at Richmond Dykes (Chatham Road)..........163

Figure 5.5a. Dispersion Curves at Richmond Dykes (Francis Road)..........164

Figure 5.5b. Shear Wave Velocity Profile at Richmond Dykes (Francis Road)..........165

Figure 5.6a. Dispersion Curves at Sea Island Site..........166

Figure 5.6b. Shear Wave Velocity Profile Sea Island Site..........167

Figure 5.7a. Dispersion Curves at Burnaby Site..........168

Figure 5.7b. Shear Wave Velocity Profile at Burnaby Site..........169

Figure 5.8a. Dispersion Curves at Annacis Site..........170

Figure 5.8b. Shear-wave Velocity Profiles at Annacis Site..........171

Figure 5.8c. Dispersion Curves based on SCPT stratigraphy at Annacis..........172

Figure 5.8d. Shear Wave Velocity Profile from assumed SCPT stratigraphy..........173

Figure 5.9a. Dispersion Curves at Delta Site..........174

Figure 5.9b. Shear Wave Velocity Profile at Delta Site..........175

Figure 5.10a. Dispersion Curves at Matsqui Site..........176

Figure 5.10b. Shear-wave Velocity Profile at Matsqui Site..........177

Figure AI.1 Configuration of Analogue-to-Digital Card..........197

Figure AI.2 Set-up Internal Counters for Data Acquisition Control..........198

Figure AI.3 Set up of gain vector for all channels..........199

Figure AI.4 Identification of channels to be scanned..........200

Figure AI.5 Account for the presence any multiplexers..........201

Figure AI.6 Set up of trigger conditions..........202

Figure AI.7 Prompt for name of site to be tested..........203

Figure AI.8 Creation of site dispersion file..........204

Figure AI.9 Prompt for filename for spacing dispersion file..........205

Figure AI.10 Prompt for receiver spacing(s) 206
Figure AI.11 Creation of spreadsheet for spacing and site dispersion files....207
Figure AI.12 Computation of data acquistion parameters. 208
Figure AI.13 Beep if trigger conditions are met. 209
Figure AI.14 Scan all on board channels 210
Figure AI.15 Demux and scale scanned channels....211
Figure AI.16 Idle till operator accepts or rejects signal. 212
Figure AI.17 Average and keep track of number of accepted signals 213
Figure AI.18 Discard signal if rejected and wait for trigger. Card 214
Figure AI.19 Compute Phase of Cross-spectrum and unwrap. 215
Figure AI.20 Calculate auto-power spectra....216
Figure AI.21 Calculate coherence. Card 217
Figure AI.22 Computation of dispersion points at acceptable coherence....218
Figure AI.23 Put acquired data in spreadsheet format. 219
Figure AI.24 Write dispersion data to disk file....220
Figure AI.25 Close all open files and exit....221
Figure AII.1 Verification of SASW-FM for Case 1....227
Figure AII.2 Verification of SASW-FM for Case 2....228
Figure AII.3 Verification of SASW-FM for Case 3....229
Figure A-III.1 Results of CPT-1 at University LRT Station....231
Figure A-III.2 Results of CPT-2 at University LRT Station....232
Figure A-IV.1 Results of CPT-1 at NAIT Experimental Site....234
Figure A-IV.2 Results of CPT-2 at NAIT Experimental Site....235
Figure A-V.1 Results of CPT-1 at Richmond Dykes (Blundell Road)....237
Figure A-V.2 Results of CPT-2 at Richmond Dykes (Blundell Road)....238
Figure A-V.3 Results of CPT-3 at Richmond Dykes (Blundell Road)....239
Figure A-V.4 Results of CPT-4 at Richmond Dykes (Blundell Road)....240

Figure A-V.5 Results of CPT-5 at Richmond Dykes (Blundell Road)....241

Figure A-V.6 Results of CPT-6 at Richmond Dykes (Blundell Road)....242

Figure A-V.7 Results of CPT-7 at Richmond Dykes (Blundell Road)....243

Figure A-V.8 Results of CPT-8 at Richmond Dykes (Blundell Road)....244

Figure A-VI.1 Results of CPT-1 at Richmond Dykes (Francis Road)....246

Figure A-VI.2 Results of CPT-2 at Richmond Dykes (Francis Road)....247

Figure A-VI.3 Results of CPT-3 at Richmond Dykes (Francis Road)....248

Figure A-VI.4 Results of CPT-4 at Richmond Dykes (Francis Road)....249

Figure A-VII.1 Results of CPT-1 at Richmond Dykes (Chatham Road)....251

Figure A-VII.2 Results of CPT-2 at Richmond Dykes (Chatham Road)....252

Figure A-VII.3 Results of CPT-3 at Richmond Dykes (Chatham Road)....253

Figure A-VIII.1 Results of CPT-1 at Sea Island Site....255

Figure A-VIII.2 Results of CPT-2 at Sea Island Site....256

Figure A-VIII.3 Results of CPT-3 at Sea Island Site....257

Figure A-IX.1 Results of CPT-1 at Burnaby Site....259

Figure A-IX.2 Results of CPT-2 at Burnaby Site....260

Figure A-IX.3 Results of CPT-3 at Burnaby Site....261

Figure A-IX.4 Results of CPT-4 at Burnaby Site....262

Figure A-IX.1 Results of Annacis Island Site....264

Figure A-X.1 Results of CPT-1 at Delta Site....266

Figure A-X.2 Results of CPT-2 at Delta Site....267

Figure A-X.3 Results of CPT-3 at Delta Site....268

Figure A-X.4 Results of CPT-4 at Delta Site....269

Figure A-XI.1 Becker Hammer Test Results at Matsqui Site....271

LIST OF SYMBOLS

a_n, b_n	Fourier coefficients
A	signal amplitude
c	generic phase velocity
$\overline{c}$	ratio of generic phase velocity to shear wave velocity
d	receiver spacing
δ	impedance contrast
δ_{ij}	Kronecker delta
E	Young's Modulus
Δf	frequency interval or resolution
Δx	distance measured on the surface of the ground
$\Delta\phi$	phase delay (radians)
$D_{xy}(f)$	convolution of the time domain signals $x(t)$ and $y(t)$.
e_{ij}	engineering strain
E	Young’s Modulus
f	linear frequency
f_s	sampling frequency
f_{max}	highest frequency in input signal
$f_{s_{min}}$	minimum sampling frequency
f_N	Nyquist frequency
f_{alias}	magnitude of aliased frequency
ϕ	scalar potential
ϕ_{true}	unwrapped phase of the cross-spectrum function
$\gamma_{xy}(f)$	root mean square coherence of the time domain signals $x(t)$ and $y(t)$.
i	$\sqrt{-1}$, complex number indicator
ψ	vector potential

k	wave number
k_v	ratio of Rayleigh-wave phase velocity to shear wave velocity
k_z	approximate ratio of depth to wavelength
K	elastic bulk modulus
$K_{xy}(f)$	mean square coherence of the time domain signals $x(t)$ and $y(t)$.
$K_{xy_{min}}$	minimum acceptable coherence
L	wavelength
L_{av}	average wavelength
λ, G	Lamé's parameters
m	number of channels
n_{CT}	number of clock ticks per second
N	total number of samples acquired during data acquisition.
r	distance from wave generating source
R	reflection coefficient
ρ	mass density
$\frac{S}{N}$	signal to noise ratio
$S_{xx}(f)$	auto-power spectrum of the time domain signal $x(t)$.
$S_{xy}(f)$	cross-power spectrum of the time domain signals $x(t)$ and $y(t)$.
σ_{ij}	stress
t	time (seconds)
Δt	time duration
t_B	time-base for data acquisition
T	period of signal
u_{ij}	displacement
$\ddot{u}_i$	second derivative of displacement with respect to time.

v_s	shear-wave velocity
v_p	compressional wave velocity
v	phase velocity
v_G	group velocity of surface waves
v_r	Rayleigh-wave velocity
v_L	Love-wave velocity
υ	Poisson's ratio
v_i	gradient of scalar potential ϕ
w_i	curl of solenoidal vector potential ψ
ω	angular frequency
x_i	coordinate direction
$x(t)$	time domain signal
$X(f)$	frequency domain signal
$X^*(f)$	complex conjugate of $X(f)$
ξ	ratio of shear- to compressional wave velocities
z	depth from the ground surface
Z	acoustic impedance

CHAPTER ONE

INTRODUCTION

1.1 ELASTIC WAVES

1.1.1 Scope

For the past half century, elastic waves have been used in both intrusive and non-intrusive in-situ tests for determining soil and pavement properties. These properties are used for site characterization purposes, pavement evaluation, design of soil structures and foundations subject to dynamic loads, construction control and monitoring as well as detection and location of subsurface anomalies. This chapter reviews the types, theory and characteristics of elastic waves. The chapter ends with a note on the applicability of measured properties for geotechnical engineering purposes.

1.1.2 Types of Elastic Waves

A wave may be described as a 'disturbance' originating from an impact or a sudden stress relief. In accordance with solid mechanics, a small-amplitude wave that does not permanently deform the medium in which it propagates is said to be elastic. Elastic waves are commonly classified on the basis of either the conditions under which they can exist or their frequency content.

Winkler (1986) noted that exploration engineers usually classify elastic waves on the basis of their frequency content (in kHz) into *seismic* (0.01 - 0.1), *sonic* (0.1 - 1.0) and *ultrasonic* (100 - 1000). On the basis of the conditions of their possible existence, elastic waves are commonly classified into *body* and *surface* waves. If the source of the wave is located in an ideal full space, then only body waves, which comprise compressional and shear waves, can propagate (Love, 1927). Compressional waves are also referred to as primary (or *P*-) waves, reminiscent of the fact that this type of body wave is the first to be detected in an earthquake record. The motion of the medium particles induced by *P*-waves is perpendicular to the wavefront (Figure 1.1a). Because they constitute the second earthquake event, shear waves are also called secondary (or *S*-) waves and propagate in one of two directions perpendicular to that of induced particle motion (Figure 1.1b). If the directions of particle motion and propagation are contained in a vertical plane, the S-wave is said to be vertically polarized, otherwise it is horizontally polarized. If a medium is not isotropic, body wave motion is difficult to dissociate into separate compressional and shear waves, but relatively small anisotropy and inhomogeneity (as found in most soils) tend to validate the assumption of separate *P*- and *S*-waves for practical purposes (Sheriff and Geldart, 1982).

If the source of disturbance, however, is situated in a bounded medium, then '*surface*' waves, which constitute the third seismic event, may also emanate (Rayleigh, 1885). They are characterized by relatively larger amplitudes compared to the two earlier seismic arrivals and are so called largely because they are more prominent in near *surface* regions. This group of waves was broadly referred to as Rayleigh waves after the first person to analyze their nature (Figure 1.1c). Lord Rayleigh (1885) found that the particle displacements caused by these surface waves were always contained in a vertical plane and that the energy diverged in only two dimensions, thus attenuating less rapidly with distance from the source than body waves. This latter observation led Lord Rayleigh (1885) to rightly predict that surface waves are of great significance in seismic phenomena.

After Rayleigh's findings, it was contended that if surface waves consisted solely of pure Rayleigh waves, then they should always possess a predominantly vertical component of motion. Such an observation, however, was not experimentally supported as the vertical component of certain surface waves had been observed to be totally absent in some cases. Love (1927) found that the existence of this horizontally polarized surface shear wave could be explained by assuming that the mass density and elasticity of shallower layers differ from that of deeper layers and showed that transverse waves could be propagated through such an outer layer without penetrating deeper and stiffer layers. Waves of this type are referred to as Love waves (Figure 1.1d) and thus require a shear low velocity zone (or LVZ).

Stoneley (1924) investigated the general problem of elastic wave propagation along the interface of two acoustically different solid media and also within a stratum bounded by thicker strata of differing elasticity. Such interface waves, which are similar to Rayleigh waves in the first instance and to Love waves in the second, are referred to as Stoneley waves. The conditions under which Stoneley waves exist have been cited by Stoneley (1924), Scholte (1947) and Ewing et al (1957). A Stoneley wave is capable of travelling along a solid-liquid interface but at a lower velocity than a Rayleigh wave at a free surface of the solid medium. If a half space is overlain by a surface layer, then Stoneley waves are possible only when the shear wave velocities in both media are almost equal and the thickness of the surface layer far exceeds the maximum input wavelength (Segel, 1977). Under such circumstances, the Stoneley wave velocity is obtainable from a fourth order equation which is a function of the elastic constants of both media and has a solution for certain specific ranges of the ratio of the shear moduli and densities. The phase velocity of a Stoneley wave, if it exists, has a value between the Rayleigh wave velocity and the greater of the shear wave velocities in both media. Stoneley waves may be best suited to the investigation of bonding and interface properties between materials and are not discussed further in this thesis.

For conditions under which both body and surface waves coexist (e.g. vertically vibrating circular source on the surface of an ideal half-space), Miller and Pursey (1955) found that approximately 67 % of the input energy propagated as Rayleigh waves, 26 % as shear waves and 7% as compressional waves.

1.1.2.1 Body Waves.

The primary objective for determining body wave velocities is to deduce the elastic parameters of the propagation medium. Terzaghi (1943) was aware of this possibility for soils and noted that the:

> *"… velocity of wave propagation depends on Young's modulus and Poisson's ratio. Strata with very different elastic constants are usually separated by fairly sharp boundaries likely to give rise to well-defined reflection and refraction phenomena. Therefore it is theoretically possible to obtain information on the elastic properties and on the thickness of the strata located beneath the surface of the earth by recording the vibrations produced by an impulse on the surface at different distances from the focus of the disturbance."*

Prior to this observation, Timoshenko and Goodier (1934) and others before them, had theoretically derived the relationship between body wave velocities and elastic parameters. This derivation is reviewed in this section, primarily because some of the intermediate equations will be referred to in later discussions.

If body waves propagate in a medium of mass density ρ and Lamé's parameters λ and G as shown in Figure 1.2, then the following rudimentary equations from elasto-dynamics may be readily derived as shown below.

Newton's Law:

$$\rho \ddot{u}_i = \sigma_{ji,j} \qquad [1.1]$$

Strain - Displacement:

$$e_{ij} = \tfrac{1}{2}(u_{i,j} + u_{j,i}) \qquad [1.2]$$

Linear Elasticity:

$$\sigma_{ij} = 2Ge_{ij} + \lambda e_{kk}\delta_{ij} \qquad [1.3]$$

Substitute (1.2) in (1.3):

$$\sigma_{ij} = G(u_{i,j} + u_{j,i}) + \lambda\delta_{ij}u_{k,k} \qquad [1.4]$$

Substitute (1.4) in (1.1) and simplify to obtain *Navier's* equation below :

$$\rho\ddot{u}_i = Gu_{i,jj} + (\lambda + G)u_{j,ji} \qquad [1.5]$$

Let the displacement vector u be represented by the sum of the gradient (v) of a scalar field (ϕ) and the curl (w) of a solenoidal vector field (ψ). Then by the Helmholtz Representation Theorem,

$$u_i = v_i + w_i \qquad [1.6]$$

where $v_i = \phi_{,i}$ and $w_i = \varepsilon_{ijk}\psi_{k,j}$

If the displacement (u_i) is irrotational, (i.e. $w_i = 0$ and $u_i = v_i$,), Navier's equations reduce to

$$\rho\ddot{v}_i = Gv_{i,jj} + (\lambda + G)v_{j,ji} \qquad [1.7]$$

or

$$\rho\ddot{\phi}_{,i} = G\phi_{,ijj} + (\lambda + G)\phi_{,jji} = (\lambda + 2G)\phi_{,jji} \qquad [1.8]$$

i.e.

$$\rho\ddot{v}_i = (\lambda + 2G)v_{i,jj} \qquad [1.9]$$

which is the dilatational or P-wave equation and shows that the P-wave velocity (v_p) is given by

$$v_p^2 = \frac{\lambda + 2G}{\rho} \qquad [1.10]$$

On the other hand, if the displacement (u_i) is solenoidal, (i.e. $v_i = 0$ and $u_i = w_i$), Navier's equations reduce to

$$\rho \ddot{w}_i = G w_{i,jj} + (\lambda + G) w_{j,ji} \qquad [1.11]$$

Since w_i is solenoidal or divergence-free, $w_{i,i} = 0$, the last equation reduces to the S-wave equation

$$\rho \ddot{w}_i = G w_{i,jj} \qquad [1.12]$$

and shows that the S-wave velocity v_s is given by

$$v_s^2 = \frac{G}{\rho} \qquad [1.13]$$

For plane polarized wave propagation, an assumption that is approximately valid if wave measurements are made outside a radius of at least two wavelengths from the generating source (Lysmer and Drake, 1972; Stokoe et al, 1978), the theory of elasticity leads to the following relationships between body wave velocities and more frequently used elastic parameters.(Timoshenko and Goodier, 1934) :

$$\nu = \frac{(\frac{v_s}{v_p})^2 - \frac{1}{2}}{(\frac{v_s}{v_p})^2 - 1} \qquad [1.14a]$$

$$E = 2\rho v_s{}^2 (1 + \nu) \qquad [1.14b]$$

$$G = \rho V_s^2 \qquad [1.14c]$$

$$K = \rho (v_p{}^2 - \tfrac{4}{3} v_s{}^2) \qquad [1.14d]$$

where υ = Poisson's ratio,

E = Young's modulus,

G = shear modulus and

K = bulk modulus.

The following observations are generally made from the foregoing discussion.

1. Due to their mode of propagation, P-waves are also referred to as dilatational, longitudinal, or irrotational as they result from the propagation of the volumetric strain state while S-waves are called transverse, equi-voluminal, distortional, or rotational because they result from the propagation of the distortional strain state.

2. For the same medium, the P-wave velocity is always greater than the S-wave velocity since the Lamé constants cannot be negative. Shear-waves are difficult to detect due to the fact they always arrive in the wake of the faster P-waves but for earthquakes, they are of much larger amplitude.

3. The ratio of shear- to compressional-wave velocities ($\frac{v_s}{v_p}$) for a given medium depends solely on its Poisson's ratio and equation [1.14] offers a quick way of estimating this parameter if the body wave velocities are known. The relationship between Poisson's ratio and $\frac{v_s}{v_p}$ (shown in Figure 1.3) shows that as Poisson's ratio decreases from the theoretical maximum value of 0.5 to zero, the body wave velocity ratio ($\frac{v_s}{v_p}$) increases from zero to a maximum value of $\frac{1}{\sqrt{2}}$, indicating that $0 \leq v_s \leq 0.7v_p$.

4. Since G vanishes for normal aqueous materials, shear waves do not propagate in such fluids. Unlike P-waves, shear wave velocities do not depend as much on pore fluids and are useful for investigating the fabric and structural stiffness of near-surface formations.

Stokoe and Hoar (1977) reported compression wave velocities of 210 - 760 m/s for dry soils and for soils with degrees of saturation less than or equal to 98%. For saturated soils, however, P-wave velocities range from 1450 - 1770 m/s. Murphy (1972) observed

P-wave velocities of about 915 m/s in submerged fills and commented that saturation in these materials is rarely found. Hoar (1982) reported shear wave velocities in the range of 120-430 m/s for most soils but indicated that velocities as low as 60 m/s and as high as 610 m/s have been measured for near-surface soft clays and deep deposits of hard clays or dense sands and gravels respectively. Competent rocks have also been reported to transmit shear waves within a velocity range of 2000-4700 m/s. Body wave velocities in earth materials are also functions of depth, existing in-situ stresses, age and cementation.

The key objective of most in-situ surface wave tests is to determine body wave velocity profiles as a function of depth. Direct measurements of body wave velocities on the ground surface are difficult to make because body waves attenuate rather rapidly on free surfaces. For a surficial distance (r) from a generating source, body waves attenuate proportionally to $\frac{1}{r^2}$ (Timoshenko, 1934). This high attenuation rate is further compounded by the fact that shear waves are very difficult to detect in the presence of compressional waves. On the other hand, surface waves are not as difficult to generate, attenuate at a rather slower rate on the surface (surface waves attenuate proportionally to $\frac{1}{\sqrt{r}}$; Timoshenko, 1934) and are easily detected at distance of several wavelengths from the source. Hence, a more convenient procedure (as used in this research) is to measure surface wave velocities and then compute the desired *P*- and *S*- wave velocities on the basis of elastodynamic relationships between body and surface wave velocities. For non-ideal media, such relationships may be derived from the theory of dispersion, discussed in Chapter 3. In the following sections, the relationships between more familiar elastic parameters and body wave velocities are reviewed followed by a review of fundamental surface wave theory

Though not commonly used in routine geotechnical analysis, the two body wave velocities may be used to completely characterize the elastic behaviour of an isotropic, homogeneous medium and can play a similar analytical role as Young's modulus and Poisson's ratio.

1.1.2.2 Surface Waves.

Rayleigh waves (or ground roll as they are usually called in exploration seismology) are the most commonly used surface waves and are propagated over the relatively 'free' surface of a solid medium. They are essentially vertically polarized shear P-SV waves. They induce elliptical particle motion that is polarized in a plane perpendicular to the direction of wave propagation, the sense being retrograde at the surface and prograde at depth. There is a transition zone in which the horizontal component of particle motion vanishes (see Figure 1.4b). Since particle motion is predominantly vertical, receivers for detecting and measuring Rayleigh waves are sensitive in the vertical direction. This implies that ground coupling may be augmented by the self weight of the receivers. Rayleigh waves are the most commonly used surface waves in non-intrusive in-situ testing primarily because they constitute almost 67% of the energy of a surface source and their geometrical damping is inversely proportional to the square root of the distance from the source as compared to body waves whose amplitudes varies inversely with the square of distance from source. The implication is that much larger volumes of material can be tested for the same source characteristics, receiver sensitivity and signal amplification.

Love waves are shear waves that propagate on the surface of a solid medium. Particle motion and the direction of wave propagation are contained in a horizontal plane. Love waves are therefore said to be horizontally polarized shear (or SH-) waves. In a formation where shear wave velocity increases with depth, Love wave velocity approaches the S-wave velocity in the surface layer at high frequencies and the S-wave velocity in the deepest layer at sufficiently low frequencies. However, they are rarely utilized in either engineering investigations or exploration seismology primarily because most standard receivers are generally vertically sensitive (and hence are unable to detect them) and available energy sources are not rich in Love waves. Another reason is that receiver ground coupling becomes crucially important in Love wave investigation due to the horizontal particle motion. Perhaps the single most important disincentive for deploying Love waves is their existential condition that the shear wave velocity in deeper layers must be greater than in shallower layers. In engineering investigations, such conditions may not be known *apriori* and hence caution recommends the use of other surface waves such as Rayleigh waves at the expense of mathematical complexity as Love wave problems are relatively simpler to solve.

1.1.3 Rayleigh Wave Formulation

Figure 1.2 shows an elastic half–space with density ρ and Lamé's parameters λ and G. If a Rayleigh wave propagates in the x_1 direction on the free surface, then the displacements (u_i) are x_3-independent and are therefore polarized in the $(x_1 - x_2)$-plane.

$$u_i = u_i(x_1, x_2, t) \qquad u_3 = 0; \qquad [1.15]$$

The displacements may be dissociated into dilatation-free and irrotational components that simultaneously satisfy the following differential equations.

$$\rho \ddot{v}_i = (\lambda + 2G) v_{i,jj} \qquad [1.16]$$

$$\rho \ddot{w}_i = G w_{i,jj} \qquad [1.17]$$

The boundary conditions governing the propagation are

$$\sigma_{2i} = 0 \qquad \text{for } x_2 = 0 \qquad [1.18]$$

$$\lim_{x_2 \to \infty} u_2 = 0 \qquad [1.19]$$

By substituting equation [1.18] in the stress-displacement equation [1.4], the first boundary condition translates into the following equations at the free surface ($x_2 = 0$).

$$u_{2,1} + u_{1,2} = 0 \qquad [1.20]$$

$$(\lambda + 2G)u_{2,2} + \lambda u_{1,1} = 0 \qquad [1.21]$$

Assume that the Rayleigh wave displacements are of the form

$$w_i = A_i e^{-ax_2 + i(kx_1 - \omega t)} \qquad [1.22]$$

$$v_i = B_i e^{-bx_2 + i(kx_1 - \omega t)} \qquad [1.23]$$

where a and b = are positive constants ensuring satisfaction of the boundary condition given in equation [1.19]

ω = angular frequency

and k is the wavenumber.

Equations [1.16] and [1.17] are satisfied if

$$-\rho\omega^2 = (\lambda + 2G)(b^2 - k^2) \qquad [1.24]$$

and

$$-\rho\omega^2 = G(a^2 - k^2) \qquad [1.25]$$

By introducing the factors h_1 and h_2 given by

$$h_1^2 = \frac{\rho\omega^2}{\lambda + 2G} \qquad [1.26]$$

and

$$h_2^2 = \frac{\rho\omega^2}{G} \qquad [1.27]$$

equations [1.24[and [1 .25] may be respectively simplified to

$$b^2 - k^2 + h_1^2 = 0 \qquad [1.28]$$

and
$$a^2 - k^2 + h_2^2 = 0 \qquad [1.29]$$

From the dilatation-free nature of w_i,

$$w_{i,i} = ikA_1 - aA_2 = 0 \qquad [1.30]$$

from which
$$A_1 = -iaA \qquad [1.31]$$

where
$$A = A_2 / k. \qquad [1.32]$$

Similarly, the irrotational nature of v_i, (i.e. $v_{1,2} - v_{2,1} = 0$) leads to

$$B_1 = -ikB \qquad [1.33]$$

where
$$B = B_2 / b \qquad [1.34]$$

The three unknowns (i.e. the wavenumber k and the amplitudes A and B) may be found from the boundary conditions and a determinantal condition. The calculation of the boundary conditions are simpler if real solutions are used instead of the complex exponentials. The displacements in equations [1.22] and [1.23] may therefore be re-written as

$$w_i = A_i e^{-ax_2}[\cos(kx_1 - \omega t) + i\sin(kx_1 - \omega t)] \qquad [1.35]$$

$$v_i = B_i e^{-bx_2}[\cos(kx_1 - \omega t) + i\sin(kx_1 - \omega t)] \qquad [1.36]$$

By substituting 1.31 and 1.33 in 1.35 and 1.36, the real components of the displacement become

$$\begin{aligned} w_1 &= Aae^{-ax_2}\sin(kx_1-\omega t) \\ w_2 &= Ake^{-ax_2}\cos(kx_1-\omega t) \\ v_1 &= Bke^{-bx_2}\sin(kx_1-\omega t) \\ v_2 &= Bbe^{-bx_2}\cos(kx_1-\omega t) \end{aligned} \qquad [1.37]$$

Boundary condition 1.21 may be written as

$$2G(v_{2,2}+w_{2,2})+\lambda v_{i,i}=0 \qquad [1.38]$$

which, upon substitution of the derivatives of the displacement potentials and suppression of the trigonometric term $\cos(kx_1-\omega t)$ yields

$$2GakA+[\lambda(b^2-k^2)+2Gb^2]B=0 \qquad [1.39]$$

Similarly, with suppression of $\sin(kx_1-\omega t)$, the boundary condition given in equation [1.20] leads to

$$(a^2+k^2)A+2bkB=0 \qquad [1.40]$$

For a nontrivial solution of equations [1.39] and 1[.40], the determinant of the coefficients must vanish i.e.

$$4Gabk^2-[\lambda(b^2-k^2)+2Gb^2](a^2+k^2)=0 \qquad [1.41]$$

By replacing λ, G, a and b with substitutes from equations [1.24], [1.25], [1.26] and [1.27], the last equation reduces to the Rayleigh wave equation

$$(2-\frac{h_2^2}{k^2})^4=16(1-\frac{h_1^2}{k^2})(1-\frac{h_2^2}{k^2}) \qquad [1\ .42]$$

which can be solved for k^2 in order to determine the propagation speed c, the amplitude ratio A / B and the decay coefficients a and b.

1.1.4 Properties of Rayleigh Waves

1. Equation [1.42] is independent of the angular frequency ω. Thus Rayleigh waves are not dispersive in an elastic half space. Dispersion only occurs in materials that are not elastic or uniform.

2. From the expressions for v_p, v_s, h_1 and h_2, it can be deduced that

$$\frac{h_1^2}{k^2} = \frac{\omega^2 / k^2}{v_p^2} = \frac{c^2}{v_p^2} \qquad [1.43a]$$

and

$$\frac{h_2^2}{k^2} = \frac{\omega^2 / k^2}{v_s^2} = \frac{c^2}{v_s^2} \qquad [1.43b]$$

from which

$$\frac{h_2^2}{h_1^2} = \frac{v_p^2}{v_s^2} \qquad [1.44]$$

where c is the propagation speed of the Rayleigh-wave in the x_1 -direction.

From equation [1.44],

$$h_2^2 < k^2$$

and therefore

$$c^2 < v_s^2 < v_p^2 \qquad [1.45]$$

The Rayleigh-wave velocity is thus less than both body wave velocities, v_p and v_s.

3. From equations [1.28] and [1.29], it can be shown that $a < b$. Therefore the horizontal displacement decays at a slower rate than the vertical component.

4. The decay of the Rayleigh-wave displacement components depends on the expression ax_2 which in turn depends on the parameter kx_2. The higher the value of this latter parameter, the greater the attenuation. Since k is proportional to frequency, the implication is that Rayleigh waves of higher frequency are attenuated more rapidly with depth than

those of low frequency. Hence high frequency Rayleigh waves are more prominent near the surface.

5. The material properties of the propagation medium are present only in terms of v_p and v_s. In terms of the body and Rayleigh wave propagation velocities, the quartic order of equation [1.42] may be reduced to a cubic in the parameter $\bar{c}$ as

$$\bar{c}^6 - 8\bar{c}^4 + 8(3 - 2\xi^2)\bar{c}^2 - 16(1 - \xi^2) = 0 \qquad [1.46]$$

where $$\bar{c}^2 = \frac{c^2}{v_s^2}$$

and $$\xi^2 = \frac{v_s^2}{v_p^2} = \frac{\frac{1}{2} - \upsilon}{1 - \upsilon},$$

υ being Poisson's ratio.

6. The expressions for displacements in equation [1.37] show that the path of any particle in the medium is elliptical with the major axis perpendicular to the free surface. At the surface, the ratio of the lengths of major to minor axes is approximately 1.5.

7. The Rayleigh wave displacement components may be written in matrix form as

$$\begin{Bmatrix} u_1 \\ u_2 \end{Bmatrix} = \begin{bmatrix} a\sin(kx_1 - \omega t)e^{-ax_2} & k\sin(kx_1 - \omega t)e^{-bx_2} \\ k\cos(kx_1 - \omega t)e^{-ax_2} & b\cos(kx_1 - \omega t)e^{-bx_2} \end{bmatrix} \begin{Bmatrix} A \\ B \end{Bmatrix} \qquad [1.47]$$

If B is expressed in terms of A (i.e. $B = \dfrac{-A(a^2 + k^2)}{2bk}$) and the trigonometric terms are suppressed,

$$u_1 \approx \frac{A(a^2 + k^2)}{2b} e^{-ax_2} \left[\frac{2ab}{a^2 + k^2} - e^{-(b-a)x_2} \right] \qquad [1.48]$$

$$u_2 \approx \frac{A(a^2 + k^2)}{2k} e^{-ax_2} \left[\frac{2k^2}{a^2 + k^2} - e^{-(b-a)x_2} \right] \qquad [1.49]$$

Figure 1.4 shows the variation of normalized vertical and horizontal displacement components with normalized depth. It may be observed that displacement components perpendicular to the free surface initially increase slightly with depth till a maximum at a depth of approximately 0.1 (actually 0.075) wavelengths and thereafter decrease monotonically but remain positive. Displacement components parallel to the free-surface decrease with depth until they vanish at some critical depth. These horizontal components continue to decrease below zero to a minimum at a depth of about half wavelength after which they increase and asymptotically approach zero. The combined particle motion is therefore on an elliptical path that is retrograde at the surface and prograde at some depth. At a depth of approximately one wavelength, the vertical amplitudes have been attenuated to about 19% of their value at the surface.

1.2 IN-SITU WAVE PROPAGATION METHODS

1.2.1 Scope

Most available seismic field procedures involve the measurement of either the velocity of elastic wave propagation in the ground or the response of structures to dynamic excitation. Methods under the latter approach subject the soil to a dynamic load and measure the resulting response characteristics. The first approach entails the determination of the velocity of body or surface waves in the ground by the measurement of either traveltimes or phase delays. Methods for directly determining body wave velocities generally fall under *intrusive* or *subsurface* tests because drilling or penetration of the ground is required. Procedures for the indirect determination of body wave velocities *via* surface wave velocities, however, do not require penetration of the soil and are called *non-intrusive* or *surface* tests. This section presents a cursory review of well-known intrusive tests and a detailed review of current non-intrusive methods.

1.2.2 Intrusive Methods.

As mentioned earlier, intrusive methods require borehole(s) or penetration for implementation. Included in this category are the crosshole, downhole, uphole, in-hole, bottom-hole and the seismic cone penetration tests. Figures 1.5 and 1.6 show schematic illustrations of these tests.

In the downhole test (Schwarz and Musser, 1972), an impulse source located on the surface generates predominantly compressional or shear waves that are received at the bottom of a single borehole. The compressional or shear wave velocity is computed simply as the ratio of the difference in consecutive receiver elevations to the difference in arrival time for the same pair of elevations, after the receiver elevations have been corrected for inclination. The use of one receiver requires accurate depth recording, verticality of the hole, synchronized triggering of source and receiver and a high resolution in time measurements. As the receiver depth increases, the signals from the impulse sources gets weaker and different sources with similar characteristics but higher energies may be required. Downhole testing at short depth intervals is potentially capable of determining changes in stratigraphy. Another modification of this test uses two receivers at a fixed spacing and has the advantage of a common source for the two elevations (Hoar, 1982).

The uphole test (Meisner, 1965) is very similar to the downhole test. The only major difference is that the positions of the source and receiver are interchanged, the receiver being on the surface and the source at the bottom of the hole. The procedure for determining body wave velocities is identical to the downhole test and shares most of the advantages and limitations of the downhole test. In addition, the surface location of the receiver makes it more vulnerable to stronger background noise whereas the requirement of a buried source places restrictions on the type of source that can be deployed.

In the in-hole method (Ogura, 1979), both receiver and source are located in the walls of a borehole. Test procedures are the same as in the uphole and downhole tests. This test, is of limited application since generated waves virtually sample the smeared and disturbed materials in the vicinity of the borehole. Difficulty may also be encountered in attaching the receiver and source to the sides of the borehole. The method, however, may be employed in evaluating the degree of disturbance caused by drilling operations.

For bottom-hole approach (Stokoe et al, 1978), an arrangement of a source and a receiver is pushed into the soil at the bottom of a borehole, was probably aimed at improving the in-hole method. Not only is the method restricted to relatively soft soils, but also the depth of penetration must exceed the probable depth of drilling disturbance for a meaningful evaluation of the results. The test is limited to relatively soft soils.

The cross-hole test (Stokoe and Hoar, 1978) requires a minimum of two boreholes for a source and one or more receivers. Any borehole deviations from the vertical must be known at all test depths since the distance between boreholes (usually 3 to 6 metres) must be reliably known. At each desired test depth, an impulse source and receiver(s) are coupled to the soil in their respective boreholes. Signals generated by the source travel through the intervening medium, desirably at the same test depth, before detection by the receivers. Synchronized triggering of source and receiver is required only if two boreholes are used. The velocity of the waves is computed as the ratio of inter-borehole distance at the test depth to the travel time. In soils where stiffness increases with depth, Andréasson (1979) observed that shear waves travel in the deeper and stiffer material and hence travel paths are not necessarily horizontal as assumed in velocity calculations. To reduce the time involved in conventional crosshole testing, and avoid drilling disturbances associated with pre-bored holes, crosshole tests have also been performed with two cone penetration rigs for pushing a receiver and a source (Baldi et al, 1988). However, tests conducted by Andréasson (1979) concluded that disturbance effects on wave velocities from drilling and pushing relatively large penetrometers are similar. Larsson and Mulabdic (1991) noted that the crosshole test is often considered the most accurate of all the intrusive tests and is more frequently used as a reference. However, it is very expensive and time-consuming to install and measure the inclination of the holes.

In the seismic cone penetration test or SCPT (Robertson et al, 1986), a geophone or accelerometer is incorporated in a conventional electric cone which is pushed into the ground. At desired depths, usually every metre, a surface source generates predominantly shear-waves which are picked up by the receiver in the cone. The shear waves are generated by hitting a surface steel beam with an instrumented hammer (Figure 1.6). Velocity computation is the same as in the downhole test. The method is restricted to relatively soft soils, and existing results have compared favourably with those from the crosshole method (Gillespie, 1990). Recent modifications of the test includes the incorporation of two receivers in the electric cone for a bettet estimate of interval traveltime (Campanella and Stewart, 1991).

Intrusive methods are limited by the requirement of one or more boreholes but are otherwise simple to analyze. In soils that are not self-supporting, well casings can affect the measurements, sometimes rendering the results difficult to interpret. Non-intrusive tests seek to overcome most of these difficulties.

1.2.3 Non-Intrusive Methods.

Non-intrusive methods comprise refraction survey, reflection survey, steady vibration and the Spectral Analysis of Surface Waves (SASW) methods. The first two methods are used more frequently in geophysical exploration work whereas the last two, also used in global geophysics, are more suited to civil engineering needs.

1.2.3.1 Seismic Refraction Method

In the seismic refraction survey, the objective is to determine the thicknesses and velocities of refracting layers and the velocity in the underlying medium. The principles of the test are illustrated in Figure1.7 which, for simplicity, shows refracted and direct waves in a two-layered medium. An array of receivers are positioned to pick up direct and refracted waves in line with a surface energy source. The main measurements in the test are the offset distances of receivers from the source and the traveltimes of direct and refracted waves at each receiver station. From the theory of the method, discussed in detail by Dobrin (1960), Richart et al (1970) and Redpath (1973), it can be shown from the geometry of the set-up in Figure 1.7 that the traveltimes (t_r) and (t_d) for a refracted and direct wave respectively are given by

$$t_r = \frac{x}{v_2} + \frac{2z\cos\theta}{v_1} \qquad [1.50]$$

and

$$t_d = \frac{x}{v_1} \qquad [1.51]$$

where x = offset distance from source to receiver,

v_1, v_2 = appropriate velocity in upper and lower medium respectively,

z = depth to the refracting surface and

θ = the critical angle of incidence.

Data processing involves plotting traveltimes of direct and refracted waves against geophone offset as shown in Figure 1.8. The velocity of the upper medium is obtained from the slope (m_d) of the direct traveltime curve as

$$v_1 = \frac{1}{m_d} \qquad [1.52]$$

and the velocity of the lower medium is similarly obtained from the slope (m_r)of the linear portion of the traveltime curve for the refracted wave.

$$v_2 = \frac{1}{m_r} \qquad [1.53]$$

The critical angle (θ) may then be calculated from the relationship

$$\theta = \sin^{-1}\frac{v_1}{v_2} \qquad [1.54]$$

The depth to the refracting surface may be calculated from the intercept time (t_1) of the refracted traveltime curve using the following equation

$$z = \frac{v_1 t_1}{2\cos\theta} \qquad [1.55]$$

The method may be extended to estimate the average body wave velocity, thickness and dip angles of each subsurface stratum of a multi-layered deposit. According to Bath (1974), Masuda (1975) analytically modified the theory to allow for complex strata orientations and geometries. Bath (1974) also indicated that Soriano, Krizek and Franklin (1977) developed the method still further for a single layer of increasing stiffness with depth. The main advantages of the method are its relative simplicity, economy and relative speed in surveying wide areas

Though the refraction method can potentially use any type of seismic wave, P-waves have been more frequently deployed primarily because of their easy and uncomplicated generation and detection. Near and below the phreatic surface, however, the dependency of P-wave velocity on the degree of saturation complicates data interpretation for geotechnical purposes. Under the latter circumstance, body S-waves have been used with limited success, resulting directly from the difficulty of coupling adequate amounts of shear energy into the soil and by the complexity of detecting the arrival of shear waves amidst the earlier arrivals of direct, reflected and refracted compressional waves. The seismic refraction method is also beset with a number of other limitations. Many authors have summarized potential practical problems associated with applying this method to near-surface deposits, which are of interest in civil engineering. Redpath (1973) concluded that thin high velocity layers are not detected if the velocity contrast with adjacent layers is high. Woods (1978) indicated that not only are low-velocity layers sandwiched between high velocity layers undetectable by refraction, but also only portions close to layer interfaces are sampled in thick layers. An additional barrier to the use of this method in developed areas is the relatively large area required by the test. Hoar (1982) noted that the receiver layout require a length three times the expected penetration depth and that velocity profiling is based on averaging algorithms which render the resulting resolution too poor for most geotechnical analyses.

1.2.3.2 Seismic Reflection Method

The primary objective of the reflection method described by Borm (1978), is to locate the depth of a subsurface layer that causes a reflection on a seismic record. The principles of the test are best illustrated in two dimensions for a two-layered horizontal system in which the body wave velocities of the lower layer are much greater than those of the upper layer Figure 1.9.

Explosive sources are exclusively used in this method and therefore the generated waves are predominantly compressional waves. The traveltime (t) required for interface reflected waves to reach the geophone at offset (x) is measured on an oscilloscope by synchronized triggering of source and geophone. In practice, an array of receivers, the spread of which is obviously not as wide as in refraction survey, are used to simultaneously find arrival times at different offsets. The relationship between reflection traveltime and offset can be simply shown to be given by

$$t^2 = \frac{1}{v^2}\left(x^2 + 4h^2\right) \qquad [1.56]$$

where v = appropriate body wave velocity in the upper layer and

h = depth to the surface of the reflecting layer.

The basic approach of a more commonly-used method of processing seismic reflection data, called the $X^2 - T^2$ method, is to graphically plot the square of traveltime against the offset. The result is a straight-line relationship, from which the depth to the reflecting surface (h) and the velocity (v)of the upper layer may be calculated from the following equations.

$$v = \sqrt{\frac{1}{m}} \qquad [1.57]$$

$$h = \frac{1}{2} v t_0 \qquad [1.58]$$

where

m = the slope

and t_0 = t^2-intercept.

Whenever conditions permit, the capability of this method to detail stratigraphy may be its main advantage . The reflection method, considered to be the most commonly used test in petroleum exploration, also finds application in marine environments where use is made of the large acoustic difference between soil and water to locate the sea-bed within centimetres. Its use, however, is severely limited on civil engineering sites due to the following reason. The fraction of wave energy reflected at an interface is inversely proportional to the impedance contrast (δ) at the interface which is defined as

$$\delta = \frac{Z_1}{Z_2} \qquad [1.59]$$

where Z_1 and Z_2 are the acoustic impedances of the media on opposite sides of the reflecting surface. The acoustic impedance (Z) of a medium is the product of its mass density (ρ)and the appropriate body wave velocity (v). When δ = 1, no wave energy is reflected and the greater the value of $|\delta - 1|$, the greater the reflection. Telford et al (1976) presented results for a sandstone-limestone interface that show that for material of the same mass density, a velocity ratio of 2:3 is required to produce a 4% reflection coefficient (R) which is a measure of the fraction of reflected energy and is defined by the equation

$$R = \left(\frac{\delta - 1}{\delta + 1}\right)^2 \qquad [1.60]$$

Telford et al (1976) also show that the reflection coefficient may be as low as 0.2% for most shallow interfaces and 0.05% for deep interfaces. The authors also noted that

> *"The sandstone-on-limestone interface is as about as large a contrast as is apt to be encountered, whereas the 'shallow interface' and 'deep interface figures are much typical of most interfaces in the earth; hence usually appreciably less than 1% of the energy is reflected at any interface. A major exception involve the bottom and surface of the ocean ...".*

The method is thus not well-suited for geotechnical engineering applications where variations of soil stiffness with depth is gradual and rarely abrupt. It must be added that the reflection technique has been used with some success in a few cases (Nyland, 1992), probably at sites where sharp variations in soil stiffness exists. Figure 1.8 also shows that reflected waves never arrive earlier than direct and refracted waves. The determination of reflected wave arrivals is therefore very complicated and requires subjective experience. Another possible difficulty is that multiple reflections within a near-surface layer may obscure and complicate detection and interpretation of arrivals from deeper layers. Its use is also limited in engineering applications by the fact that compressional waves are exclusively used and that P-wave velocities are much more dependent on the degree of saturation than on the stiffness of the soil skeleton.

In the light of the foregoing discussion, it may be concluded that the surface refraction and reflection methods are not as suitable for most geotechnical engineering applications. In the next sections, two methods based on surface waves will be reviewed

1.2.3.3 Steady-State Vibration Method.

The objectives of the steady-state vibration method are to determine the thicknesses and corresponding shear wave velocities of the layers of a soil or pavement system by determining the in-situ Rayleigh wave dispersion curve (Jones, 1950, 1955; Heukelom and Foster, 1960; Fry, 1963; Ballard, 1964). The field procedure essentially consists of the generation of steady vibrations of different but known frequencies, and the determination of their wavelengths by a trial-and-error approach.

The experimental procedure is schematically illustrated in Figure 1.10, which shows a geophone and a vibrator connected to an oscilloscope. The vibrator is set up to generate a sequence of steady pulses at a predetermined frequency (f), which then propagate towards the geophone, predominantly as Rayleigh waves (Miller and Pursey, 1955). Beginning from a location close to the vibrator, the distance to the geophone is incrementally widened until the measured wave trace is in phase with the source signal. Alternatively, two geophones may be moved relative to one another and the source until the measured signals are in phase. With the latter approach, though more expensive, any obstacles between source and geophone may be easily avoided without relocating the source. The distance from the vibrator to the nearest in-phase location of a single geophone or the shortest distance between two geophones with in-phase responses, which is equal to a wavelength (L), is recorded. To obtain a more representative wavelength, the distance between the vibrator and geophone is doubled and adjusted until source and receiver signals are in phase again. This larger in-phase distance is equivalent to two wavelengths $(2L)$ and an average wavelength (L_{av}) of the steady signal is obtained from the slope of the linear relationship between in-phase distances and number of wavelengths. This averaging technique is important in minimizing body wave effects which are not insignificant for short source-geophone distances of about one wavelength (Stokoe and Nazarian, 1984).

The use of two geophones, all of which are at least a wavelength from the source, significantly minimizes this undesired effect. The velocity of the propagating Rayleigh wave (v_r) is calculated simply as the product of frequency and wavelength

$$v_r = fL_{av}. \qquad [1.61]$$

The above procedure is repeated for each of a given set of predetermined vibration frequencies to obtain the corresponding set of wavelengths and velocities. A plot of phase velocity against wavelength is the required in-situ dispersion curve from which the layer thicknesses and shear wave velocities are to be determined, a process often referred to as inversion or system identification.

The inversion scheme in the steady vibration method is primarily based on the work by Miller and Pursey (1955), who found that approximately 67% of the energy of a vertically vibrating source on the surface of a half-space propagated as Rayleigh waves. The implication is that the waves reaching the geophones from the vibrator may be considered as Rayleigh waves. Hence the approximate relationship (see equation 1.46) between Rayleigh wave and shear wave velocities can be used to calculate shear wave velocities from corresponding Rayleigh wave velocities if the Poisson's ratio of each layer is known.

$$v_s = k_v.v_r \qquad [1.62]$$

where

v_s = shear wave velocity,

v_r = Rayleigh-wave velocity and

k_v = the ratio of Rayleigh-wave to body shear-wave velocities

k_v is identical to $\bar{c}$ and may be obtained as the appropriate solution to the Rayleigh wave equation which was given in equation [1.46] and may also be expressed as cubic in k_v^2 as.

$$k_v^6 - 8k_v^4 + 8(3-2\xi^2)k_v^2 - 16(1-\xi^2) = 0 \qquad [1.63]$$

where $$k_v^2 = \frac{v_r^2}{v_s^2} = \frac{c^2}{v_s^2}, \qquad [1.64]$$

$$\xi^2 = \frac{v_s^2}{v_p^2} = \frac{\frac{1}{2}-\upsilon}{1-\upsilon}, \qquad [1.65]$$

υ = Poisson's ratio.

For a given Poisson's ratio, ξ can be calculated and the cubic equation solved for the valid root of k_v. Alternatively, simplifying approximations may be used to calculate k_v in order to avoid solving the complex cubic equation. Within the normal range of Poisson's ratio $(0 \le \upsilon \le 0.5)$, Filipczynski et al (1966) showed that a simpler but approximate solution of equation [1.57] is

$$\frac{1}{k_v} = \frac{0.87 + 1.12\upsilon}{1+\upsilon} \qquad [1.66$$

where k_v and υ are as defined. Equation [1.66] indicates that

$$0.87 \le \frac{1}{k_v} \le 0.95 \quad \text{or} \quad 1.05 \le k_v \le 1.15 \qquad [1.67]$$

and hence the Rayleigh-wave velocity in a layer is about 10% less than the shear-wave velocity in the same layer. An assumption of Poisson's ratio in equation [1.66] therefore yields k_v, which gives the relationship between the measured Rayleigh-wave velocity (v_r) and the required shear-wave velocity (v_s). The remaining task is to relate the wavelength to the depth from the surface.

Das (1983) showed that the vertical- and horizontal- displacement components of a Rayleigh wave approach zero below a depth of about one wavelength. The statement may be verified from the variation of normalized particle displacements with normalized depth already shown in Figure 1.4. This observation appears to give some theoretical support for the assumption that a Rayleigh wave of wavelength L samples an average depth z given by

$$z = k_z L \qquad [1.68]$$

where k_z is a constant relating depth and wavelength. With the exception of the work by Jones (1953), steady-state vibration data have generally been interpreted on the basis of equations [1.66] and [1.68]. Though most researchers used k_v = 1.1, different values of k_z have been used, e.g. 0.5 (Heukelom and Foster, 1962), 1.0 (Ballard, 1964), and 0.33 (Heisey, 1981). Abbiss (1983) used a k_z of 0.5 to locate the interface between a clay subgrade and an overlying wet-mix macadam. It appears that k_z values of 0.5 and 0.3 were the common choices for tests on roads (or runways) and soil sites respectively. For most earthquake dispersion studies, a value of 0.3 is the most common choice (Nyland, 1991).

The major advantage of the steady vibration technique is its analytical simplicity because the shear-wave velocity profile is obtained directly from the field dispersion curve. It also has low initial cost and requires neither time measurement nor signal analysis. It is, however, time-consuming and impractical for investigating relatively deep-seated deposits with monochromatic signals since receiver spacings become inconveniently large. The weakness of the method also lies in its neglect of the dispersive characteristics of surface waves in the inversion process, a limitation which the Spectral Analysis of Surface Waves approach has overcome.

1.2.3.4 Spectral Analysis of Surface Waves (SASW)

The Spectral Analysis of Surface Waves (SASW) is an improvement on the steady-state vibration technique, and it employs the phenomenon of dispersion to determine the body-wave velocities of the propagation medium. It shares all the advantages of the steady vibration method but improves upon it by the deployment of a polychromatic source and a more thorough inversion scheme based on elasto-dynamic theory. Field testing is therefore much quicker, and resulting profiles are potentially more accurate. Dorman and Ewing (1962) were probably the first to employ the principles of SASW testing to determine layering and elastic parameters in a seismological context. Earlier, Jones (1953) had used surface wave dispersion principles for inversion but measured field dispersion by means of steady state vibrations. Nazarian and Stokoe (1984) used a polychromatic source and introduced the procedure to geotechnical engineering. The SASW test procedure used by Nazarian (1984) is reviewed in the following paragraphs.

In the field, a polychromatic surface wave is generated, and a dual-channel signal analyzer (see Figure 1.11) is used to compute the phase of the cross-spectrum (S_{xy}) and coherence (K_{xy}) functions from measurements at two predetermined receiver stations a distance (d) apart. A desk-top computer can be connected to the spectrum analyzer and a program, TRANSI, is used to extract field data previously stored by the analyzer. A second program, TRANSII, formats the field data for use with a mainframe or desk-top computer, the output of which is utilized by a third program, TRANS12, to calculate phase velocities and corresponding wavelengths. Finally a fourth program EXPER1 employs Heisey's (1981) recommendations to perform a statistical analysis of the data to produce a final experimental dispersion curve.

Based on Dunkin's (1965) modification of the Thomson-Haskell (1953) formulation, Nazarian (1984) calculated the dispersion curve for a stack of homogeneous, isotropic layers with assumed thicknesses, mass densities and body-wave velocities. The calculated dispersion curve, was then compared with the field dispersion curve within an interactive framework of a FORTRAN computer program called 'INVERT' (Nazarian, 1984). If both curves do not match, the user is prompted to change layer properties for repeated dispersion calculations and comparison until field and computed dispersion curves match. At this stage, the parameters of the model are assumed to be the properties of the site. The issues regarding the reliability of this latter assumption is discussed in Chapter 3.

The SASW method has a well-established theoretical basis and therefore requires neither empirical correlations nor correction factors. In developed areas, or restricted access sites, the SASW is a non-destructive test that does not require boreholes or explosives, which is preferable as chances of possible damage to existing structures are minimized. In geotechnical site exploration and foundation investigation, the primary objectives are to obtain a subsurface picture and reliable estimates of relevant soil properties to a predetermined significant depth. For structures such as underground facilities, nuclear reactor and missile sites, dams and reservoirs, tunnels, highways, airfields and large building complexes the exclusive use of boreholes may not only be slow, uneconomical and sometimes impossible but could also fail to detect isolated subsurface anomalies. Under such circumstances, the incorporation of elastic wave testing and other geophysical techniques could expedite exploration, reduce cost and provide valuable information for effectively optimizing and locating boreholes.

1.3 Geotechnical Applications of Surface Wave Measurements

Until recently, it was not uncommon to underestimate the usefulness of small-strain properties as inappropriate for the analysis of commonly occurring geotechnical foundation problems on the premise of anomaly high values. However, on-going research findings (e.g. Burland et al, 1989) continue to give increasing evidence in favour of the general applicability of small-strain parameters under both static and dynamic conditions. In his conclusion to the Ninth Bjerrum Memorial Lecture entitled "Small is Beautiful", Burland (1989) commented that :

"In the past, dynamic measurements of Young's and shear moduli have tended to give results that are so much higher than static values determined in the laboratory that the dynamic values have been discounted. However, in a number of recent cases, the accurately determined static small strain values of stiffness have been found to be very close to the values measured by dynamic methods".

The implication is that the commonly reported dichotomy between field and laboratory stiffnesses partly stemmed from the limitations and inaccuracies in strain measurement techniques in the laboratory. Two types of moduli are traditionally accepted - small-strain modulus for small deformation problems and large-strain modulus for relatively larger deformation problems. The ratio of small- to large-strain moduli may be anywhere between 1 and 10. It is now well-accepted that the two moduli are the slopes at small and large strains of the same generic modulus-strain curve shown in Figure 1.12. This figure shows the variation of normalized secant shear modulus with shear strain and indicates that the shear modulus is initially strain-independent up to a strain of approximately 10^{-4} % after which it decreases non-linearly with increasing shear strain. This phenomenon is explained by the observation that at small strains, the mechanism controlling the stress-strain response of soils depends predominantly on the stress-deformation behaviour of the particle contacts and not on the relative particle slippage associated with large deformations. Thus soils are commonly stiffer at small strains than at relatively larger strains. Hence both small and large strain moduli are required for modelling behaviour at intermediate strains.

A complete definition of the variation of material moduli with strain is of utmost importance in historical matching. In this approach, input model parameters are adjusted until analytical results are in reasonable agreement with corresponding measured values. Matching cannot be validated if the input parameters are unbounded since a criterion must be established for rejecting the theoretical model rather than the magnitudes of input parameters. Wave propagation methods thus provide the upper boundary magnitudes for deformation moduli.

In nonlinear material modelling, the initial tangent deformation moduli and Poisson's ratio are important elastic parameters for assessing and predicting material behaviour at other stress levels. The use of in-situ body wave velocities in computing these elastic parameters yield the appropriate values at strains often too small to be measured in conventional triaxial tests without significant error.

Geophysicists have long employed the velocity and other features of elastic wave propagation in measuring physical properties, locating sudden subsurface contrasts and identifying broad geological trends. Geotechnical engineers, on the other hand, only used elastic wave velocities for general reconnaissance purposes. This is changing and small-strain deformation moduli, Poisson's ratio, damping factor, cyclic stability parameters (shearing stress ratio, deformation, pore pressure) and shear strength have been listed by Woods (1978) as potentially capable of measurement by wave propagation methods.

If the in-situ shear and compression wave velocities are measured, then the low-strain linear elastic behaviour is completely determined by invoking elasticity relations to compute Poisson's ratio, bulk, shear and Young's moduli. These parameters may be used directly in the design of foundation structures subjected to dynamic loads such as earthquakes, wind, wave action, nuclear explosions, construction and machine vibration. The justification is that most dynamic loads and stress waves induce strains in the low end of a spectrum ranging from 10^{-4} % for the foundations of electron microscopes to 10^{-1} % for strong motion earthquakes and nuclear explosions (Hoardley,1985). The analytical techniques for the assessment of ground response in such cases therefore require low-strain deformation properties.

In-situ damping, which is also measurable from in-situ wave methods (as shown in Figure 1.13), is generally used in assessing the effect of vibration machinery and construction activity on the serviceability limit states of adjacent structures, the safe operation of certain sensitive instruments and the comfort of people in the vicinity. In evaluation studies and impact assessments, vibration effects can be predicted from damping measurements and the necessary precautions taken. Woods and Jedele (1985) presented a classification of earth materials based on damping coefficients.

In recent years, the in-situ shear wave velocity of a soil deposit has proved to be a key index of susceptibility to liquefaction (Stokoe et al, 1987). As shown in Figure 1.14, it may be concluded that for a given intensity and duration of ground shaking, sites with an average shear wave velocity of at least 150 m/s experienced insignificant or no damage during earthquakes in the Imperial Valley. Seed et al (1976) also classified earth materials on the basis of in-situ shear wave velocity for seismic microzonation and liquefiability assessment purposes.

One practical application of the characteristics of elastic wave propagation is the non-intrusive evaluation of ground improvement or softening processes. Elastic wave velocities, being key indices of engineering behaviour, have been in use for evaluating artificial improvement processes. Jones (1958) used the phase velocity of Rayleigh and Love waves to evaluate the effect of rolling on a predominantly sandy site. The results obtained by Jones (1958) are shown in Figure 1.15 and indicates that compaction produced large increases in phase velocity at short wavelengths but had relatively little impact at long wavelengths. For the assessment of reinstatement backfills, Winter and Selby (1990) concluded that surface wave propagation velocity was a much more sensitive measure of the degree of compaction than either dry density or CBR measurements which are also more time-consuming. Due to the non-intrusive nature of the test, no sources of weakness are introduced in the test structure. Further void ratio increases in lower layers resulting from the placement and compaction of overlying lifts are also measured by surface wave methods.

Stokoe et al (1987) used the Spectral Analysis of Surface Waves method to evaluate ground improvement by dynamic compaction. The process involves the systematic drops of heavy steel or concrete blocks onto the ground surface. The resulting impact densifies the soil. The dispersion curves before and after the dynamic compaction (Figure 1.16) shows the resulting improvement.

Jones (1953) showed that seasonal ground softening due to percolating rainfall and runoff could be measured by changes in surface wave velocities. Figure 1.17 shows that the surface wave dispersion curve was altered between January 1956 and March 1956 as the soil got wetter but velocities increased subsequently in April of that year with drying. Such non-destructive monitoring of ground softening could be useful as indicators of inadequate drainage or as a basis for preventive maintenance. The in-situ shear or compression wave velocities of rocks and stiff soils are also indicators of the type of excavation technique to be adopted and provide a basis for ripping or blasting. Whenever ripping is preferable, the correlations of compression and shear wave velocities with ripping tractor size (Caterpillar Tractor Co., 1966) facilitate estimation of excavation costs and plant allocation.

Heukelom and Klomp (1962) applied the same principles to follow the softening of a road base due to infiltration and its improvement resulting from draining. The results are shown in Figure 1.18. Curve I represents the dispersion curve just after the placement of the base. Before the wearing course was placed, however, the base was softened by runoff from intensive precipitation. Curve II shows the dispersion curve for the roadbase in the softened state. The placement of the wearing course was preceded by draining, after which the dispersion curve was determined. This is Curve III. These results show clear changes in the dispersion curves and hence that deterioration of roadbases may be determined by the measurement of wave propagation velocities.

Variations in properties of the layers of a soil structure resulting from compaction, softening due to moisture, freezing, thawing and cracking can therefore be followed. For remedial evaluation purposes therefore, wave propagation methods seem technically more appropriate for isolating weaker layers for improvement rather than the entire section.

Stratification delineation has been used to determine the extent and thicknesses of frozen and thawed ground in permafrost regions (Olson and Wright, 1991), the depth of seasonal variation (Addo and Robertson, 1991) and layer thicknesses of soil (Stokoe and Nazarian, 1984), airfields (Heukelom and Klomp, 1962) and roadways (Jones, 1962). Jones (1962) used a simplified analysis to compute the thickness and elastic properties of a concrete pavement on a well-compacted road base. A calculated thickness of 9.5 inches compared favourably with two measured core thicknesses of 9.55 and 9.85 inches. Heisey (1982) used the SASW technique to measure the thicknesses of the elements in a road structure. Figure 1.19 shows the results obtained by Heisey (1982). The capability to determine the stiffness and thickness of each layer in a roadway section is an advantage over methods which only yield an average modulus of the entire section and no thicknesses. In-situ wave measurements on roads and runways can serve to check any differences between design and as-built specifications of all layers after and during construction without introducing any sources of weakness.

Surface wave propagation methods have a potential for determining the relative magnitudes of in-situ stresses since the dispersion function is directly based on the existing stresses within the medium. Husson et al (1983) used experimentally measured Rayleigh wave velocities on the outside and inside surfaces of a pipe to compute stress profiles within the pipe material. The authors found that the results agreed well with both theoretical and experimental results published by others. A similar approach could be applied to soil in-situ.

Current trends indicate that in-situ surface wave testing, if appropriate, is preferable because of its circumvention of sampling effects (e.g. disturbance and size) and virtually unrelieved in-situ stress state. An in-situ test independent of testing equipment, it has the added advantage of preference in uneconomical-to-reproduce environments and difficult-to-sample soils and rocks.

1.4 Objectives and Outline of Research

Prior to the commencement of this research in 1988, the major components of existing surface wave instrumentation were a spectrum analyzer and a computer. The analyzer was expensive and its operation required specially trained personnel. This research primarily focused on the development of a solely microcomputerized system (without the analyzer) for collecting and analyzing Rayleigh and Love wave dispersion data and to determine in-situ shear wave velocity profiles. Such a centralization of the test enhances portability, economy, speed and produces results in the field for preliminary evaluation. It was also hoped that more surface wave testing would be performed since no new major equipment would be required.

The objectives of this research are

1. To eliminate the need for a spectrum analyzer and thereby introduce flexibility and significantly reduce the initial cost for an operational SASW testing system.
2 To microcomputerize the entire SASW field procedure for shorter post-processing times and enable on-site determination of the experimental dispersion-curve.
3. To investigate existing methods for computing theoretical Rayleigh wave dispersion curves and implement a fast scheme in a computer program for that purpose.
4. To automate the dispersion curve matching process and thus minimize the requirement for personnel with significant experience in dispersion computation.
5. To examine the possibility of incorporating Love waves into the SASW procedure

In the this chapter, the types, characteristics and some engineering applications of elastic body and surface waves were discussed. A summary and review of past and present work in both the geophysical and engineering literature have also been presented. The objectives of this research have also been outlined. The rest of this thesis is organized in the following manner:

Chapter 2 describes the implementation of the exclusive use of microcomputers for data acquisition and processing instead of the currently used expensive spectrum analyzers for acquisition and partial processing. The chapter also includes elementary information on the spectral analysis functions used in this work and concludes with a description of the computer program for data acquisition and processing.

Chapter 3 contains a review of the general theory of surface wave dispersion and a description of an automated computer program for dispersion computation for forward modelling.

Chapter 4 outlines the instrumentation, experimental set-up, field procedure as well as site selection and description. Field results and available site information from other independent tests are also presented.

Chapter 5 discusses the experimental results and the theoretical analyses of the field work described in Chapter 4.

Chapter 6 presents the conclusions and recommendations for further research and development.

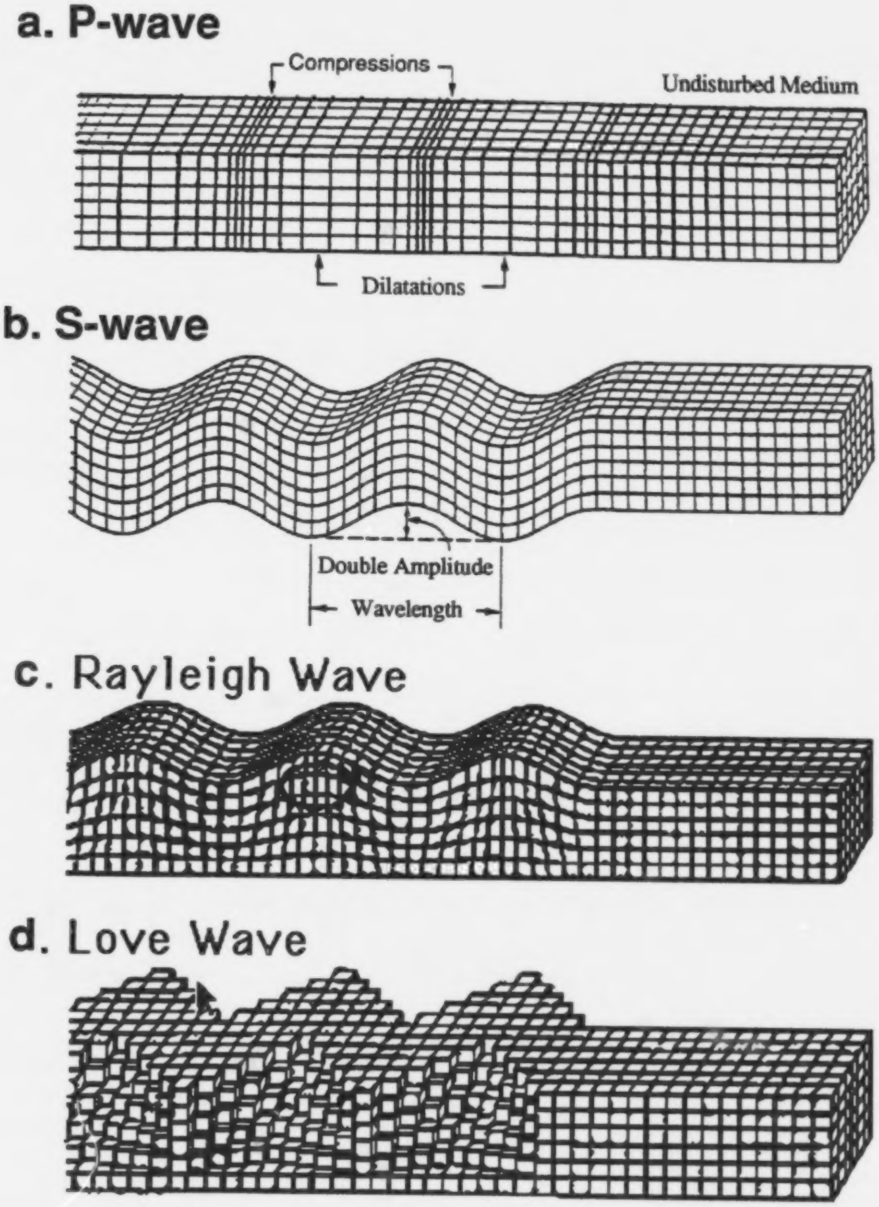
a. P-wave
Compressions
Undisturbed Medium
Dilatations
b. S-wave
Double Amplitude
Wavelength
c. Rayleigh Wave
d. Love Wave

Figure 1.1 Elastic Wave Motion (After Bolt, 1976)

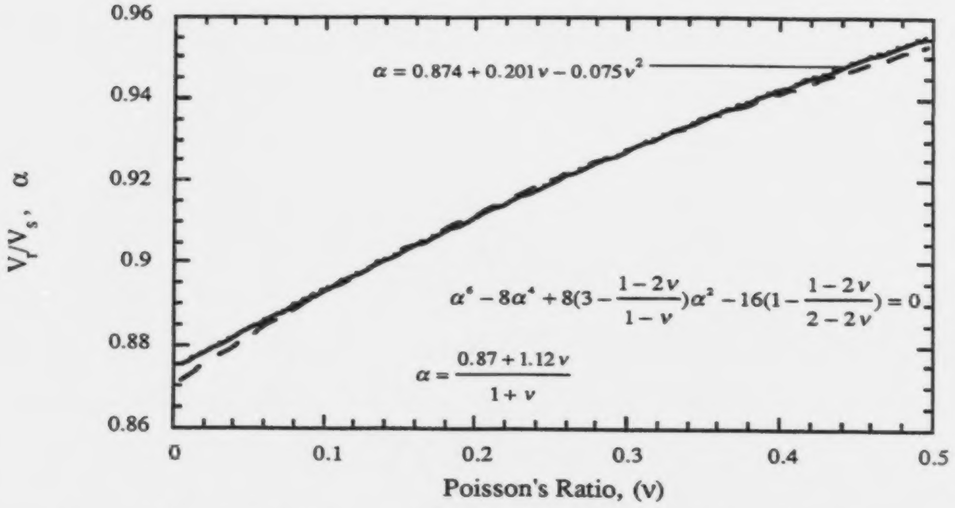

Figure 1.2 Dependence of Rayleigh Wave Velocity 0n Poisson's Ratio.

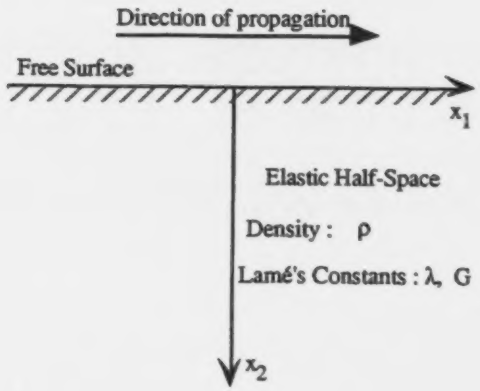
Direction of propagation
Free Surface
x_1
Elastic Half-Space
Density : ρ
Lamé's Constants : λ, G
x_2

Figure 1.3. Idealized Model for Deriving Rayleigh Wave Equation

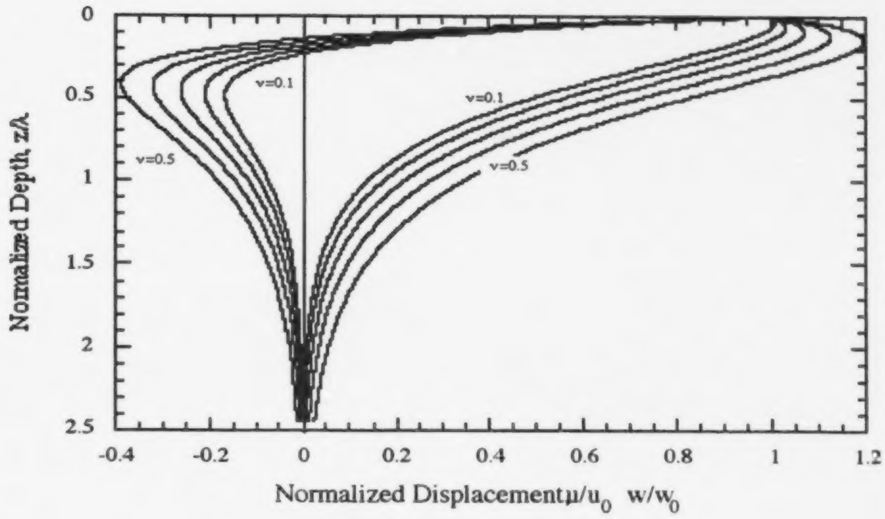

(a)

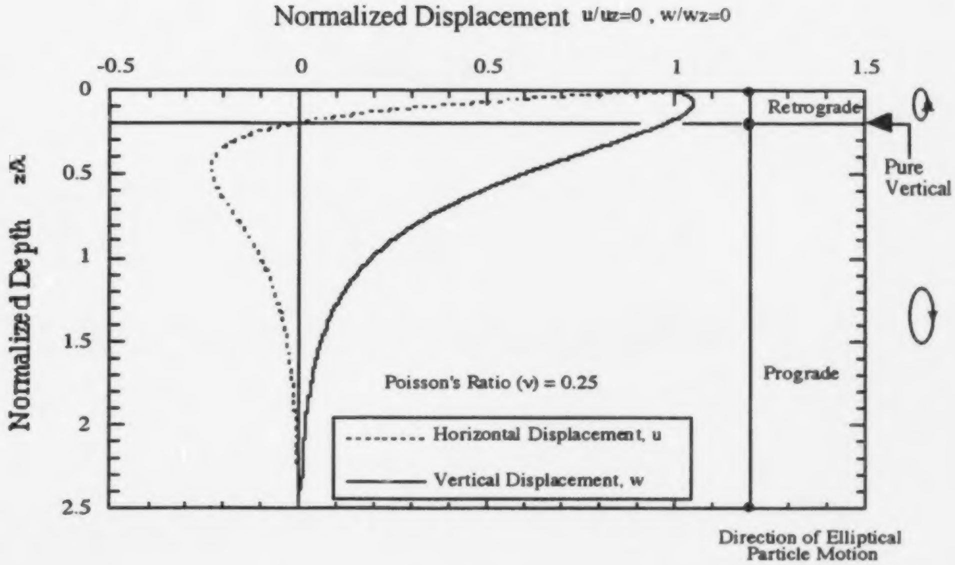

(b)

Figure 1.4 Particle Displacements in a Rayleigh Wavefield

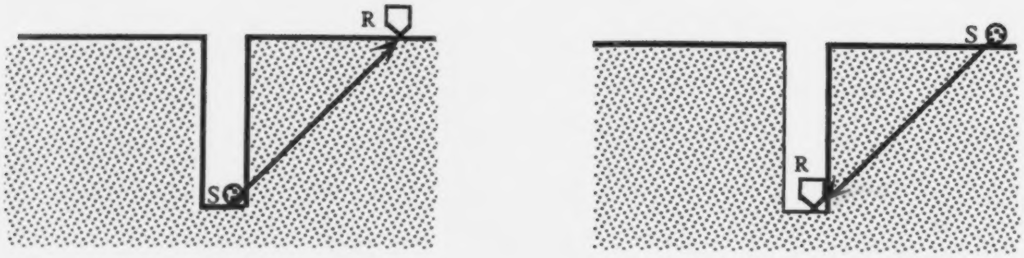

a. Up-Hole

b. Down-Hole

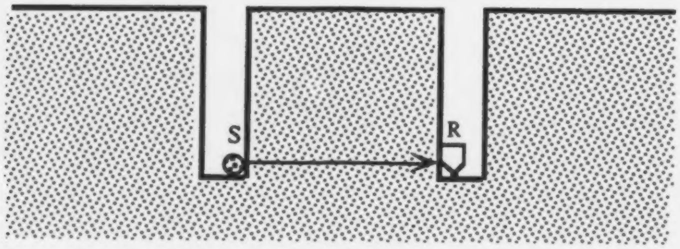

c. Cross-Hole

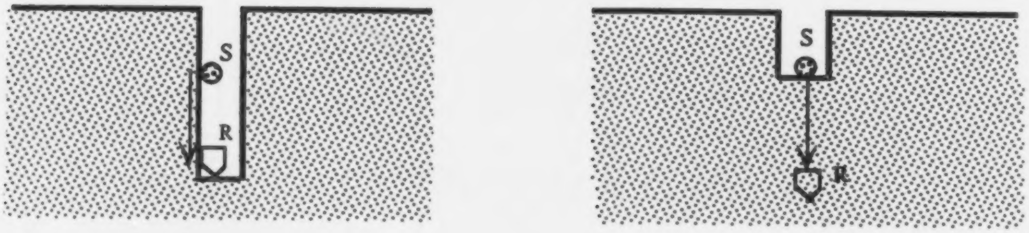

d. In-Hole

e. Bottom-Hole

Figure 1.5 Schematic representation of intrusive in-situ wave propagation methods. (Modified after Hoar, 1982)

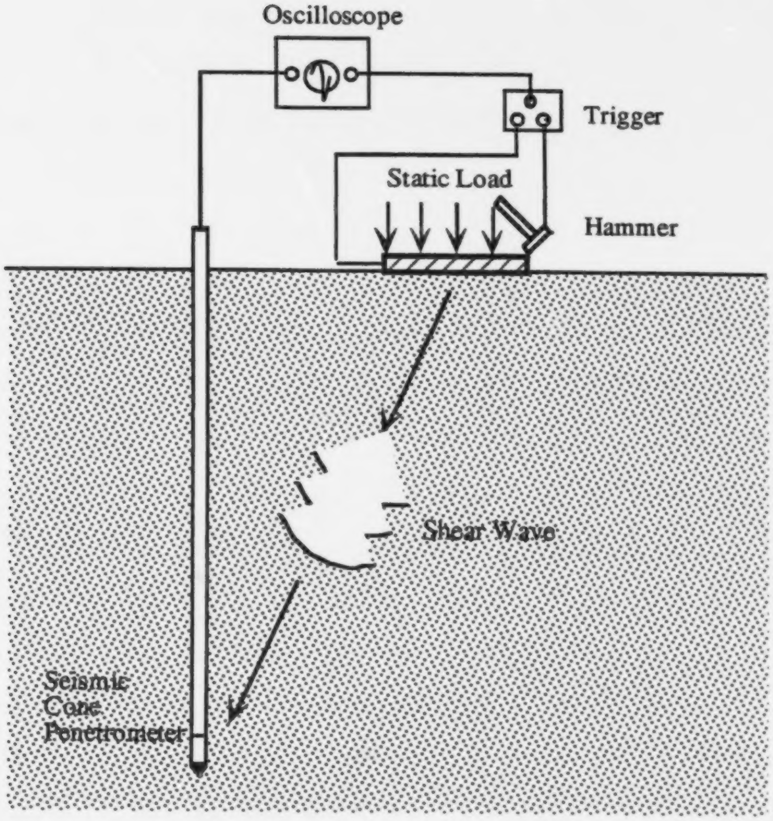
Oscilloscope
Trigger
Static Load
Hammer
Shear Wave
Seismic Cone Penetrometer

Figure1.6 Schematic Layout of Downhole Seismic Cone Penetration Test (After Robertson et al, 1986)

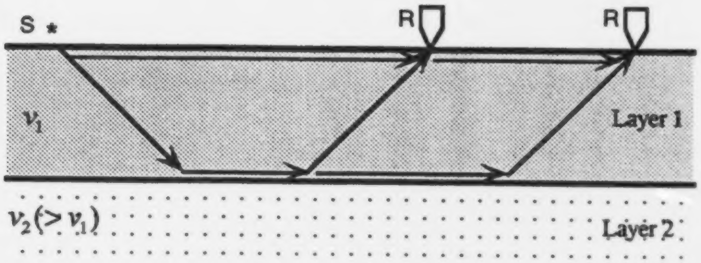
S
R
R
v_1
Layer 1
$v_2(> v_1)$
Layer 2

Figure 1.7 Seismic Refraction Method

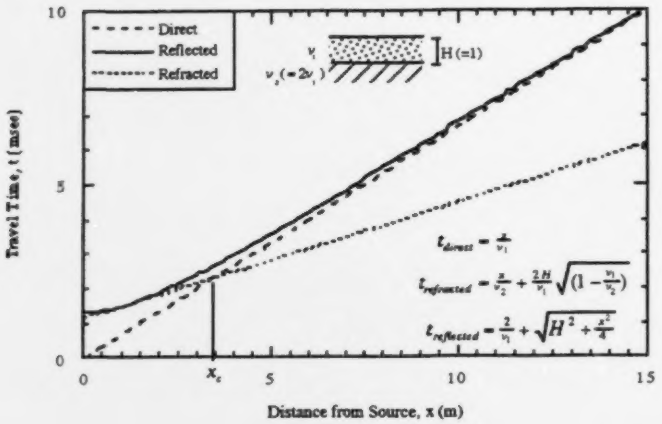

Figure 1.8 Traveltime Curves for Direct, Reflected and Refracted Waves -

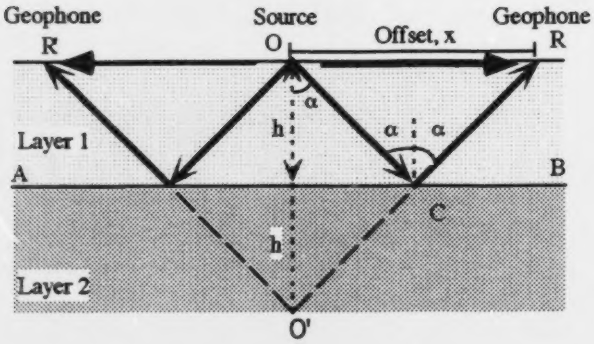
Geophone
R'
Source
O
Offset, x
Geophone
R
α
h
α
α
Layer 1
A
B
C
h
Layer 2
O'

Figure 1.9 Principles of the Seismic Reflection Method

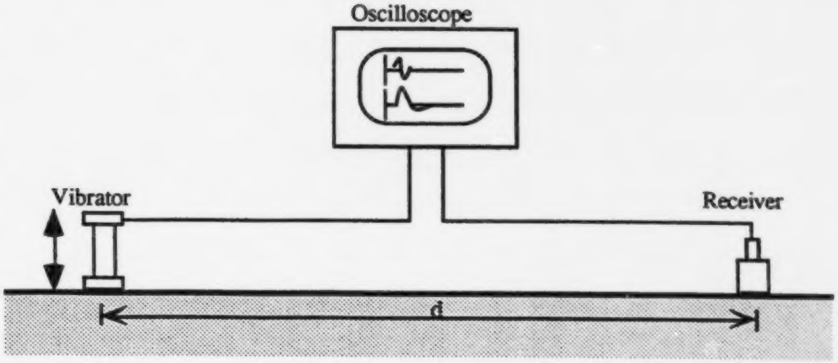
Oscilloscope
Vibrator
Receiver
d

Figure 1.10 Steady-State Vibration Method

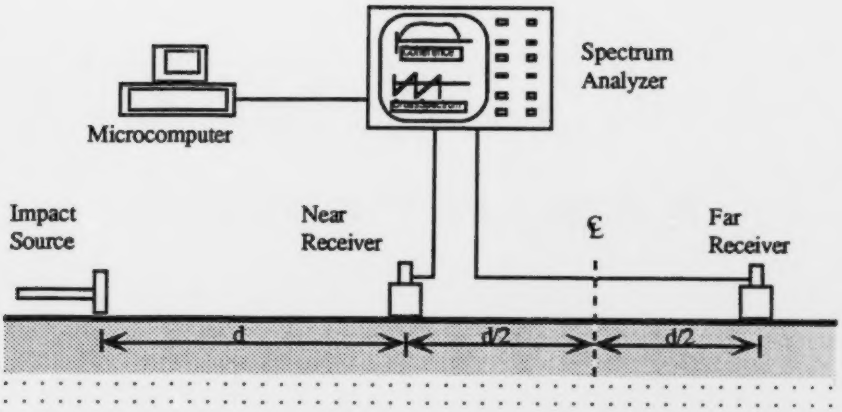
Spectrum
Analyzer
Microcomputer
Impact
Source
Near
Receiver
℄
Far
Receiver
d
d/2
d/2

Figure 1.11 The University of Texas SASW System

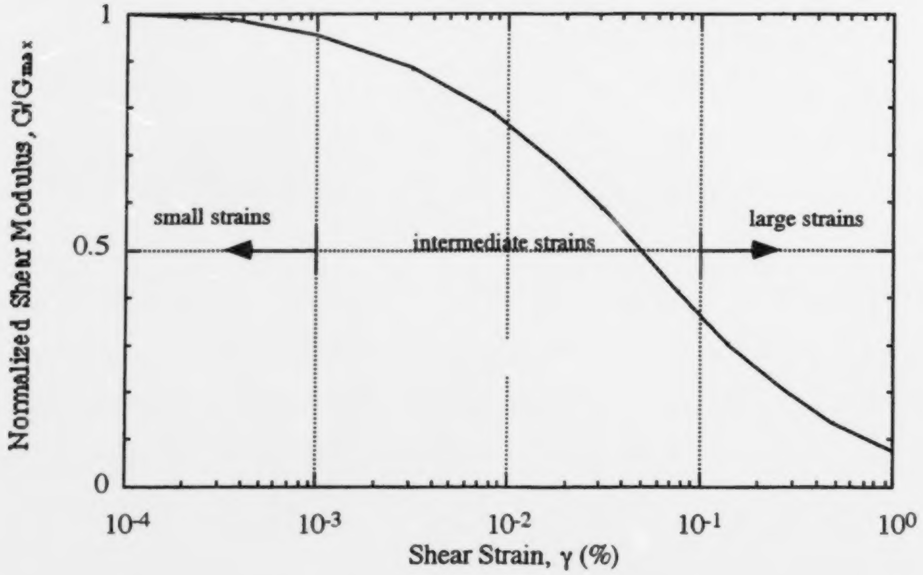

Figure 1.12 Variation of normalized shear modulus with shear strain

(Modified After Seed and Idriss, 1976)

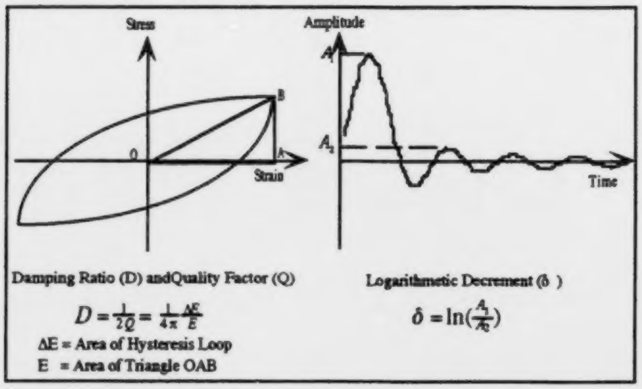
Stress
Amplitude
B
0
A
Strain
A1
A2
Time
Damping Ratio (D) andQuality Factor (Q)
D = 1/2Q = 1/4π ΔE/E
ΔE = Area of Hysteresis Loop
E = Area of Triangle OAB
Logarithmetic Decrement (δ)
δ = ln(A1/A2)

Figure 1.13 Measurement of Damping from Wave Propagation Tests

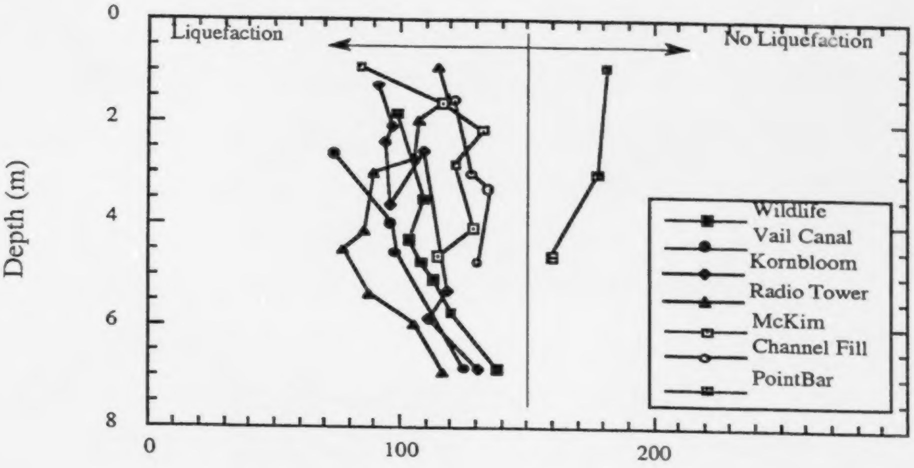

Figure 1.14 Shear wave velocity profiles of sites with previous exposure to liquefaction (Redrawn after Stokoe et al, 1987).

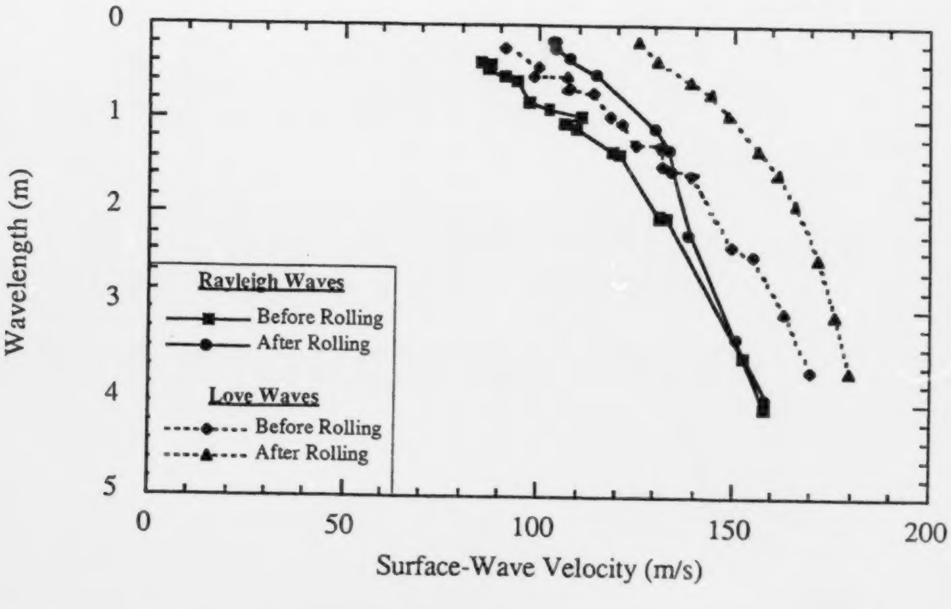

Figure 1.15. Effect of Rolling on Rayleigh and Love Wave Dispersion Curves. (After Jones, 1955)

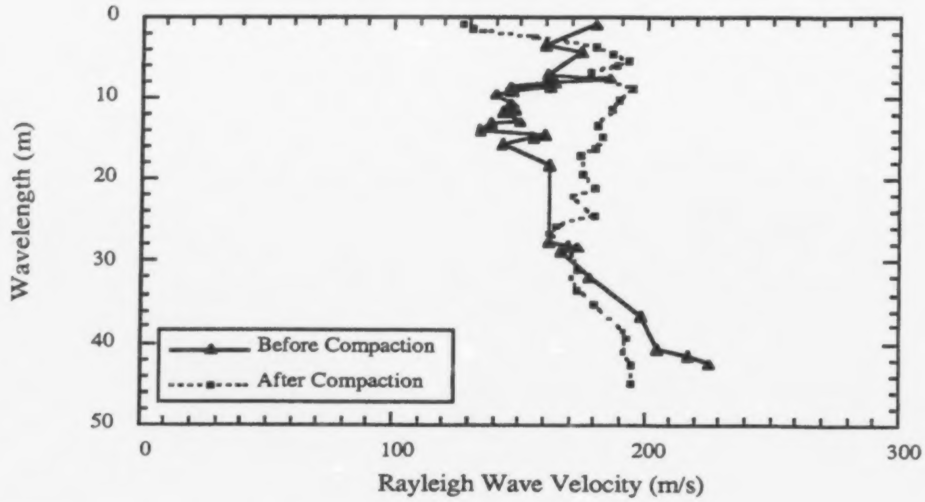

Figure 1.16 Effect of Dynamic Compaction on Rayleigh Wave Dispersion

(After Stokoe et al, 1987)

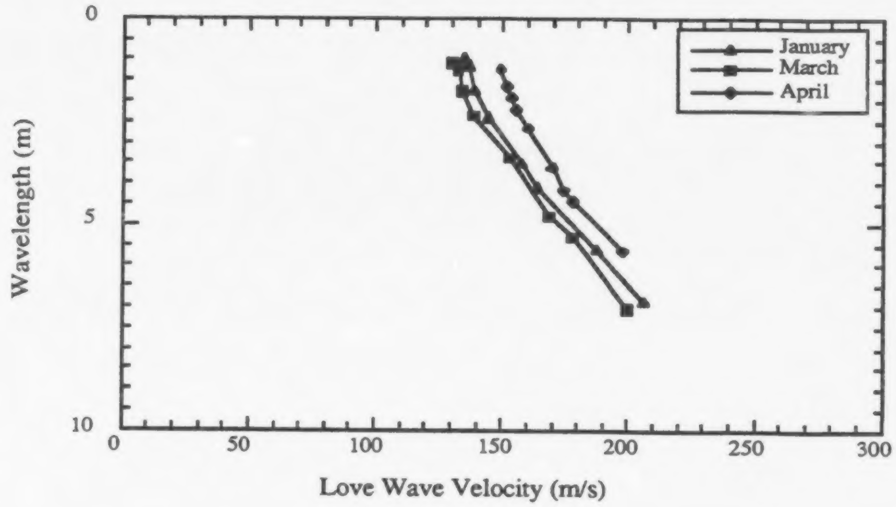

Figure 1.17 Effect of softening on Love wave dispersion
(Modified After Jones, 1953)

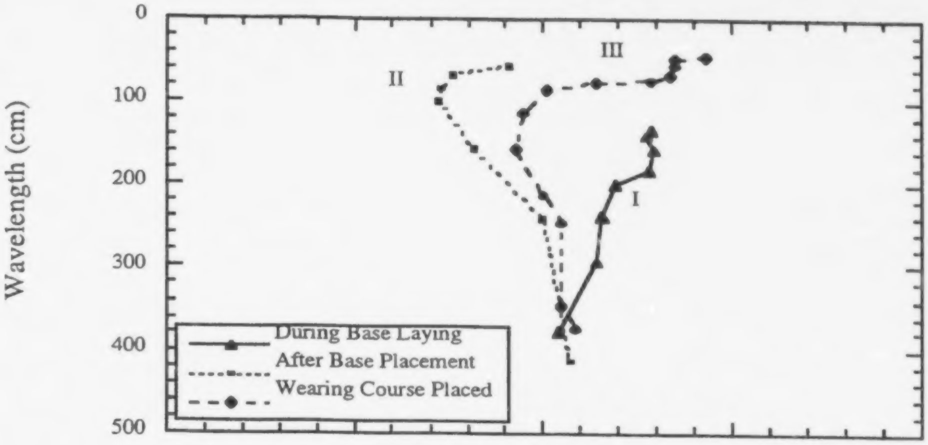

Figure 1.18 Following the effects of base softening by water (II) and gradual recovery by draining (III) on Rayleigh wave dispersion (After Heukelom and Klomp, 1962).

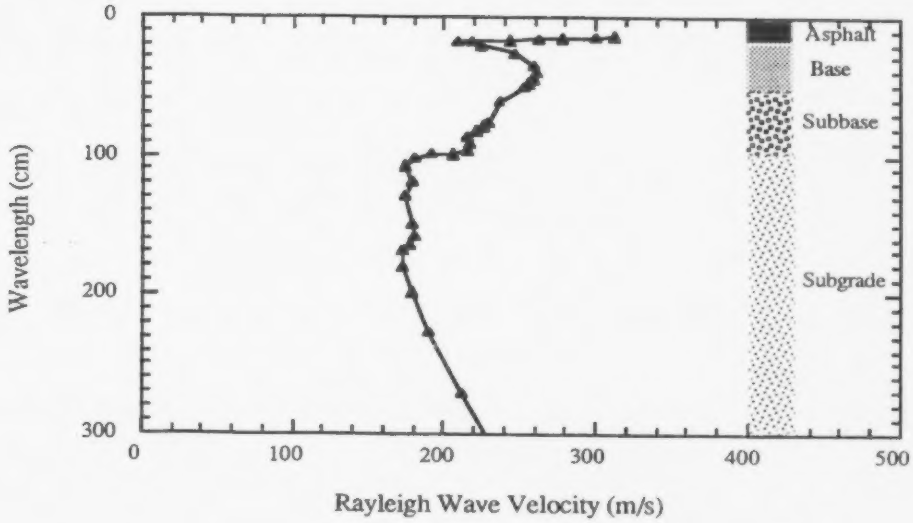

Figure 1.19 Stratification of a Pavement Structure by Surface Waves (After Heisey et al, 1982).

CHAPTER 2

SIGNAL ACQUISITION AND ANALYSIS

2.0 Introduction

In this chapter, the theory underlying *SASW-DA* (Spectral Analysis of Surface Waves -Data Acquisition) a computer program written by this author for determining the in-situ dispersion curve is presented. The sequence of operations in the program are signal acquisition, frequency domain transformation and spectral analysis, and are discussed in that order.

In current SASW data acquisition systems, a spectrum analyzer implements the necessary precautions for proper signal acquisition in hardware. To implement similar precautions in software demands the understanding of the relevant principles so as to avoid any pitfalls and appreciate any limitations. The proposed scheme (Figure 2.1) eliminates the need for a spectrum analyzer and uses a microcomputer for the entire field procedure. The advantages of such a microcomputerized system, compared with available alternative instrumentation systems, are very attractive and are discussed at the end of the chapter.

2.1. Signal Acquisition

Signal acquisition involves procedures that ensure that a measured signal is a true representation of the original analogue signal and that no information is lost in the measurement process. The general procedure for acquiring an analogue signal involves detection with receivers, analogue filtering with known minimal phase shift and adequate sampling to eliminate aliasing as well as sufficient amplification to ensure that the signal magnitudes are measurable with a satisfactory degree of accuracy. The details of these procedures are discussed in this section.

2.1.1 Sampling Rate

If an analogue signal is sampled at an evenly spaced time interval Δt, then the sampling rate (or frequency) f_s is defined as the reciprocal of this constant time interval i.e.

$$f_s = \frac{1}{\Delta t} \qquad [2.0]$$

If the time interval is measured in seconds, then the sampling rate is the number of samples acquired per second and is probably the most important parameter in the design of the sampling process. As discussed below, an underestimated sampling rate would lead to errors that could invalidate the digitized signal.

Associated with every sampling interval, Δt , is a parameter called the Nyquist frequency f_N defined as

$$f_N = \frac{1}{2\Delta t} = \frac{f_s}{2} \qquad [2.1]$$

The Nyquist frequency has two important repercussions in signal acquisition theory. The first is a consequence of Shannon's Sampling Theorem which states that, if a continuous input signal $x(t)$, sampled at a time interval Δt, did not contain any frequencies less than the Nyquist frequency, then the acquired signal is a true representation of the original signal. If the frequency spectrum of $x(t)$ is $X(f)$, then this condition may be expressed mathematically as

$$X(f) = 0 \quad \text{for all} \quad |f| > f_N \qquad [2.2]$$

Essentially, the sampling theorem implies that the total information content of a signal is obtained by sampling at a minimum frequency equal to twice the maximum frequency contained in the signal i.e.

$$f_{s_{\min}} \geq 2 f_{\max} = \frac{1}{\Delta t} \qquad [2.3]$$

where

$f_{s_{\min}}$ = sampling frequency (Hz),

$f_{\max}$ = highest frequency content in the input signal (Hz)

Δt = maximum sampling interval (sec)

This requirement for the proper sampling of a continuous signal is called the Nyquist criterion. It essentially stipulates the minimum sampling rate requirement for complete recovery of a waveform without any loss of information and implies that finer sampling does not necessarily result in more accurate signal representations.

The second repercussion is related to sampling a continuous signal with unknown frequency content or that is not band-width limited to less than the Nyquist frequency. In such an instance, all frequencies higher than the Nyquist criterion are not correctly represented in the acquired signal but spuriously parade in the acquired signal as frequencies lower than the Nyquist. Any frequency f for which $f > f_N$ appear in the acquired signal as a frequency of magnitude f_{alias} given by

$$f_{alias} = f - f_N \qquad [2.4]$$

This phenomenon corrupts signals and is called aliasing because some frequencies take on magnitudes other than their own by overfolding at the Nyquist frequency (also called the folding frequency as a result). Figure 2.2 shows an instance when aliasing may occur if the necessary precautionary measures are not taken before sampling. A mathematical explanation for aliasing is that for every sinusoid $x_1(t)$ given by

$$x_1(t) = \cos[\pi(n+\varepsilon)t + \phi] \qquad [2.5]$$

there is another sinusoid $x_2(t)$ given by

$$x_2(t) = \cos[\pi(n-\varepsilon)t + \phi] \qquad [2.6]$$

which has the same sample values at some equally spaced sample points such as shown in Figure 2.2. The equality of the sample values follow from the following trigonometric identity

$$\cos[\pi(n+\varepsilon)t + \phi] - \cos[\pi(n-\varepsilon)t + \phi] = -2\sin(n\pi t)\sin(n\varepsilon t + \phi) = 0 \qquad [2.7]$$

where n and t are integers

Once a continuous signal is discretely sampled without analogue tape recording, there is nothing that can be done to undo the effects of aliasing. A way to find out if aliasing has occurred is to examine the Fourier transform of the digitized signal. If the transform approaches zero at either end of the spectrum, then aliasing was unlikely to have occurred. If the transform approaches any other value, then aliasing cannot be ruled out. The basis of this criterion is the observation that the transform of an adequately sampled signal is zero outside a range of $2f_N$ centered on DC.

Aliasing is a direct consequence of inadequate discrete sampling at evenly-spaced intervals and is avoidable by sampling at unequal intervals. The problem with unequal-interval sampling is that it complicates data acquisition and transformation into the frequency domain. For simplicity and convenience, it is better to sample at equal intervals and ensure that Nyquist criterion is met. In the SASW test, however, the frequency content of impact signals is not known *apriori*. The maximum frequency is thus unknown and hence the Nyquist criterion cannot be readily applied. A two-step procedure implemented to eliminate aliasing in program SASW-DA is:

1. A maximum frequency is imposed on the input signal before sampling by analogue filtering with known minimal phase shift.
2. A minimum sampling rate greater than twice the imposed maximum input frequency is used to sample the continuous signal.

The procedure for estimating the maximum test frequency at a site is given below:

1. Estimate the shear modulus (G) and mass density (ρ) of the surface layer.
2. Calculate the corresponding shear wave velocity, v_s ($v_s = \sqrt{\frac{G}{\rho}}$)
3. Estimate the Rayleigh wave velocity, v_R $(= \frac{v_s}{1.1})$.
4. Estimate depth to center of surface layer, z.
5. Estimate wavelength required to sample surface layer, L $(= \frac{z}{2})$.
6. Estimate required maximum frequency, f $(= \frac{v_R}{L})$.

Maximum frequencies of 600 - 1200 Hz and up to about 40 kHz are adequate for most soils and pavements respectively. In both cases, the stiffness and thickness of the surface layer determine the minimum sampling frequency.

2.1.2 Number of Samples

The number of samples to be acquired in a time record depends on the nature and duration of the signal as well as the intended method of analysis. In the SASW test, the signals may originate from a vibrator, random noise, hammer impact or "chirp" source. If the signal is periodic, then sufficient samples should be acquired to clearly establish its shape and other characteristics. In the case of transient signals, samples should be taken throughout the entire duration of the signal or appropriate windowing techniques must be applied to the acquired data.

The fast Fourier transform is readily implemented if the number of acquired samples is a power of 2. If the number of samples (N) is not a power of 2 after fulfilling the above and Nyquist criteria, the sampled data should be padded with zeros up to the nearest power of two i.e.

$$N = 2^k \qquad [2.8]$$

where k is a positive integer.

The number of samples may also be limited by other factors such as the speed of discretization of the signals if the analogue-to-digital converter in use is not fast enough to acquire the required samples in a limited time.

2.1.3 Filtering

Filtering is the process of removing certain unwanted frequencies in a given range from a polychromatic signal. This may be achieved in either analogue or digital mode. Analogue filtering is achieved by passing the signal through a hard-wired circuit specially designed to attenuate the specified frequency bandwidth(s) before sampling. Such a circuit is frequently used for anti-aliasing purposes. Digital filtering is achieved by multiplying the signal with a given transfer function.

Four main types of filter exist, namely low-pass, high pass, band-pass and band stop, with the names reflecting their functions. The characteristics of all four types are shown in Figure 2.3, which shows the variation of the ratio of the output to input amplitudes with frequency for ideal and real filters. A band-pass filter is essentially a low- and a high-pass filter with the appropriate frequencies connected in series whereas in the band stop, the same filters are connected in parallel. An ideal filter is one in which the signal is not attenuated at all in the pass-band but is completely attenuated everywhere in the stop band and whose phase shift within the pass-band varies linearly with frequency. Real filters do not completely and abruptly attenuate signals in the stop band and may have a nonlinear phase shift variation with frequency. The frequency at which the amplitude has been attenuated by 3dB compared with the input amplitude is called the corner frequency. In other words, if the amplitude of the input is A_1, then the corner frequency (also called the -3dB point) is the frequency at which the amplitude is A_2 such that

$$3 = \begin{cases} 20\log_{10}\left(\dfrac{A_1}{A_2}\right) & \text{for mean square amplitudes} \\ 10\log_{10}\left(\dfrac{A_1}{A_2}\right) & \text{for root mean square amplitudes} \end{cases} \qquad [2.9]$$

In the simplest case, an active filter has a capacitor for each cut off frequency it is designed for. Thus low- and high-pass filters have a single capacitor each whereas bandpass and bandstop filters have two each. Such a filter is called a first-order filter. The order of a filter is the number of capacitors per cut-off frequency. In general, the higher the filter order, the closer the characteristics approach the ideal case i.e. the slope of the response curve in the stop band become steeper. An estimate of the roll-off (in dB/octave) of a simple filter is approximately six times the filter order (Turner, 1988). Filters of increasing order approach the ideal in different ways. The class of a filter defines the way in which its characteristics approach the ideal. Examples of filter classes are Butterworth, Chebyshev, Cauer and Bessel. The characteristics of all four filters are shown in Figures 2.4 to 2.7.

The response of Butterworth filters is characterized by a smooth variation with frequency (which is its main advantage) and attenuates at a rate proportional to the cut-off frequency outside the pass band. The disadvantage of Butterworth filters is the slow roll-off between the pass and stop bands. In the pass band, Chebyshev filters reduces peak error as it accounts for the maximum difference between ideal and desired responses. The advantages of Chebyshev filters over Butterworth filters are its more abrupt transition between the pass and stop bands for filters of low order, a smaller absolute error and higher execution speed. Its disadvantage is probably the equi-ripple response in the pass band. Elliptic (or Cauer) filters minimize peak error by distributing it over the pass and stop bands. The magnitude response of elliptic filters is characterized by equi-ripples at all frequencies. For the same order filter, the elliptic has the steepest roll-off at the cut-off frequency and are therefore popular if a low order filter is required. Bessel filters have a maximally flat response in both magnitude and phase. As such, they are generally used in cases where phase magnitudes are crucial and must be reserved. In addition, phase response in the pass-band is approximately linear, a key advantage of this class of filters. Like the Butterworth filter, a high-order is required to substantially minimize errors.

From the foregoing discussion, a low-pass Bessel filter, properly designed to minimize and linearize phase shifts appears to be the best choice for SASW data analysis.

2.1.4 Averaging

Averaging (or stacking in geophysics) is the process of determining the mean of a number of repeatable records in an ensemble. The technique is simple in that a repetitive signal is acquired a desired number of times and each acquisition is added to the sum of all previous acquisitions. The average is then calculated as a simple mean i.e. the sum is divided by the number of records. Ambient noise is generally random in nature and therefore tend to have zero mean. Hence averaging tends to minimize the contribution of background or white noise but strengthens the actual signals due to the repetitive nature of the latter. This signal enhancement is illustrated in Figure 2.8.

For a true zero-mean noise, *signal enhancement* or the improvement in signal-to-noise ratio for a number of averages is proportional to the square root of the number of averages. Thus the ambient noise minimization initially improves with the number of records in the ensemble but becomes insignificant as the number of records gets large. In exploration geophysics, it is not uncommon to average as high as 128 records in a single ensemble. In general, if the number of signals averaged is n_A then the signal improvement is approximately equal to $3\log_2 n_A$ dB, given that the buried noise is a true zero-mean noise. Based on the findings of Heisey (1981), Nazarian (1984) recommended five signals for SASW averaging. It should be borne in mind that the number of times a signal is averaged depends on how noisy it is (which in turn depends on the test environment), the time available for testing and the computing speed and memory available. Ramirez (1985) recommends that a repetitive signal must be averaged at least 32 times so as to reduce low-level noise and minimize noise due to time jitter. In general, preliminary testing at a site should be done to determine the noisiness of signals and hence the number of signals to average for the desired improvement.

Averaging may be performed in either the time or frequency domain. Randall (1967) noted that averaging in the frequency domain results in a reduction of quantization noise and an increase in the dynamic range of the data.

2.1.5 Windowing

The fast Fourier transform or FFT (described in the next section) is a tool for transforming data in the time domain into the frequency domain. The Fourier integral, on which the FFT is based, assumes implicitly that a sampled time record is repeated at every window length throughout time. Hence if the data to be transformed does not constitute a repeatable record (e.g. an integer number of periods), the record to be transformed will not bear any resemblance to the original analogue record from which the sample was obtained. If such a record is transformed in the frequency domain, energy will be smeared throughout the frequency domain. This smearing phenomenon is called leakage and is a direct consequence of the finite time record of acquired samples since no leakage occurs if an infinite theoretical record is transformed. Windowing is the process of multiplying a time domain record by certain functions before transformation into the frequency domain for the purposes of minimizing power leakage into adjacent frequencies.

To avoid leakage, the time record to be transformed must be repeatable else the record should be multiplied by an appropriate window to reduce the effects of leakage. Windows available for this purpose include the exponential, Hanning and Hamming types. If an impact signal is acquired in such a way that the first and last amplitudes in each record is zero, then windowing is not required. If steady vibrations are used for SASW testing, effort must be made to acquire at least a full period of samples or the acquired data should be appropriately windowed.

2.2 Signal Analysis

Signal analysis involves the mathematical calculations required to calculate the desired attributes of a waveform and may be performed in the time or frequency domain. A decision must be made under given circumstances regarding the better domain for analysis. Given that mathematical and computational skills and facilities are available, there appears to be a general preference for frequency domain analysis because of one or more of the following:

1. Many systems only respond to a limited frequency band in which they have strong resonances and hence experimental studies can be restricted to this range.

2. The complexity of certain computations reduces when performed in the frequency domain (e.g. convolution degenerates to multiplication).

3. Frequency analysis clarifies signal amplitudes by dissociating them into amplitudes and phases, because the noisiness of a signal is often contained in its phase spectrum.

4. An input at a specific frequency gives output only at the same frequency and hence frequency analysis offers a way of treating individual frequencies without regard to events at other frequencies.

5. The frequency content of a signal often reveals diagnostic information about the source and probable cause of the signal (e.g. mechanical signature analysis)

It must be borne in mind, however, that results from time and frequency analyses are different representations of the same answer and show detail in different respects. In SASW testing, the two main functions required are the phase lag and the coherence of each frequency component in an impact signal measured at two stations collinear with the impact source. Since an impact signal is generally polychromatic in nature, frequency domain transformation is required to identify the individual frequency components.

2.2.1 Frequency Domain Transformation

The mathematical tool for transformation of signals from the time to the frequency domain is the fast Fourier transform which in turn is a numerical implementation of the Fourier

Integral. In this section, the relevant aspects of Fourier analysis used in this research are discussed.

Figure 2.9 shows a three dimensional illustration of the graphical relationship between a sinusoidal signal in the time and frequency domains. From a theoretical standpoint, therefore, the two representations are projections of the same signal onto different planes.

2.2.1.1 The fast Fourier Transform.

This thoerem is the basis of most frequency domain analyses. It is well described in most testbooks. Hence only the relevant aspects and background pertaining to this research is reviewed.

Fourier's theorem, first propounded in 1807, essentially states that any function $x(t)$, fulfilling certain criteria (referred to as Dirichlet's conditions) can be expressed as an infinite series of trigonometric functions (called a Fourier series) i.e.

$$x(t) = \frac{a_0}{2} + \sum_{n=1}^{\infty}(a_n \cos n\omega_0 t + b_n \sin n\omega_0 t) \qquad [2.10]$$

where the coefficients a_0, a_n and b_n (called Fourier coefficients) are given by

$$a_n = \frac{2}{T}\int_{\frac{-T}{2}}^{\frac{T}{2}} x(t)\cos n\omega_0 t \; dt \qquad [2.11]$$

$$b_n = \frac{2}{T}\int_{\frac{-T}{2}}^{\frac{T}{2}} x(t)\sin n\omega_0 t \; dt \qquad [2.12]$$

$$\omega_0 = \frac{2\pi}{T} \qquad [2.13]$$

T = fundamental period of the waveform.

Dirichlet's conditions are generally sufficient but not all necessary for the transformation and may be briefly summarized as follows:

1. $x(t)$ must have a finite number of discontinuities in any period.
2. $x(t)$ must have a finite number of turning points in any period.
3. $x(t)$ must be absolutely integrable in any period T, i.e. $\int_{-\infty}^{\infty} x(t)dt < \infty$

Most natural phenomena satisfy Dirichlet's conditions (which also imply that $x(t)$ must possess a finite period) and hence Fourier analysis is generally applicable to most physically realizable waveforms. By invoking de Moivre's theorem, i.e.

$$e^{in\theta} = \cos n\theta + i \sin n\theta \qquad [2.14]$$

the series may be rewritten as:

$$x(t) = \sum_{n=-\infty}^{\infty} c_n e^{int} \qquad [2.15]$$

where

$$c_n = \frac{1}{T}\int_{-\frac{T}{2}}^{\frac{T}{2}} x(t)e^{-in\omega t}dt = \begin{cases} \frac{1}{2}(a_n + ib_n) & n > 0 \\ \frac{a_0}{2} & n = 0 \\ \frac{1}{2}(a_n + ib_n) & n < 0 \end{cases} \qquad [2.16]$$

If a Fourier series can be written for a waveform, then the components of the series constitute a complete description of the frequency content of the waveform.

The Fourier series is strictly restricted to periodic functions. However, this restriction may be removed by allowing the period T to approach infinity to give the Fourier Integral i.e.

$$x(t) = \frac{1}{2\pi}\int_{-\infty}^{\infty} F(\omega)e^{i\omega x}d\omega \qquad [2.17]$$

where
$$F(\omega) = \int_{-\infty}^{\infty} x(t)e^{-i\omega x}dt \qquad [2.18]$$

$F(\omega)$ is the frequency-domain equivalent of $x(t)$ and contains the amplitude and phase information of all the frequencies in $x(t)$. Equations [2.17] and [2.18] are respectively called the forward and reverse transforms and are used to transform signals to and from the time into the frequency domains.

In practice, acquired signals are represented by a finite set x_k of N (which for simplicity is assumed to be even) discrete samples given by

$$x_k = x(t_k) = x(k\Delta t) \quad k \in \{0,1,2,......,N-1\} \qquad [2.19]$$

where Δt is the sampling interval. Since there are only N input time-domain samples, the same number of frequency-domain output points is obtained within the range $-f_N$ to f_N at the discrete frequency values given by

$$f_m = \frac{m}{N\Delta t} \quad m \in \left\{\frac{-N}{2},..........,\frac{N}{2}\right\} \qquad [2.20]$$

Under such circumstances, the Fourier integral is approximated numerically by a discrete sum

$$X(f_m) = \int_{-\infty}^{\infty} x(t)e^{i2\pi f_m t}dt \approx \Delta t\sum_{k=0}^{N-1} x_k e^{i2\pi k\frac{m}{N}} \qquad [2.21]$$

This numerical approximation is called the Discrete Fourier Transform (DFT) X_m of the N points x_k . The discrete inverse Fourier Transform may be similarly expressed as

$$x_k \approx \frac{1}{N}\sum_{k=0}^{N-1} X_k e^{-i2\pi k\frac{m}{N}} \qquad [2.22]$$

and can recover the set of the input time samples. For an N-point DFT, N^2 main operations are required for the evaluation of the transform. Depending on the complexity, the average number of samples needed to reasonably simulate a realistic waveform could be in the order of 1000, and thus render the procedure time inefficient.

The Fast Fourier Transform (or FFT) is an algorithm for efficiently evaluating the discrete Fourier transform with a smaller number of mathematical operations. Since the algorithm is discussed in most introductory textbooks on digital signal processing, only the main principles and methodology are reviewed.

The DFT of an N-point record may be represented by the sum of two $\frac{N}{2}$-point discrete transforms formed respectively from the even- and odd-numbered samples in the original record (Press et al, 1988). If N is an integer power of 2 (i.e. $N = 2^k$), then application of the above lemma can be continued recursively until the original record has been subdivided to transforms of unit length. The Fourier transformation of a record of unit length is an identity operation that copies its input to its output. The key issue is figuring out which input value in the time record corresponds to which output value in the frequency record. This is achieved by bit reversal reordering. This reordering process calculates the binary representation of the position of each sample point and reverses the bits (i.e. zeroes and ones are interchanged) to find the corresponding position in the frequency array.

The relative superiority of the FFT algorithm over the DFT is shown in the fact that for an N $(= 2^k)$ point DFT, the FFT algorithm reduces the number of operations from $N^2$to $N \log_2 N$. For a detail treatment of the FFT, reference can be made to Cooley and Tukey (1965).

2.3 Spectral Analysis

The investigation of elastic wave velocities has generally been pursued along either direct traveltime or phase lag measurement. The former approach measures the arrival times of successive distinguishable wave types whereas the latter involves a study of the shape of each frequency content of the wave. Spectral analyses functions are used to compute phase lag and coherence values for each constituent frequency in the impact signal. Until the advent of powerful computers and efficient numerical algorithms, waveform analysis was rarely performed due to the lengthy and tedious computations involved in its implementation. For the purposes of this work, the waveform approach is adopted.

2.3.1 Determination of Phase Velocity

The phase velocity (c) is the ratio of distance travelled by a monochromatic signal to the traveltime taken i.e.

$$c = \frac{\Delta x}{\Delta t} \qquad [2.23]$$

where $\Delta x = x_2 - x_1$, is the linear distance between any two receiver stations and

Δt = interstation traveltime.

The time lag Δt between the stations is given by

$$\Delta t = \frac{\Delta \phi}{\omega} \qquad [2.24]$$

where $\Delta \phi$ = interstation phase delay and

$\omega (= 2\pi f)$ is the angular frequency. [2.24a]

Assuming that a signal has been dissociated into its frequency components, the task is to compute the difference in phase delay of each component between two stations of known distance apart. A direct but tedious method is to compute the variation of phase with frequency at each two station and find the difference at each frequency. An easier approach is to calculate an artificial function from the measured signals at each station such that the phase of this new function at any frequency equals the phase lag of the original signal at the same frequency. Such a function is called the cross-spectrum.

The phase lag between two stations is obtainable from the deconvolution of the signal $x(t)$ observed at one station with respect to the signal $y(t)$ observed at another. In the frequency domain representation, deconvolution of $x(t)$ with respect to $y(t)$ is equivalent to

$$D_{xy}(f) = \frac{X(f)}{Y(f)} = \frac{X(f)Y^*(f)}{|Y(f)|^2} \qquad [2.25]$$

The deconvolution function, D_{xy}, contains information on both the interstation phase delay and the attenuation. However, the use of deconvolution to determine phase lag is not convenient for two reasons. First, the complex division of the two signals in the above equation could lead to a zero-denominator situation at some data points. Extra precautionary programming steps must therefore be taken to avoid such situations since they may lead to computer crashes. Secondly, the deconvolution process is very sensitive to noise. At frequencies where noise is predominant, the amplitudes are generally small. Division by the square of a small number (which is still small for noise levels normally encountered), the results of deconvolution become highly and erroneously amplified.

There is a two-step method around the problem. First, a digital filter may be applied to the data before the deconvolution process to minimize the noise content which, under most circumstances, are contained in the high frequency range. A low-pass digital filter with the appropriate cutoff frequency may be applied to the data to remove unwanted high frequency noise. A wide variety of digital filters exist e.g. Butterworth, elliptical or Cauer, Chebyschev and Bessel. A Butterworth low-pass filter is also maximally flat within the pass band and zero in the stop band. A Butterworth filter is therefore suitable for the purpose. For detail information on digital filters, reference may be made to Hamming (1983). Second, it may be observed that the numerator of D_{xy} contains the entire phase information of the signal which is essentially the cross-spectrum of the two signals. The interstation phase delay function can therefore be calculated from the cross-spectrum (i.e. the Fourier transform of the cross-correlation of the two signals). Landisman et al (1969) were the first to propose the use of the cross-spectrum for the measurement of interstation phase delay.

The cross-spectrum, S_{xy}, of any two signals, $x(t)$ and $y(t)$, is defined as the product of the Fourier transform $X(f)$ of one of the signals and the complex conjugate $\overline{Y}(f)$ of the Fourier transform $Y(f)$ of the second signal, i.e.

$$\overline{S_{xy}} = \overline{X(f)} * \overline{Y^{*}(f)} \qquad [2.26]$$

The arithmetical proof that the phase of the cross-spectrum of two signals actually gives the phase lag between them is simple as illustrated in Figure 2.10, which shows the phasor representation of the measured signals in an Argand space. The phase difference between the signals $\Delta\phi$ is given by

$$\Delta\phi = \phi_1 - \phi_2 \qquad [2.27]$$

The tangent of the phase difference can then be expressed as

$$\begin{aligned}
\tan(\Delta\phi) &= \tan(\phi_1 - \phi_2) \\
&= \frac{\tan\phi_1 - \tan\phi_2}{1 + \tan\phi_1 \tan\phi_2} \\
&= \frac{\frac{y_1}{x_1} - \frac{y_2}{x_2}}{1 + \frac{y_1}{x_1}\frac{y_2}{x_2}} \\
&= \frac{x_2 y_1 - x_1 y_2}{x_1 x_2 + y_1 y_2} \qquad [2.28]
\end{aligned}$$

The cross-spectrum, S_{xy}, of the two signals is

$$S_{xy} = (x_1 + iy_1)\cdot(x_2 - iy_2) \qquad [2.29]$$

$$= x_1x_2 + y_1y_2 + i(x_2y_1 - x_1y_2)$$

The tangent of the phase (ϕ) of the cross-spectrum is the ratio of the imaginary component to the real component i.e.

$$\tan\phi = \frac{x_2y_1 - x_1y_2}{x_1x_2 + y_1y_2} \qquad [2.30]$$

It follows from equations 2.28 and 2.30 that the phase of the cross-spectrum is equal to the required phase lag.

The variation of typical cross-spectrum phase with frequency is shown in Figure 2.11. The magnitude of the phase is generally in modulo-2π format i.e. phase is restricted to a range of 2π. The phase magnitudes in this format cannot be readily used in equation 2.24.and must be converted to the continuous representation format by the following equation

$$\phi_{true} = \phi + 2n\pi \qquad [2.31]$$

The constant $2n\pi$ is due to the fact that the Fourier transform yields phase information only for angles between -π to π (called modulo-2π phase) and it is necessary to add or subtract the appropriate integral multiples of circles to insure continuity of the phase curve. The process of conversion from modulo-2π to continuous representation format is called unfolding.

ϕ_{true} is now in the correct format for substitution in into equation [2.24]. For each frequency, the angular frequency can be calculated from equation [2.24a] and the time lag from equation [2.24]. The receiver spacing and time lag may then be used in calculating the velocity of each frequency component.

2.3.2 Signal Quality

As signals propagate from the source to the receivers, they become tainted with other undesirable signals from other sources in the vicinity of the test location. Such undesirable signals are grouped under the term 'noise' which is technically defined as any type of disturbance that can mask a signal of interest. The concept of noise is therefore relative as a noise of given characteristics may be unimportant in certain cases but may lead to gross misinterpretation in some other cases.

Noise may be coherent or incoherent. Coherent noise is characterized by a distinct apparent velocity, predicted onset and a fairly narrow bandwidth. Incoherent noise is composed of unpredictable signals of random amplitude and onset and is often referred to as ambient noise (or microseisms in areas prone to earthquakes). Such noise is believed to be due to winds, sea waves and unintentional man-made disturbances. Because incoherent noise is random, uncorrelated and has a broad spectrum, it is also called white noise. Its presence is revealed by a spike located at the zero-lag position in an auto-power spectrum. Microseisms are generally present and act as background vibration for any signal that travels in the ground. In the SASW test, high-frequency noise is generally encountered, though noise at other frequencies have also been detected. Incoherent noise is generally minimized by adequate signal averaging. The effect of coherent noise can only be minimized or eliminated by ignoring the frequencies common to the signal and the noise.

One way of indirectly determining the quality of a signal at a particular frequency is to determine the coherence between the source and measured signals at that frequency. A pair of signals x and y are said to be coherent if they bear resemblance to each other.

The root mean square coherence function between any two time-domain signals represented by x and y is the ratio of their cross-power spectrum to the square root of the product of their auto-spectra

$$\overline{\gamma_{xy}(f)} = \frac{\overline{S_{xy}(f)}}{\sqrt{\overline{S_{xx}(f)}}\sqrt{\overline{S_{yy}(f)}}} \qquad [2.32]$$

where $S_{xy}(f)$ = cross-spectrum obtained by separately averaging the co- and quad spectra over a number of data records and

S_{xx}, $S_{yy}(f)$ = are averaged power spectra over the same number of data records.

If x and y are the measured signals from two receivers, then the coherence is a measure of the portion of the output power spectrum of the signal measured at the second receiver due to the signal measured at the first. The coherence function is only applicable to averaged signals since it is trivially perfect for a single pair of data records. However, on averaging several records, it is only when there is no noise that the coherence has a value of unity. A coherence of unity indicates exact identity between x and y. Poor coherence is frequently encountered and may be attributed to leakage errors, poor signal-to-noise ratios, system non-linearity and/or extraneous noise. A typical variation of root mean square coherence with frequency is shown in Figure 2.12.

The quality of a signal may be assessed from the magnitude of its signal-to-noise ratio, which is related to the root mean square coherence by the following formula:

$$\frac{S}{N} = \frac{\overline{\gamma_{xy}^2(f)}}{1 - \overline{\gamma_{xy}^2(f)}} \qquad [2.33]$$

High values of $\frac{S}{N}$ indicate little noise. The ratio may be improved by enlarging the signal (using a stronger source), lessening the noise, especially coherent noise (by a suitable detector array) and by using a detector of suitable response (i.e. its frequency bandwidth must be outside that of the dominant noise).

2.4 Determination of in-situ Dispersion Curve

Two types of velocities, namely phase velocity and group velocity, are associated with waveforms. The phase velocity (v) is the speed at which a monochromatic signal travels and the group velocity (v_G) is the speed at which the energy of the waveform is propagated. The relationship between the two types of velocity was given by Timoshenko and Goodier (1934) as

$$v_G = v + k\frac{dv}{dk} \qquad [2.34]$$

where v_G = group velocity

v = phase velocity

k = wave number = $\frac{2\pi}{L}$

L = wavelength

In an inhomogeneous medium, group and phase velocities are unequal because the waveform changes shape during propagation, resulting in a variation of group velocity with wavenumber. Information on the elastic properties of the medium are obtainable from phase velocity and since the latter is readily measured in the field, it is more convenient for that purpose. For most natural and man-made ground, phase velocity varies with wavelength. This variation is called dispersion. Generally, the longer the wavelength, the greater the depth at which the wave travels. Thus if the material stiffness varies with depth, the phase velocity - wavelength relationship also varies similarly.

The phase velocity of a monochromatic signal between two stations at a known distance apart is given by

$$v = \frac{\omega}{\phi} d \qquad [2.35]$$

where v = phase velocity,

$\omega (= 2\pi f)$ is the angular frequency,

ϕ = phase lag,

d = receiver distance.

The preceding equation is used to calculate the phase velocity of all frequencies at which the root mean square coherence (K_{xy}) is greater than a predetermined minimum ($K_{xy_{min}}$) i.e.

$$K_{xy} \geq K_{xy_{min}} \qquad [2.36]$$

Heisey (1982) recommended that a second criterion, based on the wavelength and the interstation distance, be used to ignore certain frequencies or wavelengths. This criterion is expressed as

$$\frac{L}{3} \leq d \leq 2L \qquad [2.37]$$

where L = the wavelength of the signal

d = interstation distance.

The reasons behind this recommendation is readily appreciated. Rayleigh waves of short wavelength attenuate at a faster rate than those of long wavelength. Hence at a sufficient distance form the source (i.e. long enough to avoid the so-called near-field effects of elastic body waves), amplitudes of short wavelength signals may be attenuated to an such an extent that they are dominated by background noise. The lower limit on wavelength is thus aimed at eliminating those wavelengths that may be undesirably influenced by background noise as a result. Rayleigh waves are not fully developed until after some distance from the source. The upper limit appears to be responding to this observation in the case when the interstation distance equals the distance from source to near receiver. Under such circumstances, the argument is that wavelengths greater than the upper limit are not fully developed by the time the signal arrives at the first station. A more important reason for the upper limit, in this author's opinion, is the observation by Jones (1958) that the principal mode of propagation of Rayleigh waves was always obtained with receivers nearer the source. Jones (1958) observed that higher velocities were obtained at long distances due to higher propagation modes. From theoretical studies, Sanchez-Salinero (1987) recommended that only wavelengths less than half the interstation distance be included in the determination of the experimental dispersion curve. The basis of this recommendation was that the influence of body waves are negligible and that Rayleigh waves are fully developed within a short distance from the source. In an independent study, Hiltunen and Woods (1990) found that for source-receiver distances less than twice the interstation distance, the influence of body waves is negligible.

Although Heisey's criteria were used in the early stages of the research, it was found that a more appropriate procedure is to discriminate frequencies (or wavelengths) on the basis of an appropriate minimum coherence, calculate phase velocities and plot the dispersion curve without regard to wavelength magnitudes but ensuring that the source-near-receiver distance is at least a metre. One then finds that phase velocities at wavelengths which are influenced by the factors discussed above are orders of magnitude higher or lower than the majority of the dispersion points. It is not difficult to identify such behaviour from variations in actual material stiffness since a high resolution in wavelength gives a lot of dispersion points in small range for cross-comparison. The reason for this departure from Heiseys criteria was the requirement to truncate a particularly continuous dispersion curve that matches independent test results because the interstation distance-wavelength criterion was not met. An example of this situation will be discussed later in Chapter 5.

2.5 A Computerized SASW System

For a proper evaluation of a computerized SASW system, the current instrumentation systems will be reviewed as a basis for comparison. Figure 2.13 shows two SASW instrumentation systems in published use as well as the computerized alternative just described in this chapter. In the first approach, a dedicated instrument is used to acquire and store waveform data for later analysis with a computer. In the second and widely used approach, a spectrum analyzer is used to acquire waveform data which is then transferred to a connected microcomputer for further processing and analysis. The third approach is to use a microcomputer for both data acquisition and analysis. The components of wave generation and detection are therefore identical in all three systems. The difference occurs in how the waveform data are acquired and processed. As described below, it is the acquisition and processing that controls the system cost and processing time.

A dedicated instrument is specialized for SASW data acquisition only and may thus be very simple to operate. However, the instrument cannot be used for anything else and is therefore not economical. The spectrum analyzer is the most expensive component in the second instrumentation type, about four to five times the cost of the computer attached to it. It is very versatile, powerful and fast in a lot of other applications beside SASW. The main advantage of using a spectrum analyzer, compared with the third alternative, is the fact that the engineer does not have to be concerned with the intricacies of data acquisition and computer programming. A computerized system has the following advantages

1. Cost is considerably reduced as a result of the elimination of the spectrum analyzer.

2. Time for transferring and verifying data files from analyzer to computer is saved. Such file transfer often requires commercial translators and hence data acquisition must be stopped before transfers can be made. Time lost in file transfer can therefore be substantial.

3. Depending on the speed of the analogue-to-digital converter installed in the computer, any number of receivers can be monitored by a computerized system for little or no extra cost. However, the cost of a four-channel spectrum analyzer is almost twice the cost of a similar dual-channel analyzer. This is an important aspect, since the use of receiver arrays substantially reduces testing times in the field.

4. The potential for automation is greater with a computerized system than with any other instrumentation system since data acquisition, spectral analysis and forward modelling can be merged into a single computer program.

A limitation of this approach, if it may be called so, is that data acquisition must be done in software and therefore requires some understanding of electronics and computer programming. However, upcoming object-oriented programming environments (e.g. C++) have reusable program codes that require minor modification for specialized projects. For an economical and flexible use of equipment, it may be concluded that, it is better to specialize software rather than hardware.

2.6 Program SASW-DA

SASW-DA (Spectral Analysis of Surface Wave - Data Acquisition) is a computer program written by the author in two similar programming languages, C (Kernighan and Ritchie, 1978) and G (Vose and Gregg, 1986) for acquiring and processing waveform data. C is well-known and requires no description. G is a graphical language developed by

National Instruments of Austin, Texas and is used in a software development environment called **LabVIEW** (i.e. **Lab**oratory **V**irtual **I**nstruments **E**ngineering **W**orkbench). Currently, SASW-DA runs on only Apple Macintosh computers with a minimum of 5 megabyte random access memory and running system version 6.0.7 or later. Other hardware requirements include a data acquisition card (NB-MIO-16-9), a direct memory access card with a GPIB interface (NB-DMA-8-G), a high resolution display monitor and an interface between the receivers and the computer. The interface was designed and built for the purposes of this research and is described in chapter 4.

Computer programs developed in LabVIEW are called virtual instruments because the user interface (called front panel in G terminology) is similar to the front panel of a real instrument . Figure 2.14 shows the user interface or front panel of SASW-DA. The actual program (called a diagram) is event-driven and hidden from the user. The inputs to the program are:

1. the name of the site and receiver spacings
2. maximum frequency of waves to be sampled and digitized.
3. time-base for data acquisition
4. total count or number of samples to be taken
5. vector of channels to be scanned
6. vector of gain constants for amplification
7. trigger conditions - slope and level
8. number of signals to average for a given spacing.

The name of the site is used for the creation of a folder (or directory) that will contain all dispersion files from that site. A dispersion file contains four columns of data namely wavelength, coherence, phase delay and phase velocity.

The total count is the number of samples to be recorded for all channels. Thus if there are m channels and n samples are required per channel, then the total count (N) is given by

$$N = m.n \qquad [2.38]$$

where N is forced to take the magnitude of the nearest power of 2. The maximum frequency ($f_{\max}$) is estimated from the guidelines given earlier in this chapter. This frequency is the cut-off frequency to which all analogue low-pass filters will be set. The sampling interval is then calculated from

$$\Delta t = \frac{1}{2mf_{\max}} \qquad [2.39]$$

The time-base is the resolution of the clock to be used in data acquisition timing and must be selected from the available options. Each time base value corresponds to the indicated number of ticks per second. The time interval for sampling is expressed in terms of the time-base as

$$\Delta t = t_B . n_{CT} \qquad [2.40]$$

where Δt = maximum sampling interval.

t_B = time base and

n_{CT} = the number of clock ticks in the interval.

Each signal acquired is transformed into the frequency domain by the fast Fourier transform. The coherence and cross-spectrum functions are computed for each frequency component. A running average of coherence and cross-spectrum is performed till the specified number of signals at a given spacing have been acquired. The averaged phase delays are then unwrapped and used to calculate the phase velocity at all frequencies for which the specified minimum coherence criterion is satisfied.

The output files from all spacings are then merged to produce a dispersion file for the site. As it is often useful to examine the data from each spacing before merging, an option to leave dispersion files intact is incorporated into the program. The flow chart of the main operations in the program is shown in Figure 2.15.

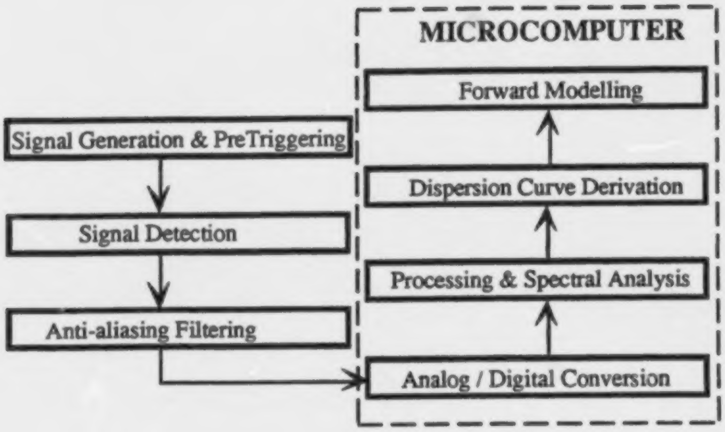
MICROCOMPUTER
Forward Modelling
Signal Generation & PreTriggering
Dispersion Curve Derivation
Signal Detection
Processing & Spectral Analysis
Anti-aliasing Filtering
Analog / Digital Conversion

Figure 2.1. Schematics of SASW Testing Without A Spectrum Analyzer.

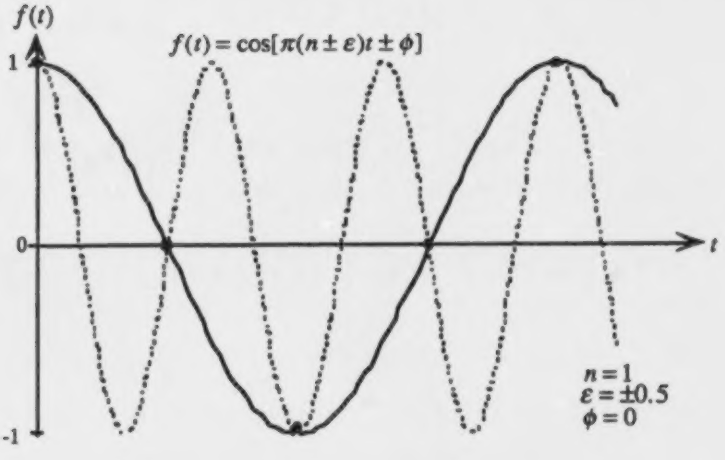

Figure 2.2 . The Phenomenon of Aliasing

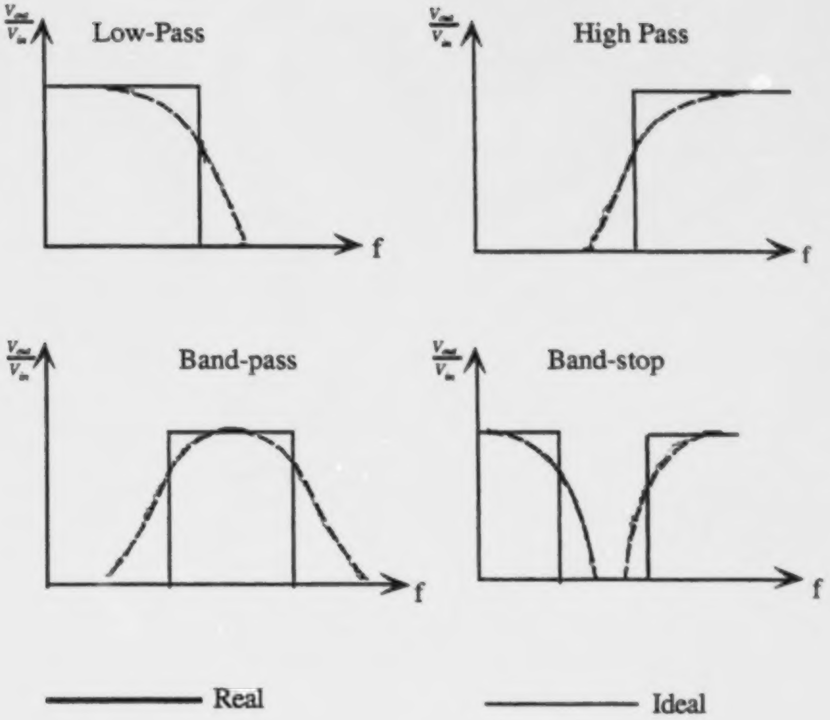
$\frac{V_{out}}{V_{in}}$
Low-Pass
f
$\frac{V_{out}}{V_{in}}$
High Pass
f
$\frac{V_{out}}{V_{in}}$
Band-pass
f
$\frac{V_{out}}{V_{in}}$
Band-stop
f
Real
Ideal

Figure 2.3 . Types of Filters.

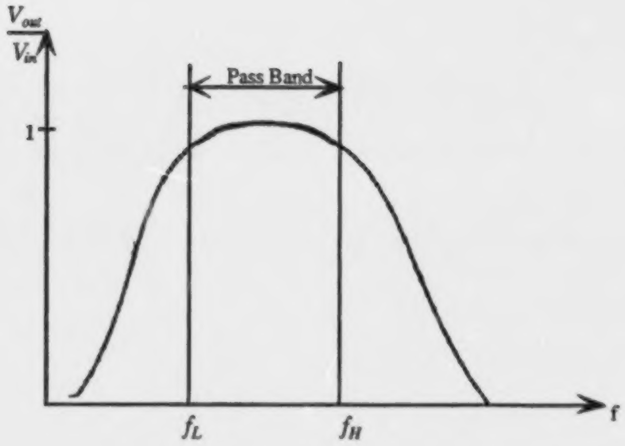
$\frac{V_{out}}{V_{in}}$
Pass Band
1
f_L
f_H
f

Figure 2.4 Characteristics of a Butterworth filter.

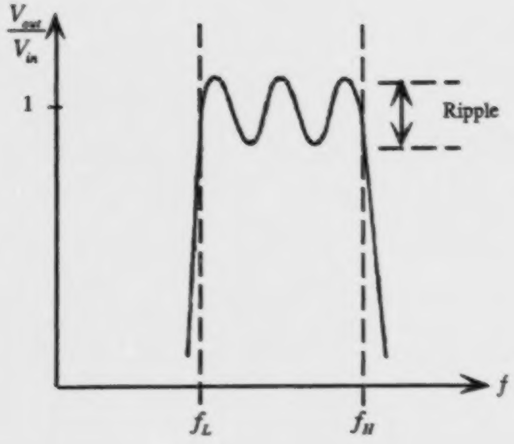

$\frac{V_{out}}{V_{in}}$
1
Ripple
f
f_L
f_H

Figure 2.5 Characteristics of a Chebyschev filter.

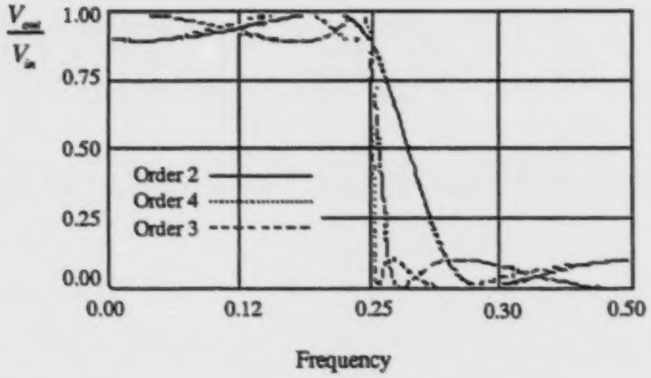

Figure 2.6 Characteristics of a Cauer Filter.

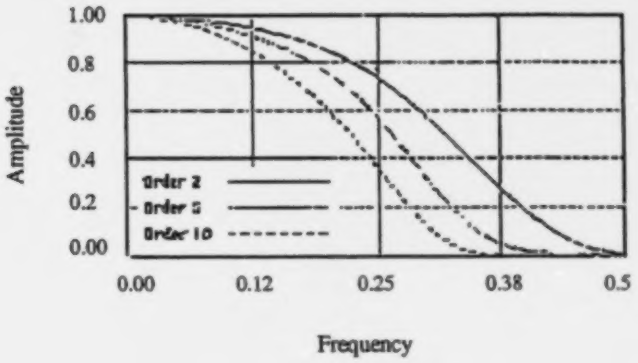

(a) Magnitude response

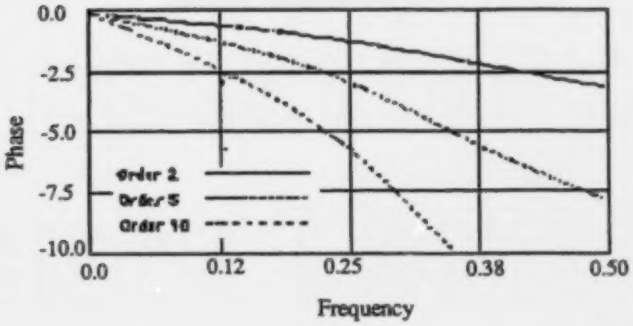

(b) Phase Response

Figure 2.7 Characteristics of a Bessel Filter.

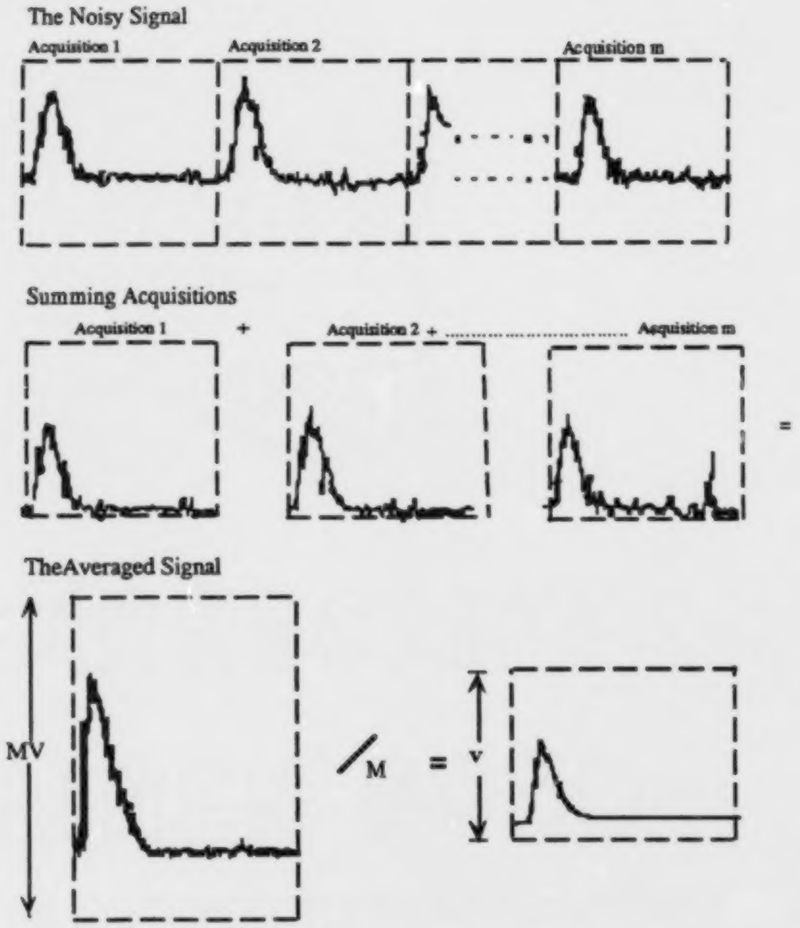
The Noisy Signal
Acquisition 1
Acquisition 2
Acquisition m
Summing Acquisitions
Acquisition 1
+
Acquisition 2 +
Acquisition m
=
TheAveraged Signal
MV
/M
=
v

Figure 2.8 Noise Reduction by Signal Averaging (After Ramirez, 1985)

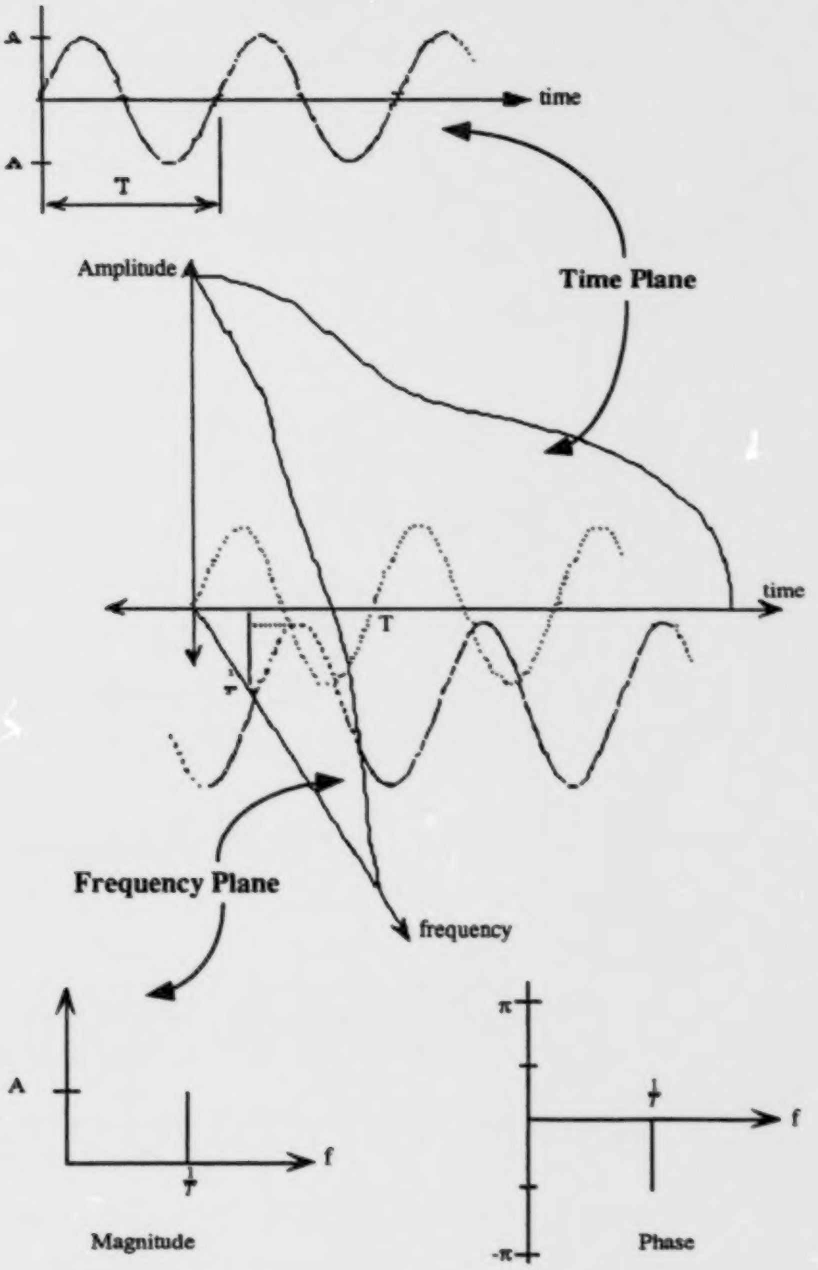
A
A
time
T
Amplitude
Time Plane
time
T
1/T
Frequency Plane
frequency
A
f
1/T
Magnitude
π
-π
1/T
f
Phase

Figure 2.9 Time-Frequency Domain Transformation (After Ramirez, 1985)

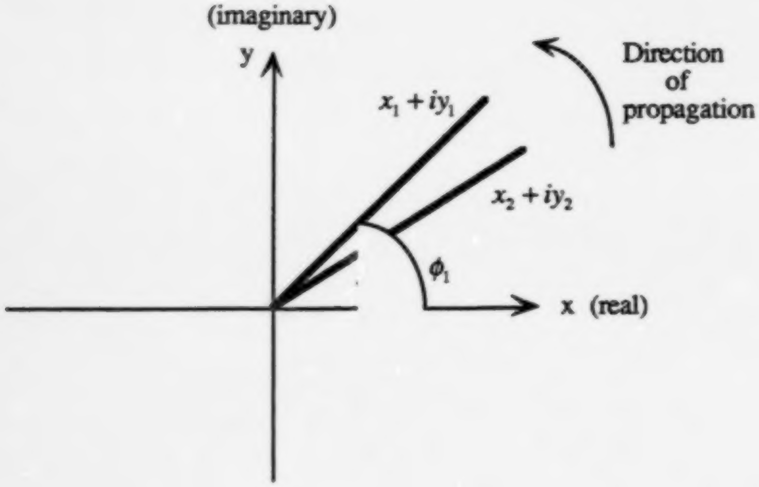
(imaginary)
y
$x_1 + iy_1$
Direction of propagation
$x_2 + iy_2$
ϕ_1
x (real)

Figure 2.10 Determination of Phase Lag from Cross-Spectrum

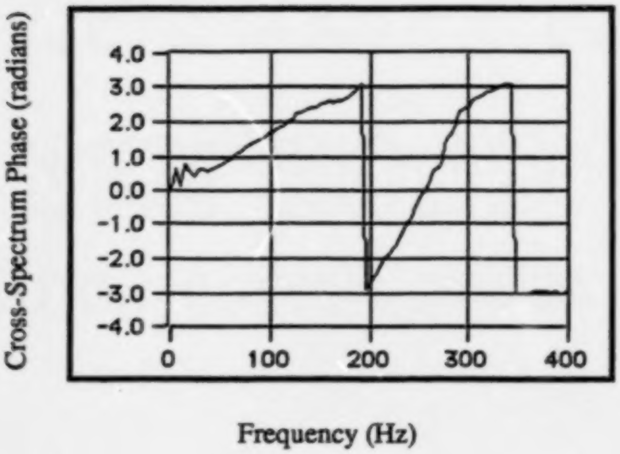

Figure 2.11 Typical variation of cross-spectrum phase with frequency.

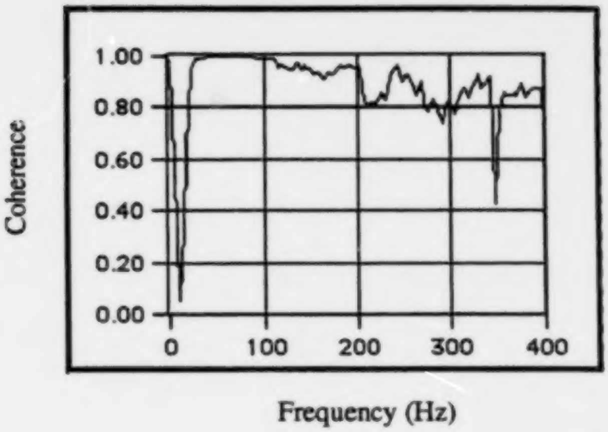

Figure 2.12 Typical variation of coherence with frequency.

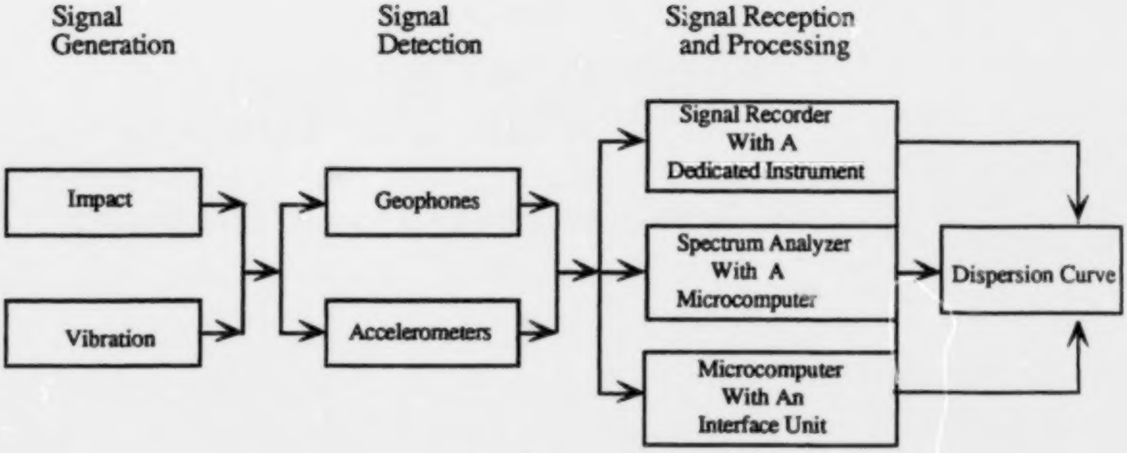
Signal Generation
Signal Detection
Signal Reception and Processing
Impact
Vibration
Geophones
Accelerometers
Signal Recorder With A Dedicated Instrument
Spectrum Analyzer With A Microcomputer
Microcomputer With An Interface Unit
Dispersion Curve

Figure 2.13. SASW Instrumentation System.

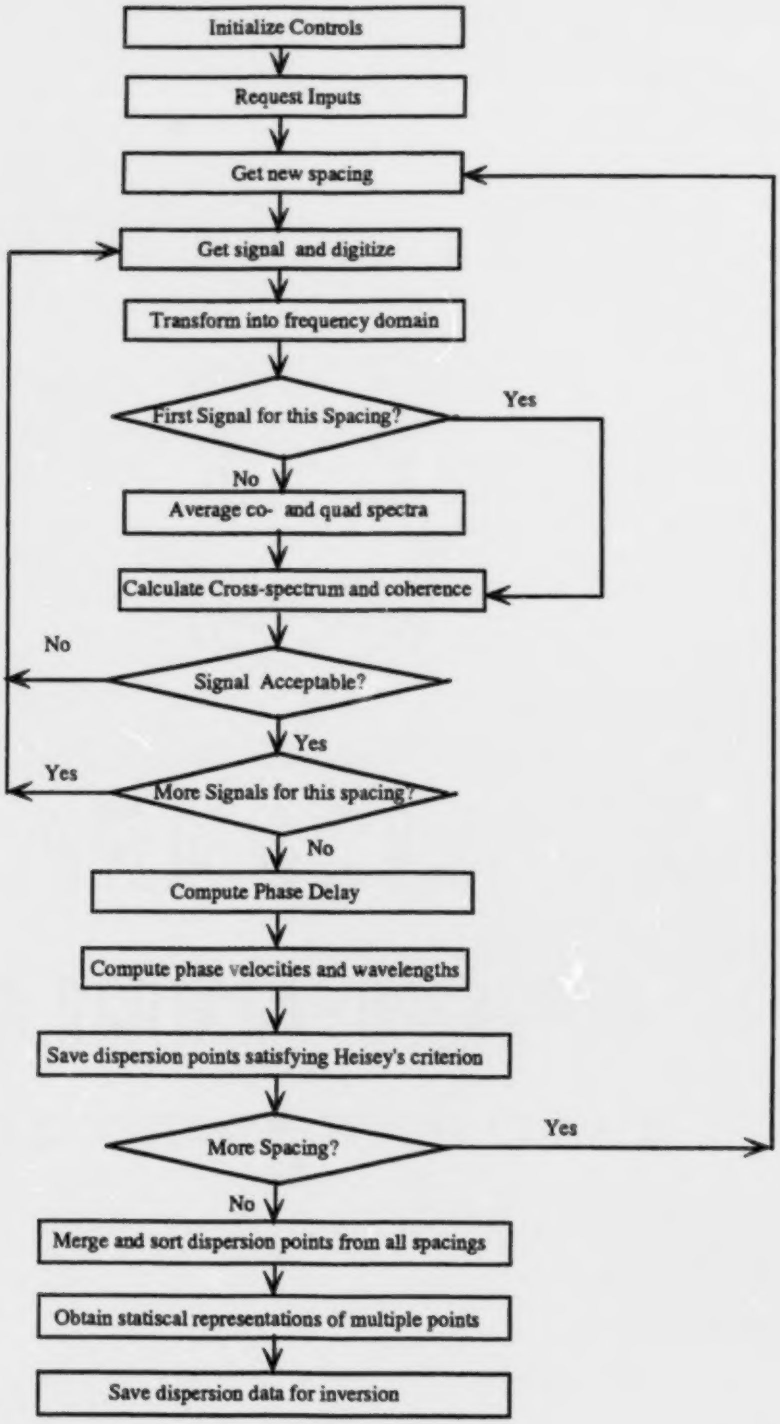
Initialize Controls
Request Inputs
Get new spacing
Get signal and digitize
Transform into frequency domain
First Signal for this Spacing?
Yes
No
Average co- and quad spectra
Calculate Cross-spectrum and coherence
No
Signal Acceptable?
Yes
Yes
More Signals for this spacing?
No
Compute Phase Delay
Compute phase velocities and wavelengths
Save dispersion points satisfying Heisey's criterion
More Spacing?
Yes
No
Merge and sort dispersion points from all spacings
Obtain statiscal representations of multiple points
Save dispersion data for inversion

Figure 2.14 Flow Chart of program SASW-DA.

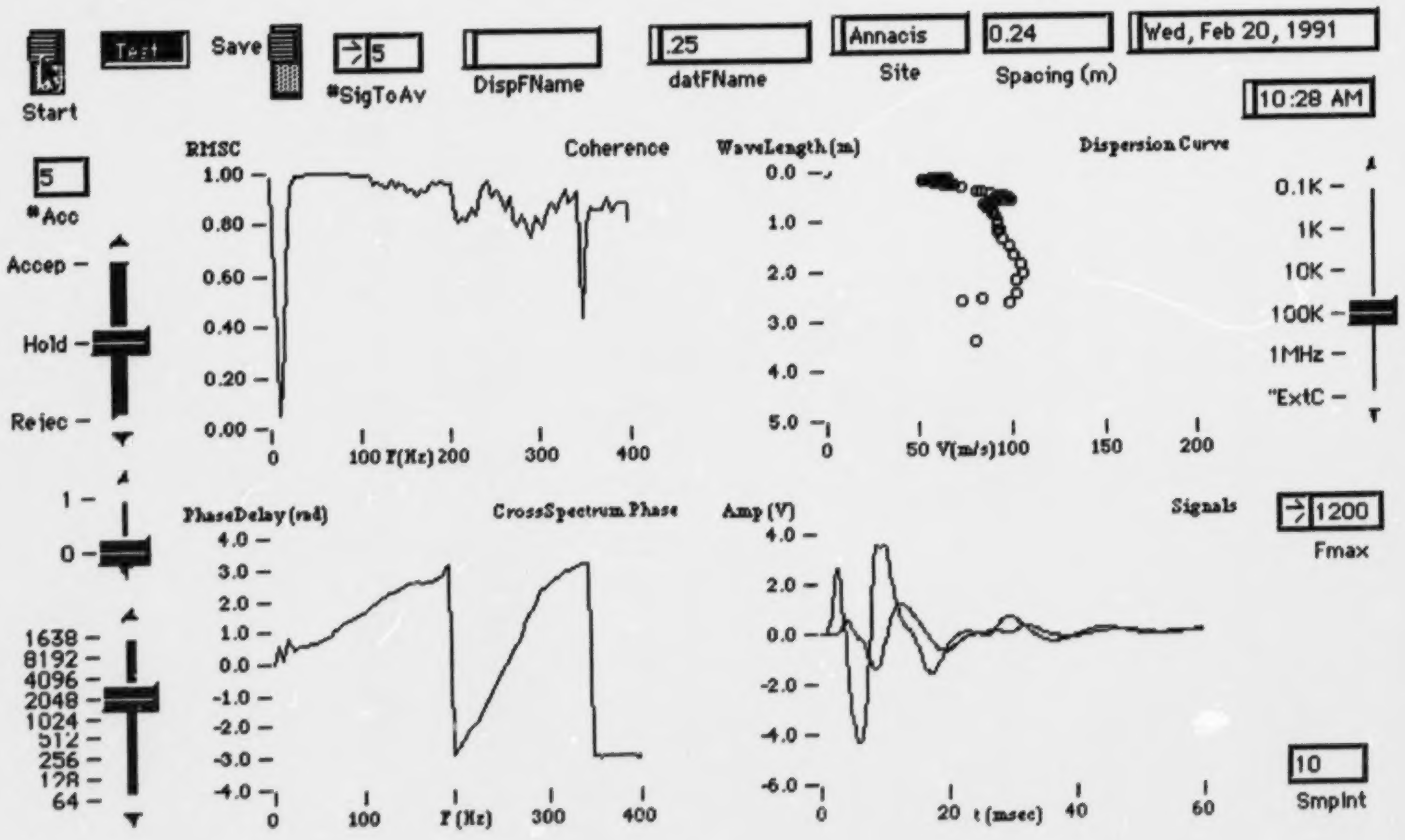

#SigToAv: 5
DispFName:
datFName: .25
Site: Annacis
Spacing (m): 0.24
Wed, Feb 20, 1991
10:28 AM
#Acc: 5
Fmax: 1200
SmpInt: 10

Start
Test
Save
Accep
Hold
Rejec
1
0
1638
8192
4096
2048
1024
512
256
128
64
RMSC
Coherence
1.00
0.80
0.60
0.40
0.20
0.00
0
100 F(Hz) 200
300
400
WaveLength (m)
Dispersion Curve
0.0
1.0
2.0
3.0
4.0
5.0
0
50 V(m/s) 100
150
200
0.1K
1K
10K
100K
1MHz
"ExtC
PhaseDelay (rad)
CrossSpectrum Phase
4.0
3.0
2.0
1.0
0.0
-1.0
-2.0
-3.0
-4.0
0
100
F (Hz)
300
400
Amp (V)
Signals
4.0
2.0
0.0
-2.0
-4.0
-6.0
0
20 t (msec)
40
60

Figure 2.15. Front Panel of program SASW-DA.

CHAPTER 3

FORWARD MODELLING

3.1 Introduction

The subject of this chapter is the process of determining the layering and shear wave velocity profile associated with a given experimental dispersion curve - a process that is variously called *inversion* in seismology and *system identification* in structural dynamics but is hereafter referred to as *forward modelling*.

It is well-known that for each possible mode of propagation, only one dispersion curve can be calculated for a given shear wave velocity profile and that the theoretical principles underlying the computation of this dispersion curve are well-established. This problem of determining an associated dispersion curve is called the direct problem. Given a specific dispersion curve, it is also well-documented that more than one shear wave velocity profile can be associated with the dispersion curve (Knopoff, 1961; Alekseev, 1962; Thrower, 1965; Mora, 1988). The solution of the inverse problem (i.e. determining the profile associated with a given dispersion curve) is therefore non-unique. According to Mora (1988), the reason for this non-uniqueness is due to the fact that the inverse mapping from dispersion curve to structural model is highly non-linear. Hence given a specific dispersion curve, the recourse is to iteratively find the structure whose dispersion curve is identical to the given curve. Such an approach, requires only the solution to the direct or forward problem and is called forward modelling.

In this chapter, the computation of the theoretical dispersion curve associated with a given layering and shear wave velocity profile is discussed.

3.2 Historical Background

The pioneering work on the theoretical treatment of surface wave dispersion in a multi-layered medium may be accredited to Sezawa (1927). However, it was not until 1950 that Thomson laid a concise theoretical framework for the application of matrix methods to the solution of surface wave dispersion problems. Thomson succeeded in minimizing the extensive arithmetical work in Sezawa's formulation and showed that the relationship between phase velocity and frequency could be expressed by the vanishing of a determinant whose elements were implicit functions of phase velocity, wavelength, density and the elastic moduli (or body wave velocities) of the constituent layers.

Unfortunately, Thomson (1950) erroneously imposed continuity of strains at layer interfaces instead of displacements. Haskell (1953) pointed out and corrected the error and then reformulated what is now referred to as the Thomson-Haskell method described below. The subsurface profile of most sites can be approximated by a layered structure overlying an ideal half space such as shown in Figure 3.1. The layers are horizontal, isotropic, homogeneous, of infinite lateral extent and parallel to each other and to the free surface. The phase velocity of a surface wave travelling in the x–direction depends on its wavelength (L) as well as the thicknesses (h), mass densities (ρ), compression (v_P) and shear (v_S) wave velocities of the individual layers. If the wave is of Rayleigh type, then there are four boundary conditions (continuity of two stress and two displacement components) at each interior interface and two boundary conditions (vanishing of two stress components) at the free surface. Thus for an n-layered model, there are 4n-2 boundary conditions. The number of boundary conditions degenerate to 2n-1 if the wave is Love type since there is only one displacement and one stress continuity at an interior interface and one stress component vanishes at the surface. Each boundary condition yields a homogeneous linear equation in the unknowns (i.e. the stresses and displacements) of which there are as many as there are boundary conditions. Such a system of equations possesses a nontrivial solution if the determinant of the coefficient matrix vanishes. Equating the determinant to zero yields the dispersion equation which implicitly expresses the dependence of phase velocity on wavelength

The Thomson-Haskell approach solved the dispersion equation by finding the modal roots of the determinant of a matrix that relates displacement and stresses at the surface to those in the half space. As shown later, the arithmetic involved the difference of products that should be identically zero but are not, due to round-off errors. At high frequencies, these differences which should have been eliminated are multiplied by very large numbers and hence errors are introduced into the calculations. As a result, unacceptably poor resolution was inevitable at short wavelengths.

This numerical difficulty, inherent in the original Thomson-Haskell solution at high frequencies, was variously circumvented by Dunkin (1965), Thrower (1965) and Watson (1970) by techniques that algebraically operated on second and third order sub-determinants of layer matrices and thereby eliminated the problematic terms before computing products. These improved approaches, however, were initially disadvantaged by the requirement of more computer memory and time with respect to the Thomson-Haskell solution as programmed by Press et al (1961).

Other alternative formulations of the solution to the direct problem have been given by Knopoff (1964), Gilbert and Backus (1966) and Kausel and Roesset (1981). Lysmer and Drake (1972) used the finite element method to solve the forward problem while Boore (1972) used the finite difference scheme. Randall (1967) programmed Knopoff's (1964) algorithm for Rayleigh waves and reported shorter computation time than for the Thomson-Haskell method. Gilbert and Backus (1966) adopted a more generalized procedure, referred to as the propagator matrix method which is applicable to layers with properties that are not constant within the layer. In the special case of the homogeneous layer model, the Backus and Gilbert approach reduces to the Thomson-Haskell solution.

On the assumption that layers behave as free plates, Jones (1962) computed the dispersion for a road structure and showed that experimental results agreed fairly well with this approximate theory. The purpose of the free plates assumption was to simplify the direct problem by turning all complex velocities into real ones. Thrower (1965) showed that the free plates analysis was limited in application to certain velocity ranges and to only some of the modes experimentally observed on pavements. Thrower (1965) therefore extended Jones' approach to include many layers on a half space and hence obtained a partial solution to the complex velocity problem. Though he found only the real roots of the dispersion equation, he succeeded in largely avoiding the characteristic numerical difficulties without recourse to super-precision arithmetic. A limited analysis and extensive experimentation on surface wave dispersion in road structures have also been carried out by Bergstrom and Linderholm (1946), Fry (1963), Heukelom and Foster (1960), Heukelom and Klomp (1962) and Ballard and Chang (1973).

3.3 Forward Modelling

The procedure generally adopted in this strategy employs a technique that requires only solutions to the direct problem in order to find the inverse mapping. The procedure formulated by Gilbert and Backus (1966) and described by Aki and Richards (1980) was adopted. Unlike other approaches, this method avoids the use of scalar and vector potentials and deals directly with the engineering parameters of displacements and stresses. For the original treatment of the subject, the reader is referred to the formulation by Gilbert and Backus (1966).

3.3.1 Rayleigh Wave Dispersion Function

The particle displacement in a medium due to the passage of a Rayleigh wave may be mathematically expressed as

$$\begin{Bmatrix} u_1 \\ u_2 \\ u_3 \end{Bmatrix} = \begin{Bmatrix} r_1 e^{i(kx_1 - \omega t)} \\ 0 \\ i r_2 e^{i(kx_1 - \omega t)} \end{Bmatrix} \qquad [3.2]$$

where r_1 and r_2 are positive real functions of wavenumber (k), depth x_3 and angular frequency (ω). x_1 is the surficial radial distance from the source and t is the time of propagation. A real and positive nature r_1 and r_2 is required to ensure that the specified displacement field represents Rayleigh wave motion.

The stress-strain

$$\sigma_{ij} = \lambda \varepsilon_{kk} \delta_{ij} + 2G\varepsilon_{ij} \qquad [3.3]$$

and strain-displacement equations

$$\varepsilon_{ij} = \frac{1}{2}(u_{i,j} + u_{j,i}) \qquad [3.4]$$

may be combined to give the stress-displacement equation

$$\sigma_{ij} = \lambda u_{k,k} \delta_{ij} + G(u_{i,j} + u_{j,i}) \qquad [3.5$$

from which the stress field may be derived as

$$\begin{Bmatrix} \sigma_{11} \\ \sigma_{22} \\ \sigma_{33} \\ \sigma_{31} \\ \sigma_{23} \\ \sigma_{12} \end{Bmatrix} = \begin{Bmatrix} i(\lambda \frac{dr_2}{dx_3} + k(\lambda + 2G)r_1) \\ i(\lambda \frac{dr_2}{dx_3} + k\lambda r_1) \\ i((\lambda + 2G)\frac{dr_2}{dx_3} + k\lambda\, r_1) \\ G(-kr_2 + \frac{dr_2}{dx_3}) \\ 0 \\ 0 \end{Bmatrix} e^{i(kx_1 - \omega t)} \qquad [3.6]$$

The stress components σ_{33} and σ_{31} are required by compatibility to be continuous in x_3 and may be respectively re-written as

$$\sigma_{31} = r_3\, e^{i(kx_1 - \omega t)} \qquad [3.7]$$

$$\sigma_{33} = i\, r_4\, e^{i(kx_1 - \omega t)} \qquad [3.8]$$

By comparing equations [3.7] and [3.8] with equation [3.6], r_3 , $\frac{dr_1}{dx_3}$, r_4 and $\frac{dr_2}{dx_3}$ can be shown to be given by the following expressions

$$r_3 = G\left(\frac{dr_1}{dx_3} - kr_2\right) \qquad [3.9]$$

$$\frac{dr_1}{dx_3} = kr_2 + \frac{1}{G} r_3 \qquad [3.10]$$

$$r_4 = k\lambda\, r_1 + (\lambda + 2G)\frac{dr_2}{dx_3} \qquad [3.11]$$

$$\frac{dr_2}{dx_3} = \frac{-k\lambda}{\lambda + 2G} r_1 + \frac{1}{\lambda + 2G} r_4 \qquad [3.12]$$

By substituting the expressions for stresses and partial derivatives of r_1 and r_2 with respect to x_3 into the equation of motion [3.13]

$$\rho \ddot{u}_i = \sigma_{ij,j} \qquad [3.13]$$

and assuming a source free condition everywhere (i.e. zero body force) it can be shown that

$$\frac{dr_3}{dx_3} = (4k^2G\frac{\lambda+G}{\lambda+2G} - \rho\omega^2)r_1 + (\frac{k\lambda}{\lambda+2G})r_4 \qquad [3.14]$$

$$\frac{dr_4}{dx_3} = -\rho\omega r_2 - kr_3 \qquad [3.15]$$

Equations [3.10], [3.12], [3.14] and [3.15] may be re-written in matrix notation as

$$\frac{d}{dx_3}\begin{Bmatrix} r_1 \\ r_2 \\ r_3 \\ r_4 \end{Bmatrix} = \begin{bmatrix} 0 & k & \frac{1}{G} & 0 \\ \frac{-k\lambda}{\lambda+2G} & 0 & 0 & \frac{1}{\lambda+2G} \\ \frac{4k^2G(\lambda+G)}{\lambda+2G} - \rho\omega^2 & 0 & 0 & \frac{k\lambda}{\lambda+2G} \\ 0 & -\rho\omega^2 & -k & 0 \end{bmatrix}\begin{Bmatrix} r_1 \\ r_2 \\ r_3 \\ r_4 \end{Bmatrix} \qquad [3.16]$$

Equation [3.16] is a coupled first order differential equation of the form

$$\frac{d\mathbf{r}}{dx_3} = [\mathbf{A}]\mathbf{r} \qquad [3.17]$$

where $[\mathbf{A}]$ is an $n x n$ $(n = 4)$ matrix that depends on the layer parameters λ, G, ρ, ω and

$$\mathbf{r} = \mathbf{r}(x_3) = \begin{Bmatrix} r_1 \\ r_2 \\ r_3 \\ r_4 \end{Bmatrix} \qquad [3.18]$$

is a column vector giving the depth dependence of particle displacement and stress (referred to as the motion-stress vector) and is related to the displacements and stresses by the following relationship

$$e^{i(kx_1-\omega t)} = \begin{Bmatrix} u_1 \\ u_3 \\ \sigma_{31} \\ \sigma_{33} \end{Bmatrix} \qquad [3.19]$$

The next task is to solve the differential equation [3.17] with the following boundary conditions:

$$\begin{cases} \lim\limits_{x_3 \to \infty} r_1 = 0 \\ \lim\limits_{x_3 \to \infty} r_2 = 0 \end{cases} \qquad \text{for zero traction at the free surface and}$$

$$\begin{cases} r_3 = 0 \\ r_4 = 0 \end{cases} \qquad \text{for no motion at infinity (i.e. the radiation condition)}$$

Under the above boundary conditions, non-trivial solutions of equation [3.17] exist only for certain pairs of values of ω and k. In the next section, the matrix propagator method for solving this differential equation is described. For a stack of homogeneous layers overlying a half space, this method simplifies to the Haskell-Thomson matrix approach. The propagator approach is preferred because it is more general and hence can be applied to cases where material properties are not constant within a layer.

3.3.2 Love Wave Dispersion Function

The equations leading to the Love wave dispersion equation are similar to the Rayleigh wave development. Therefore only the relevant and particular equations are given below. The displacement field of Love waves may be represented by

$$\begin{Bmatrix} u_1 \\ u_2 \\ u_3 \end{Bmatrix} = \begin{Bmatrix} 0 \\ l_1 \\ 0 \end{Bmatrix} e^{i(kx_1 - \omega t)} \qquad [3.20]$$

where l_1 is a function of k, ω and x_3. The stress-displacement function is also given as

$$\begin{Bmatrix} \sigma_{11} \\ \sigma_{22} \\ \sigma_{33} \\ \sigma_{31} \\ \sigma_{23} \\ \sigma_{12} \end{Bmatrix} = \begin{Bmatrix} 0 \\ 0 \\ 0 \\ 0 \\ G\dfrac{dl_1}{dx_3} \\ iGkl_1 \end{Bmatrix} e^{i(kx_1-\omega t)} \tag{3.21}$$

The stress component σ_{23} is continuous at the interfaces and is therefore continuous with depth. This dependence on depth x_3 may be expressed as

$$\sigma_{23} = l_2 e^{i(kx_1-\omega t)} \tag{3.22}$$

where l_2 is a function of k, ω and x_3.

Comparison of [3.22] and [3.21] shows that

$$\frac{dl_1}{dx_3} = \frac{1}{G} l_2 \tag{3.23}$$

The equation of motion in the x_2-direction may be expressed in terms of l_1 and l_2 as

$$-\rho\omega^2 l_1 = G\left(\frac{d^2 l_1}{dx_3{}^2} - k^2 l_1\right) \tag{3.24}$$

into which [3.23] may be substituted to eliminate the second-order derivative to give

$$\frac{dl_2}{dx_3} = (k^2 G - \rho\omega^2) l_1 \tag{3.25}$$

Equations [3.23] and [3.25] may be written in matrix form as

$$\begin{Bmatrix} l_1 \\ l_2 \end{Bmatrix} = \begin{bmatrix} 0 & \dfrac{1}{G} \\ k^2 G - \rho\omega^2 & 0 \end{bmatrix} \begin{Bmatrix} l_1 \\ l_2 \end{Bmatrix} \tag{3.26}$$

which is of a similar form as the Rayleigh wave equation

$$\frac{d}{dx_3}(\ell) = \mathbf{A}\ell \qquad [3.27]$$

3.4 Solution by Propagator Matrix Method

Gilbert and Backus (1966) showed that the propagator matrix $\mathbf{P}(x_3, x_{3_0})$ defined by

$$\mathbf{P}(x_3, x_{3_0}) = \mathbf{I} + \int_{x_{3_0}}^{x_3} \mathbf{A}(\zeta_1) d\zeta_1 + \int_{z_0}^{z} \mathbf{A}(\zeta_1) \int_{z_0}^{\zeta_1} \mathbf{A}(\zeta_2) d\zeta_2 d\zeta_1 + \cdots\cdots \qquad [3.28]$$

where $\mathbf{I}$ is a unit matrix of order n is a solution of the differential equations [3.17] and [3.27]. For a stack of homogeneous layers shown in Figure 3.1, the matrix $\mathbf{A}$ is independent of depth x_3 and is therefore a constant for each layer. In this case, the propagator matrix takes the following form

$$\mathbf{P}(x_3, x_{3_0}) = \mathbf{I} + (x_3 - x_{3_0})\mathbf{A} + \tfrac{1}{2}(x_3 - x_{3_0})^2 \mathbf{A}\mathbf{A} + \cdots = e^{(x_3 - x_{3_0})\mathbf{A}} \qquad [3.29]$$

Hildebrand (1952) showed that any function of a square matrix $\mathbf{M}$ with distinct eigenvalues $m_k (k = 1, 2 \ldots, n)$ can be expanded by Sylvester's formula which is defined as

$$F(\mathbf{M}) = \sum_{k=1}^{n} F(m_k) \frac{\prod_{r \neq k} (\mathbf{M} - m_r \mathbf{I})}{\prod_{r \neq k} (m_k - m_r)} \qquad [3.30]$$

For Rayleigh waves, the eigenvalues (m) of matrix $\mathbf{A}$ may be shown to be given by

$$m \in \{\pm\gamma, \pm\upsilon\} \qquad [3.31]$$

where $\gamma = \sqrt{k^2 - \frac{\omega^2}{v_P^2}}$ and $\upsilon = \sqrt{k^2 - \frac{\omega^2}{v_S^2}}$

Substituting the matrix $\mathbf{A}$ and its eigenvalues into equation [3.30], the elements of the propagator matrix are found to be given by (Aki and Richards, 1980):

$$\mathbf{P} = \left\{ \begin{matrix} p_{11} & p_{12} & p_{13} & p_{14} \\ p_{21} & p_{22} & p_{23} & p_{24} \\ p_{31} & p_{11} & p_{33} & p_{34} \\ p_{41} & p_{42} & p_{43} & p_{44} \end{matrix} \right\} \qquad [3.32]$$

where

$$p_{11} = p_{33} = 1 + \tfrac{2G}{\omega^2\rho}[2k^2 \sinh^2 \tfrac{\gamma(x_3 - x_{3_0})}{2} - (k^2 + \upsilon^2)\sinh^2 \tfrac{\upsilon(x_3 - x_{3_0})}{2}] \qquad [3.33]$$

$$p_{12} = -p_{43} = \tfrac{kG}{\omega^2\rho}[(k^2 + \upsilon^2)\tfrac{\sinh \gamma(x_3 - x_{3_0})}{\gamma} - 2\upsilon \sinh \upsilon(x_3 - x_{3_0})] \qquad [3.34]$$

$$p_{13} = \tfrac{1}{\omega^2\rho}[k^2 \tfrac{\sinh \gamma(x_3 - x_{3_0})}{\gamma} - \upsilon \sinh \upsilon(x_3 - x_{3_0})] \qquad [3.35]$$

$$p_{14} = -p_{23} = \tfrac{2k}{\omega^2\rho}[\sinh^2 \tfrac{\gamma(x_3 - x_{3_0})}{2} - \sinh^2 \tfrac{\upsilon(x_3 - x_{3_0})}{2}] \qquad [3.36]$$

$$p_{21} = -p_{34} = \tfrac{kG}{\omega^2\rho}[(k^2 + \upsilon^2)\tfrac{\sinh \gamma(x_3 - x_{3_0})}{\gamma} - 2\gamma \sinh \gamma(x_3 - x_{3_0})] \qquad [3.37]$$

$$p_{22} = p_{44} = 1 + \tfrac{2G}{\omega^2\rho}[2k^2 \sinh^2 \tfrac{\upsilon(x_3 - x_{3_0})}{2} - (k^2 + \upsilon^2)\sinh^2 \tfrac{\gamma(x_3 - x_{3_0})}{2}] \qquad [3.38]$$

$$p_{24} = \tfrac{1}{\omega^2\rho}[k^2 \tfrac{\sinh \upsilon(x_3 - x_{3_0})}{\upsilon} - \gamma \sinh \gamma(x_3 - x_{3_0})] \qquad [3.39]$$

$$p_{31} = \tfrac{G^2}{\omega^2\rho}[4k^2 \gamma \sinh \gamma(x_3 - x_{3_0}) - (k^2 + \upsilon^2)^2 \tfrac{\sinh \upsilon(x_3 - x_{3_0})}{\upsilon}] \qquad [3.40]$$

$$p_{32} = -p_{41} = 2G^2(k^2 + \upsilon^2)p_{14} \qquad [3.41]$$

$$p_{42} = \tfrac{G^2}{\omega^2\rho}[4k^2 \upsilon \sinh \upsilon(x_3 - x_{3_0}) - (k^2 + \upsilon^2)^2 \tfrac{\sinh \gamma(x_3 - x_{3_0})}{\gamma}] \qquad [3.42]$$

It can be shown from the definition of the propagator matrix that

$$\mathbf{P}(x_{3_0}, x_{3_0}) = \mathbf{I} \qquad [3.43]$$

from which the relevant attribute of the propagator matrix emerges i.e.

$$\mathbf{f}(x_3) = \mathbf{P}(x_3, x_{3_0})\mathbf{f}(x_{3_0}) \qquad [3.44]$$

The right-hand side of equation [3.44] can also be shown to be a solution of the differential equations [3.17] and [3.27], and gives $\mathbf{f}(x_{3_0})$ at $x_3 = x_{3_0}$. The propagator matrix thus generates the motion-stress vector at x_3 by operating on the corresponding vector at x_{3_0} when both x_3 and x_{3_0} are in the same layer.

The propagator matrix $\mathbf{P}(x_3, x_{3_0})$ for $x_{3_k} < x_3 < x_{3_{k-1}}$ is found from

$$\mathbf{f}(x_3) = \mathbf{P}(x_3, x_{3_{k-1}})\mathbf{P}(x_{3_{k-1}}, x_{3_{k-2}})\cdots\mathbf{P}(x_{3_1}, x_{3_0})\mathbf{f}(x_{3_0}) = \mathbf{P}(x_3, x_{3_0})\mathbf{f}(x_{3_0}) \qquad [3.45]$$

and thus

$$\mathbf{P}(x_3, x_{3_0}) = e^{(x_3 - x_{3_k})\mathbf{A}_k} \prod_{l=1}^{k-1} e^{(x_{3_l} - x_{3_{l-1}})\mathbf{A}_l} \qquad [3.46]$$

The radiation boundary condition cannot be directly applied to the motion stress vector but may be applied to the magnitudes of downward and upward going waves in the underlying half space. Therefore the motion-stress vector has to be related to these waves, which may be represented by

$$\mathbf{w} = \begin{Bmatrix} P^{\setminus} \\ S^{\setminus} \\ P^{/} \\ S^{/} \end{Bmatrix} \qquad [3.47]$$

$$\begin{Bmatrix} r_1 \\ r_2 \\ r_3 \\ r_4 \end{Bmatrix} = \mathbf{F}\mathbf{w} = F \begin{Bmatrix} P^{\setminus} \\ S^{\setminus} \\ P^{/} \\ S^{/} \end{Bmatrix} \qquad [3.48]$$

where $\mathbf{F}$ is given as

$$\mathbf{F}=\frac{1}{\omega}\left\{\begin{bmatrix} v_p k & v_s \upsilon & v_p k & v_s v \\ v_p \gamma & v_s k & -v_p \gamma & -v_s k \\ -2v_p Gk\gamma & -v_s G(k^2+\upsilon^2) & 2v_p Gk\gamma & v_s G(k^2+\upsilon^2) \\ -v_p G(k^2+\upsilon^2) & -2v_s Gk\upsilon & -v_p G(k^2+\upsilon^2) & -2v_s Gk\upsilon \end{bmatrix}\begin{bmatrix} e^{-\gamma x_3} & 0 & 0 & 0 \\ 0 & e^{-\upsilon x_3} & 0 & 0 \\ 0 & 0 & e^{\gamma x_3} & 0 \\ 0 & 0 & 0 & e^{\upsilon x_3} \end{bmatrix}\right\}$$

[3.49]

F is a product of a matrix consisting of the eigenvectors of **A** and a diagonal matrix whose non-zero elements are the corresponding vertical phase factors. For surface waves, both eigenvectors are real and positive and hence all the elements of **F** are real numbers.

$$F^{-1}=\frac{v_s}{2v_p G\gamma\upsilon\omega}\left\{\begin{bmatrix} e^{\gamma x_3} & 0 & 0 & 0 \\ 0 & e^{\upsilon x_3} & 0 & 0 \\ 0 & 0 & e^{-\gamma x_3} & 0 \\ 0 & 0 & 0 & e^{-\upsilon x_3} \end{bmatrix}\begin{bmatrix} 2v_s Gk\gamma\upsilon & -\beta Gv(k^2+v^2) & -\beta kv & \beta\gamma v \\ -v_p G\gamma(k^2+\upsilon^2) & 2\alpha Gk\gamma v & \alpha\gamma v & -\alpha k\gamma \\ 2v_s Gk\gamma\upsilon & -\beta Gv(k^2+v^2) & \beta\gamma v & \beta\gamma v \\ -v_p G\gamma(k^2+\upsilon^2) & -2\alpha Gk\gamma v & -\alpha\gamma v & -\alpha k\gamma \end{bmatrix}\right\}$$

[3.50]

The amplitude of the upward and downward going waves in the half space can now be related to the motion stress vector at the free surface as follows:

$$\mathbf{w}_{n+1}=\mathbf{F}_{n+1}{}^{-1}\mathbf{r}_{n+1} \qquad [3.51]$$

$$=\mathbf{F}_{n+1}{}^{-1}\mathbf{r}_{n} \qquad [3.52]$$

$$=\mathbf{F}_{n+1}{}^{-1}\mathbf{P}(x_{3_n},x_{3_0})\mathbf{r}(x_{3_0}) \qquad [3.53]$$

i.e. $$\mathbf{w}_{n+1}=\mathbf{B}\mathbf{r}(x_{3_0}) \qquad [3.54]$$

where **B** is given by

$$\mathbf{B}=\mathbf{F}_{n+1}{}^{-1}\mathbf{P}(x_{3_n},x_{3_0}) \qquad [3.55]$$

The elements of matrix **B** are thus functions of the elastic parameters of the layers, the frequency and the wavenumber of the surface wave. On substituting the boundary conditions, equation [3.54] may be expressed as

$$\begin{Bmatrix} P_{n+1}{}^{\backslash} \\ S_{n+1}{}^{\backslash} \\ 0 \\ 0 \end{Bmatrix} = \begin{bmatrix} B_{11} & B_{12} & B_{13} & B_{14} \\ B_{21} & B_{22} & B_{23} & B_{24} \\ B_{31} & B_{32} & B_{33} & B_{34} \\ B_{41} & B_{42} & B_{43} & B_{44} \end{bmatrix} \begin{Bmatrix} r_1(x_{3_0}) \\ r_2(x_{3_0}) \\ 0 \\ 0 \end{Bmatrix} \qquad [3.56]$$

For a non-trivial solution of equation [3.56], the following the determinantal equation must be true.

$$\begin{vmatrix} B_{31} & B_{32} \\ B_{41} & B_{42} \end{vmatrix} = 0 \qquad [3.57]$$

Equation [3.57] is the dispersion equation to be solved for valid pairs of ω and k.

For the Love wave problem, the boundary conditions are

$l_2 = 0$ at $x_3 = 0$ (i.e. vanishing surface traction at the surface)

$\lim_{x_3 \to \infty} l_2 = 0$ (i.e. zero motion at infinite depth)

The solution to the differential equation is the same as that for Rayleigh waves. The eigenvalues (υ) in this case are given by

$$\upsilon = \pm\sqrt{k^2 - \frac{\omega^2}{v_s{}^2}} \qquad [3.58]$$

The corresponding propagator matrix, $\mathbf{P}(x_3, x_{3_0})$, is given by

$$\mathbf{P}(x_3, x_{3_0}) = e^{(x_3 - x_{3_0})\mathbf{A}} = \begin{bmatrix} \cosh \upsilon(x_3 - x_{3_0}) & \frac{1}{\upsilon G}\sinh \upsilon(x_3 - x_{3_0}) \\ \upsilon G \sinh \upsilon(x_3 - x_{3_0}) & \cosh \upsilon(x_3 - x_{3_0}) \end{bmatrix} \qquad [3.59]$$

The corresponding equivalents of matrix **F** and vector **w** for Love waves are given below.

$$\mathbf{F} = \begin{bmatrix} e^{-\upsilon(x_3 - x_{3_0})} & e^{\upsilon(x_3 - x_{3_0})} \\ -\upsilon G e^{-\upsilon(x_3 - x_{3_0})} & \upsilon G e^{\upsilon(x_3 - x_{3_0})} \end{bmatrix} \qquad [3.60]$$

$$\mathbf{w} = \begin{bmatrix} S^{\backslash} \\ S^{\prime} \end{bmatrix} \qquad [3.61]$$

The vector **w** may thus be expressed as

$$\mathbf{w} = \mathbf{F}^{-1}\boldsymbol{\ell}$$

which on application to the motion stess vector at $x_3 = x_{3_n}$ gives

$$\mathbf{w}_{n+1} = \mathbf{F}^{-1}\mathbf{P}(x_{3_n}, x_{3_0})\boldsymbol{\ell}(x_{3_0}) = \mathbf{B}\boldsymbol{\ell}(x_{3_0}) \qquad [3.62]$$

or

$$\begin{Bmatrix} S^{\backslash}_{n+1} \\ S^{\prime}_{n+1} \end{Bmatrix} = \begin{bmatrix} \mathbf{B}_{11} & \mathbf{B}_{12} \\ \mathbf{B}_{21} & \mathbf{B}_{22} \end{bmatrix} \begin{Bmatrix} l_1(x_{3_0}) \\ l_2(x_{3_0}) \end{Bmatrix} \qquad [3.63]$$

By applying the radiation and stress-free surface boundary conditions, equation [3.63] reduces to

$$\begin{Bmatrix} S^{\backslash}_{n+1} \\ 0 \end{Bmatrix} = \begin{bmatrix} \mathbf{B}_{11} & \mathbf{B}_{12} \\ \mathbf{B}_{21} & \mathbf{B}_{22} \end{bmatrix} \begin{Bmatrix} l_1(x_{3_0}) \\ 0 \end{Bmatrix} \qquad [3.64]$$

For a non-trivial solution of equation [3.64]

$$\mathbf{B}_{21} = 0 \qquad [3.65]$$

Equation [3.65] is the dispersion equation for Love waves.

Equations [3.57] and [3.64] have the form:

$$f(c, L, v_{P_1}, v_{S_1}, h_1, \rho_1, v_{P_2}, v_{S_2}, h_2, \rho_2, \ldots. v_{P_n}, v_{S_n}, h_n, \rho_n) = 0 \qquad [3.66]$$

and thus can only be solved numerically. The procedure used in solving the above dispersion equation for a given signal frequency ω_1 is as follows:

1. Assume a trial value of wavenumber, k

2. For the assumed values of ω_1 and k, calculate the appropriate determinantal equation for a given set of layer parameters.

3. Slightly perturb the value of k and minimize the value of the determinant.

4. Locate the value of k (say, k_1) at which the determinant is zero.

5. Calculate the corresponding phase velocity v_r $(\frac{\omega_1}{k_1})$.

6. Calculate the wavelength L $(= \frac{2\pi}{k_1})$

A number of pairs of values of v_r and L are found as described above. A plot of v_r against L is the desired dispersion curve.

In solving the determinantal equation, it is often possible to find a number of values of k (called roots of the equation) that satisfy the equation. These different roots constitute the various propagation modes. The root with the least magnitude is called the fundamental. The root just higher than the fundamental is called the first mode and so on. The root described above is the fundamental and hence it must be ensured that there are no smaller roots than the values of k_1.

A numerical difficulty that occurs at high Rayleigh wave frequencies (or short wavelengths) has been well documented by Dunkin (1965) and Schwab and Knopoff (1970). If extended precision (i.e. 16 decimal places) is enforced in dispersion computations, then this difficulty occurs when the following condition is approximately satisfied.

$$\frac{H}{L} = 3x10^{\frac{14.3-s}{12.4}} \qquad [3.67]$$

where H = depth to the half space

L = wavelength

s = desired number of significant figures in computed wave velocity.

The cause of this difficulty is in the evaluation of the matrix $\mathbf{B}$ which may be expressed as

$$\mathbf{B} = \mathbf{L}\Lambda\mathbf{R} \qquad [3.68]$$

where Λ is the matrix of phase factors (Λ) given by

$$\Lambda = \begin{bmatrix} e^{-\gamma x_3} & 0 & 0 & 0 \\ 0 & e^{-\nu x_3} & 0 & 0 \\ 0 & 0 & e^{\gamma x_3} & 0 \\ 0 & 0 & 0 & e^{\nu x_3} \end{bmatrix} \qquad [3.69]$$

At large values of $\frac{H}{L}$, some diagonal elements in the above matrix become very large. The evaluation of certain expressions in the determinantal equation [3.57] such as

$$e^{2\gamma x_3}(l_{33}r_{31}l_{43}r_{32} - l_{43}r_{31}l_{33}r_{32}) \qquad [3.70]$$

which should be zero, results in finding the difference of very large numbers. This difference will yield a small number and if the factor $e^{2\gamma x_3}$ is large, the product becomes large as well and cause a loss in significant figures. This difficulty led to the various forms of the Haskell (1953) -Thomson(1950) matrix method. This technique constructs the dispersion function by building layer matrices that relate components of the motion stress vector at one interface to the next interface, beginning from the interface with the half space. The product of all the layer matrices then relates the motion stress vectors at the surface and within the half space. Dunkin (1965), Thrower (1965) and Watson (1970) developed modifications of the original formulation that overcame the precision problem. These modifications are generally referred to as delta-matrix methods, of which the fastest and most efficient is the formulation by Watson (1970).

The alternative algorithm for computing the dispersion function was proposed by Knopoff (1964) and did not contain the numerical difficulty in the Thomson-Haskell method (Schwab, 1970). In this method, the full determinantal form of the dispersion function is constructed before it is decomposed into sub-matrices that relates the motion stress vectors of adjacent layers. Knopoff's method overcomes the precision control error by a technique called the layer reduction method in which the lower part of the layered structure is replaced by a half-space at increasingly shallower depths for waves of higher frequency. Randall (1967) developed a computer program for calculating the dispersion function based on Knopoff's method and showed the validity of the approach. Schwab (1970) made a pair of modifications to Knopoff's algorithm that increased computation speed. These modifications were the elimination of complex arithmetic and the prior evaluation of certain expressions in that determinant that were identically zero. This modified version is referred to as the '"fast" form of Knopoff's method.

A review of all the methods for computing the surface wave dispersion function was presented by Schwab and Knopoff (1970). Their findings, shown in Table 1, indicate that the fast form of Knopoff's method is by far the fastest of all the tested methods. Knopoff's method was therefore used in this study computing the value of the determinant, primarily because it was the fastest (Schwab , 1970).

In practice, it is required to calculate a set of layer parameters that will produce a dispersion curve identical to an experimentally determined curve. In this case, the various values of ω for which k_1 values must be found are those of the experimental dispersion curve. In almost all cases, the set of initially calculated v_r values will not match the experimental velocities. When this happens, the elastic parameters of the layers must be adjusted and the calculations repeated until the calculated and experimental dispersion curves match to a desired degree. The difficulty with this approach is that unless one is knowledgeable in dispersion computations, it is not readily obvious from the dispersion curve misfit, which parameters to change, whether to decrease or increase the selected parameters and by how much.

In the next section, a procedure to automatically adjust the layer parameters until a fit is achieved is described.

3.5 Matching Dispersion Curves

The technique of dispersion curve matching by iteratively updating the preceding guess until computed and experimental dispersion curves match according to a least square measure of fit was probably first adopted by Dorman and Ewing (1962). If the parameter updates are small, then at each iteration linearity may be assumed and function perturbations are obtainable via a linear relationship or constant increments..

The process of matching theoretical and experimental dispersion curves is one of optimization. For an assumed set of layer parameters $(h_i,\rho_i,v_{p_i},v_{s_i},)$, a set of theoretical dispersion points (L_i,v_{T_i}) is calculated and compared with an experimentally determined set (L_i,v_{E_i}). The layer parameters are adjusted until the two sets of points match according to a given figure-of-merit-function. This matching requirement may be expressed as the minimization of the differences between the corresponding magnitudes of phase velocities. If the sum of least squares is chosen as the merit function, then the matching process reduces to minimizing the following residual.

$$\sum_{i=1}^{n}(v_{T_i}(h_k,\rho_k,v_{p_k},v_{s_k})-v_{E_i})^2 \qquad [3.71]$$

where n = number of dispersion points,

k = layer number,

v_{T_i} = theoretical phase velocity at wavelength L_i,

v_{E_i} = experimental phase velocity at the same wavelength L_i.

After minimizing the sum of least squares, the goodness of fit of the parameters needs to be estimated. Thus the process of matching dispersion curves involves the estimation of best-fit parameters, error estimates on the parameters and a statistical measure of the goodness-of-fit. In this section, a procedure for matching theoretical and experimental curves is described. The sum of least square criterion is used as a merit function and the simplex algorithm for function minimization.

3.5.1 The simplex algorithm

A simplex is a geometrical figure with one more vertex than the dimension of the space in which it is defined. Examples of simplices are a triangle in a two-dimensional space and a tetrahedron in a three-dimensional space. If the number of layer parameters to be optimized is m, then the algorithm calculates the residuals at m assumed points. Each of the assumed points therefore has $m+1$ coordinate directions - m of which represent each of the parameters to be optimized and the last is the residual at that point. A plot of the residuals against the corresponding points produces an $m+1$ response surface, which is therefore a simplex in the factor-space.

Let the m points be represented by P_j,and the residual at P_j be represented by y_j. The residuals y_j are then ranked in order of magnitude. Let the point with the highest residual y_{i_H} be P_H and the point with the lowest residual y_{i_L} be P_L. Furthermore, let $\overline{P}$ be the centroid of all points except P_H and $[P_M P_K]$ be the distance between any points P_M and P_K. At each stage of the minimization process, the objective is to find the point with the highest residual and replace it with a new point with a smaller residual by three main operations called reflection, contraction and expansion.

The reflection of P_H gives a point P^* whose coordinates are obtained from the coordinates of P_H by the following relationship

$$P^* = (1+\alpha)\overline{P} - \alpha P_H \qquad [3.72]$$

where α is positive constant called the reflection coefficient and is typically assumed to be 1.0. P^* is thus located on the line segment between $\overline{P}$ and P_H but on the other side of the hyperplane containing all points but opposite P_H. If α is assumed to be 1.0, then

$$\left[P^*\overline{P}\right] = \alpha\left[P_H\overline{P}\right] = \left[P_H\overline{P}\right] \qquad [3.73]$$

The residual (y^*) is then calculated at P^*. If $y_{i_L} < y^* < y_{i_H}$, then the reflection operation produced a new minimum (i.e. a better point) and so P_H. is replaced by P^*. If $y^* < y_{i_L}$, then a new point P^{**} is then calculated from P^* by an expansion operation defined as.

$$P^{**} = \gamma P^* + (1-\gamma)\overline{P} \qquad [3.74]$$

where γ is an expansion coefficient greater than unity and is defined as

$$\gamma = \frac{P^{**}\overline{P}}{P^*\overline{P}} \qquad [3.75]$$

If the residual (y^{**}) at P^{**} is such that $y^{**} < y_{i_L}$, then P_H is replaced with P^{**}. and the process is restarted. However, if $y^{**} > y_{i_L}$, then P_H is replaced with P^* before restarting the process.

If P^* is such that $y^* > y_i$ for all values of y_i where $i \neq H$,, then whichever of y_H and y_{i_H} is smaller becomes the new P_H. In this case, the next step is to contract the new P_H by the following formula

$$P^{**} = \beta P_H + (1-\beta)\overline{P} \qquad [3.76]$$

where β is a contraction coefficient with a value between 0 and 1. The value of β is given by

$$\beta = \frac{P^{**}\overline{P}}{P^{*}\overline{P}} \qquad [3.77]$$

P_H is then replaced with P^{**} and the process restarted unless $y^{**} > \min(y^*, y_{i_H})$ which means that the contracted is worse than the better of the y_{i_H} and y^*. For this failed contraction, all P_j's (except P_L) are replaced by new ones using the following formula before restarting the process.

$$P_j = \frac{P_j + P_L}{2} \qquad [3.78]$$

The flow chart of the above algorithm is shown in Figure 3.2 and details of the algorithm are given by Nelder and Mead (1965).

The criterion for halting iterations is based on the magnitude of the standard error (calculated as shown in the following equation) exceeding a specified minimum.

$$\varepsilon = \sqrt{\frac{\sum (y_i - \overline{y})^2}{n}} \qquad [3.79]$$

In the above equation, n is the number of points and $y_i - \overline{y}$ is the difference between calculated and measured functional values.

The incidence of false convergence is a problem found in almost all minimization routines. In the simplex algorithm, false convergence may occur if the response surface has long curved valleys with steep sides. Under such circumstances, the convergence criterion recommended by Powell (1964) may be used to reduce the possibility of false convergence This complex convergence criterion requires perturbing the first minimum found and repeating the method to find a second minimum, followed by exploration along the line segment joining the two mininma.

The simplex method is simple as it does not require derivatives of any order or numerical integration. This allows discontinuous functions to be optimized and also minimizes round-off error incurred in calculating derivatives. However, it is not as fast as other sophisticated algorithms such as Powell's (1964) method. The objective in this work was to demonstrate that the process of dispersion curve matching can be computerized. Further research is required to incorporate a faster optimization scheme.

3.6 Program SASW-FM

SASW-FM (stands for Spectral Analysis of Surface Wave -Forward Modelling) is a computer program for calculating a theoretical dispersion curve that matches a given in-situ curve. The program is written in C but short portions of the code are in assembly language for processing speed.

The following inputs are required by the program SWAGE-FM and must be stored in an ASCII text file in the order given in Appendix 3.1.

1. The type of wave (Rayleigh or Love)

2. The height of water on the ground surface, if inundated.

3. Maximum number of iterations

4. Number of parameters to be optimized

5. Number of coordinates per dispersion point (=2 for a two dimensional dispersion curve).

6. Number of measured dispersion points.

7. The Poisson's ratio of all layers including the half space, starting from the surface.

8. The mass density (kg/m^3) of all layers including the half space, starting from the surface.

9. The magnitudes of the parameters to be optimized (i.e. the assumed thicknesses of all layers excluding the half space and the assumed shear wave velocity of all layers including the half space). The layer thicknesses must precede the shear wave velocities.

10. The allowable change per iteration in the parameters to be optimized, expressed as a fraction of the magnitude of the corresponding parameter.

11. The maximum allowable error in the parameters to be optimized. The preset value of the standard error for halting the iterations must be appended as the last allowable error.

12. The measured dispersion points, one point per line.

The sequence of operations in SASW-FM after the inputs are read may be summarized as follows:

1. The initial guess of shear-wave velocity and thickness for each layer may be made from the experimental dispersion curve using the simple-axis transformation procedure from steady vibration analysis i.e.

$$v_S = 1.1v_R \qquad [3.80]$$

$$z = 0.5L \qquad [3.81]$$

2. Values of mass density and Poisson's ratio for each layer are estimated and compressional wave velocity is calculated from the theory of elasticity using.

$$v_p = v_s\sqrt{\frac{1-\upsilon}{\frac{1}{2}-\upsilon}} \qquad [3.82]$$

3. The determinantal equation is then computed for the profile at an experimentally measured wavelength using the fast form of Knopoff's method, the only unknown being the phase velocity (c).
4. The principles of the intermediate-value theorem are used to bracket the minimum value of c and Brent's (1973) algorithm to calculate the root.
5. Steps 3 and 4 are repeated for each experimentally measured wavelength. Corresponding wavelengths and phase velocities are plotted to give the theoretical dispersion curve.
6. Using Nelder and Mead's (1965) simplex algorithm and a least-squares-criterion, the parameters of the model are adjusted until a set of best-fit parameters are found for which wavelengths and phase velocities match the experimental relationship to a predetermined accuracy.

For most soil structures, the dispersion function is insensitive to Poisson's ratio, mass density and compressional wave velocity (Dorman and Ewing, 1962). The reason is partly because only ratios of mass density appear in the function. For most soils, this ratio is almost always less than 2 and Poisson's ratio is always positive but less than 0.5. In relation to the very large numbers in the dispersion function, this insensitivity is not surprising. The insensitivity to the P-wave velocity may be due to its narrow range around an average value of1500 m/s for most saturated soils.

A sample output of the program is shown in Appendix II.1. The best-fit layer thicknesses and shear wave velocities, the experimental and fitted dispersion points and the standard error (which indicates the goodness of fit) are shown. The standard deviation refers to the distribution of the coordinates of the vertices of the final simplex.

To ensure that program SASW-FM was producing correct results, a set of three synthetic profiles (provided by Professor Stokoe of the University of Texas at Austin) were tested. The three cases comprise a single layer on a stiffer half-space, a single layer on a softer half space and a stiff sandwich layer between a softer upper layer and a lower half space. The results of these benchmark tests, presented in Appendix II.3, show that SASW-FM produced the expected results in all three cases.

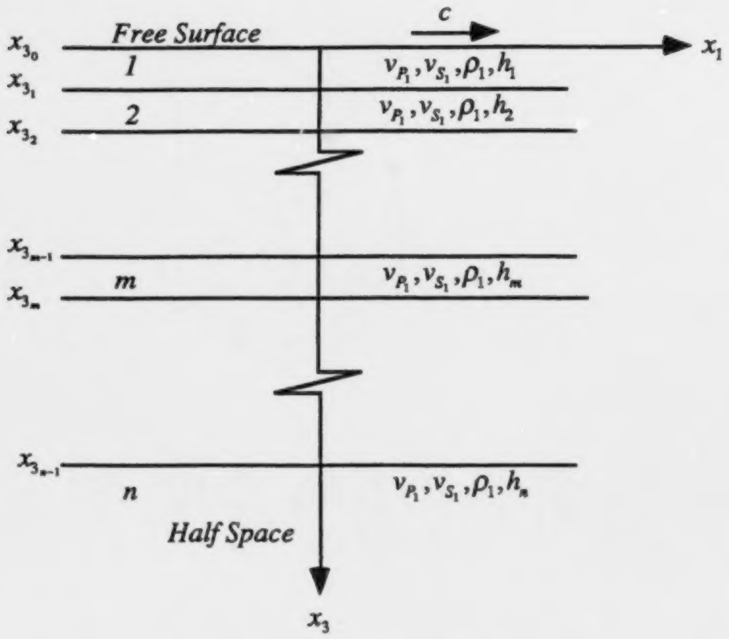
c
x_{3_0}
Free Surface
x_1
1
$v_{P_1}, v_{S_1}, \rho_1, h_1$
x_{3_1}
2
$v_{P_1}, v_{S_1}, \rho_1, h_2$
x_{3_2}
$x_{3_{m-1}}$
m
$v_{P_1}, v_{S_1}, \rho_1, h_m$
x_{3_m}
$x_{3_{n-1}}$
n
$v_{P_1}, v_{S_1}, \rho_1, h_n$
Half Space
x_3

Figure 3.1. The Homogeneous Layer Model

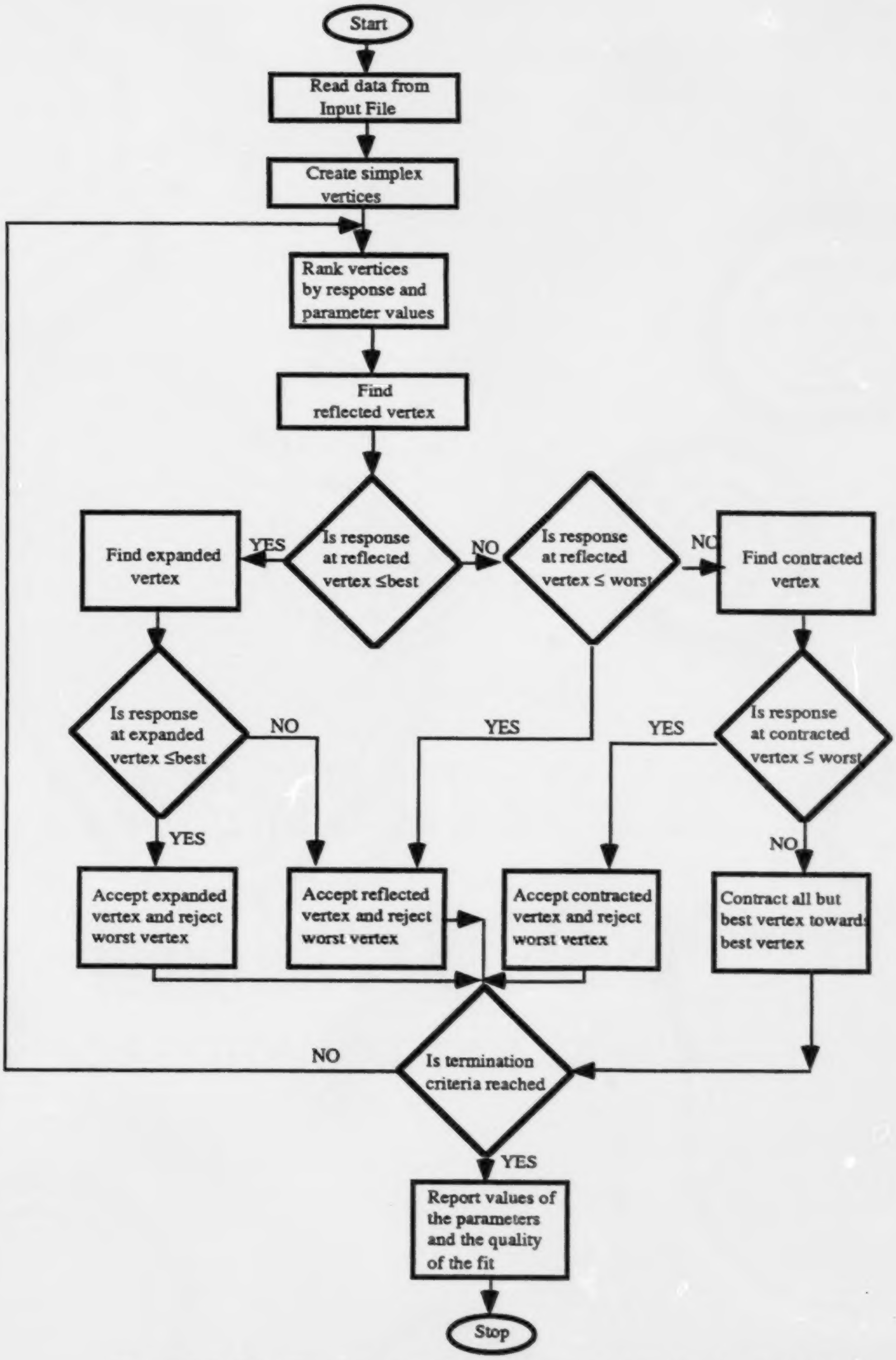
Start
Read data from Input File
Create simplex vertices
Rank vertices by response and parameter values
Find reflected vertex
Is response at reflected vertex ≤best
YES
Find expanded vertex
NO
Is response at reflected vertex ≤ worst
NO
Find contracted vertex
Is response at expanded vertex ≤best
NO
YES
YES
YES
Is response at contracted vertex ≤ worst
NO
Accept expanded vertex and reject worst vertex
Accept reflected vertex and reject worst vertex
Accept contracted vertex and reject worst vertex
Contract all but best vertex towards best vertex
NO
Is termination criteria reached
YES
Report values of the parameters and the quality of the fit
Stop

Figure 3.2. The Simplex Algorithm (After Caceci and Cacheris, 1984).

Table 3.1. Time Estimates for Rayleigh Wave Dispersion Computations
(After Schwab and Knopoff, 1970)

TECHNIQUE	VERSION	RELATIVE COMPUTATION TIME	LOSS OF PRECISION CONTROL FEATURE
Thomson-Haskell	Original "Fast" Form	1.12	No
	Original form for computing layer matrix products	1.4	No
	Reduced-δ-matrix form	1.38	Yes
	δ–matrix form	1.47	Yes
Knopoff	"Fast" Form	1.00	Yes
	Analog of reduced-δ-matrix form	1.38	Yes
	Analog of δ-matrix form	1.47	Yes

CHAPTER FOUR

EQUIPMENT DEVELOPMENT AND FIELD TESTING

4.1 Introduction

The field procedure and equipment developed at the University of Alberta for performing SASW testing are described in this chapter. The system uses a microcomputer to acquire and analyze surface wave data in the field. The details of the computer programs for analyzing signals and forward modelling were respectively discussed in Chapters Two and Three. In this chapter only the hardware implementation is described, followed by the testing procedure used in the field.

4.2 Equipment Development

4.2.1 Energy Sources

Since the type of signal generated influences how the signal is detected, processed and analyzed, it seems appropriate to review the possible types that can be generated by available energy source. Randall, 1977 presented the schematic classification of signals in which the basic categories were stationary and non-stationary.

Stationary signals are such that their average properties are independent of time and the length of sample record. Such signals may be either deterministic (i.e. the signal amplitude at any time can be predicted) or random (i.e. only statistical characteristics are predictable). Random signals have a continuously-distributed spectrum but deterministic signals consist of only sinusoids at discrete frequencies and are further subdivided into periodic and quasi-periodic signals. The frequencies in a periodic signal are harmonics (or integer multiples) of a specific fundamental frequency whereas the frequencies in a quasi-periodic signal are not harmonics. Any signal that does not satisfy the criteria for stationary type may be described as non-stationary and may be divided into continuous and transient signals. A transient signal is one that has initial and final amplitudes of zero, whereas a continuous non-stationary signal is one that is considerably longer than the duration of interest.

The energy required to generate surface waves may be produced from an impact, explosive or vibration. The desired characteristics of appropriate energy sources are repeatability, directionality, low-noise content (or body wave content) and a wide frequency bandwidth of sufficient amplitude. A wide range of sources have been used for surface wave generation (Woods, 1978). Included in the list are drop weights, to-and-fro track-motion, hand-held hammers, SPT (Standard Penetration Test) hammers, gas guns, water cannons and more complicated mechanical systems. Nazarian (1984) used mechanical sources of different weights varying from a 56 g chisel to a 140-lb SPT hammer.

A set of hammers with weights varying from 0.5 to 20 LB were used in this research. In general, the heavier the hammer, the lower the frequencies generated. All hammers were instrumented with an accelerometer for pretriggering purposes. The signals generated at direct impact of these hammers with the testing surfaces often did not contain high or low enough frequencies to sample material at very shallow or deep depths. This problem was somehow overcome by indirect hammer impacts on steel, wooden, rubber or stone pads laid on the testing surface. Such a generation technique results in transient non-stationary signals. A pretrigger is therefore required in order to measure the entire signal. A pretriggering mechanism is built into the system developed in this research and is described in a later section. If pretriggering is unavailable, then special windowing techniques have to be employed to minimize leakage in the frequency domain. This is the case when triggering is based on one of a pair of receivers in the SASW test.

A better and more reliable but initially expensive alternative is to use an electromagnetic vibrator with a wide force capacity range and a built-in programmable interface (e.g. General Purpose Interface Bus (GPIB) or RS-232/422). Such a vibrator can be controlled from the microcomputer to step sequentially through a predetermined set of desired frequencies that may not all be available with impact systems. For the SASW system used in this research, vibrator interfacing can be implemented at no extra cost since the direct memory access (DMA) card installed in the microcomputer is equipped with GPIB control features. This feature is built into most modern spectrum analyzers. The added advantage is that such a vibrator would not only reduce personnel required to perform the test from to two to one but also enhance testing speed and signal repeatability, a saving and improvement that would eventually be justified.

Abbiss and Ashby (1986) used background noise in a seismic test to determine ground moduli with some success.

4.2.2 Receivers

Amplitudes of particle motion due to the propagation of elastic waves could be as small as $0.4x10^{-9}$ mm (Gardner, 1938) and vary over a wide dynamic range of about 100 dB. Wave motion detectors therefore need not only comply with a high-sensitivity requirement but also cover a wide dynamic range. Detectors must also have a repeatable frequency response within the expected operational range and cause the least phase distortion to the signal. The three basic types of motion detectors are acceleration, velocity and displacement sensors.

Acceleration transducers or accelerometers, as the name connotes, detect motion by measuring accelerations. Among the principlea of operation commonly used in accelerometer design is the phenomenon of piezoelectricity. A piezoelectric material is one that develops an electric charge when subjected to stress (and consequent deformation). Examples of piezoelectric materials are quartz, Rochelle salt or artificially polarized ferroelectric ceramics from compounds such as barium titanate, lead zirconate and lead metaniobate. If an elastic wave impinges on a quartz crystal, the induced deformation generates electric charges on its surfaces to oppose the disturbance. The surface charges in turn produce a voltage signal dependent on the acceleration of the disturbance. A schematic sketch of an accelerometer construction is shown in Figure 4.1. The ratio of the voltage or charge output to the input acceleration is referred to as the sensitivity of the accelerometer. Accelerometers are useful over a wide range of frequencies (1 to 20,000 Hz) and temperature. They are also rugged and operate fairly well under severe conditions due to their solid state construction. They also tend to have high natural frequencies and perform well in this range. As a result of their small sizes, a requirement for closely-spaced measurements and a fairly frequency-independent response over a wide range. Nazarian (1984) reported better results when testing with accelerometers than other receivers. According to Nazarian (1984), the reason for this observation was that accelerometers tend to suppress the level of environmental noise.

Velocity sensors or geophones are instruments which produce an electrical output proportional to the magnitude of motion of the surface onto which they are mounted and are either electromagnetic or piezoelectric in nature. The electromagnetic geophone operates on the principle of voltage generation as a result of differential movement of a coil suspended in a permanent magnetic field (see Figure 4.2). The ratio of the electrical output of a geophone to the mechanical input is known as its transductivity and depends on the strength of the magnetic field, the number of turns in the coil and the relative velocity of the coil with respect to the magnet.

In operation, the coil of a geophone continues to oscillate long after the causative motion has subsided. In practice, the motion of the coil is attenuated by winding it on a metal former and/or by resistors shunted across the terminal of the geophone. The degree of damping (called a damping ratio and expressed as percentage of the critical) influences the amplitude and phase responses which are often displayed in specification curves for the particular geophone. Over-damping reduces detection sensitivity while insufficient damping accentuates oscillation after the particle motion has subsided. Traditionally, about 70% damping of the critical value is accepted as optimum for most purposes. It is not advisable to use a geophone for the detection of signals with frequencies lower than the natural frequency since the response is considerably reduced and the transductivity may not be constant in this range. It is often directional and must be oriented along the axis of maximum sensitivity. Specially designed geophones have also been used for sensing motion in three perpendicular directions.

Hydrophones are used in water-covered areas for detecting seismic waves. Unlike geophones, they are insensitive to movements but respond to changes in water pressure caused by an impact. Thus, they are less disturbed by turbulent flows in rapids. The principle of operation is similar to the geophone except that the generated voltage is dependent on the pressure changes.

The magnitude of a signal detected at a receiver station depends on the characteristics of the source, the elastic properties of the propagation medium and the impulse response of the recording instruments. Some transducers, especially accelerometers, have high electrical impedance and produce low-power signals that are rapidly dissipated. Preamplifiers may be therefore have to be fitted to adjust these characteristics or to compensate for non-standard transducer sensitivity by conditioning the signal to a reference sensitivity. By incorporating integration networks into such accelerometers, velocity and displacement can be measured from the acceleration signal.

The characteristics of the geophones used in this research are shown in Table 4.1 The properties of the geophones with serial numbers 8626, 8627 and 8628 have similar electrodynamic or transductivity constants and were used for the most part of the field testing.

4.2.3 Source-Receiver Configuration.

Two main arrangements of source and receivers are used in SASW testing. These are the common receiver midpoint and common source configurations. The common receiver midpoint (or CRMP) geometry is a source-receiver configuration in which two receivers are always equidistant from an imaginary centerline. The source is placed in line with the receivers and the distance to the nearer receiver is the same as the receiver spacing. This arrangement is shown in Figure 4.2(a). The common source (CS) configuration is shown in Figure 4.2(b). In this arrangement, the locations of the source and one receiver remain unchanged during the test. The second receiver is moved further away from the other receiver for a new test. For speed and less work, the CS configuration is better since only one receiver has to be coupled for additional spacings. For offshore work, however, the CS method appears to be more attractive since one receiver is more readily moved and positioned than the all the receivers and the source.

The common source and common receiver midpoint configurations are direct consequences of the traditional use of a dual channel spectrum analyzer. For a long time, these instruments had only two channels and hence the number of receivers was restricted. Though modern signal analyzers have more than two channels, the cost is proportionally higher and are uneconomical for use in only SASW testing. The use of a microcomputer for data acquisition removes this restriction. Any number of channels may be used, depending on the speed of the analogue-to-digital converter installed in the computer. With this flexibility, almost all the spacings shown for either CS or CRMP configurations can be tested with s single array. The result is a much shorter testing time and costs.

The distance between the source and near receiver depends on factors such as the minimum distance required for Rayleigh waves to be fully established, the attenuation characteristics of the medium between the source and receiver, the distance required for body wave amplitudes to be sufficiently attenuated and the amplitude level of the source signal. Based on theoretical studies, Lysmer (1968) indicated that, at a distance of two and a half wavelengths from the source, surface waveforms are virtually fully established. The spacing of the geophones or the distance from source to the far-receiver also depends on the above factors but largely on the signal amplitude. Based on experimental studies, Heisey (1981) recommended that the receiver spacing be made equal to the source-near receiver distance. This recommendation was the result of the observation that data from this configuration were least noisy and has since been unofficially incorporated into the SASW test procedure.

For a frequency range of 2-3 kHz and a source-near receiver distance several times the inter-receiver spacing, Nazarian (1984) obtained low coherence values. It appears that at far distances from the source, low coherence values may be due to the fact that background noise may be of the same order of magnitude as the signal amplitudes. Thus there is a need to correlate the source-near receiver distance with the strength of the source and the attenuation characteristics of the intervening medium.

Heisey (1981) concluded that material velocity, sampling depth, frequency range, substructural damping characteristics and equipment sensitivity determine receiver spacing, for which an optimum spacing between a half and three wavelengths was recommended. Nazarian (1984) pointed out that since substrata velocities are initially unknown, the said range cannot be employed prior to testing. The latter author then recommended that various spacings be used in the field to determine wavelengths and velocities and thereafter ignore spacings that do not satisfy Heisey's criterion. However, an inherent error exists in using prospective rejectable spacings to compute criteria that would be used in discriminating against the same spacings. This approach could also be excessively wasteful and needs refinement.

4.2.4 Receiver Coupling

Receiver coupling is the process of ensuring that receivers are properly bonded to the test surface such that both move in unison. Improper coupling, often the cause of a large number of errors that are often attributed to background noise, results in the measurement of distorted signal amplitudes. Coupling methods include resting on the test surface, bonding to the surface, slight pushing into the surface, nailing and embedding flush with the surface. The type of coupling used depends on the nature of the test surface and on the characteristics of the receiver. Surface resting is suitable for receivers that are relatively heavy. The test surface has to be relatively level for this type of coupling and even in that case response to low signal levels would be poor. Most receivers generally require some form of bonding, Examples of bonding agents are which are honey, plaster of Paris and phenyl salicyclate. Receivers with spiked bases may be readily pushed into soft test surfaces.

The geophones used in this research had flat bases and had to be bonded to the test surface. The choice of flat geophone bases was due to planned field work in the winter, when the frozen surface cannot be penetrated by spike-based receivers. Dry ice was primarily used as a bonding agent and was found to give strong bonding that was easily broken with a gentle horizontal tap. The geophones weighed a little over 1 kg and hence the self weight also enhanced the coupling.

The type of wave to be detected by the receivers also influences the degree of coupling. On the test surface, Rayleigh waves induce particle displacements that are largely vertical. Such particle displacements are readily picked up, compared with horizontal displacements due to Love waves. The horizontal polarization of Love waves is one of the many disincentives for their use in SASW and other tests.

4.2.5 Signal Acquisition and Recording

The electrical voltage or charge transformed from mechanical energy of the source is transmitted by cables to recording unit. Traditionally, this unit is a spectrum analyzer, a photographic film or a magnetic tape where the signals are amplified if necessary, before they are recorded. The set-up of the microcomputer was used for signal acquisition is described below.

The Apple Macintosh computer, model IIcx was selected for purpose. The choice of a Macintosh microcomputer was based on its user-friendly interface and the high graphics capabilities. Secondly, LabVIEW was only available on the Apple Macintosh. LabVIEW (stands for **Lab**oratory **V**irtual **I**nstrument **E**ngineering **W**indow) is an iconic programming environment for developing applications by creating on-screen control panels to emulate test instruments data acquisition and analysis. The Model IIcx was acquired because of its suitable combination of cost, relatively small size and the fact that it was near the high end of technology in 1988 when this research began. Faster computers are available that may be more advantageous in a lot of other ways than processing speed.

Installed in the computer are a direct memory access (DMA) card and a data acquisition (A/D) card. The purpose of the DMA is to assist the central processing unit (CPU) with the handling of data once it has been digitized. This makes the CPU available for faster rates of acquisition which is performed by the A/D card. The models of the A/D and DMA cards are NB-MIO-16-9 and NB-DMA-8-G, both of which are manufactured by National Instruments. Within the computer, the two cards are connected via a 50 pin RTSI cable. The A/D card has a maximum sampling rate of 100 kHz , a maximum of 8 channels for differential and 16 channels for single ended inputs. For most soil sites, this means that an array of four receivers can be used at sampling rates of over 20 kHz. Generally frequencies of less than 1 kHz are required in soil investigations and hence a longer receiver array can be used.

The interface between the geophones and the microcomputer is provided in a small locally–made box, 150 x 100 x100 mm which is given a generic name "interface control unit" (ICU). The circuit diagram of the board in the ICU is shown in Figure 4.3. The ICU is a locally-made housing unit containing circuits for external triggering, filtering and interface connections, directly or indirectly, from the receivers as well as a provision for remotely discriminating between waveform data by the push of a button. The inputs into the ICU are signals from the receivers and an accelerometer attached to the hammer source. The ICU is connected via a 50-pin ribbon cable to the A/D card. If a generated signal satisfies the minimum trigger conditions, an LED is lit and data acquisition is initiated on the A/D card. The level and slope of the trigger signal is adjustable.

A provision for incorporating an anti -aliasing filter in the ICU circuit was not implemented for time reasons. As a result, a special purpose anti-alias filter processed the signal before entering the ICU. It is recommended that the design and construction of the

ICU be improved and completed by incorporating anti-alias filters for each of the four channels on the ICU. The number of channels could also be increased to eight.

4.2.6. Equipment Assembly

Figure 4.4 shows a schematic set-up of the field equipment. The microcomputer is connected via the interface control unit (ICU) to a filter, into which leads from a maximum array of four receivers may be connected. The NB MIO 16 and DMA-8-G cards are installed in slots 2 and 3 of the microcomputer. Slot 1 contains the high resolution graphics card. Also shown in the same figure is an instrumented hammer for surface wave generation.

An existing desk was modified for mounting and securing the computer, ICU and other accessories. The desk is designed that it can be pushed into the back of a middle-sized van. For safety during transportation, the mounting desk is equipped with fasteners for securing the computer and its accessories. The computer may be powered by a portable generator or may run off the battery of the transporting vehicle. Due to signal disturbances from the tires of a running vehicle, it is preferable to use generators, from which the signals are conditioned for constant output voltage.

4.3 Site Selection.

The following locations in western Canada were selected for field testing:

1. University LRT Station, Edmonton, Alberta

2. NAIT Experimental Test Site, Edmonton, Alberta
3. Ricmond Dykes at Blundell Road, Richmond, B.C.
4. Richmond Dykes at Francis Road, Richmond, B.C.
5. Richmond Dykes at Chatham Road, Richmond, B.C.
6. Sea Island Site, Vancouver, B.C.
7. Burnaby Site, Burnaby, B.C.
8. Annacis Site, Annacis Island, B.C.
9. Delta Site, Delta, B.C.
10. Matsqui Site

The above sites were selected in conjunction with ConeTec Investigations Limited (an in-situ testing company based in Vancouver). The selection criteria included availability of shear wave velocity profiles from recent seismic cone penetration tests and site accessibility. Most of the selected sites were in British Columbia where the various stratigraphies were not known.

As the primary reason for field testing was to evaluate the developed SASW equipment and computer programs for analysis, results of SCPT tests were not made available until forward modelling was completed. In Chapter Five, the SASW data obtained in the field at all the above sites will be discussed and compared with SCPT data.

4.4 Field Procedure

Two geophones were used for testing at all the sites. However at one of the sites, an array of four geophones were also used to obtain thllhhe shear wave velocity profile. The procedure for testing was the same for all sites and may be itemized as follows:

1. Two perpendicular lines are demarcated with ropes and pegged at each end. The length of the lines are approximately twice as long as the maximum spacing anticipated at the site. The purpose of these lines are to guide the positioning of the geophones, which must be collinear, from test to test. The generator is then powered on. Free running of the generator allows the voltage to stabilize before any power is drawn from it.

2. The location at one end of one of the lines is selected as the impact point. The following distances in metres are then measured and identified along the line :12.0, 10.0, 8.0, 6.0, 5.0, 4.5, 4.0, 3.5, 3.0, 2.5, 2.0, 1.5, 1.0, 0.5 and 0.2. These locations are the positions of one of the geophones during the test. One receiver is fixed at the origin of measurement.

3. Beginning with the largest receiver spacing, dry ice is used to couple the geophones to the ground surface. The reason for starting with the larger spacing is that hammer impacts disturb surfaces that are outside the range of subsequent spacings.

4. While the geophones bond to the surface, the data acquisition system is powered on. The procedure described in Chapter 2 for estimating the highest test frequency is used to calculate the highest frequency for the site. The inputs for SASW-DA are then entered as they are requested for.

6. Trial tests are conducted to find the noisiness in the signals due to the background and to ascertain how hard to hit the ground in order to obtain reasonable amplitudes. If the signals are found to be noisy, and this is usually the case, the number of averages required to substantially reduce the noise level is determined. The number of signals required averaged between 5 and 30. The trials tests are also used to establish communication signs between the hammer and computer operators. This is helpful and saves a lot of walking back and forth since the testing vehicle is usually about 10-15 metres from the source location.

7. The actual test is then started by a hammer impact with the geophones at the largest spacing. The signals detected by the two geophones are displayed in real time in the time domain on the video display. After the acquisition, SASW-DA (the computer program) waits for the operator to accept or reject the signal. Criteria for acceptance of the signal include signal similarity with the trial signals, acquisition of the entire signal (i.e. the amplitude of the signal must start from zero and end at zero) and the amplitude at a later time should not exceed the highest initial amplitude (this occurs when the hammer operator is unable to control the rebound of the hammer after an impact). The criterion for acceptability, based on visual inspection of the captured signal, is operator-dependent must be improved for full automation. A better way to discriminate signals is to keep an alias of the averaged properties before updating. The updated average may therefore be accepted if the coherence is improved and rejected if worsened.

8. If the signal is accepted, SASW-DA proceeds to calculate and graphically display the phase of the cross-spectrum and the coherence in real time. SASW-DA then waits for the next trigger.

9. The system controller then signals for another impact which is subsequently processed. This step is repeated till the preset number of signals are acquired for averaging. SASW-DA performs a running average and can therefore be stopped if the preset number of signals is found to be too high.

10. On acquiring the preset number of signals, SASW-DA displays the dispersion curve for that spacing and simultaneously save it on disk. The procedure is repeated for all the other spacings. It takes approximately 2 hours to complete all the spacings previously listed.

After SASW-DA acquires the dispersion points for all the spacings, the dispersion curve for the site based on a minimum preset minimum coherence may be written to file. This is not an automatic feature and must be intentionally enabled. The reason is that there is an occasional site where the analysis of dispersion data must be based on a coherence less than the minimum already set in the program. Another reason is to encourage users to initially look at the dispersion from all the spacings before combining them. Such observations show spacings that yield the best data for a given impact source and receivers.

During the preliminary stages of field testing, it was found that reversing the position of the source did not produce any significantly different results if the test site is fairly level. This is probably because the geophones used were identical in most pertinent characteristics. Secondly, the use of fewer instruments may also have contributed in minimizing phase shifts due to instrument impulse responses. Another observation made was that the number of spacings mentioned above very much exceeded the optimum number of spacings to produce the same curve. Instead of a large number of consecutive receiver spacings, a single receiver array may be used to determine the complete dispersion curve for a site if signals of the appropriate frequency bandwidths can be generated.

In the next chapter, the results obtained from the field testing are discussed.

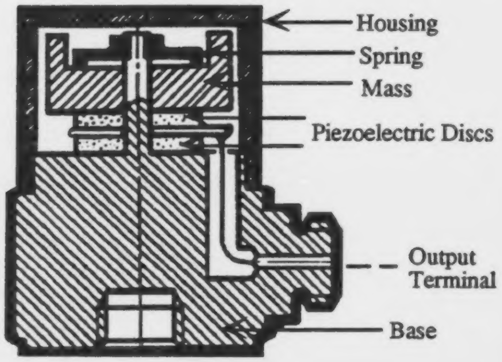
Housing
Spring
Mass
Piezoelectric Discs
Output Terminal
Base

(a) The Piezoelectric Accelerometer (After Bruel and Kjær, 1978)

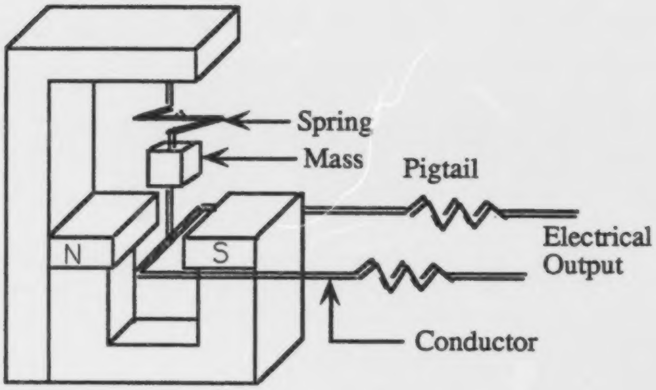
Spring
Mass
Pigtail
N
S
Electrical Output
Conductor

(b). Basic Geophone Construction

Figure 4.1 Schematics of Signal Receivers

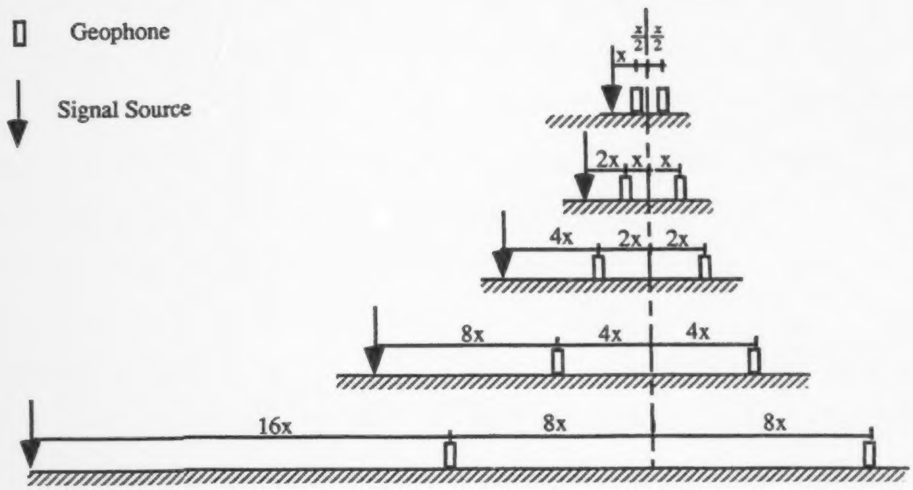
Geophone
Signal Source
x
x/2
x/2
2x
x
x
4x
2x
2x
8x
4x
4x
16x
8x
8x

(a) Common Receiver Mid-Point Geometry

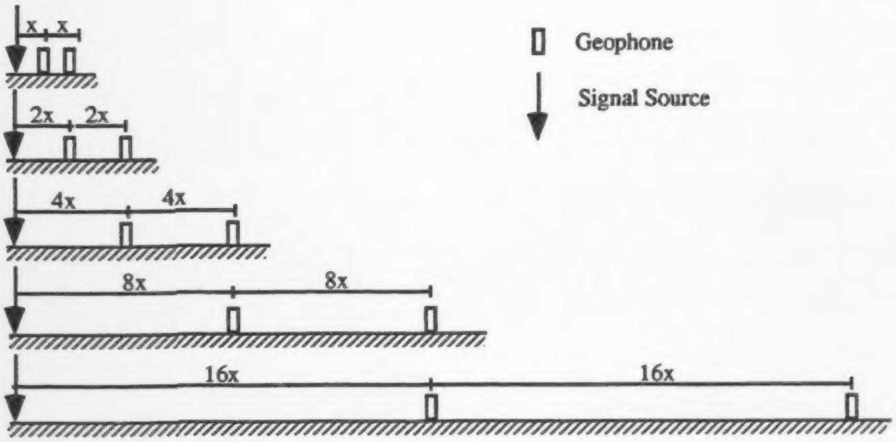
Geophone
Signal Source
x
x
2x
2x
4x
4x
8x
8x
16x
16x

(b) Common Source Geometry

Figure 4.2 Types of SASW Source-Receiver Set-Up.

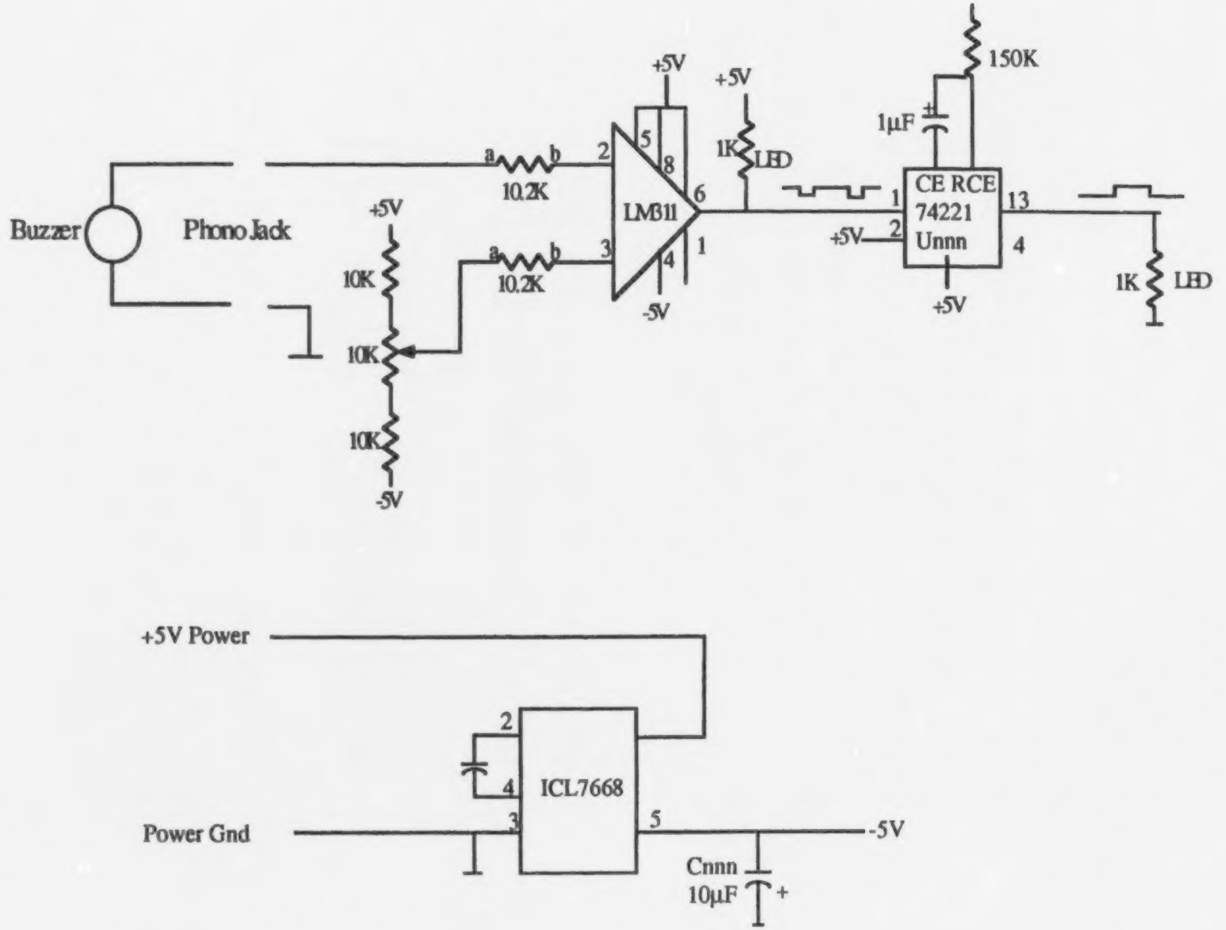
Buzzer
Phono Jack
+5V
10K
10K
10K
-5V
a
b
10.2K
a
b
10.2K
2
3
5
8
6
1
4
LM311
+5V
-5V
+5V
1K
LED
1μF
150K
1
2
+5V
CE RCE
74221
Unnn
13
4
+5V
1K
LED
+5V Power
Power Gnd
2
4
3
ICL7668
5
-5V
Cnnn
10μF
+

Figure 4.3 Main Circuit diagram of the interface control unit.

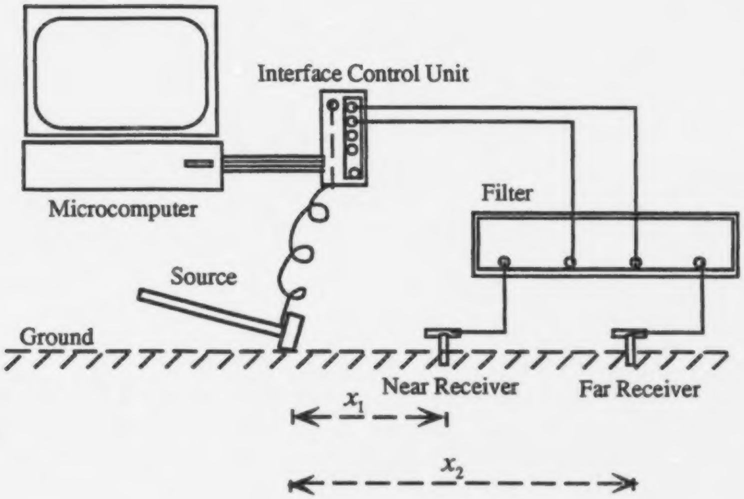
Interface Control Unit
Microcomputer
Filter
Source
Ground
Near Receiver
Far Receiver
x_1
x_2

Figure 4.4. University of Alberta SASW System

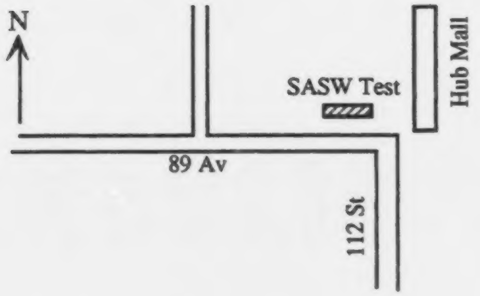
N
SASW Test
Hub Mall
89 Av
112 St

Figure 4.5(a). Location of University of Alberta LRT Station (Edmonton Site)

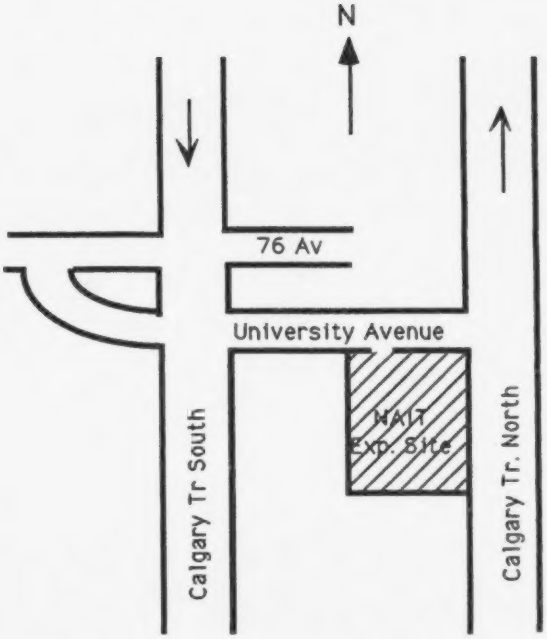
N
76 Av
University Avenue
NAIT
Exp. Site
Calgary Tr South
Calgary Tr. North

Figure 4.5(a). Location of NAIT Experimental Site (Edmonton Site)

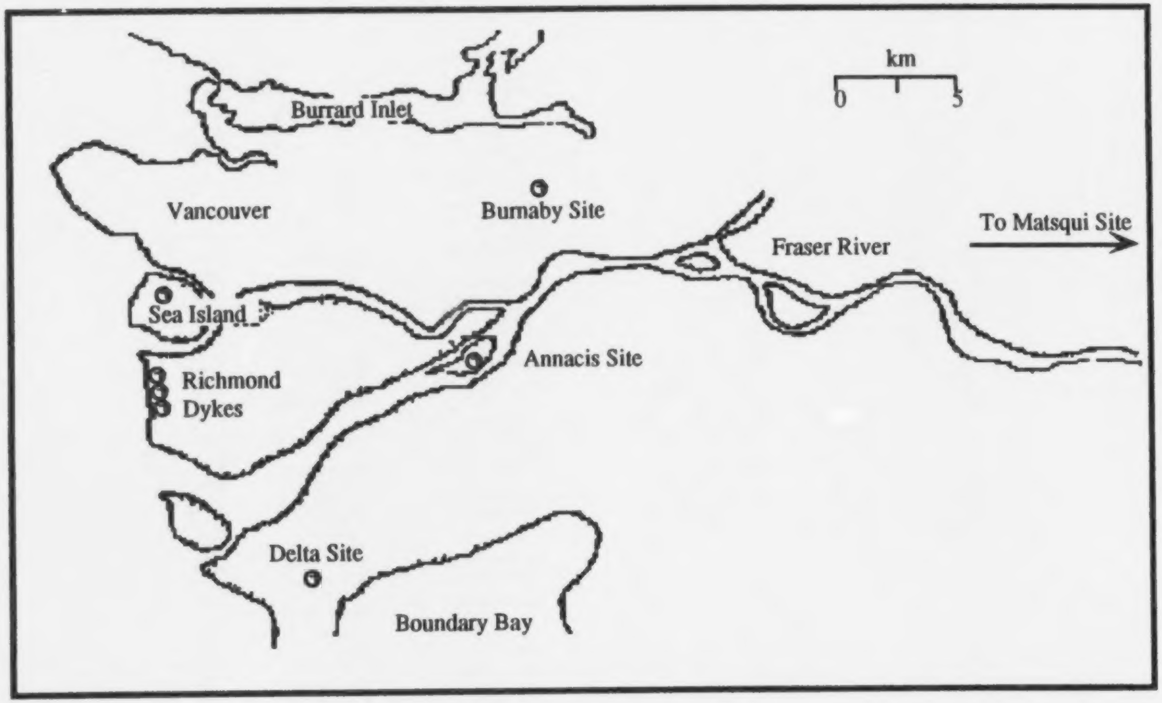
km
0
5
Burrard Inlet
Vancouver
Burnaby Site
To Matsqui Site
Fraser River
Sea Island
Annacis Site
Richmond
Dykes
Delta Site
Boundary Bay

Figure 4.6(a). Test Sites in the Greater Vancouver Area

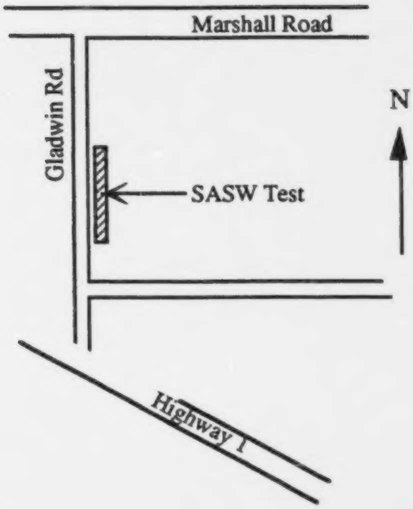
Marshall Road
Gladwin Rd
N
SASW Test
Highway 1

Figure 4.6(b). Location of Selected Sites in British Columbia

Serial No	**8625**	**8626**	**8627**	**8628**
General Information				
Case Height (cm)	13.0	13.0	13.0	13
Case Diameter (cm)	7.6	7.6	7.6	7.6
Total Mass (kg)	2.15	2,15	2.15	2.15
Operating Pressure Under Water (psi)	500	500	500	500
Polarity of Voltage produced at terminals when both suspended masses move towards the base	Negative	Negative	Negative	Negative
Calibration Coil				
No. of Turns	12	12	12	12
Resistance (Ω) at 20°C	5.7	6.3	6.3	5.6
Signal Coil				
Turns/coil for each of 2 coils	4950	4950	4950	4950
Electrodynamic Constant (V/cm/s)	2.795	2.756	2.756	2.756
Resistance(Ω) at 20°C	5481	5521	5571	5571
Leakage to Case (MΩ at 500V)	>100	>100	>100	>100
Calibration Constant (Dynes/Ampere)	39.2	40.9	41.1	42.3
Resonant Frequency f_O(Hz)	1.009	0.972	0.980	1.01
Suspended Mass (g)	972.8	966.6	973.8	968.2
Open Circuit Damping (percentage of critical damping)	0.253	0.253	0.253	0.259

Table 4.1 Characteristics of Geophones Used in Research

CHAPTER 5

ANALYSIS AND DISCUSSION OF RESULTS

5.0 Introduction

The in-situ dispersion curves measured at all the sites listed in the last chapter and the determination of the shear wave velocity profiles associated with these measured curves are discussed in this chapter. For evaluation of the results, the shear wave velocities obtained from forward modelling are compared with results from seismic cone penetration tests at the same or close to the tested locations.

The agreement and differences are discussed and probable reasons for observed discrepancies are suggested. The discussion is planned around the ten sites. Two plots are presented for each site. The first shows the measured in-situ and the calculated dispersion curves. The second plot shows the variation of shear wave velocity with depth obtained from forward modelling (SASW) compared with seismic cone penetration test (SCPT) results. Where available, the stratigraphy of the sites as inferred from the tip resistance, sleeve friction and pore pressure measurements made during the SCPT, are also shown alongside the shear wave velocity profiles.

For all test sites, the goodness of the match between in-situ and calculated dispersion curves is evaluated on the basis of the standard deviation parameter.
Mathematically, the standard deviation (or error) is defined by

$$\sigma = \sqrt{\frac{\sum (c_{exp} - c_{calc})^2}{n-1}} \qquad [5.1]$$

where σ = standard error,

c_{exp} = in-situ phase velocity,

c_{calc} = calculated phase velocity,

n = number of dispersion points.

A perfect match of the in-situ and calculated dispersion curves results in zero standard error whereas an average phase velocity difference of 10 m/s between the two results in a standard error of 10, if the number of dispersion points is large. The magnitude of this parameter is therefore a measure of the departure of the calculated dispersion points from the corresponding measured in-situ dispersion points. The smaller this value, the better the match.

5.1. University LRT Station.

The Light Rail Transit (LRT) station at the University of Alberta is located at the north-west corner of 112 Street and 89th Avenue. This site was selected because of its proximity to the Civil Engineering Department (where this research was based) and more importantly to a planned deep excavation for tunneling purposes. The excavation could provide information from which the stratigraphy of the near surface could be established or verified.

The first test at the site was performed in the summer of 1990. Instrumented mechanical hammers of different sizes and two geophones were respectively used for signal generation and detection. The test procedure followed the guidelines outlined in the previous chapter. The test lasted approximately two hours during the day. Without interference from curious pedestrians, the test could have taken less time. This was the very first site tested and many tests were done at this site to ensure the system was functioning properly.

Another set of tests was performed with an array of four geophones. This was readily done since the system currently allows for a maximum of five channels. Only four geophones of the same make were available and hence were used for the array. This particular test was not aimed at obtaining the shear wave velocity profile but to verify that all four channels of the developed system were working properly. Testing with an array of four receivers in an evening took a little over twenty minutes at this site. The signals were found to be less noisy and the usual repetitions of signal generation due to noisiness was avoided. Noisiness of signals during the day requires more averaging than at night resulting in longer testing times. This could be very important in testing on busy pavements.

The in-situ dispersion curve obtained at this site using two receivers is shown in Figure 5.1a. The curve shows the wavelength ranging from small values to about 18 m while the measured Rayleigh-wave phase velocity varied from about 180 m/s at the surface to 220 m/s at the longest wavelength of 18 m. The two other dispersion curves are also shown in Figure 5.1(a). These are the initial and optimized dispersion curves obtained from forward modelling. The analysis was based on an assumed layered soil model from the steady vibration processing of Rayleigh wave data discussed in Chapters 1 and 3. The number of layers and the magnitude of the layer parameters were based on the shape, curvature and position of the dispersion curve in the phase velocity-wavelength space. The calculations of the initial dispersion curve and the iteration of the assumed model parameters until a matching dispersion curve was found, were all done by the computer program SASW-FM, which was described in the last chapter. The sum of least squares criterion was used for evaluating the degree of the match. The smaller this parameter, the better the match. A better measure of this parameter, the root mean square deviation, was calculated and found to be 2.62 as shown in Table 5.1.

The shear-wave velocity profile associated with the final dispersion curve is shown in Figure 5.1(b). Also shown in the same figure is the corresponding profile from one of two seismic CPT performed at this site, both of which are shown in Appendix III. The shear wave velocity profiles from both SCPT results were almost identical and hence only one of them is presented. Shear wave velocities from the SASW test varied from about 118 m/s at the ground surface to about 340 m/s at a depth of approximately 9.3 m. The shear wave velocity from the SCPT starts from about 140 m/s at a depth of 1.5 m to 340 m/s at a depth of 10.7 m. The SCPT had to be stopped because the soil at about 10 m deep was too stiff for pushing the cone with a 24-ton rig. Detail results of the cone penetration test is shown in Appendix III. Although the SASW tests gave results up to approximately 15 m deep, only results to the same depth range as the SCPT tests are shown for comparison purposes.

The stratigraphy at this site, shown alongside the plot, is based on data from excavation and cone penetration tests and is also found to be consistent with local construction knowledge in the area. The site is overlain with a metre of clay fill which is underlain by almost 7 m of a stiff silty clay. A 4-m thick of fine dense sand at about 8 m depth is also underlain by a stiff glacial till. As can be seen from the plot, it was near the transition of dense sand to stiff till that the SCPT had to be stopped.

According to the SCPT procedure, shear wave velocities are not usually determined for the first metre because the cone is pushed for an initial metre before the test is stopped for the determination of shear wave velocity. Thus no SCPT velocity data is available for the top clay fill layer which is a metre deep. The SASW test shows that the S-wave velocity in the clay layer is about 180 m/s in the upper half and 260 m/s in the lower half. Within the upper half of the stiff silty clay layer, the shear wave velocities from both tests are in good agreement. In the lower half, however, the velocities differ by as much as 60 m/s, a difference that is accentuated by the way SCPT data is traditionally plotted as shown in the figure. If plotted as the results should be, i.e. constant velocity for each metre of depth increment. The reason for this difference could be due to the fact that shear wave velocities measured in the SASW method are influenced by the stiffness of adjoining deeper layers while the velocities from the SCPT are not. In this case the lower stiff till influenced the velocities in the lower portions of the clay layer. The degree to which layer stiffnesses are affected by adjoining layers depend on the velocity contrast.

The dispersion curve obtained at this site with an array of four geophones is shown in Figure 5.1c. Forward modelling was not done for this case primarily for the reasons stated above - to ensure that the dispersion curves for a pair and an array of geophones were identical.

5.2. NAIT Experimental Test Site, Edmonton, Alberta

This site is located at the south-west corner of Calgary Trail North and University Avenue in Edmonton, Alberta. Two seismic CPT profiles were performed and showed that ground conditions consisted of 5 to 6 m of a firm silty clay overlying a very dense glacial till. The results of the CPT are shown in Appendix IV. SASW tests using Rayleigh waves were performed adjacent to the locations of the two SCPT profiles. The experimental and computed dispersion curves are shown in Figure 5.2a. Results of the SASW analysis is compared with the SCPT shear wave velocity data in Figure 5.2b.

The in-situ dispersion curve was not identically matched after a large number of iterations. This is due to the presence of local minima on the residual surface and may be overcome by slightly altering the layer parameters. This was done but the first few trials only yielded curves that slowly approached the experimental. Due to time constraints and computer speed requirements, this iteration could not be continued. However, the fair agreement with the seismic CPT results indicate that this match is fair.

The seismic cone could not be pushed deeper than 5 m and thus results were only obtained for this depth range. As can be seen in Figure 5.2b, the shear wave velocities from the two tests do not match in the top 2.5 m. The reason for this difference lies in the timing of the tests. The SCPT was performed in the summer while the SASW was performed in the winter. The different timing of the results accidentally give indications of the effect of seasonal temperature variation on shear wave velocity at this site. Both methods, however, agree fairly well. The SCPT was unable to penetrate the dense glacial till below a depth of 6 m. However, the SASW was able to measure shear wave velocity to a depth of about 12 m.

5.3. Richmond Dykes at Blundell Road, Richmond, B.C.

A total of eight SCPT profiles were made along the dyke at Blundell Road, in Richmond, B.C. The results of the 8 tests are shown in Appendix V. The ground conditions consist of about 1 m of a sand and gravel surface fill overlying about 4 m of a clayey silt and clay fill. Underlying this is a deep deposit of loose to medium dense sand and silty sand to a depth of about 35 m.

SASW tests employing Rayleigh waves were performed along the crest of the dyke. The measured and theoretical dispersion curves are shown in Figure 5.3a. The Rayleigh wave phase velocities varied from about 95 m/s at short wavelengths to about 240 m/s at wavelengths of about 25 m. A good match of the dispersion curves was obtained at this site. The shear wave velocities shown in Figure 5.3b indicates that the results of the SASW tests and the SCPT shear wave velocity data were in good agreement for the most part. Large differences are observed in the shear wave velocities in the uppermost layer. Another look at the unfiltered dispersion points, showed that some of the points that were rejected according to Heisey's criteria did have phase velocities that would have translated into shear wave velocities much higher than those obtained but still less than the SCPT velocities at the surface. The seismic cone penetration test is also influenced by signal noisiness near the surface and errors are introduced as a result. This difference in surface velocities could also be due to a localized stiff zone since the SASW sample a much larger volume of soil than the seismic cone.

An interesting observation at this site is that the usual wavelength-depth ratio of 2 does not apply in this case. This ratio is almost equal to unity in this case. It may be recalled that some previous researchers used a ratio of unity in interpreting dispersion curves. It appears that it was not a poor assumption. It also illustrates that the simple interpretation procedure may be flawed in some cases where shear wave velocity increases with depth. In this case, the presence of the stiff crust at the surface probably invalidated the k_z value of 0.5. k_z, it may be recalled is the ratio of depth to wavelength in the simple interpretation procedure.

5.4. Richmond Dykes at Francis Road, Richmond, B.C.

Four seismic cone penetration tests were performed along the dyke at Francis Road in Richmond, B.C. The results, shown in Appendix VI, that the ground conditions were similar to the Blundell Road subsurface profile described earlier.

Measured and computed dispersion curves are shown in Figure 5.4a. The experimental and theoretical dispersion curves are almost identical. Figure 5.4b.is a plot of the shear wave velocity profiles from the seismic cone penetration and SASW tests. The seismic CPT shows a high velocity surface layer that was not picked up by the SASW. Observation of all the CPT profiles shows that this surface crust did not show up at some of the locations. Thus this lack of agreement could be due to this localized effect. In general, the SASW test samples a larger volume of ground than the seismic cone. Hence the velocities of localized pockets of stiff material tend to be lowered by any adjoining low velocity zones. The good agreement between the shear wave velocity profiles below the surface crust demonstrate the applicability of the method.

5.5. Richmond Dykes at Chatham, Road, Richmond, B.C.

Three CPT tests were performed at this site which is close to the Francis Road dyke. The ground conditions are similar the Francis Road site. All three CPT results are shown in Appendix VII. The dispersion curves, shown in Figure 5.5a, match quite well. The phase velocities decrease slightly from 140 m/s at short wavelengths before increasing again to about 160 m/s at a wavelength of approximately 160 m/s.

The shear wave velocities from the SCPT and SASW are shown in Figure 5.5b. The profiles show significant differences in shear wave velocities between 3 and 7 m. This occurs when the SCPT picks up a layer with a relatively lower shear wave velocity. As is discussed later, another site also showed significant difference in shear wave velocities in the vicinity of low velocity zones.

5.6. Sea Island Site, Vancouver, B.C.

Four seismic cone penetration tests were performed at this site which lies to the north of Vancouver International Airport in Richmond, BC. The CPT results are presented in Appendix VIII. The ground conditions consist of approximately 2 m of soft silts and clays overlying a medium dense sand deposit to a depth of about 15 m. Underlying the sand is a deep deposit of approximately normally consolidated clayey silt.

The measured and theoretical dispersion curves are shown in Figure 5.6a. Rayleigh wave SASW was performed in the same general area as the SCPT. Results of the SASW analyses are compared with the SCPT shear wave velocity data and shown in Figure 5.6b. Fair agreement is observed between the two methods. The shear wave velocity increases with depth from a value of about 100 m/s near the surface to about 220 m/s at a depth of about 18 m.

5.7. Burnaby Site, Burnaby, B.C.

Four seismic cone penetration tests were performed at this site located in Burnaby, B.C. All CPT results are presented in Appendix IX. The ground conditions consist of approximately 5 m of fill overlying about 2 m of sand which is in turn underlain by a deposit of very soft clay. This site was particularly soft and large amounts of energy were expended in exciting the ground.

Experimental and calculated Rayleigh wave dispersion curves for this site are shown in Figure 5.7a. Figure 5.7b shows a plot of the shear wave velocity profiles obtained from both procedures. The seismic cone penetration test could not be performed in the top 5 m because the soil was too weak to support even the self weight of the cone and attached rods in this depth range. The SASW test was able to determine the shear wave velocities in the top layers and also matched the SCPT profile in the depths where results were obtained by both methods.

The theoretical dispersion curve exhibits anomalous behaviour at a depth of approximately 5 m. The problem is due to the fact that the root finding algorithm reached the maximum number of trials before converging on a root close enough to the real root. Associated errors were therefore incurred. The computer program for matching the dispersion curve has been modified but a more powerful computer is required to handle the required memory

5.8. Annacis Site, Annacis Island, B.C.

The location of this site was shown in Figure 4.6(a) of Chapter 4. One seismic CPT was performed at this site and the results are shown in Appendix X. The CPT results showed that the site consists of a 3.5 m sand fill over 12.5 m of a soft organic silty clay. This silty clay is underlain by about 13.5 m of a medium dense sand which is in turn underlain by normally consolidated clayey silt with thin sand layers.

The dispersion curves at this site is shown in Figure 5.8(a) and the shear wave velocities in Figure 5.8(b). The differences in the results are significant. The reason may be found in the presence of the organic layers in the stratigraphy at this site. The mass density ratio between normal and organic soils is approximately equal to two. Since the presence of the organic layer was not known prior to forward modelling, this contrast in density was not accounted for as all layers were assumed to have the same mass density. This assumption is fair for most soils. In the forward modelling, that cannot be explained except for the presence of the shear wave velocity decrement in the organic layer. Nazarian (1984) made similar observations of deviations in shear wave velocity profiles for sites where low velocity zones were sandwiched between higher velocity layers.

Figures 5.8(c) and (d) show the corresponding profiles when the density contrast is accounted for. Though the results compare better with the seismic CPT results, further research is required to enable the identification of soil structures with low velocity zones from the measured in-situ dispersion curve.

5.9. Delta Site, Delta, B.C.

This site is located in the north-east corner of 56th Street and 28th Avenue. Four seismic cone penetration tests were performed at this site and Appendix XI shows the results obtained. All four tests indicate that the top 7.5 m consists of a layer of soft to firm silt underlain by a compact to dense sand layer to a depth of approximately 16 m. Underneath the compact sand is a 2 m -thick layer of very compact silt which overlies compact to dense sand with occasional thin silt layers to a depth of about 30 m.

The in-situ dispersion curve and the corresponding matching theoretical curve are shown in Figure 5.9a. The match could be improved upon by further iteration. Figure 5.9b shows the shear wave velocity profiles from both tests. There is good agreement which should get better with better matching of the dispersion curves.

5.10. Matsqui Site

This site is located at the south-east corner of Marshall Road and Gladwin Road in Matsqui, B.C. The seismic CPT could not be performed because of large gravel and cobbles that made it impossible to push the cone. Becker hammer test at the site (see results in Appendix XII) showed that the site consisted of medium to dense sand with trace gravel to a depth of about 2.5 m. Below this is a 3.5 m thick layer of silt containing sub-rounded gravels and cobbles. Under this layer is a mixture of gravel and cobbles to a depth of approximately 30 m.

The dispersion curve and the shear wave velocity profile at this site are shown in Figure 5.10 (a) and 5.10 (b). There is no shear wave velocity data from the seismic cone because the site was too stiff for cone penetration. The velocities appear to be consistent with the profiles inferred from the Becker hammer tests.

5.11 Summary

The results show that the SASW equipment and the computer programs developed in this research are working as designed. Further modifications in the experimental and analytical computer programs are required to improve the rate and quality of the convergenceat which the theoretical dispersion curve converge on the in-situ curve.

The interpretation of the in-situ dispersion curves was done without any prior knowledge of the site conditions or the stratigraphy. If the layering at the site is known, the determination of shear wave velocities would be quicker and the time spent in the field would be considerably shortened.

For sites where layer anomalies are absent, i.e. the absence of very soft and very stiff sandwiched layers, the theoretical dispersion curve tends to converge faster on the in-situ curve e.g. at Richmond Dykes (Francis Road). The forward modelling of the sites with layers of lighter organic material appears to be the most difficult if the density contrast is not known prior to the analysis. The results obtained at Annacis site indicated that such layers could lead to misinterpretation of in-situ dispersion curves. The second stage in the analysis at this site assumed a density ratio of 2 between the upper fill and the organic layer. The improved match illustrates the effect of the density contrast between the layers. Caution is therefore required on sites where dispersion curves are initially difficult to match. In such cases, it is recommended that the local geology maps be consulted.

The sources used did not always generate signals of the desired frequencies. This was a major setback and further research in the design of suitable signal sources is required. Vibrators with programmable interfaces is probably the best option as these can be designed to generate signals of the appropriate frequency and strength.

The most difficult aspect of the test is the definition of the in-situ dispersion curve. Better and consistent guidelines are required to ensure standardization. This subject was discussed in chapter 2.

It would have been appropriate to re-analyze the in-situ dispersion curves based on the stratigraphy inferred the seismic CPT. This requires a computer program that can perturb or fix all four layer variables of thickness, mass density, shear and compressional wave velocities. The computer program written in this research perturbed only two variables - thickness and shear wave velocity, though all four layer parameters may be perturbed. The reason lies in the fact that optimization of the dispersion curves is extremely slow on the computer used in this research. A faster computer will enable the processing of dispersion data with perturbation of all four layer parameters.

The observed discrepancies between measured and calculated dispersion curves may be attributed to the possibility that not only stiffness but also of material damping affects the theoretical dispersion curve. In the forward modelling process, material damping was assumed to have negligible effect on the theoretical dispersion curve. The reason for this asumption lies in the observation that, for most soils, there is little or no measurable hysteretic behaviour at strains of 10-4 % or smaller. However, this may not be the case during surface wave propagation and further research is required in this area. It is known that rocks exhibit anelastic behaviour and geophysicists introduce a quality factor (Q) of at least 100 (Nyland, 1991) to reflect this anelasticity. This is accounted for in dispersion theory by giving the elastic constants a small imaginary part and thus making them complex. This approach may be extended to soils - except that unlike rocks, material damping for soils is highly likely to be frequency-dependent and thus complicate the problem.

Another possible explanation for some of the observed dicrepancies between measured and calculated curves is the relatively small number of layers used in the matching process. Soils with steep stiffness gradients will only be well-represented by a large number of thin uniform layers or sub-layers with some velocity variation. A large number of layers results in long computing times and iterative calculations become too slow. As previously discussed, a faster computer will better serve this purpose.

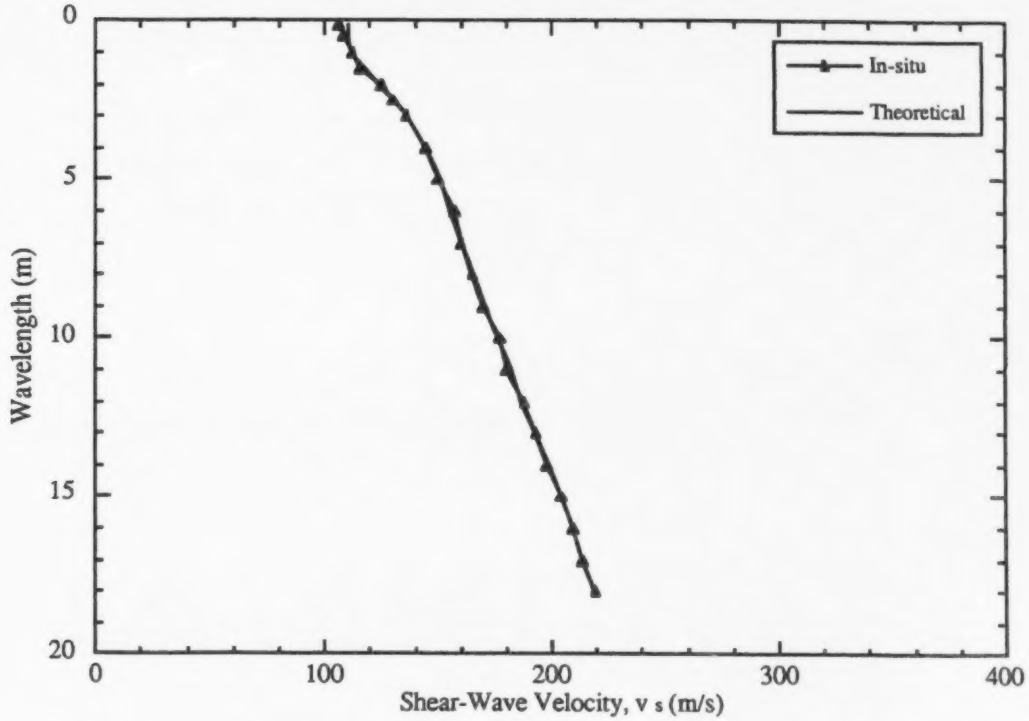

Figure 5.1a Dispersion Curves at University LRT Station.

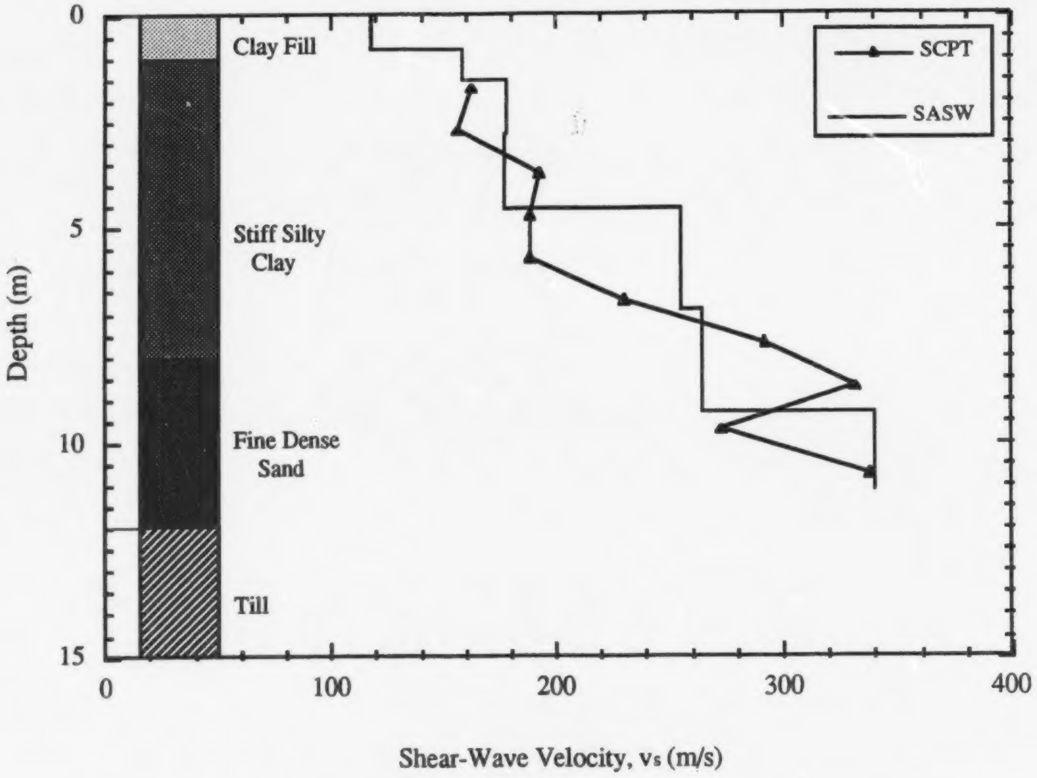

Figure 5.1b. Shear Wave Velocity Profile at University LRT Station.

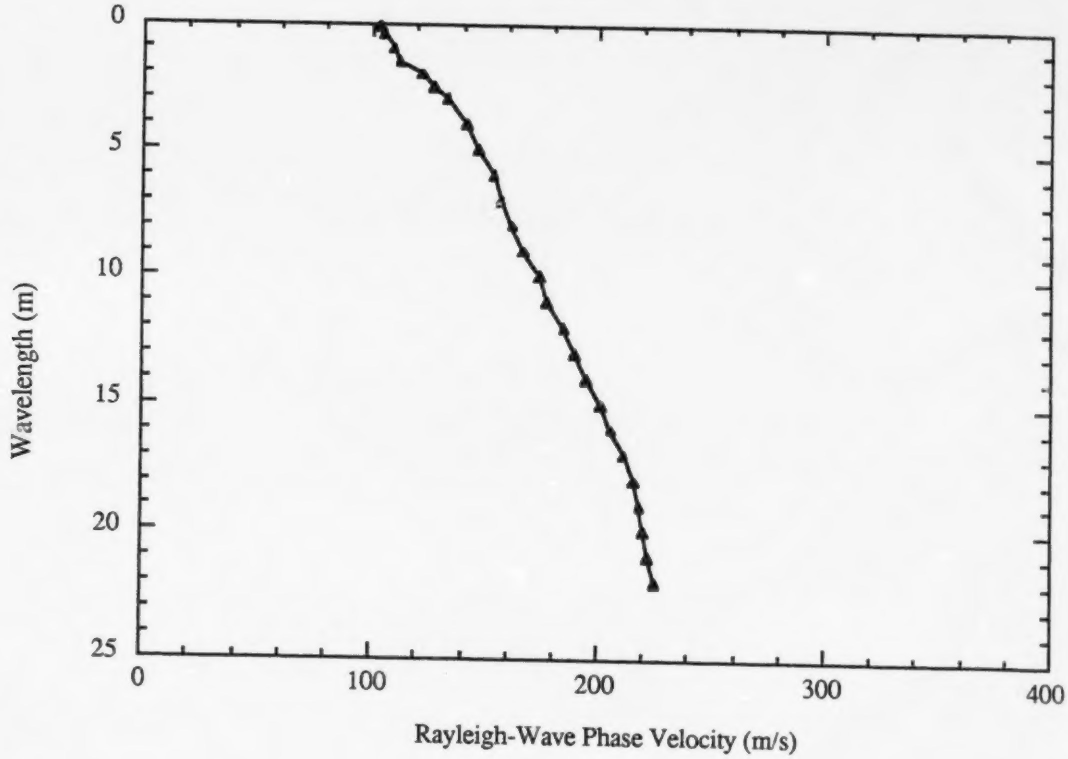

Figure 5.1c. Dispersion Curve from Four-Array Receiver at University LRT Station

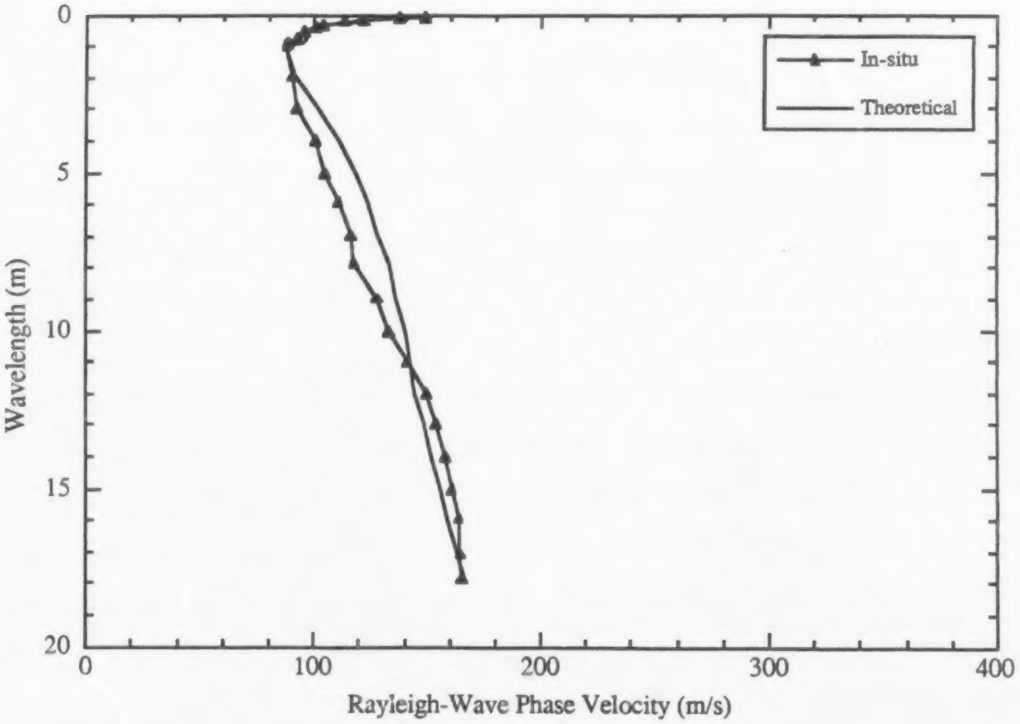

Figure 5.2a. Dispersion Curves at NAIT Experimental Site

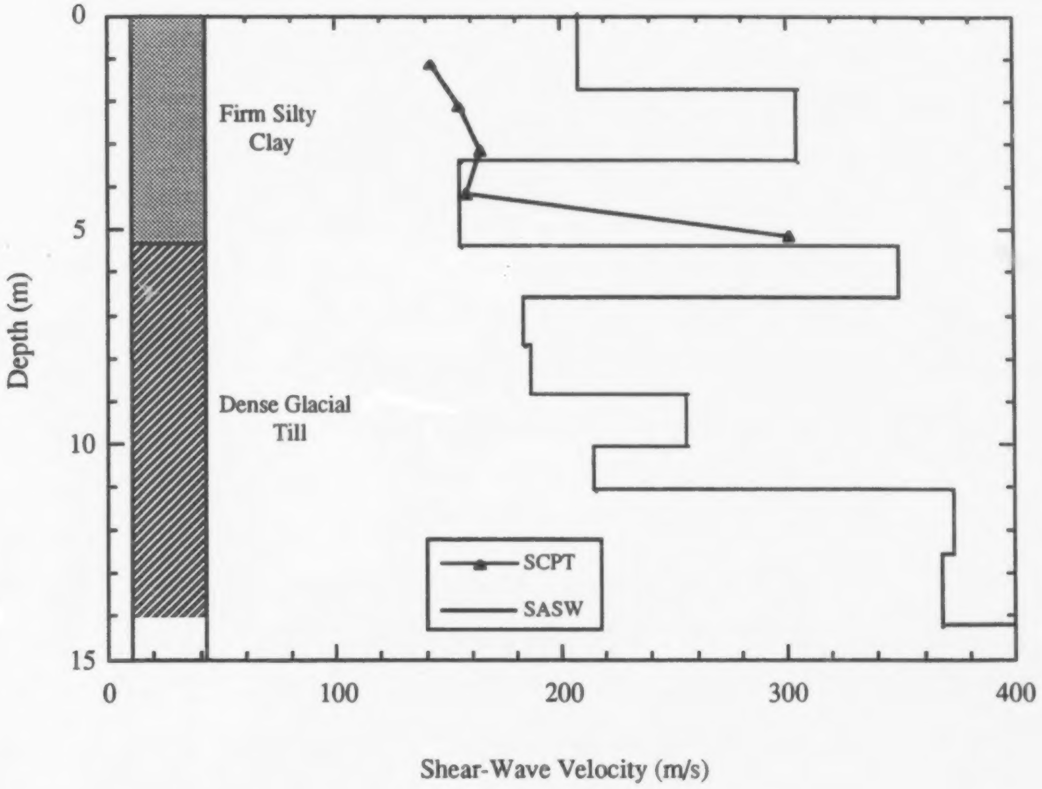

Figure 5.2b. Shear Wave Velocity Profile at NAIT Experimental Site

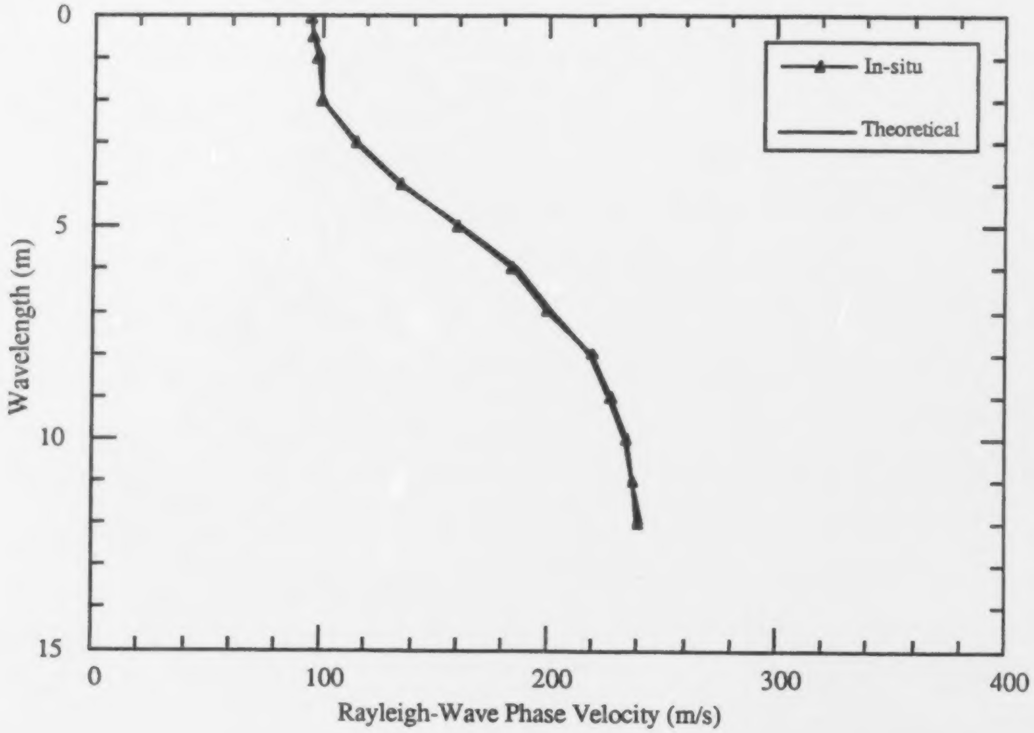

Figure 5.3a. Dispersion Curves at Blundell Road Dyke

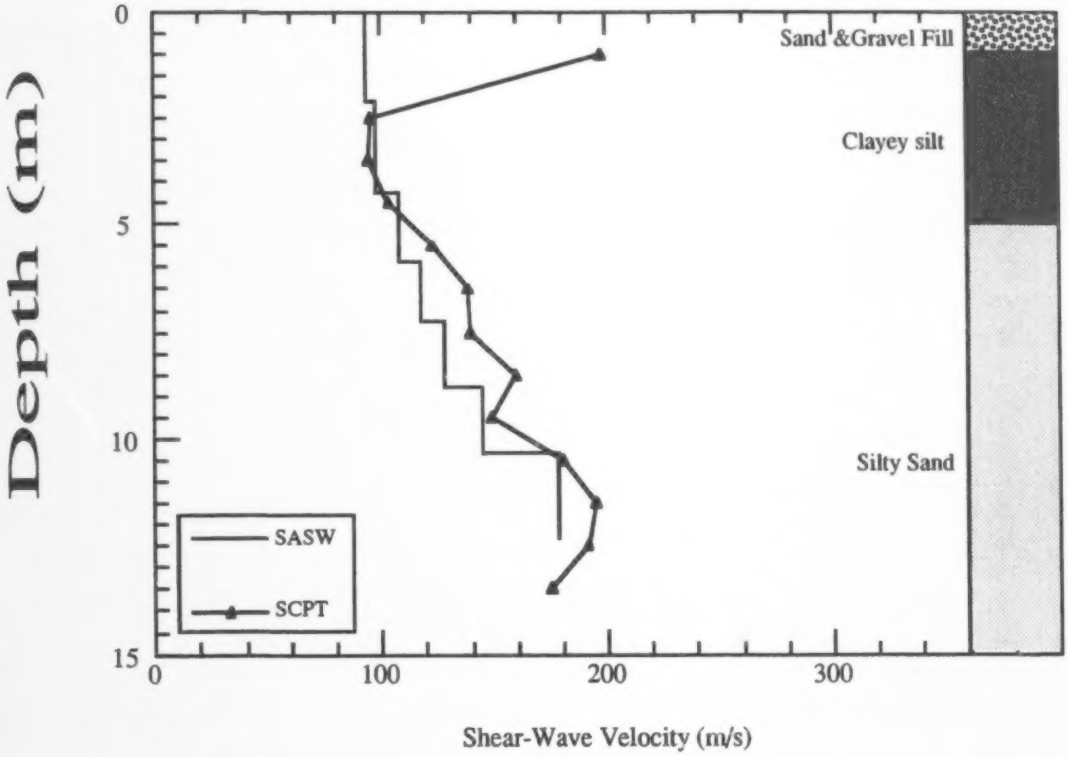

Figure 5.3b. Shear Wave Velocity Profile at Blundell Road Dyke

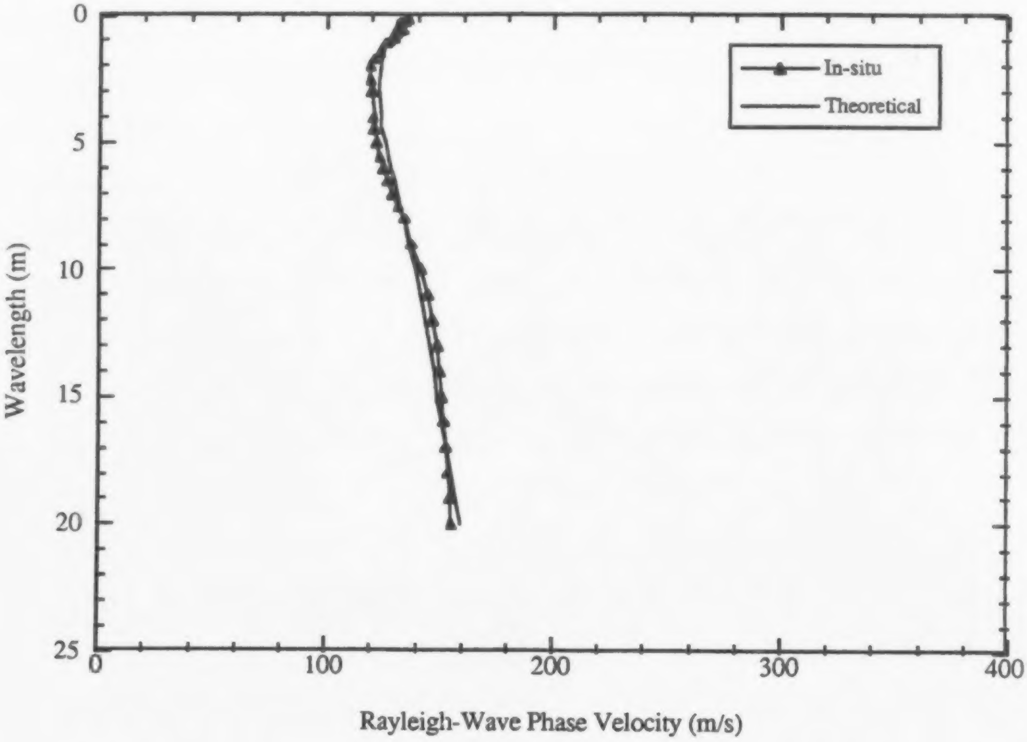

Figure 5.4a. Dispersion Curves at Chatham Road Dyke Site

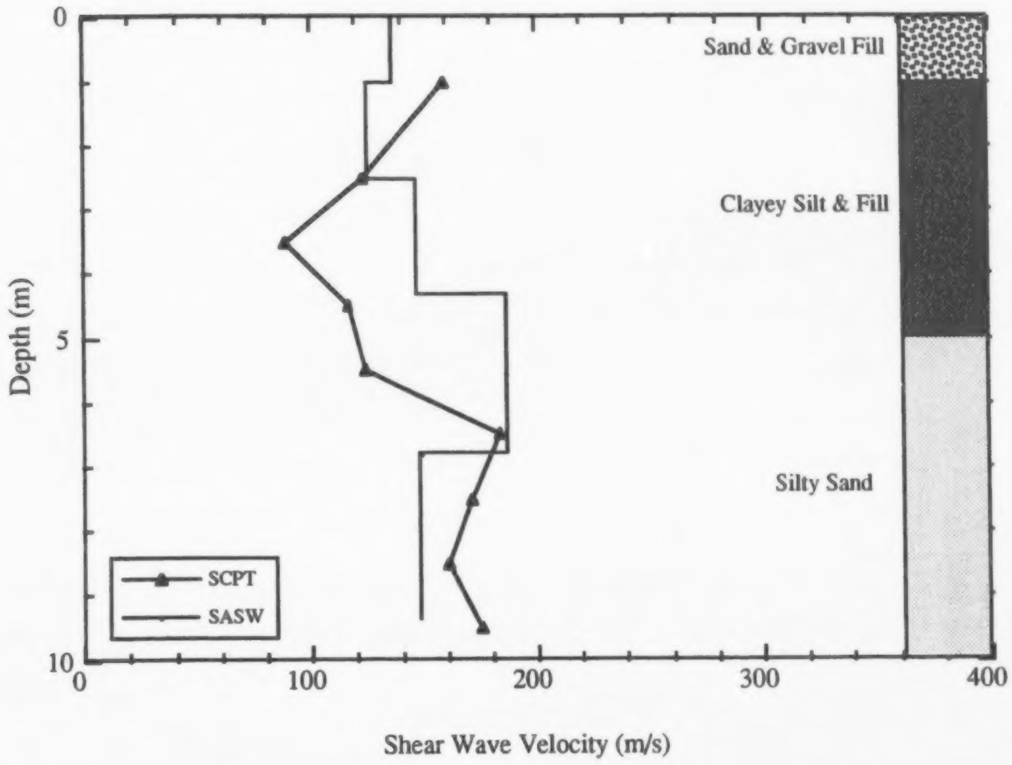

Figure 5.4b. Shear Wave Velocity Profile at Chatham Road Dyke Site

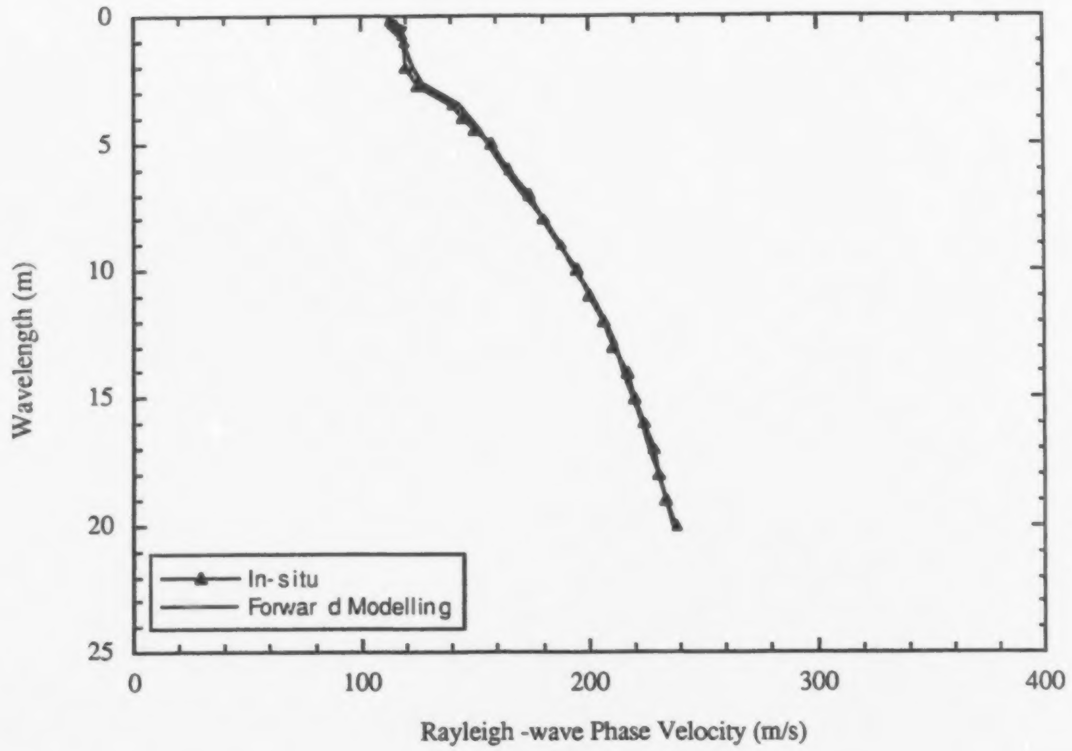

Figure 5.5a. Dispersion Curves at Francis Road Dyke Site

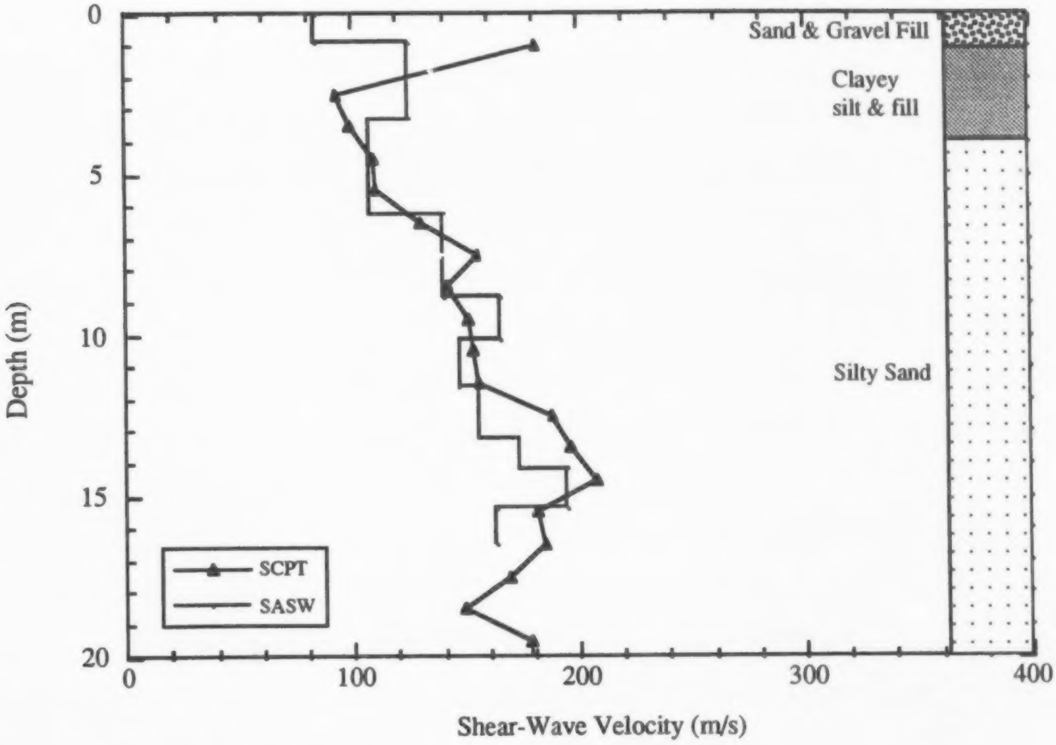

Figure 5.5b. Shear Wave Velocity Profile at Francis Road Dyke Site

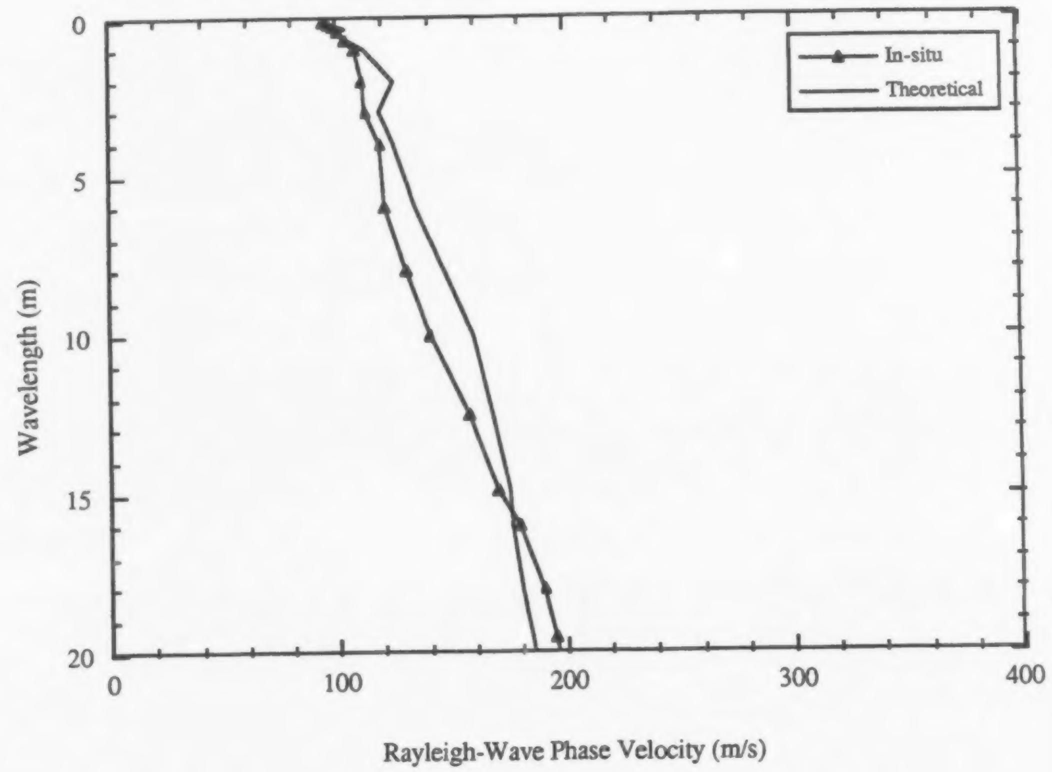

Figure 5.6a. Dispersion Curves at Sea Island Site

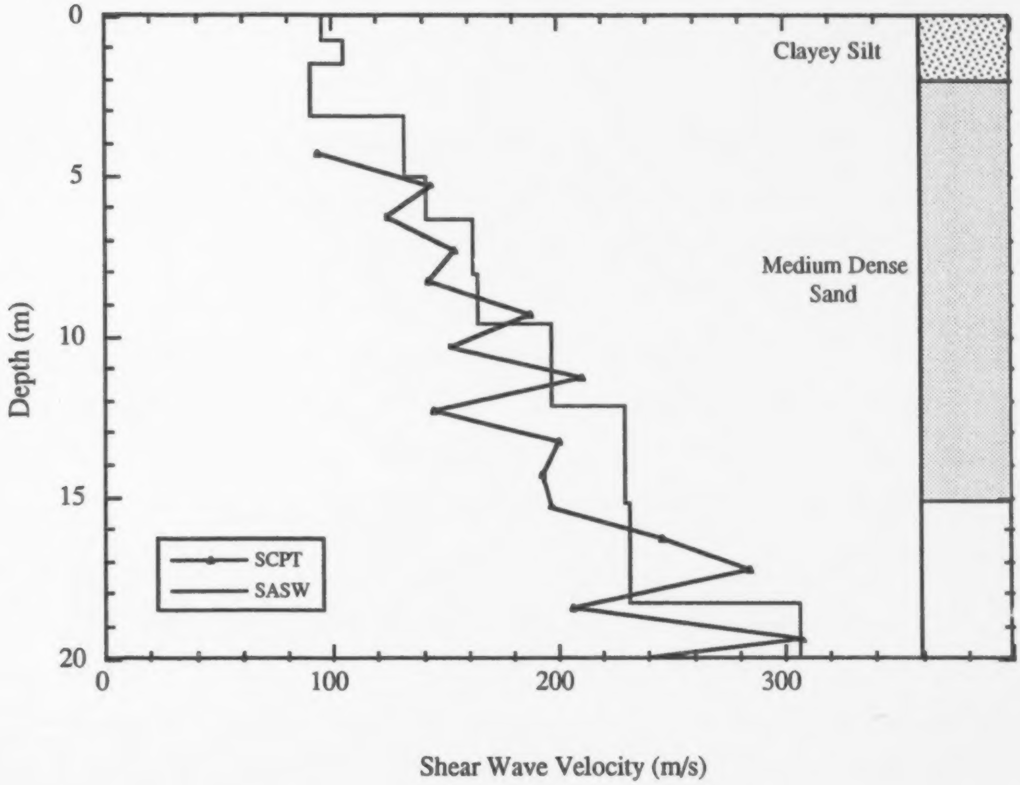

Figure 5.6b. Shear Wave Velocity Profile Sea Island Site.

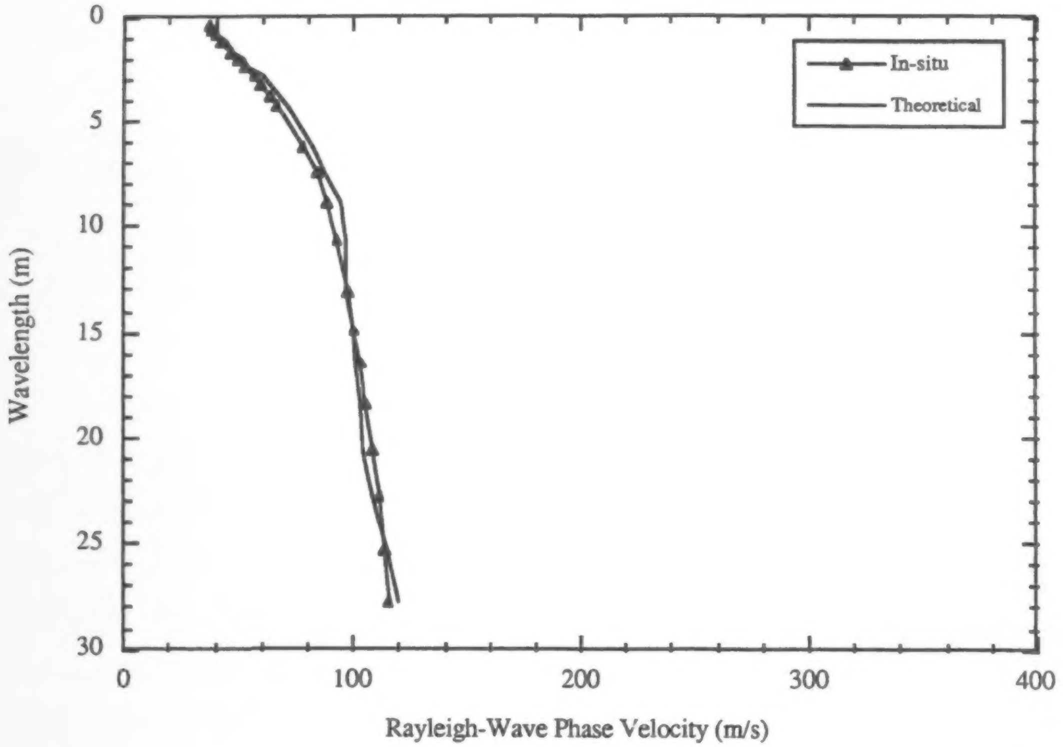

Figure 5.7a. Dispersion Curves at Burnaby Site.

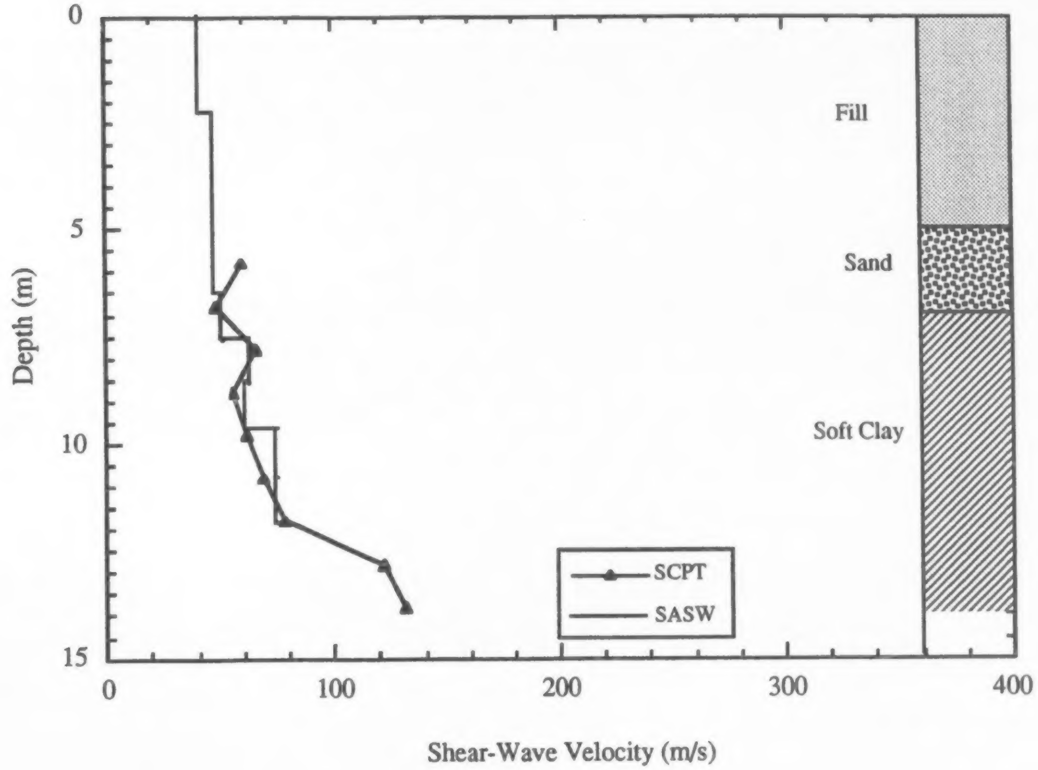

Figure 5.7b. Shear Wave Velocity Profile at Burnaby Site.

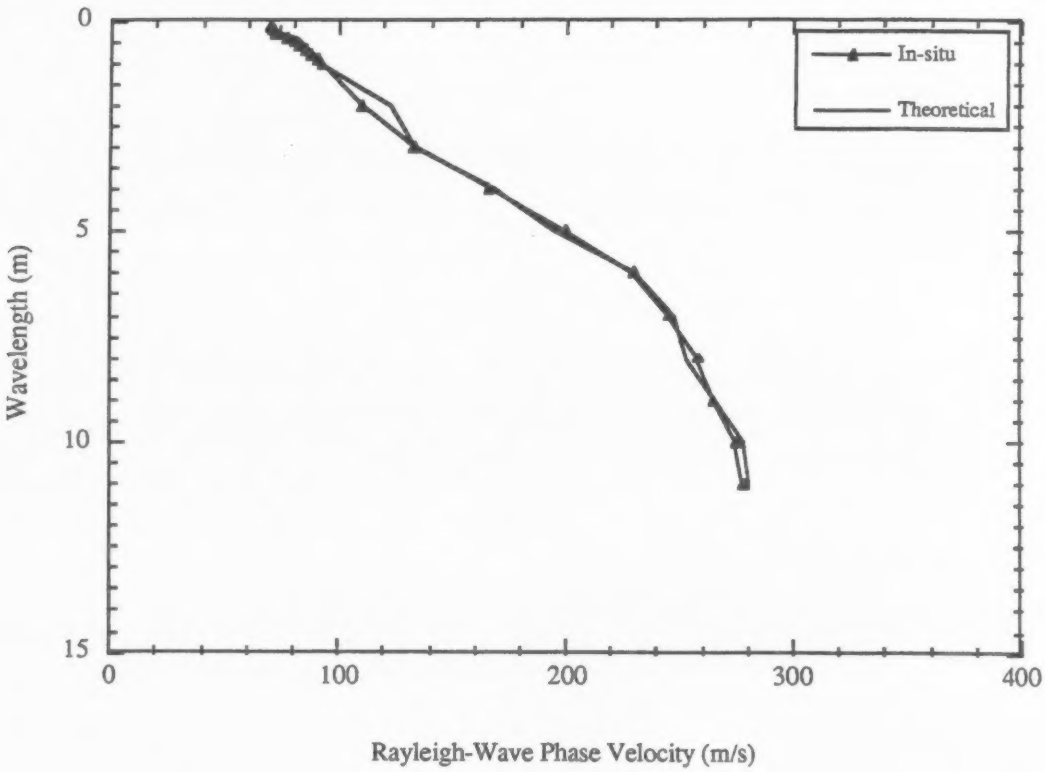

Figure 5.8a. Dispersion Curves at Annacis

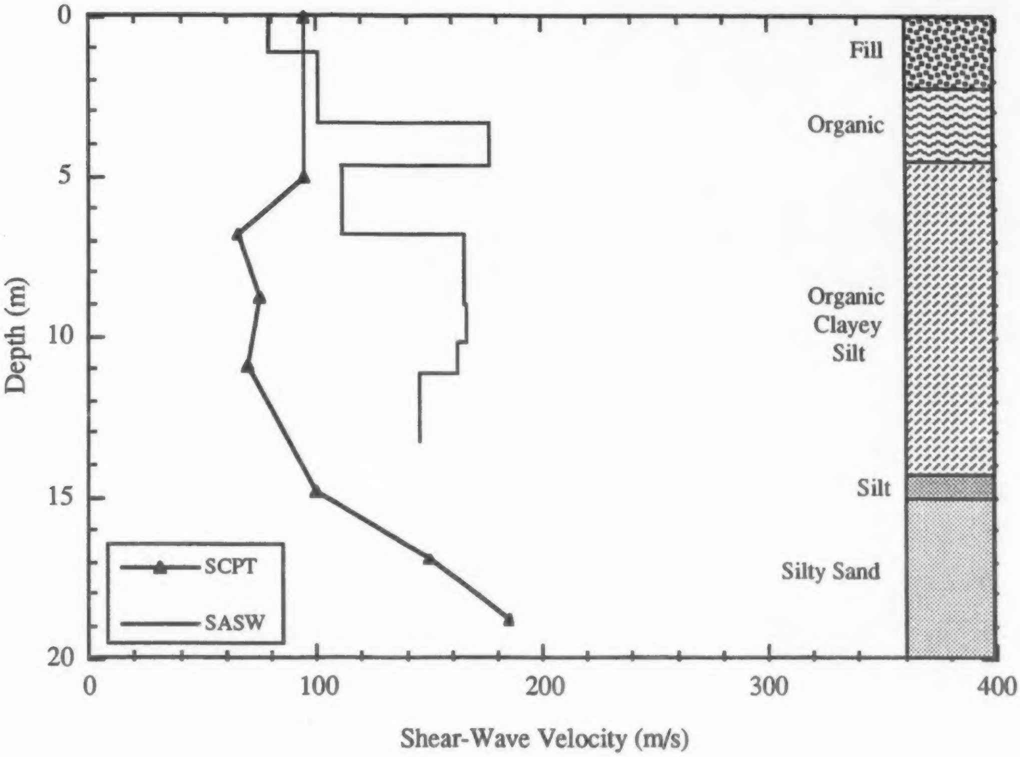

Figure 5.8b. Shear-wave Velocity Profiles from SASW and SCPT at Annacis Site

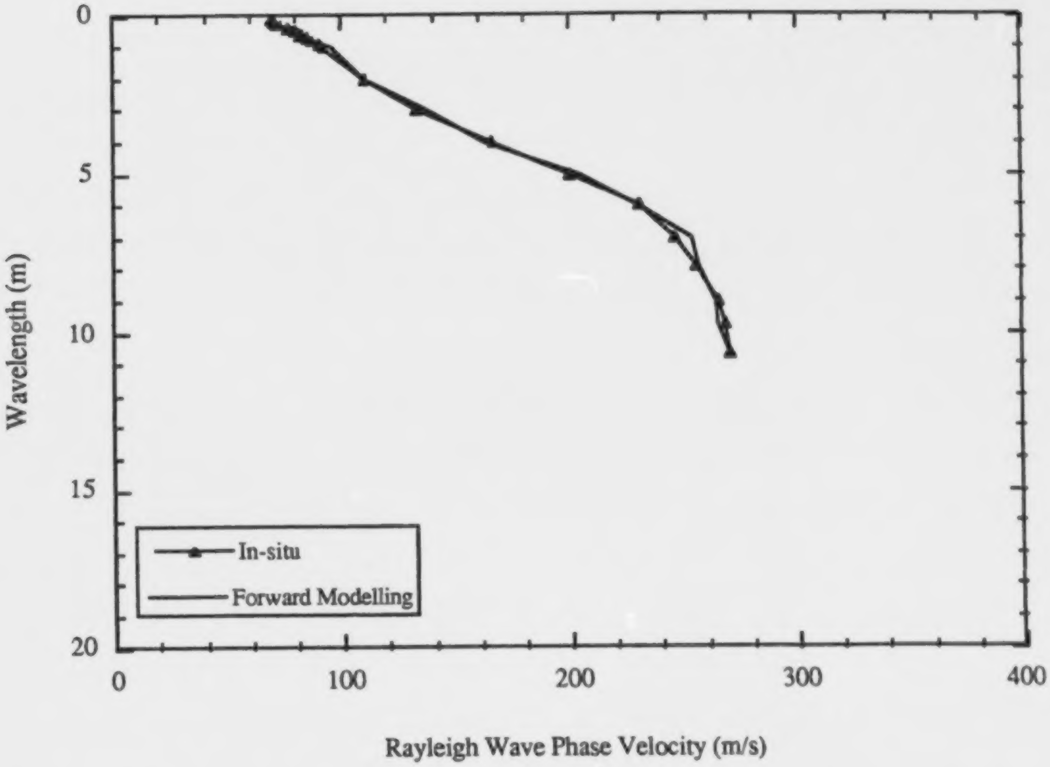

Figure 5.8c. Dispersion Curves based on SCPT stratigraphy at Annacis.

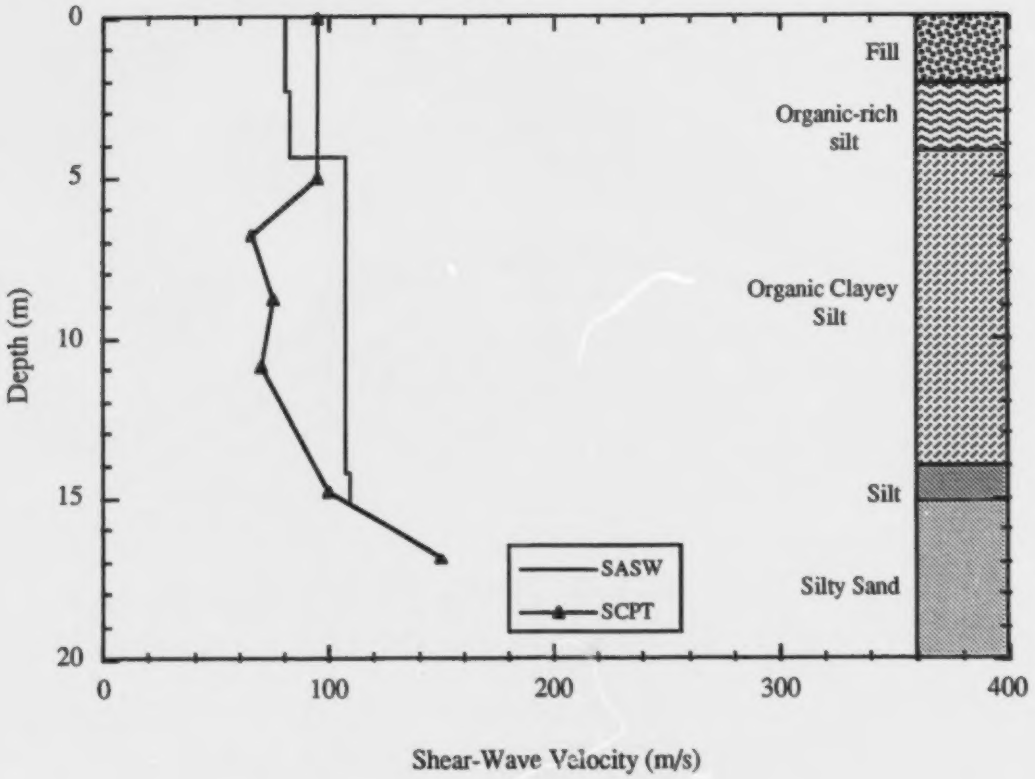

Figure 5.8d. Shear Wave Velocity Profile from assumed SCPT data at Annacis.

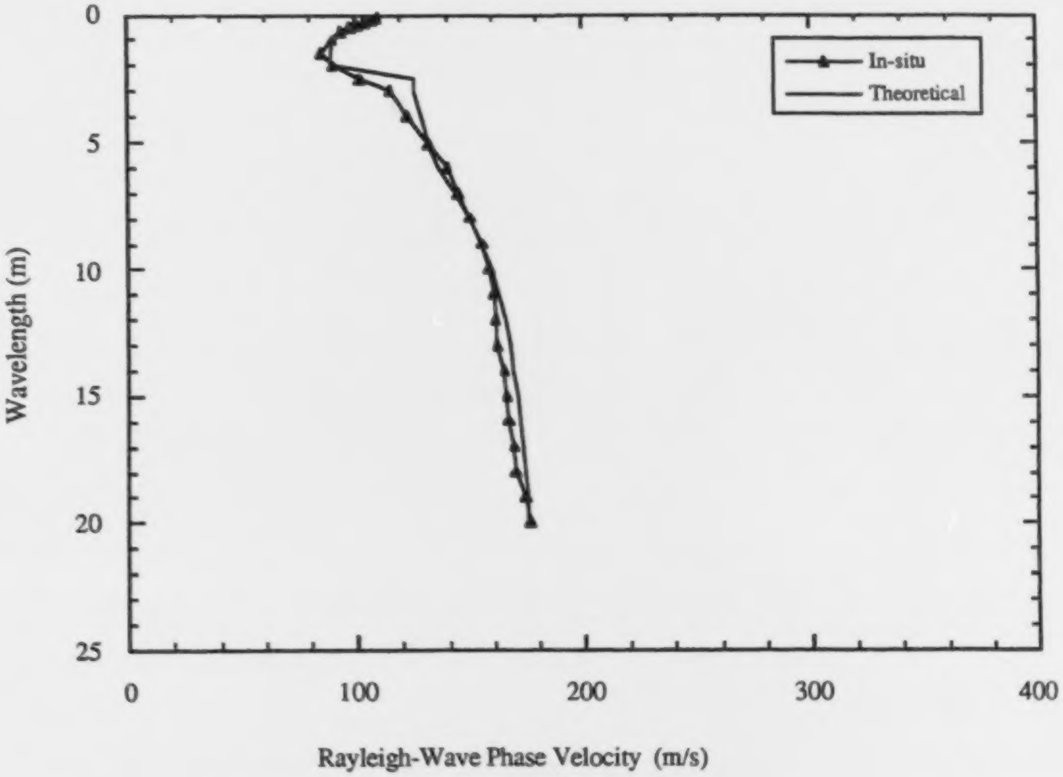

Figure 5.9a. Theoretical and In-situ Dispersion Curves at Delta Site.

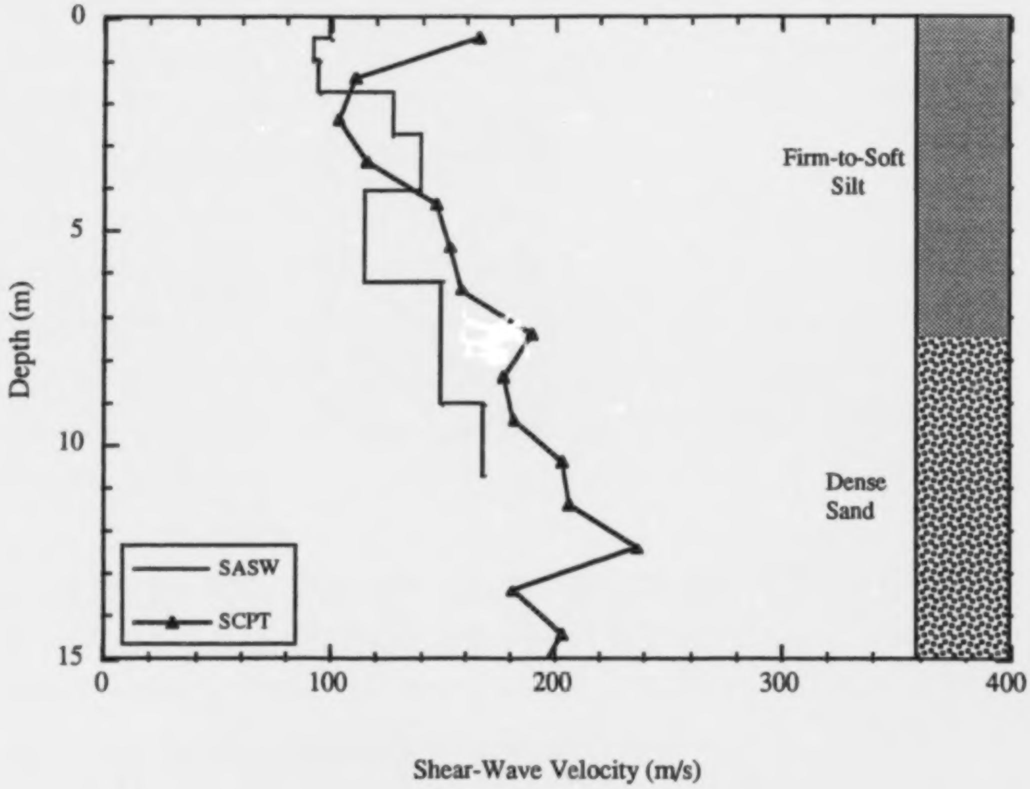

Figure 5.9b. Shear Wave Velocity Profile at Delta Site.

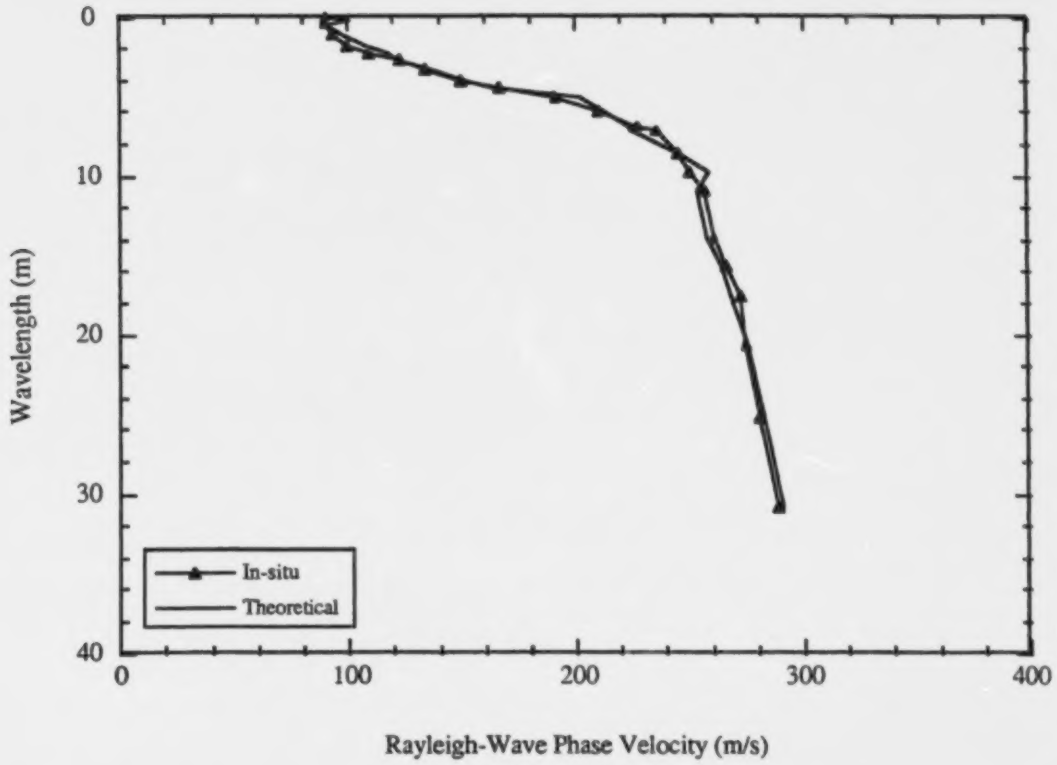

Figure 5.10a. Theoretical and In-situ Dispersion Curves at Matsqui Site.

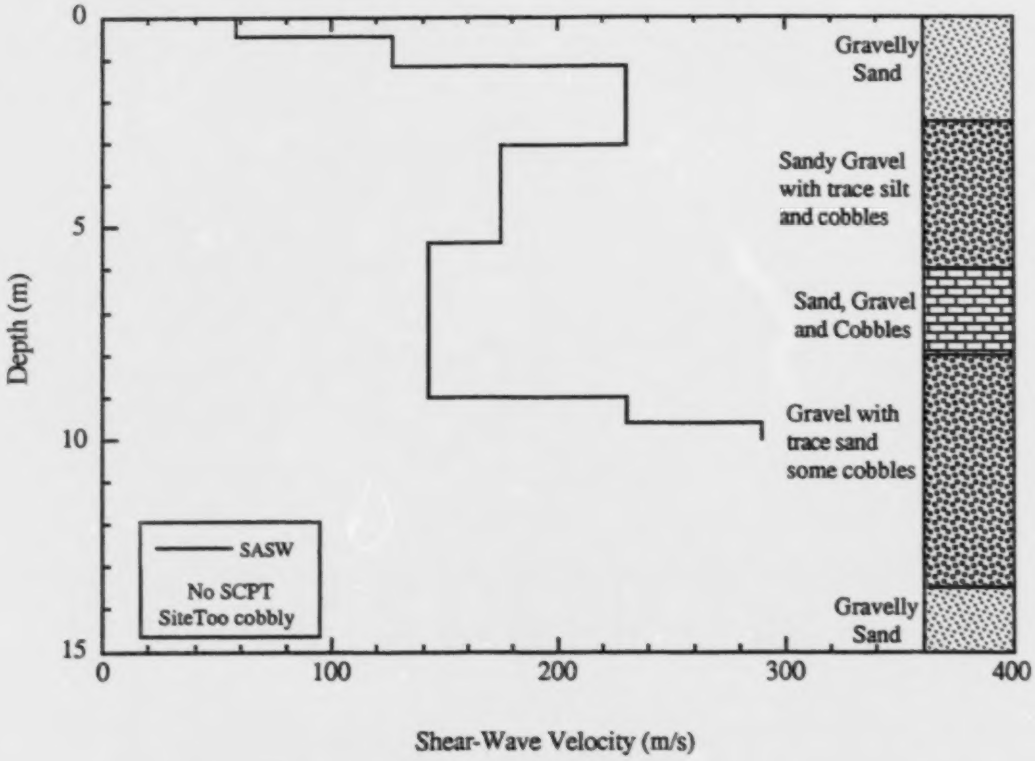

Figure 5.10b. Shear-wave Velocity Profile at Matsqui Site.

Table 5.1. Measures of Fit between Theoretical and Experimental Dispersion Curves

Test Location	Standard Deviation	Standard Error
University LRT Station	2.62	1.85
NAIT Experimental	3.71	1.85
Blundell	2.31	1.25
Chatham	1.12	0.4
Francis	1.17	0.44
Sea Island	3.88	1.91
Burnaby	4.35	3.07
Annacis	-	-
Delta	1.25	0.81
Matsqui	1.4	0.98

CHAPTER 6

CONCLUSIONS AND RECOMMENDATIONS

6.1 Summary

The SASW technique requires no boreholes and is fast and economic to perform. The test is well-suited to sites where access may be difficult for large equipment or where subsurface conditions make it difficult to perform the seismic cone penetration test.

A modified version of the Spectral Analysis of Surface Wave technique has been developed. The equipment for field testing has been trimmed and simplified, the analysis speed has been improved and automated. This system is based on a microcomputer programmed to acquire waveform data and perform the relevant spectral analyses and forward modelling. The equipment and analysis programs were evaluated at ten different sites in western Canada and have both shown to be working effectively at some sites but not so well at other sites. For most of the sites, shear wave velocity profiles obtained using the SASW method compared well with profiles independently determined using the seismic cone penetrometer.

The microcomputer based system reduces the cost of equipment and allows on-site determination of the field dispersion curve. Hence preliminary interpretation can be made during testing on a site. The automation of the inversion process also reduces the reliance on experienced personnel to perform the forward modelling. Secondly, the restriction on the number of receivers has been removed. The number of receivers is now user-defined and is limited only by the speed of the data acquisition cards installed in the microcomputer.

6.2 Conclusions

The conclusions that can be drawn from this research may be outlined as follows:

1. A microcomputer has been equipped and programmed to acquire, analyze and determine in-situ surface wave dispersion curves on site. This represents an elimination of the single most expensive equipment required for SASW testing, while extending the uses of the attached microcomputer. This micro-computerization has reduced the cost for an operational SASW system, saved the time spent in transferring files from the analyzer to the microcomputer in existing instrumentation systems and brought the SASW technique closer to automation.

2. An array of more than two receivers can now be used in the SASW test procedure as a result of the elimination of the restriction imposed by the commonly used dual-channel spectrum analyzer. This represents an economic saving over the use multi-channel spectrum analyzers for array testing.

3. Results indicate that one receiver spacing may be used in defining the entire dispersion curve for a site if signals of the appropriate frequencies are generated by the source. The use of dispersion points from many receiver spacings for defining the in-situ dispersion curve is a good research idea in that the effect of small layer inclinations tend to be averaged off. For most sites, this approach may be too time-consuming from a commercial standpoint since too much duplication of the dispersion points occur from spacing to spacing.

4. The algorithm on which the dispersion calculations in this research are based, is reported to be one of the fastest forward modelling algorithms.

5. Forward modelling calculations have been extended to include the dispersion of Love waves. Though SASW-FM contains this feature, more testing is required to ensure that results are consistent with those from other independent forward modelling programs.

6. The process of matching the in-situ and theoretical dispersion curves has been automated and hence does not require intervention or extensive knowledge of surface wave dispersion theory.

6.3 Recommendations

The technique of non-intrusively determining the low-strain elastic properties and thicknesses of soil and pavement layers by surface wave dispersion is very attractive. For increased use of the technique, the following areas require further research.

1. The procedure for defining the in-situ dispersion curve needs to be carefully reviewed and standardized. Such a step would enable the comparison of results from other researchers in other countries. Current criteria for defining the in-situ curve differ extensively and are even contradictory in some cases e.g. which wavelengths are acceptable for the definition of the curve and which are not. On many occasions, the application of Heisey's criteria would have meant the rejection of certain portions of an otherwise continuous dispersion curve. The recommendations by Sanchez (1988) which is based on theoretical studies, directly contradicts Heisey's criteria. Heisey's criteria were used initially in this research, but need to be further scrutinized.

2. It appears that the in-situ dispersion curve measured in the field from combining dispersion points from a number of spacings is assumed to be due to the fundamental mode of propagation. Throughout this research, it was abundantly clear that phase velocities measured at larger receiver spacings appear to be higher than at smaller

spacings for the same wavelength. Jones (1958) reported similar observations when performing a steady vibration test on soils. This observation is important for the definition of the fundamental mode. The dispersion curves measured in the field need be dissociated into the appropriate propagation modes. This subject requires further study. It appears that the effect of the role played by higher modes may be one of the empirical basis for Heisey's criteria.

3. The SASW method in this research was based on Rayleigh waves generated from a vertical hammer impact. Further investigations into other sources of energy are required in an effort to increase the range of frequencies generated and hence increase the detail and depth capability of the method.

4. Shear wave velocities are dependent on the in-situ stress levels in the directions of propagation and particle displacements. Thus measurement of shear wave velocities in different directions may be used to determine measures of these native stresses.

BIBLIOGRAPHY

ABBISS, C. P. 1981. Shear wave measurements of the elasticity of the ground. Geotechnique, Vol. 31, No. 1, pp. 91-104.

ABBISS, C. P. and ASHBY, K. D. 1984. Determination of ground moduli by a seismic noise technique on land and on the sea bed. Geotechnique, Vol. 34, pp. 445-450.

ADDO, K.O. and ROBERTSON, P.K. 1991. Shear wave velocity mesurement of soils using Rayleigh waves. Proceedings of the 44th Canadian Geotechnical Conference, Calgary, Alberta, Vol. 1, pp. 11.1-11.10.

AKI, K. and RICHARDS, P.G. 1980. Quantitative Seismology. W. H. Freeman, San Francisco, California, 557 pp.

ALEKSEEV, A.S. 1962. Some converse problems in wave propagation theory. Bulletin of the Academy of Sciences, Russia, Vol. 11 , pp. 1-11.

ANDREASSON, B. 1979. Deformation characteristics of soft, high-plastic clays under dynamic loading conditions. PhD Dissertation, Department of Civil Engineering, Chalmers University of Technology, Gothenburg, Sweden.

BALDI, G., BRUZZI, D., SUPERBO, S., BATTAGLIO, M. and JAMIIOLKOWSKI, M. 1988. Seismic cone in Po River sand. Proceedings of the First International Symposium on Penetration Testing (ISOPT-1), Orlando, Florida, Vol. 2, pp. 643-650.

BALLARD (JR), R.F. 1964. Determination of soil shear moduli at depths by in-situ vibratory techniques. United States.Army Engineer Waterways Experiment Station, Corps of Engineers, Vicksburg, MS, MP No. 4-691, 9 pp.

BALLARD (JR), R.F. and CHANG, F.K. 1973. Rapid Subsurface Exploration: Report 1: Review of selected geophysical techniques. U.S. Army Engineers Waterways Experiment Station, Corps of Engineers, Vicksburg, MS, S-69-30, 17 pp.

BATH, M. 1974. Spectral Analysis in Geophysics. Elsevier, Amsterdam, 563 pp.

BERGSTRÖM, S.G. and LINDERHOLM, S. 1946. A dynamic method for determining average elastic properties of surface soil layers. Proceedings, Handlingar, Svenska Forskningsintitutet för Cement och Betong vid Kungl, Techniska Högskolan i Stockholm, Vol. 7, pp. 1-47.

BOLT, B.A. 1976. Nuclear explosions and earthquakes. W.H. Freeman and Company, San Francisco, California, 309 pp.

BOORE, D.M. 1972. Finite difference methods for seismic wave propagation in heterogeneous materials. Methods in Computational Physics, Vol. 11, pp. 1-37.

BORM, G.W. 1977. Methods from exploration seismology - reflection, refraction and borehole prospecting. Dynamical Methods in Soil and Rock Mechanics, Vol. 3, pp. 87-112.

BRENT, R.P. 1973. Algorithms for minimization without derivatives. Prentice-Hall, Englewood Cliffs, New Jersey.

BURLAND, J.B. 1989. "Small is beautiful" - the stiffness of soils at small strains. Canadian Geotechnical Journal, Vol. 26, pp. 499-516.

CACECI, M.S. and CACHERIS, W.P. 1984. Fitting curves to data - the simplex algorithm is the answer. Byte, Vol. 9, No. 5, pp. 340-362.

CAMPANELLA, R.G. and STEWART, W.P. 1991. Downhole seismic cone analysis using digital signal processing. Proceedings, Second International Conference on Recent

Advances in Geotechnical Earthquake Engineering and Soil Dynamics, St. Louis, Missouri, pp. 77-82.

CATERPILLAR TRACTOR COMPANY. 1966. Handbook of ripping. Preoria, III edition, Caterpillar Tractor Company.

COOLEY, J.W. and TUKEY, J.W. 1965. An algorithm for the machine calculation of complex Fourier series. Mathematics of Computation, Vol. 19, pp. 297-301.

DAS, B.M. 1983. Fundamentals of soil mechanics. Elsevier, Oxford.

DOBRIN, M.B. 1960. Introduction to geophysical prospecting. McGraw-Hill Book Company, New York, 435 pp.

DORMAN, J. and EWING, M. 1962. Numerical inversion of seismic surface wave dispersion data and crust-mantle structure in the New York - Pennsylvania Area. Journal of Geophysical Research, Vol. 67, No. 13, pp. 5227-5241.

DUNKIN, J.W. 1965. Computation of modal solutions in layered, elastic media at high frequencies. Bulletin of the Seismological Society of America, Vol. 55, pp. 335-358.

DZIEWONSKI, A. M. and HALES, A.L. 1972. Numerical analysis of dispersed surface waves. Methods in Computational Physics, Vol. 11, pp. 39-85.

EWING, W. M., JARDETZKY, W.S. and PRESS, F. 1957. Elastic waves in layered media. McGraw-Hill Book Company, New York.

FILIPCZYNSKI, L., PAWLOWSKI, Z. and WEHR, J . 1966. Ultrasonic methods of testing materials. Butterworths, London, UK.

FRY, Z.B. 1963. A procedure for determining elastic moduli of soils by field vibratory techniques. U.S. Army Engineers Waterways Experiment Station, Corps of Engineers, Vicksburg, MS, MP No. 4-577.

FUTTERMAN, W. I. 1962. Dispersive body waves. Journal of Geophysical Research, Vol. 67, pp. 5279-5291.

GARDNER, D.H. 1938. Measurement of relative ground motion in reflection recording. Geophysics, Vol. 3, pp. 40-45.

GILBERT, F. and BACKUS, G.E. 1966. Propagator matrices in elastic wave and vibration problems. Geophysics, Vol. 31, pp. 326-332.

GILLESPIE, D.G . 1989. Evaluating velocity and pore pressure data from the cone penetration test. PhD Dissertation, Department of Civil Engineering, University of British Columbia, Canada, 183 pp.

HAMMING, R.W. 1983. Digital filters (Second Edition). Signal Processing Series, Prentice Hall, Englewood Cliffs, New Jersey.

HARDIN, B.O. and Drnevich, V.P. 1972. Shear modulus and damping in soils: measurement and parameter effects. Journal of the Soil Mechanics and Foundation Engineering Division, ASCE, Vol. 95, No. SM6, pp. 603-624.

HASKELL, N. A. 1953. The dispersion of surface waves on multilayered media. Bulletin of the Seismological Society of America, Vol. 43, pp. 17-34.

HEISEY, J.S. 1982. Determination of in-situ shear wave velocity from spectral analysis of surface waves. MSc. Thesis, Department of Civil Engineering, University of Texas at Austin, TX, 300 pp.

HEUKELOM , W. and KLOMP, A.J.G. 1962. Dynamic testing as a means of controlling pavements during and after construction. Proceedings of the International Conference on Structural Design of Asphalt Pavements, Ann Arbor, Michigan, pp. 667-679.

HEUKELOM, W. and FOSTER C.R. 1960. Dynamic testing of pavements. Proceedings of the ASCE Journal of Soil Mechanics and Foundation Division, New York, No. SM1, Part 1, Vol. 86, pp. 1-28.

HILDEBRAND, F.B. 1952. Methods of applied mathematics. Prentice Hall, New Jersey.

HILTUNEN, D.R. and WOODS, R.D. 1988. SASW and crosshole test results compared. Proceedings of the ASCE Specialty Conference, Geotechnical Engineering Division, Vol. G, SP No. 20, pp. 279-289.

HILTUNEN, D.R. and WOODS, R.D. 1989. Influence of source and receiver geometry on the testing of pavements by the surface waves method. Nondestructive Testing of Pavements and Backcalculation of Layer Moduli. ASTM STP 1026, A.J. Bush (III) and J.Y. Baladi (Editors), pp. 138-154.

HOAR, R. J. 1982. Field measurement of seismic wave velocity and attenuation for dynamic analyses. Ph.D Dissertation, Department of Civil Engineering, University of Texas, Austin, Texas, 478 pp.

HOARDLEY, P.J. 1985. Measurement of dynamic soil properties. A.A. Balkema, Amsterdam, Netherlands, pp. 349-405.

HUSSON, D., BENNETT, S.D. and KINO, G.S. 1983. Materials Evaluation, American Society for Nondestructive Testing, Vol. 43, pp. 92-100.

JONES, R. 1949. Measurement of the thickness of concrete pavements by dynamic methods: a survey of the difficulties. Magazine of Concrete Research, January, pp. 31-34.

JONES, R. 1949. The non-destructive testing of concrete. Magazine of Concrete Research, June, pp. 67 - 77.

JONES, R. 1953. In-situ measurement of the dynamic properties of soil by vibration methods. Geotechnique, Vol. 8, pp. 1-21.

JONES, R. 1955. A vibration method for measuring the thickness of concrete road slabs in situ. Magazine of Concrete Research, pp. 97-102.

JONES, R. 1962. Surface wave technique for measuring the elastic properties and thickness of roads: theoretical development. British Journal of Applied Physics, Vol. 13, pp. 21-29.

KAUSEL, E. and ROESSET, J. M. 1981. Stiffness matrices for layered soils. Bulletin of the Seismological Society of America, Vol. 71, No. 6, pp. 1743-1761.

KERNIGHAN, B.W. and RITCHIE D.M. 1978. The C Programming Language (second edition). Prentice Hall- Englewood Cliffs, New Jersey, 272 pp.

KNOPOFF, L. 1964. A matrix method for elastic wave problems. Bulletin of the Seismological Society of America, Vol. 54, No. 1, pp. 431-438.

KOLSKY, H. 1952. Stress waves in solids. Dover Publications, New York, 213 pp.

KROHN, C.E. 1983. Geophone ground coupling, Geophysics, Vol. 49, No. 6, pp. 722-731.

LANDISMAN, M., DZIEWONSKI, A. and SATO, Y. 1969. Geophysical Journal of the Royal Astronomical Society, Vol. 17, pg. 369.

LARSSON, R. AND MULABDIC, M. 1991. Shear moduli in Scandinavian clays. Swedish Geotechnical Institute, Report No. 40, Linkoping, Sweden, 127 pp.

LOVE, A.E.H . 1927. Some Problems of geodynamics. University Press, Cambridge, U.K.

LYSMER, J. and DRAKE, L.A. 1972. A finite element method for seismology. Methods in Computational Physics, Vol. 11, pp. 181-216.

MEISNER, R. 1965. P- and SV-Waves from uphole shooting. Geophysical Prospecting, Vol. 13, No. 3, pp. 433-459.

MILLER, G. F. and PURSEY, H. 1955. On the partition of energy between elastic waves in a semi-infinite solid. Proceedings of the Royal Society of London, Series A, Mathematical and Physical Sciences, Vol. 233, pp. 55-59.

MORA, P. 1988. Elastic wavefield inversion and the adjoint operation for the elastic wave equation. Mathematical Geophysics, Vlaar, N.J., Nolet G., Wortel, M.J.R., Cloetingh, S.A.P.L. (Editors), D. Reidel Publishing Company, Dordrecht, Holland, pp. 117-137.

MURPHY, V.J. 1972. Geophysical engineering investigation techniques for microzonation. Proceedings of the International Conference on Microzonation for safer construction: Research and Application, Vol. 1, Seattle, WA, pp. 131-159.

NAZARIAN, S . 1984. In situ determination of elastic moduli of soil deposits and pavement systems by spectral analysis of surface waves method. PhD Dissertation, Department of Civil Engineering, University of Texas at Austin, Austin, TX, 453 pp.

NELDER, J.A. and MEAD, R. 1964. A simplex method for function minimization. The Computer Journal, Vol. 7, pp. 308-313.

NIJBOER, L.W. and METCALF, C.T. 1962. Dynamic testing at the AASHO road test. Proceedings of the International Conference on Structural Design of Asphalt Pavements, Ann Arbor, Michigan, pp. 713-721.

Nyland, E. 1991. Personal Communication. Department of Physics. University of Alberta, Edmonton, Alberta, Canada.

OGURA, K. 1979. Development of a suspension type S-wave log system. Oyo Corporation, Technical Note TN-34, ,Tokyo, Japan, 23 pp.

OLSON, L.D. 1991. Measurement of subsurface, deep foundation and slab/subgrade conditions with in situ seismic, sonic and vibration methods. American Society of Civil Engineers, pp.

PRESS, F., HARKRIDER, D. and SEAFELDT, C.A. 1961. A fast convenient program for computation of surface-wave dispersion curves in multi-layered media. Bulletin of the Seismological Society of America, Vol. 51, No. 4, pp. 495-502.

PRESS, W.H., FLANNERY, B.P., TEUKOLSKY, S.A. AND VETTERLING, W.T. 1988. Numerical Recipes in C. Cambridge University Press, New York, 735 pp.

RAMIREZ, R.W. 1985. The FFT fundamentals and concepts. Prentice-Hall, Englewood Cliffs, New Jersey, 178 pp.

RANDALL, M.J. 1967. Fast programs for layered half-space problems. Bulletin of the Seismological Society of America, Vol. 57, No. 6, pp. 1299-1315.

RAYLEIGH, J.W.S. 1885. On waves propagated along the plane surface of an elastic solid. Proceedings of the London Mathematical Society, United Kingdom, Vol. 17 (Series 1), pp. 4-11.

REDPATH, B.B. 1973. Seismic refraction exploration for engineering site investigation. United States Army Engineer Waterways Experiment Station, Corps of Engineers, Vicksburg, MS, Technical Report TRE-73-4, 52 pp.

RICHART, F. E., HALL, J. R. and WOODS, R. D. 1970. Vibrations of soil and foundations. Englewood Cliffs, New Jersey, 414 pp.

RIX, G. J. 1988. Experimental study of factors affecting the spectral analysis of surface waves method. PhD Dissertation, Department of Civil Engineering, University of Texas at Austin, TX, 315 pp.

ROBERTSON, P.K., CAMPANELLA , R.G., GILLESPIE, D. and RICE, A. 1986. Seismic cone penetration test to measure in-situ shear wave velocity. ASCE Journal of Geotechnical Engineering, Vol. 112, No. 8, pp. 791-803.

SANCHEZ-SALINERO, I. 1987. Analytical investigation of seismic methods used for engineering applications. PhD Dissertation, Department of Civil Engineering, University of Texas at Austin, TX 401 pp.

SCHOLTE, J.G. 1947. The range of existence of Rayleigh and Stonely waves. Monthly Notices of the Royal Astronomical Society, Geophysics Supplement, Vol. 5, pp. 120-126.

SCHWAB, F.A. 1970. Surface wave computations: Knopoff's method. Bulletin of the Seismological Society of America, Vol. 60, No. 5, pp. 1491-1520.

SCHWAB, F.A. AND KNOPOFF, L. 1970. Surface-wave dispersion computations. Bulletin of the Seismological Society of America, Vol. 60, No. 2, pp. 321-344.

SCHWAB, F.A. and KNOPOFF, L . 1972. Fast surface wave and free mode computations. Academic Press, New York, pp. 87-180.

SCHWARZ, S.C. and MUSSER, M. 1972. Various techniques for making in-situ wave velocity measurements - a description and evaluation. Proceedings of the International Conference on Microzonation for Safer Construction, Research and Application, Vol. II, Seattle, WA, pp. 593-608.

SEED, H.B., MURARKA, R., LYSMER, J. and IDRISS, I.M. 1976. Relationships of maximum velocity, distance from source and local site conditions for moderately strong earthquakes. Bulletin of the Seismological Society of America, Vol. 66, No. 4, pp. 1323-1342.

SEGEL, L.A. and HANDELMAN, G.H. 1977. Mathematics applied to continuum mechanics. Dover Publications Incorporated, New York, 590 pp.

SEZAWA, K. 1927. Dispersion of Elastic Waves propagated on the Surface of Stratified Bodies and on Curved Surfaces. Bulletin of the Earthquake Research Institute (Japan), Vol. 3, pp. 1-18.

SHERIFF, R.E. and GELDART, L.P. 1982. Exploration seismology Vol. 1: History, theory and data acquisition. University Press, Cambridge, 253 pp.

STOKOE (II), K.H. 1980. Field measurement of dynamic soil properties. ASCE Specialty Conference on Civil Engineering and Nuclear Power, Knoxville, TN, 31 pp.

STOKOE (II), K.H. and HOAR, R.J. 1977. Field measurement of shear wave velocity by crosshole and downhole seismic methods. Proceedings of the Conference on Dynamical Methods in Soil and Rock Mechanics, Karlsruhe, Germany, Vol. III, pp. 115-137.

STOKOE (II), K.H. and WOODS, R.D. 1972. In-situ shear wave velocity by cross-hole method. Journal of the Soil Mechanics and Foundations Division, ASCE, Vol. 98 No. SM5, pp. 443-460.

STOKOE (II), K.H., ARNOLD E.J., HOAR, R. J., SHIRLEY, D.J. and ANDERSON, D.G. 1978. Development of a bottom-hole device for offshore shear wave velocity measurement. Proceedings of the Tenth Annual Offshore Technology Conference, Houston, Texas, pp. 1367-1380.

STONELEY, R. 1924. Elastic waves at the surface of separation of two solids. Proceedings of the Royal Society of London, Series A, Mathematical and Physical Sciences, Vol. 106, pp. 416-428.

TAKAHASHI, T. 1955. Analysis of the dispersion curves of Love waves. Bulletin of the Earthquake Research Institute (Japan), Vol. 33, pp. 287-295.

TELFORD, W.M., GELDART, L.P., SHERIFF, R. E. AND KEYS, D. A. 1984. Applied geophysics. Cambridge University Press, New York, 860 pp.

TERZAGHI, K. 1943. Theoretical soil mechanics. John Wiley & Sons, New York, 510 pp.

THOMSON, W.T. 1950. Transmission of elastic waves through a stratified solid medium. Journal of Applied Physics, Vol. 21, No. 2, pp. 89-93.

THROWER, E.N. 1965. The computation of the dispersion of elastic waves in layered media. Journal of Sound and Vibration, Vol. 2, No. 3, pp. 210-226.

TIMOSHENKO, S.P. and GOODIER, J.N. 1934. Theory of elasticity. McGraw- Hill Book Company, London, United Kingdom, 567 pp.

TOKIMATSU, K., KUWAYAMA, S. and TAMURA, S. 1991. Liquefaction potential evaluation based on Rayleigh wave investigation and its comparison with field behaviour. Proceedings, Second International Conference on Recent Advances in Geotechnical Earthquake Engineering and Soil Dynamics, St. Louis, Missouri, Vol. 1, pp. 357-364.

TURNER, J. D. 1988. Instrumentation for engineers. McMillan Education Limited, London, United Kingdom, 222 pp.

VOSE, G.M. and GREGG, W. 1986. LABVIEW: Laboratory Virtual Instrument Engineering Workbench. Byte, Vol. 11, No. 9, pp. 84-92.

WATSON, T.H. 1970. A note on fast computation of the dispersion of Rayleigh-wave dispersion in the multi-layered elastic half space. Bulletin of the Seismological Society of America, Vol. 60, No. 1, pp. 161-166.

Winkler, K.W. 1986. Estimates of velocity dispersion between seismic and ultrasonic frequencies. Geophysics, Vol. 51, No. 9, pp. 183-189.

WINTER, M.G. and SELBY, A.R. 1990. The measurement of reinstatement backfill quality by a non-intrusive method. Field Testing in Engineering Geology, Geological Society, Engineering Geology Special Publication, No. 6, pp. 275-285.

WOODS, R. D. and JEDELE, L. P. 1985. Energy-attenuation relationships from construction vibrations. Vibration problems in geotechnical engineering, Gazetas, G. and Selig, E.T. (Editors), ASCE, New York, pp. 229-246.

WOODS, R.D. 1978. Measurement of dynamic soil properties. Proceedings of the ASCE Geotechnical Engineering Division, Specialty Conference on Earthquake Engineering and Soil Dynamics, Pasadena, California, Vol. 1, pp. 91-178.

TURNER, J. D. 1988. Instrumentation for engineers. McMillan Education Limited, London, United Kingdom, 222 pp.

VOSE, G.M. and GREGG, W. 1986. LABVIEW: Laboratory Virtual Instrument Engineering Workbench. Byte, Vol. 11, No. 9, pp. 84-92.

WATSON, T.H. 1970. A note on fast computation of the dispersion of Rayleigh-wave dispersion in the multi-layered elastic half space. Bulletin of the Seismological Society of America, Vol. 60, No. 1, pp. 161-166.

Winkler, K.W. 1986. Estimates of velocity dispersion between seismic and ultrasonic frequencies. Geophysics, Vol. 51, No. 9, pp. 183-189.

WINTER, M.G. and SELBY, A.R. 1990. The measurement of reinstatement backfill quality by a non-intrusive method. Field Testing in Engineering Geology, Geological Society, Engineering Geology Special Publication, No. 6, pp. 275-285.

WOODS, R. D. and JEDELE, L. P. 1985. Energy-attenuation relationships from construction vibrations. Vibration problems in geotechnical engineering, Gazetas, G. and Selig, E.T. (Editors), ASCE, New York, pp. 229-246.

WOODS, R.D. 1978. Measurement of dynamic soil properties. Proceedings of the ASCE Geotechnical Engineering Division, Specialty Conference on Earthquake Engineering and Soil Dynamics, Pasadena, California, Vol. 1, pp. 91-178.

APPENDICES

APPENDIX I.

I. SASW-DA PROGRAM SEQUENCE

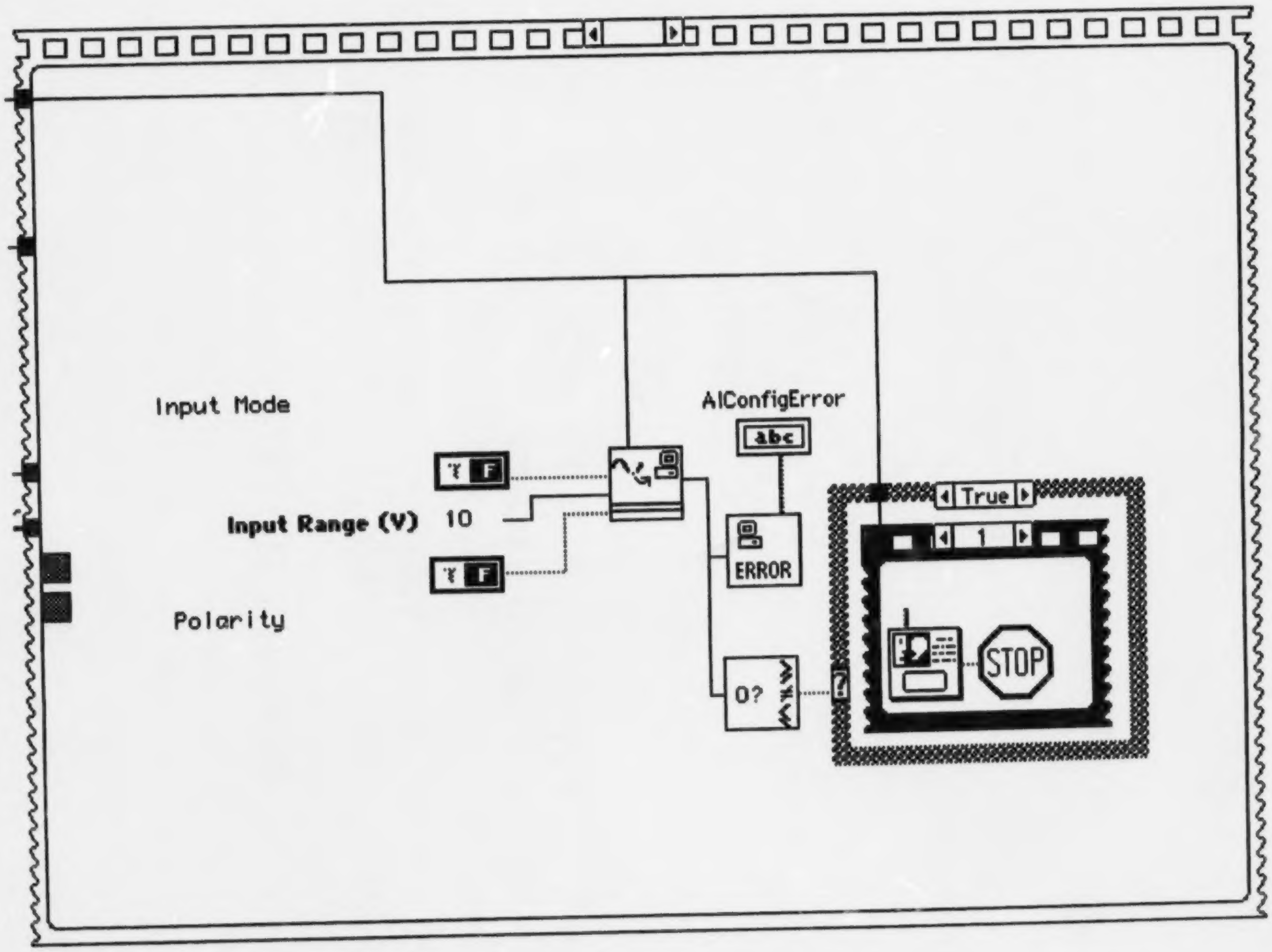
Input Mode
Input Range (V)
10
Polarity
AIConfigError
abc
ERROR
0?
True
1
STOP

Figure AI.1 Configuration of Analogue-to-Digital Card

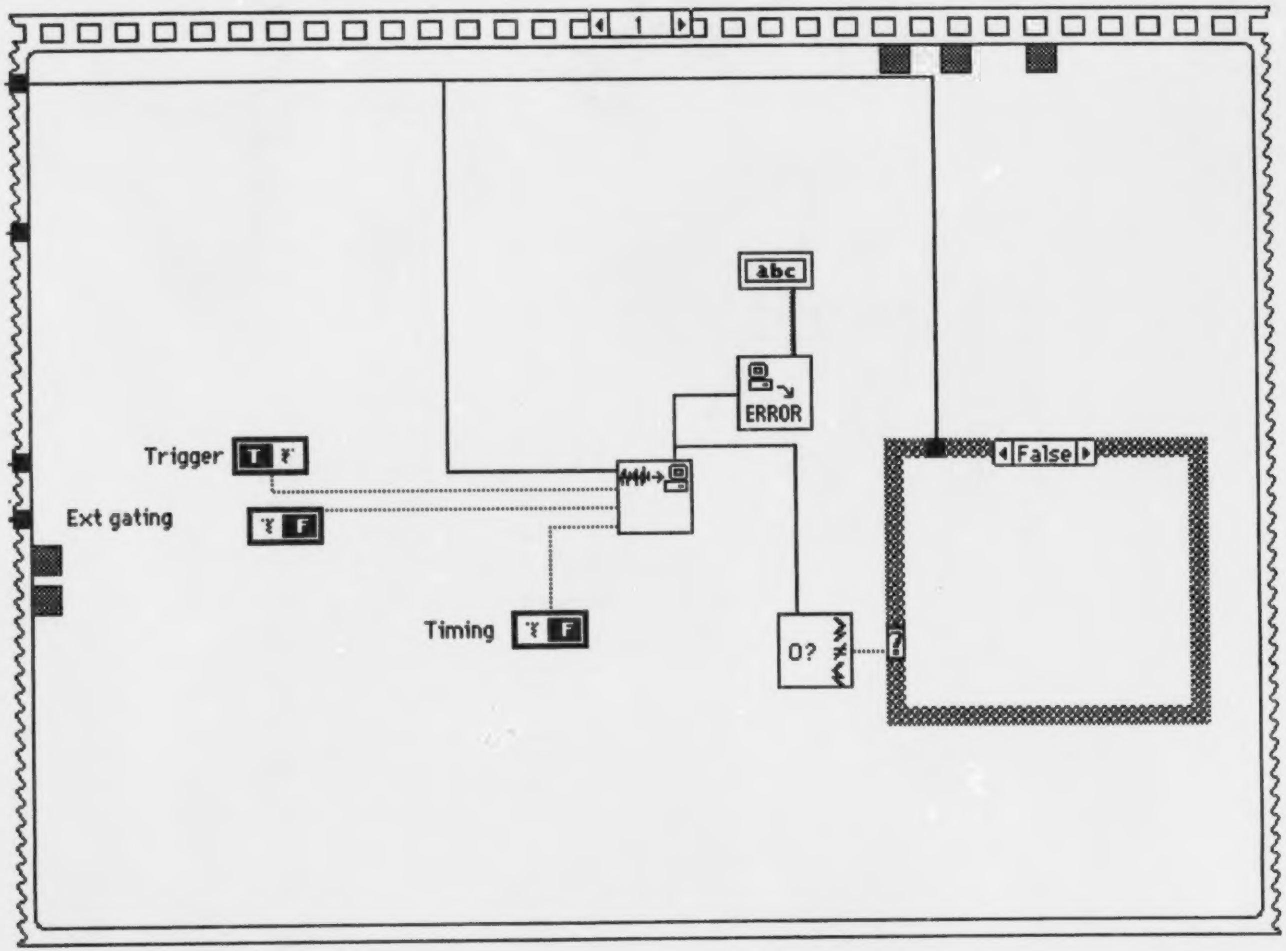
1
abc
ERROR
Trigger
T
F
Ext gating
T
F
Timing
T
F
0?
False
?

Figure AI.2 Set-up Internal Counters for Data Acquisition Control

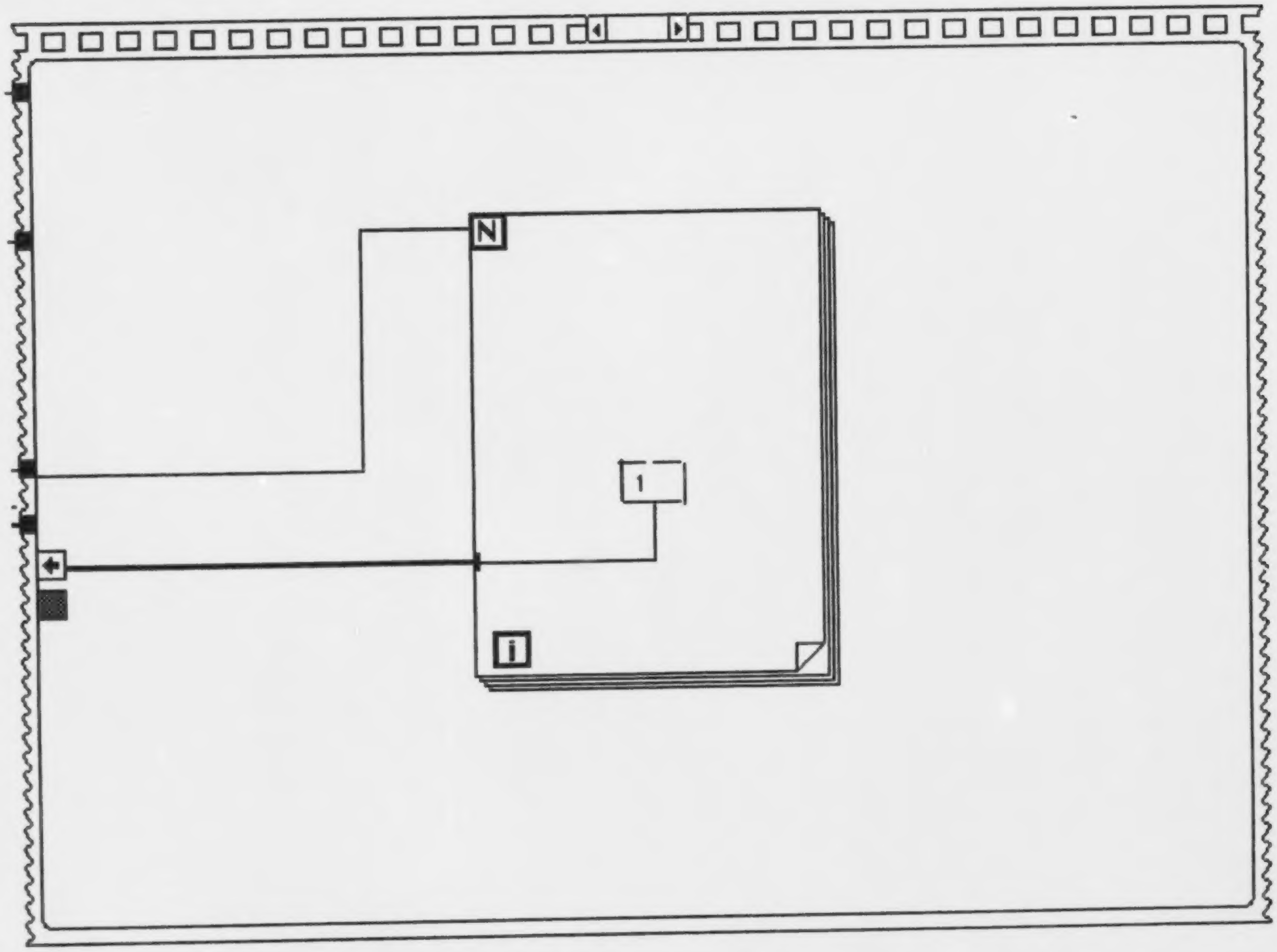

Figure AI.3 Set up of gain vector for all channels

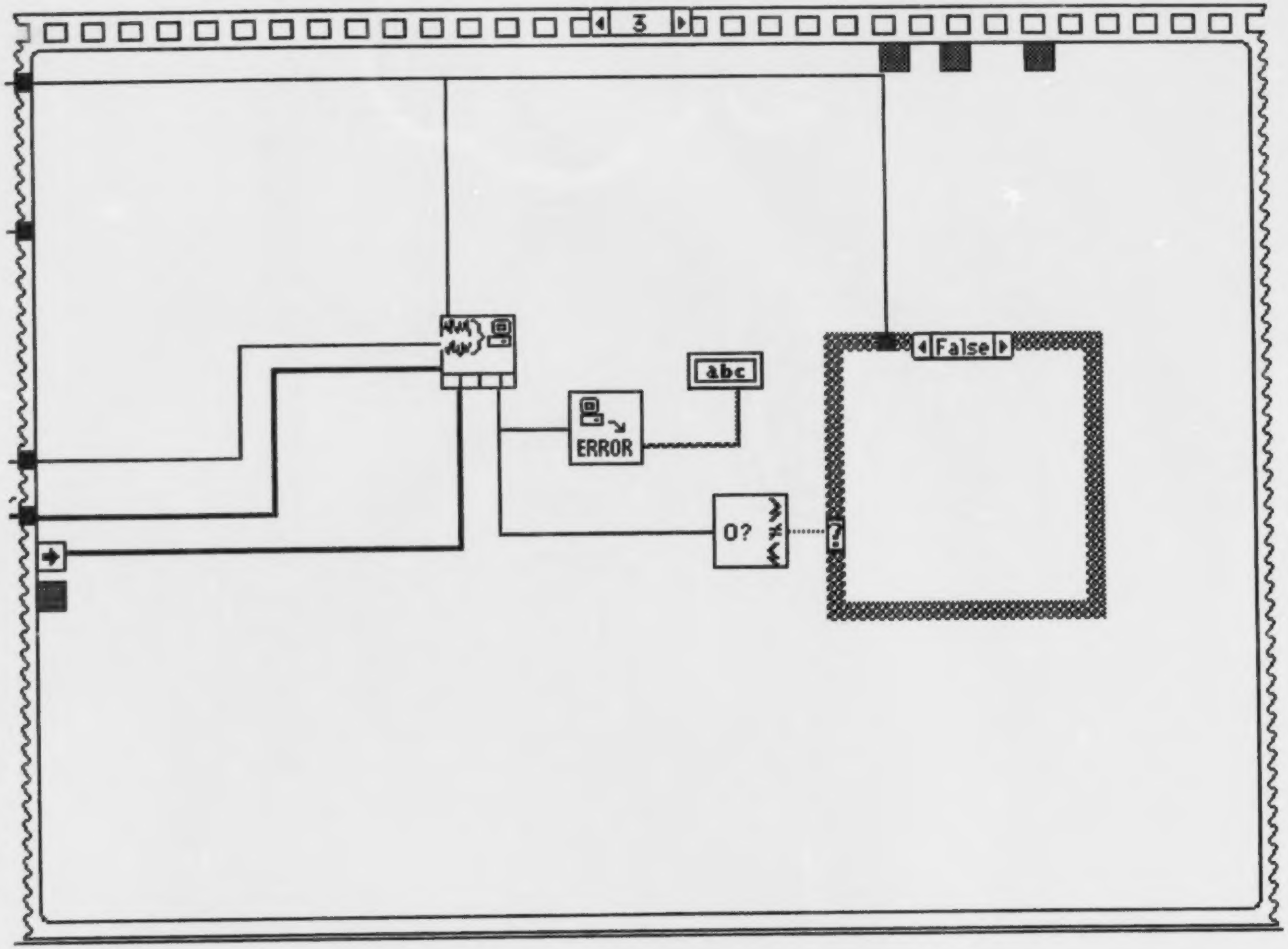
3
False
abc
ERROR
0?

Figure AI.4 Identification of channels to be scanned.

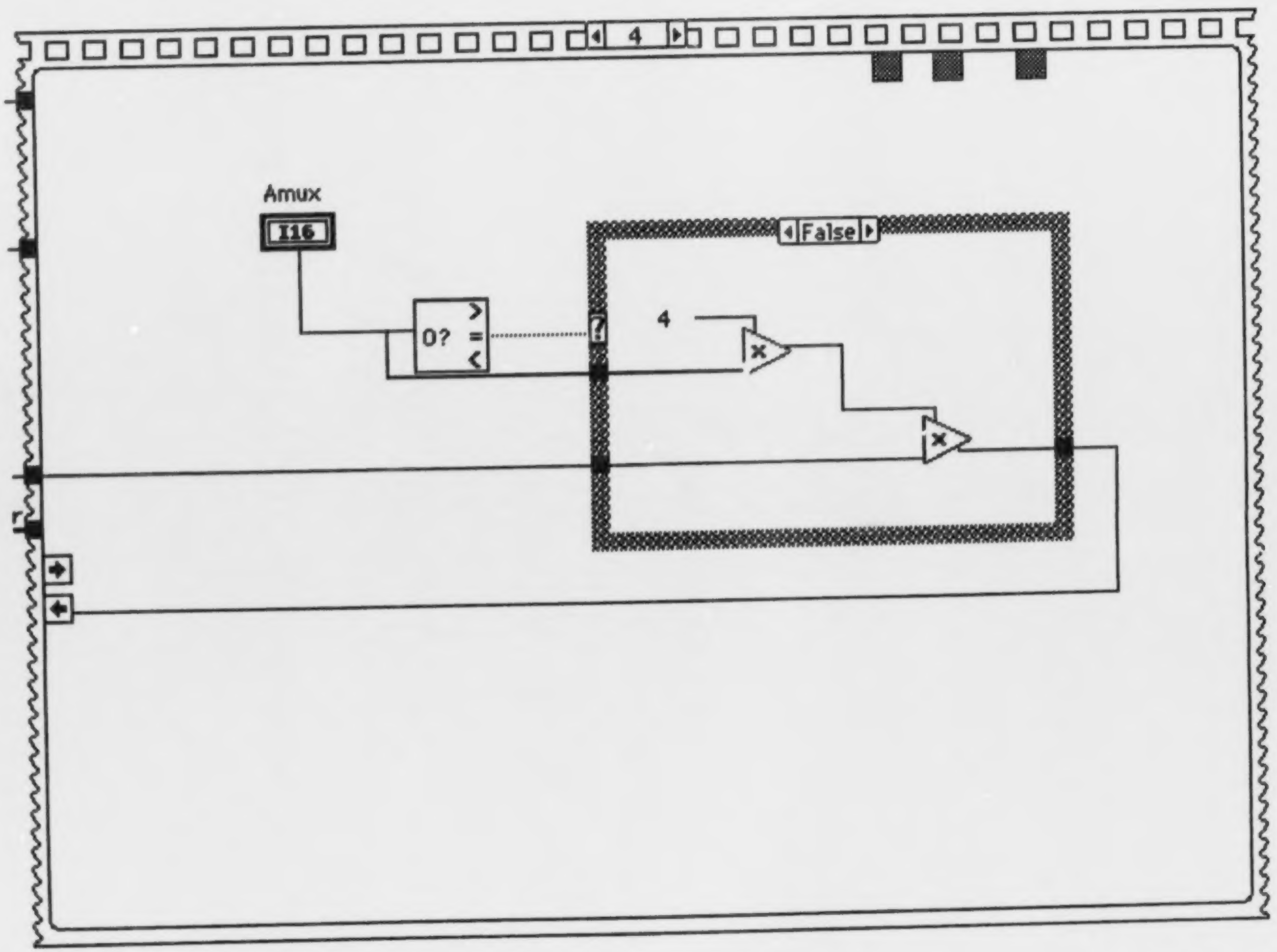
4
Amux
I16
0?
>
=
<
False
4
x
x

Figure AI.5 Account for the presence any multiplexers.

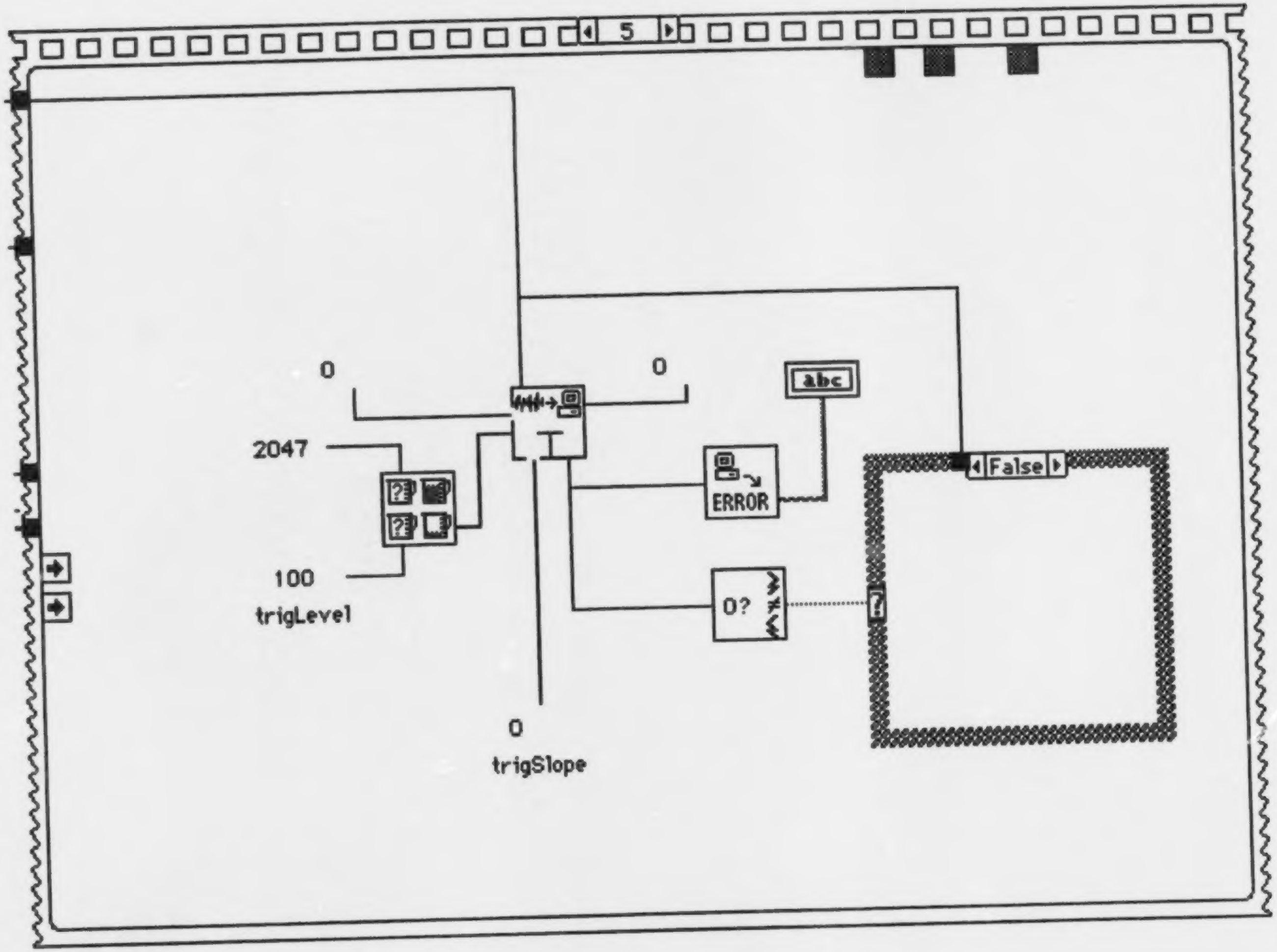
5
0
0
2047
100
trigLevel
0
trigSlope
ERROR
abc
0?
False

Figure AI.6 Set up of trigger conditions

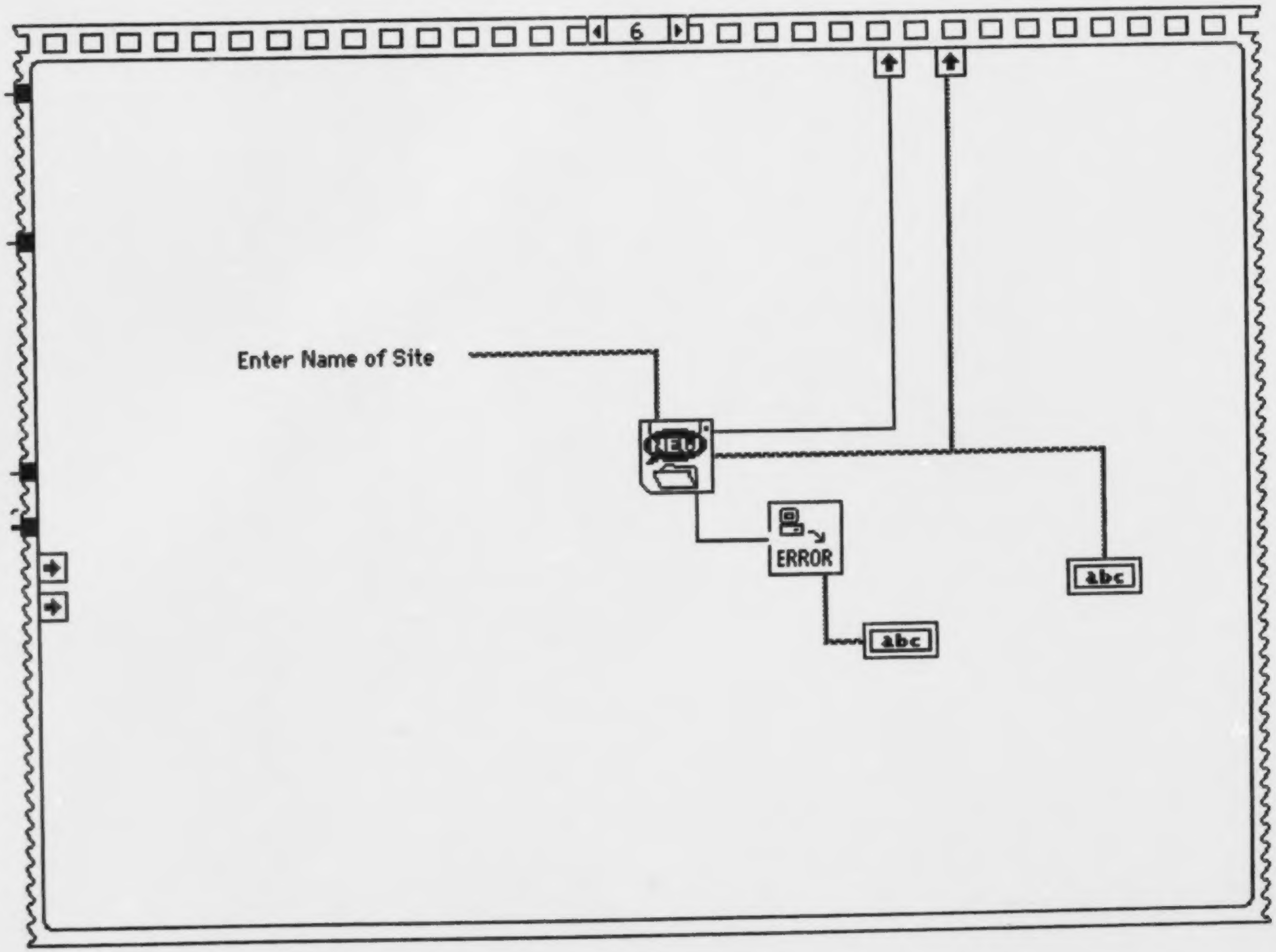
6
Enter Name of Site
NEW
ERROR
abc
abc

Figure AI.7 Prompt for name of site to be tested.

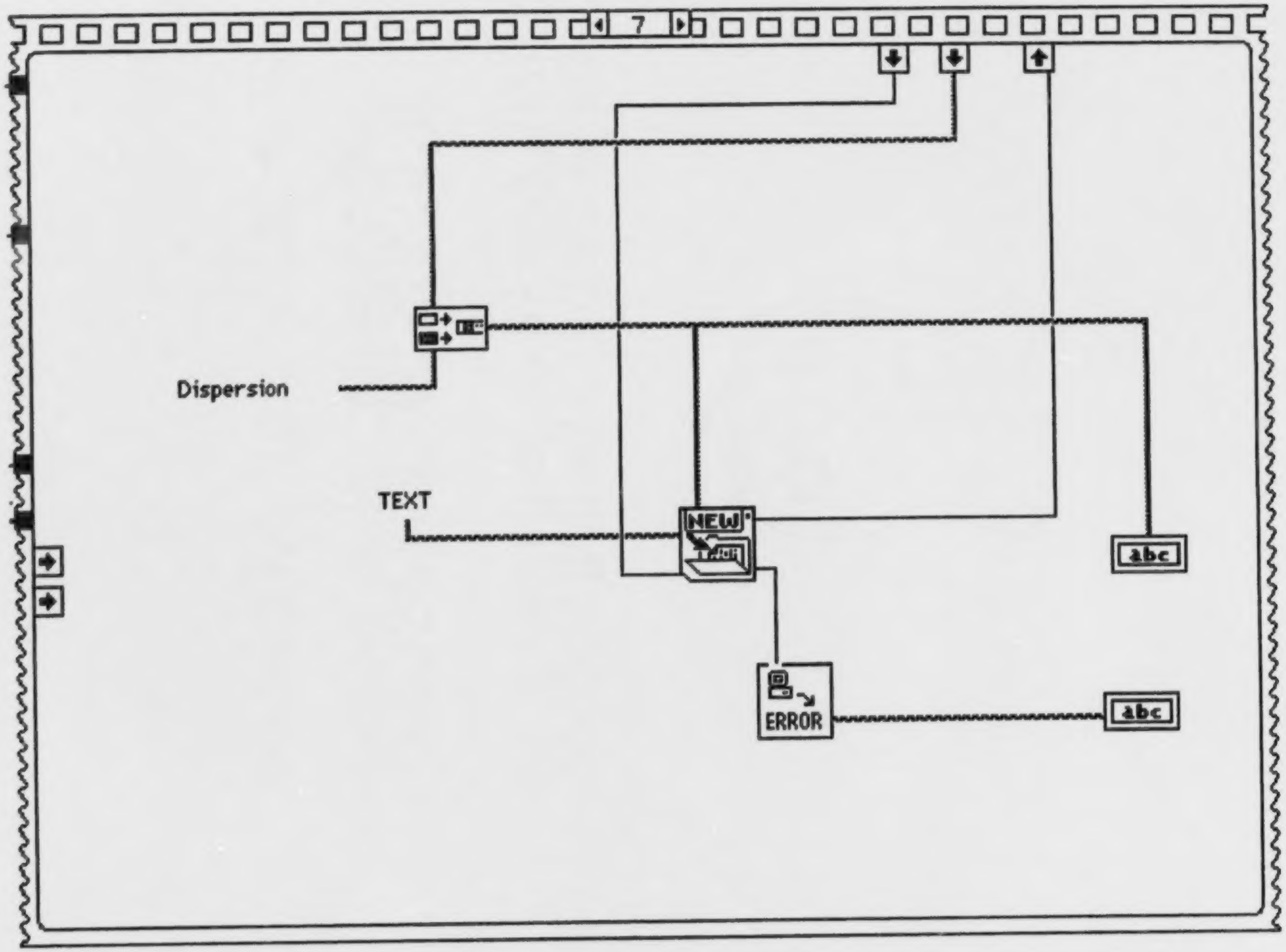
7
Dispersion
TEXT
NEW
ERROR
abc
abc

Figure AI.8 Creation of site dispersion file.

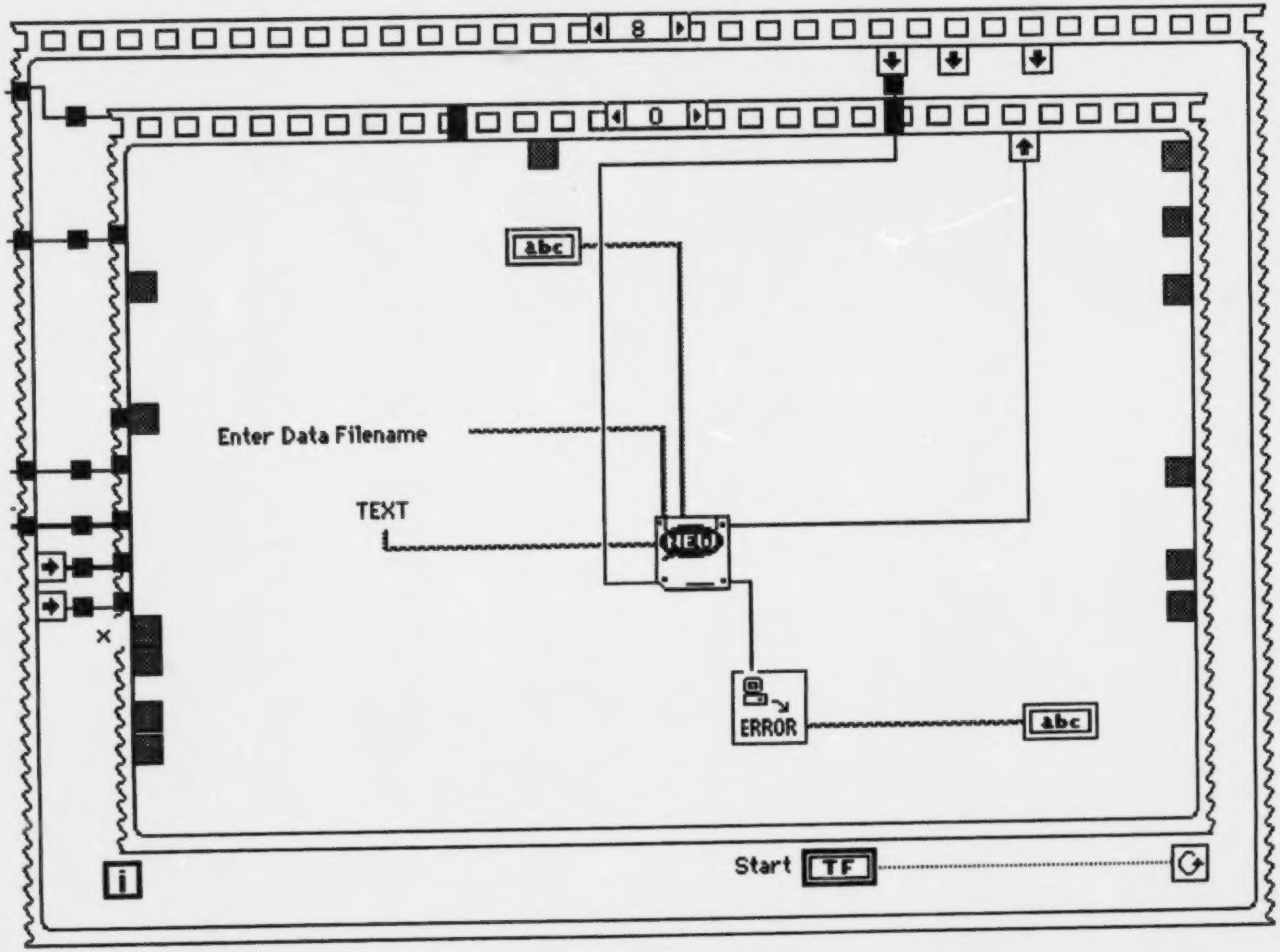
8
0
abc
Enter Data Filename
TEXT
NEW
ERROR
abc
Start
TF
i
×

Figure AI.9 Prompt for filename for spacing dispersion file

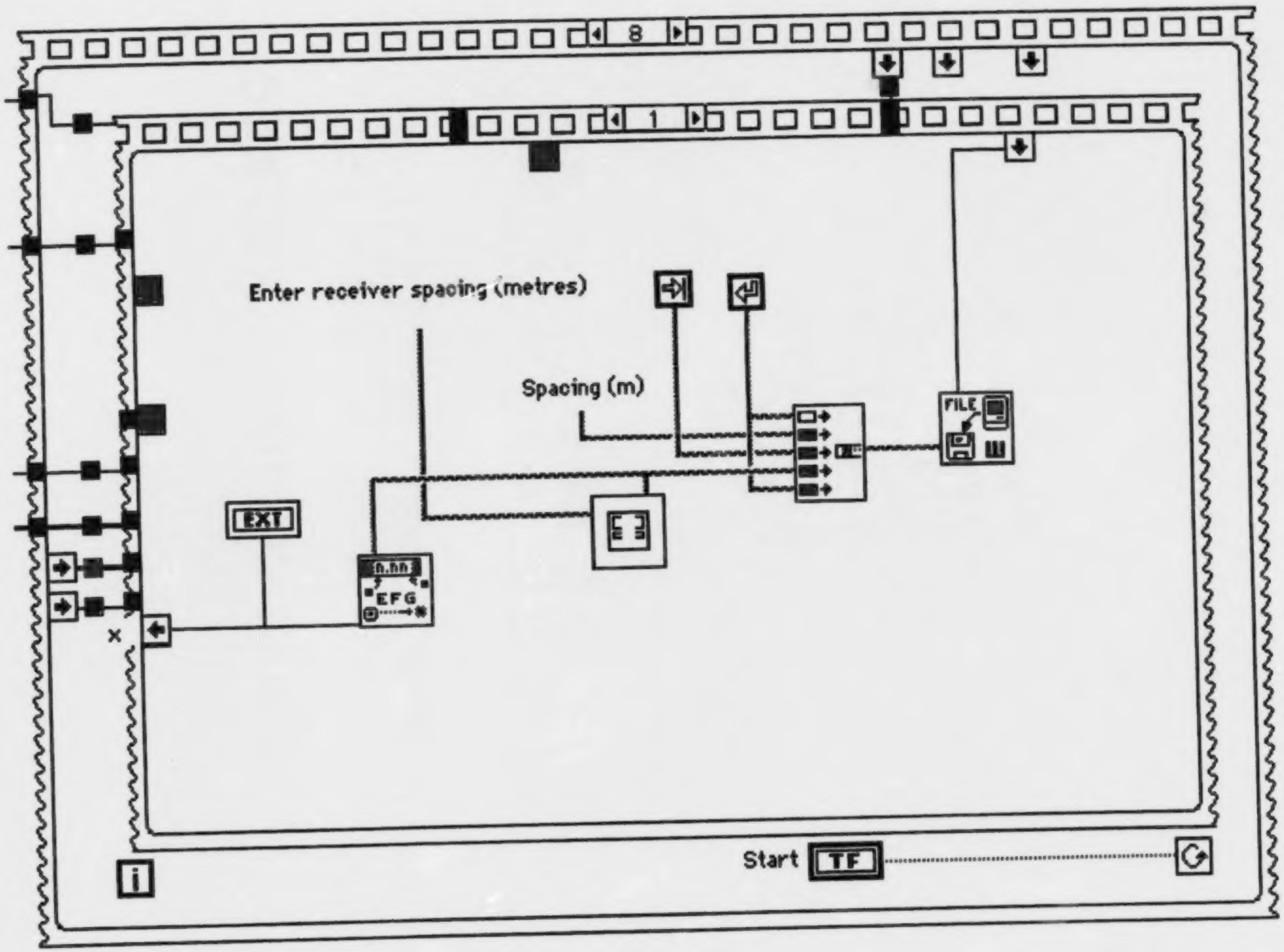
8
1
Enter receiver spacing (metres)
Spacing (m)
FILE
EXT
EFG
TF
Start

Figure AI.10 Prompt for receiver spacing(s)

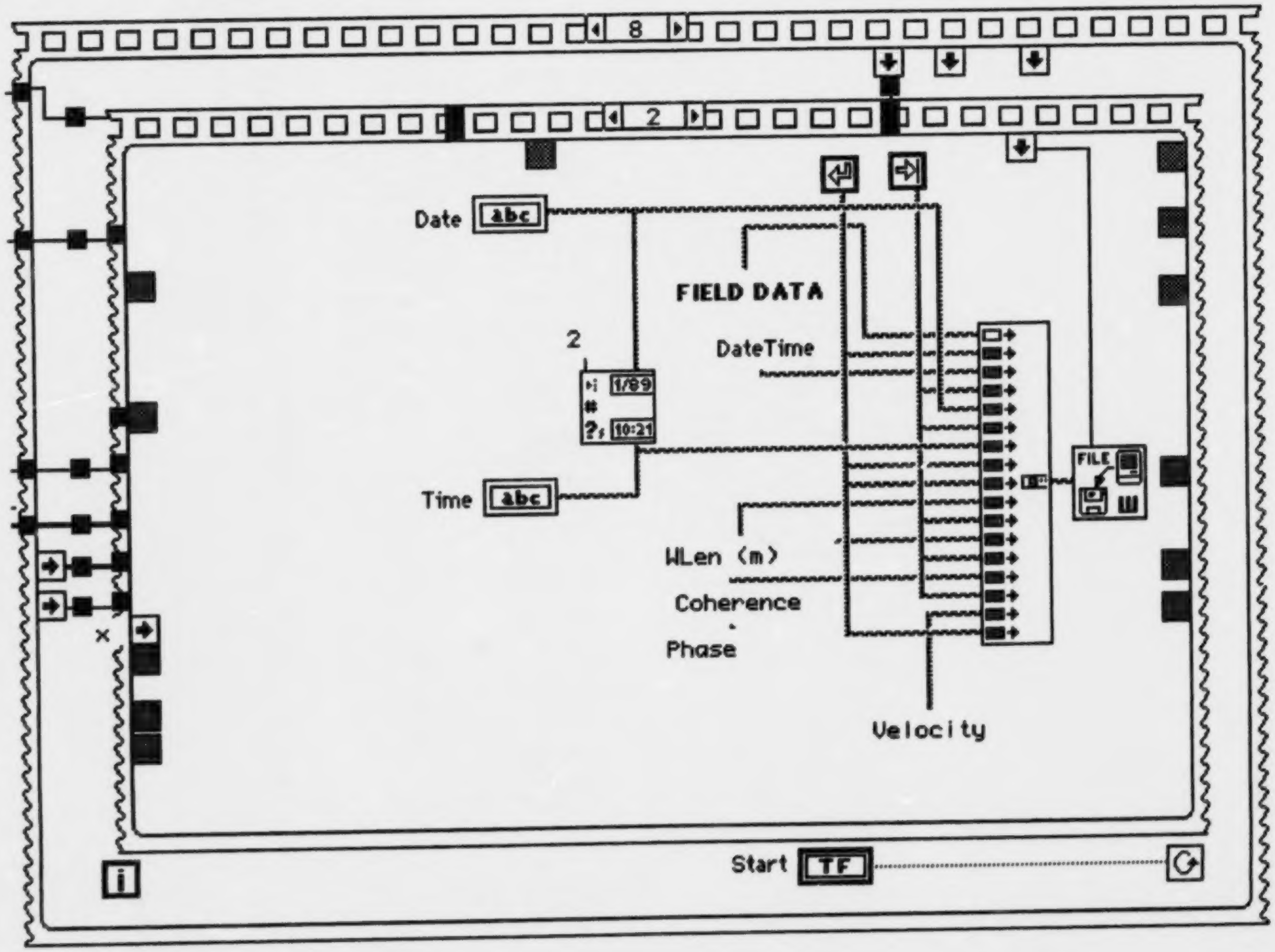
8
2
Date
abc
FIELD DATA
DateTime
2
1/89
10:21
Time
abc
WLen (m)
Coherence
Phase
Velocity
FILE
x
Start
TF

Figure AI.11 Creation of spreadsheet for spacing and site dispersion files

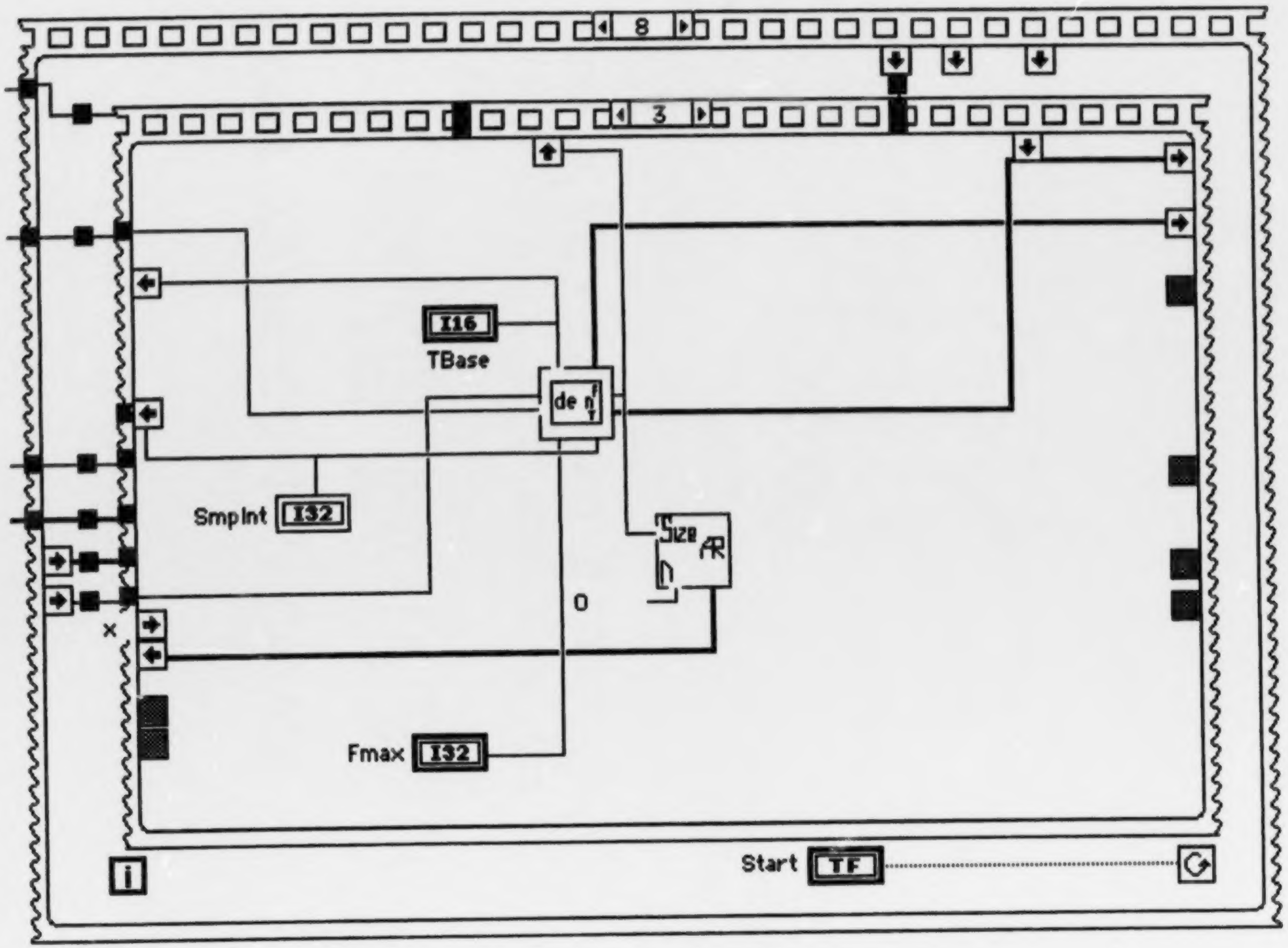
8
3
I16
TBase
Smp Int
I32
Size
0
Fmax
I32
Start
TF
i
×

Figure AI.12 Computation of data acquistion parameters.

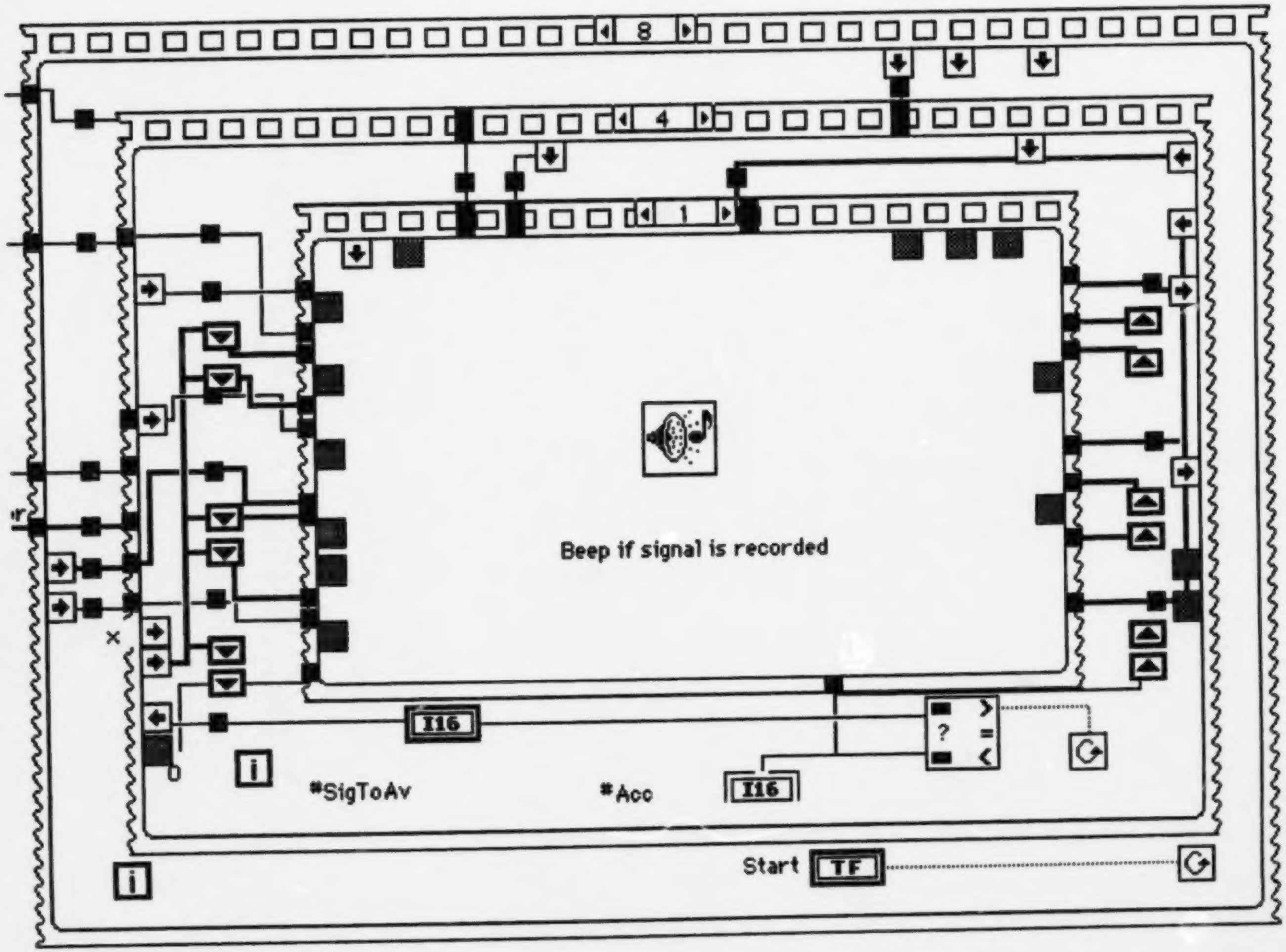
8
4
1
Beep if signal is recorded
I16
I16
#SigToAv
#Acc
?
Start
TF
i
i

Figure AI.13 Beep if trigger conditions are met.

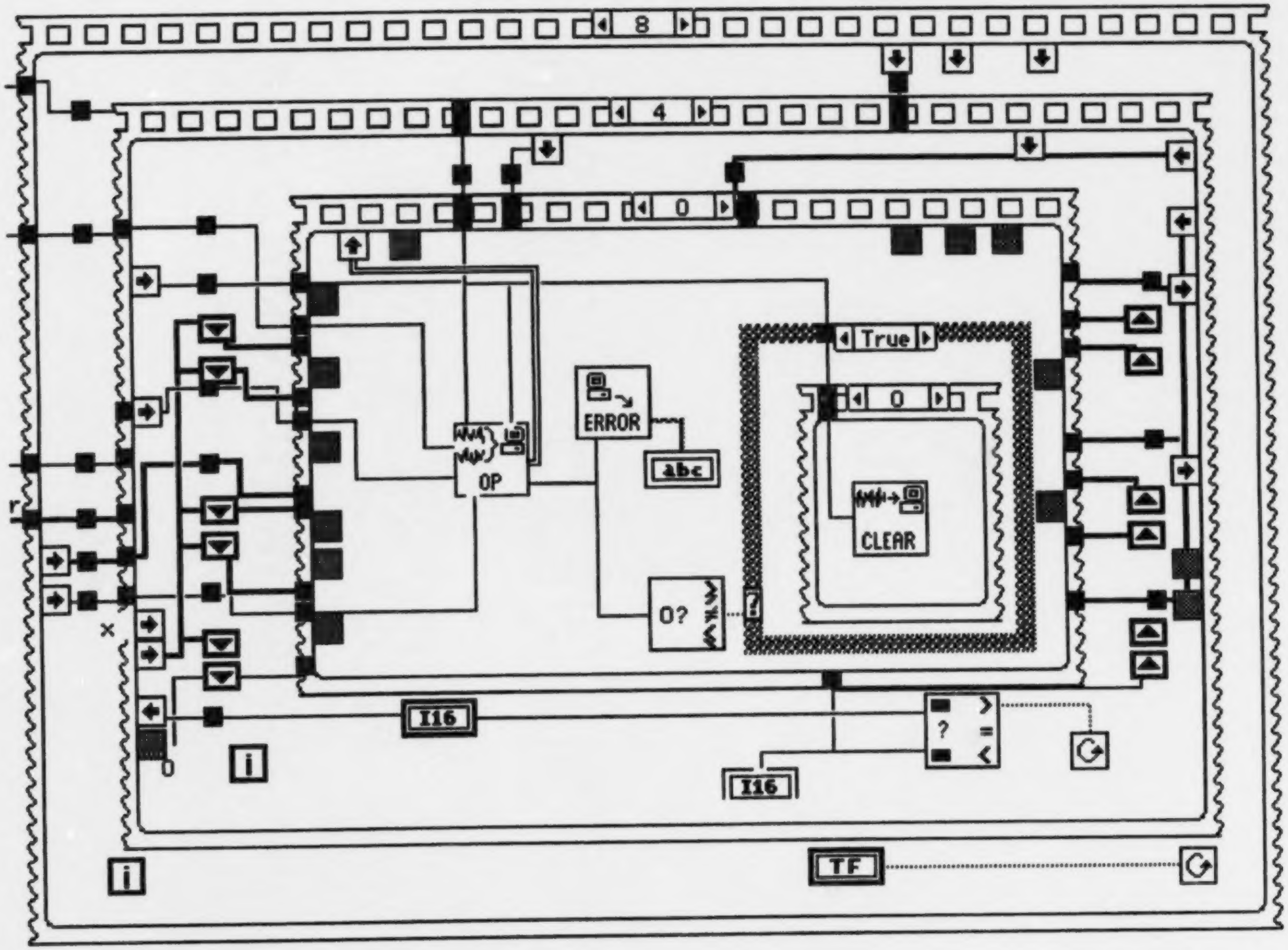
8
4
0
True
0
ERROR
abc
OP
CLEAR
0?
I16
I16
TF

Figure AI.14 Scan all onboard channels

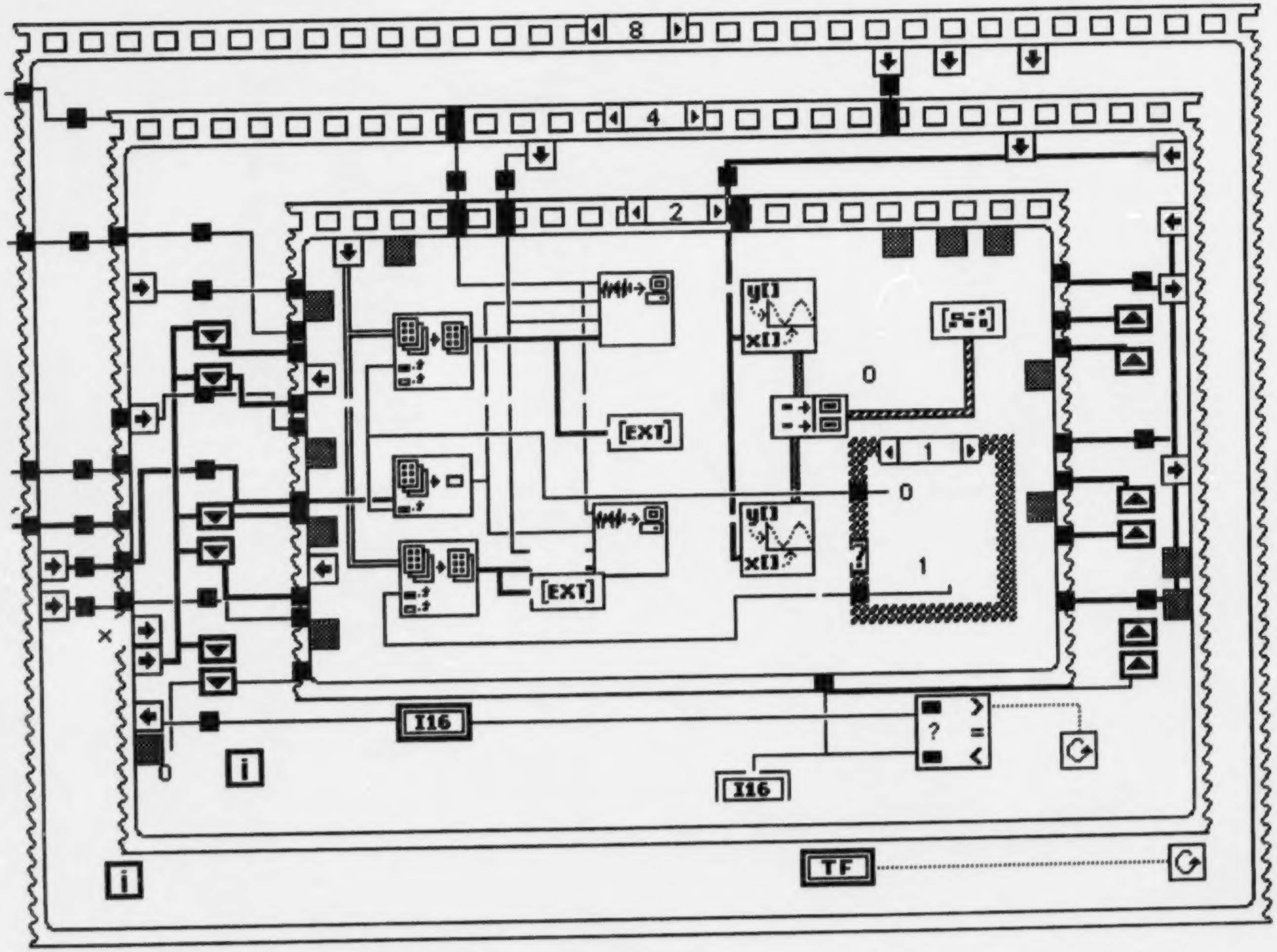
8
4
2
1
0
0
1
[EXT]
[EXT]
I16
I16
TF
y[]
x[]
y[]
x[]
?

Figure AI.15 Demux and scale scanned channels

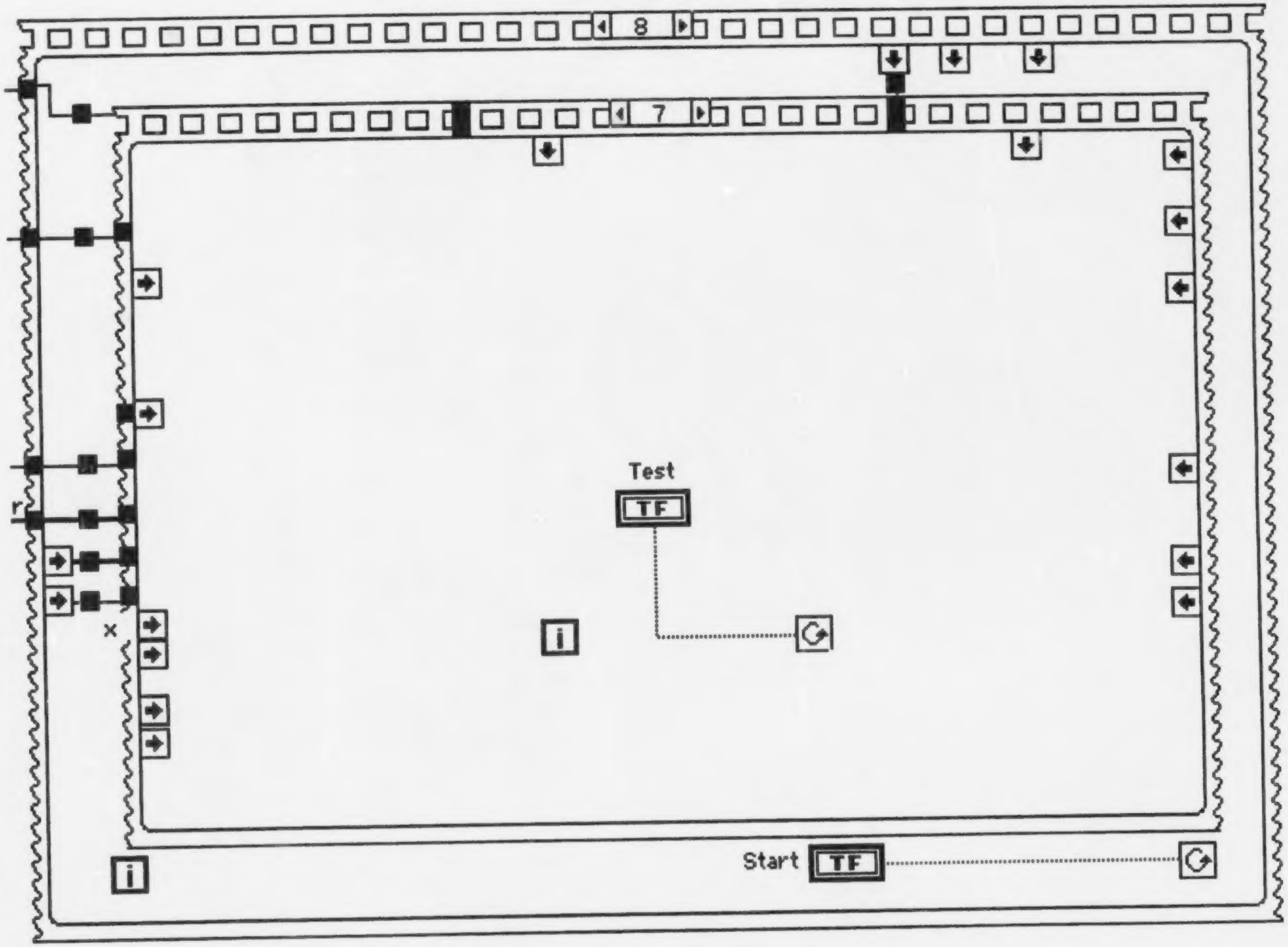
8
7
Test
TF
i
r
x
Start
TF
i

Figure AI.16 Idle till operator accepts or rejects signal.

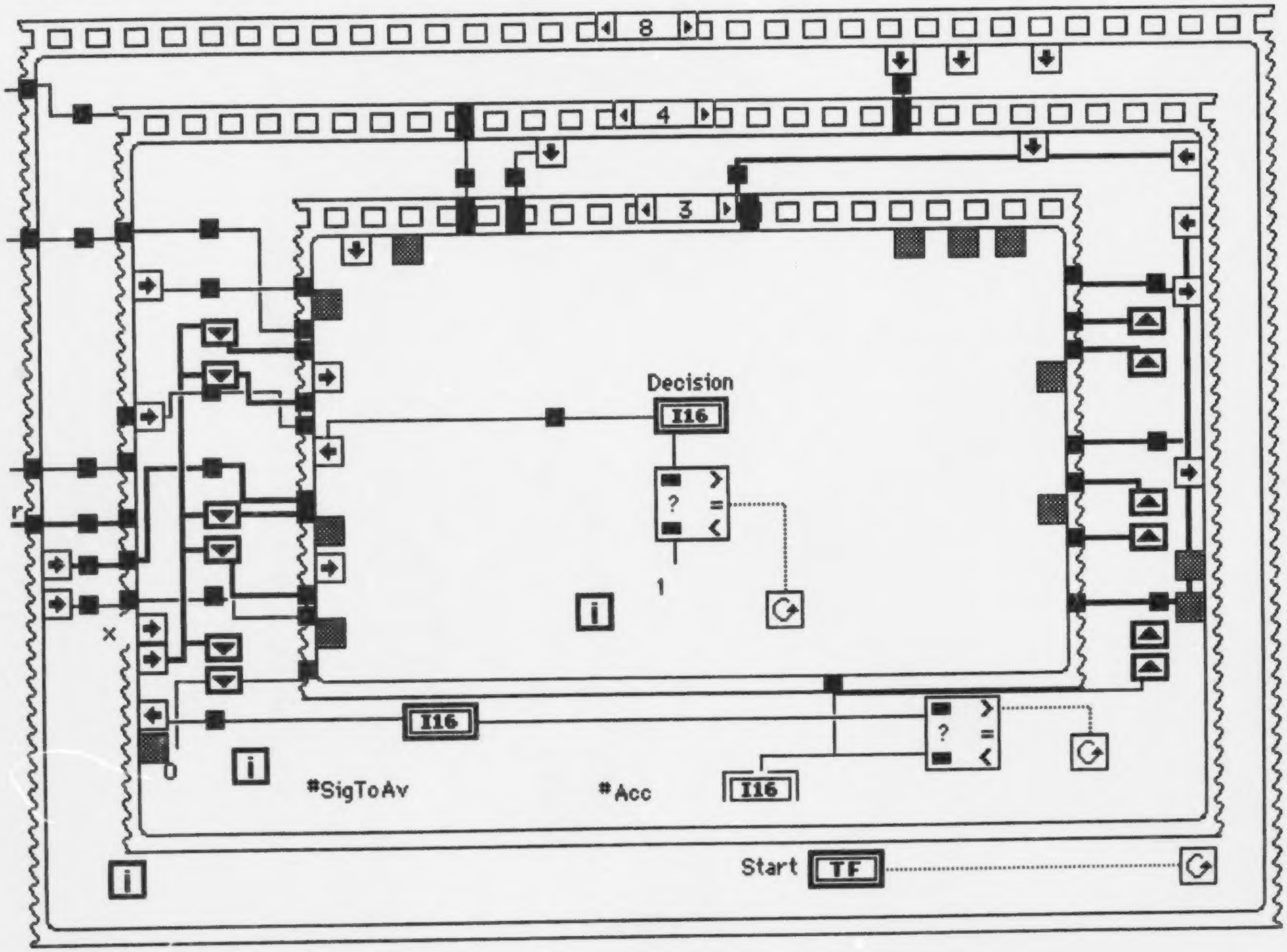
8
4
3
Decision
I16
?
1
I16
#SigToAv
#Acc
I16
?
r
x
0
Start
TF

Figure AI.17 Average and keep track of number of accepted signals

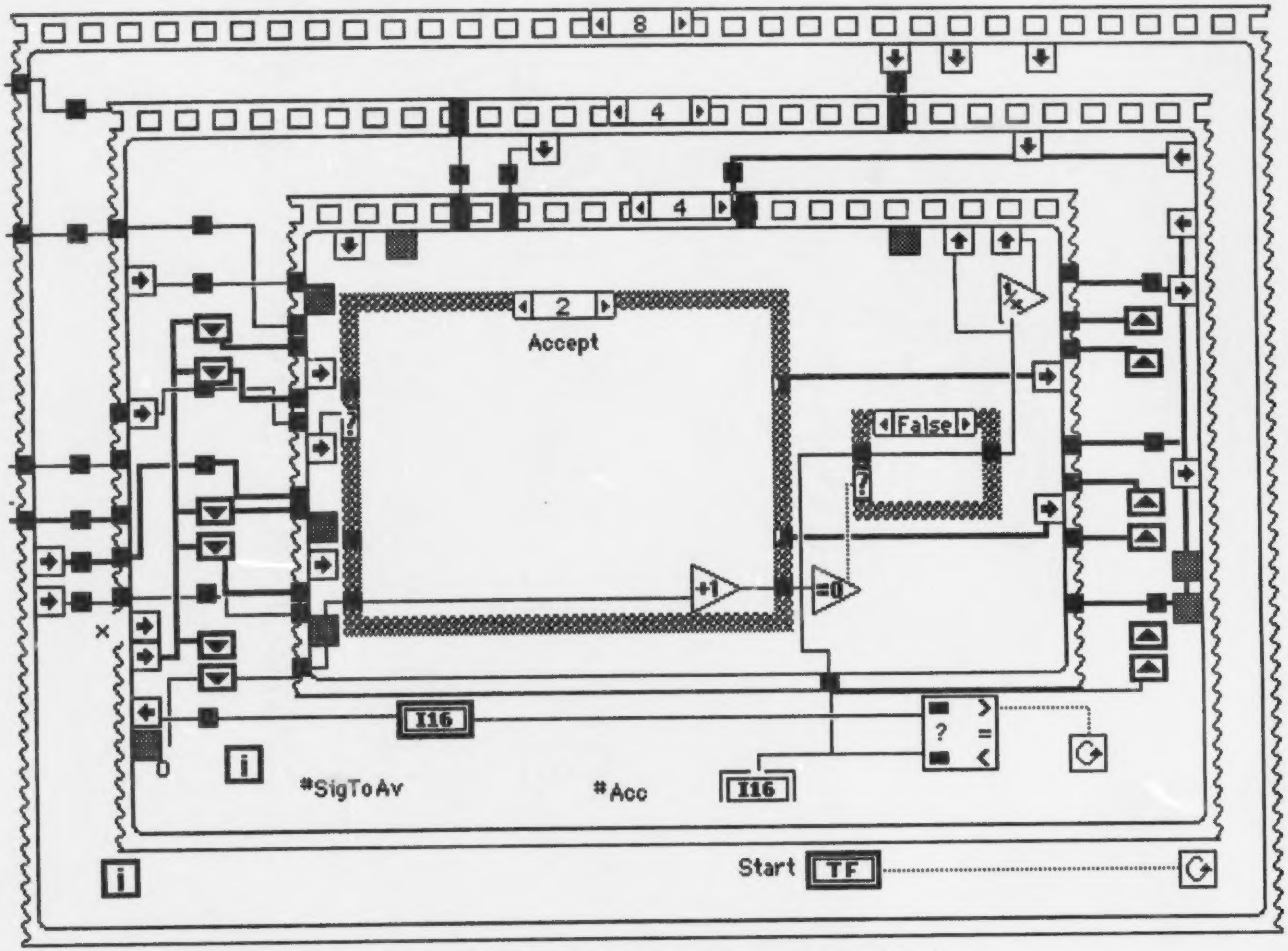
8
4
4
2
Accept
False
+1
=0
1/x
?
I16
I16
#SigToAv
#Acc
Start
TF
i
i

Figure AI.18 Discard signal if rejected and wait for trigger.

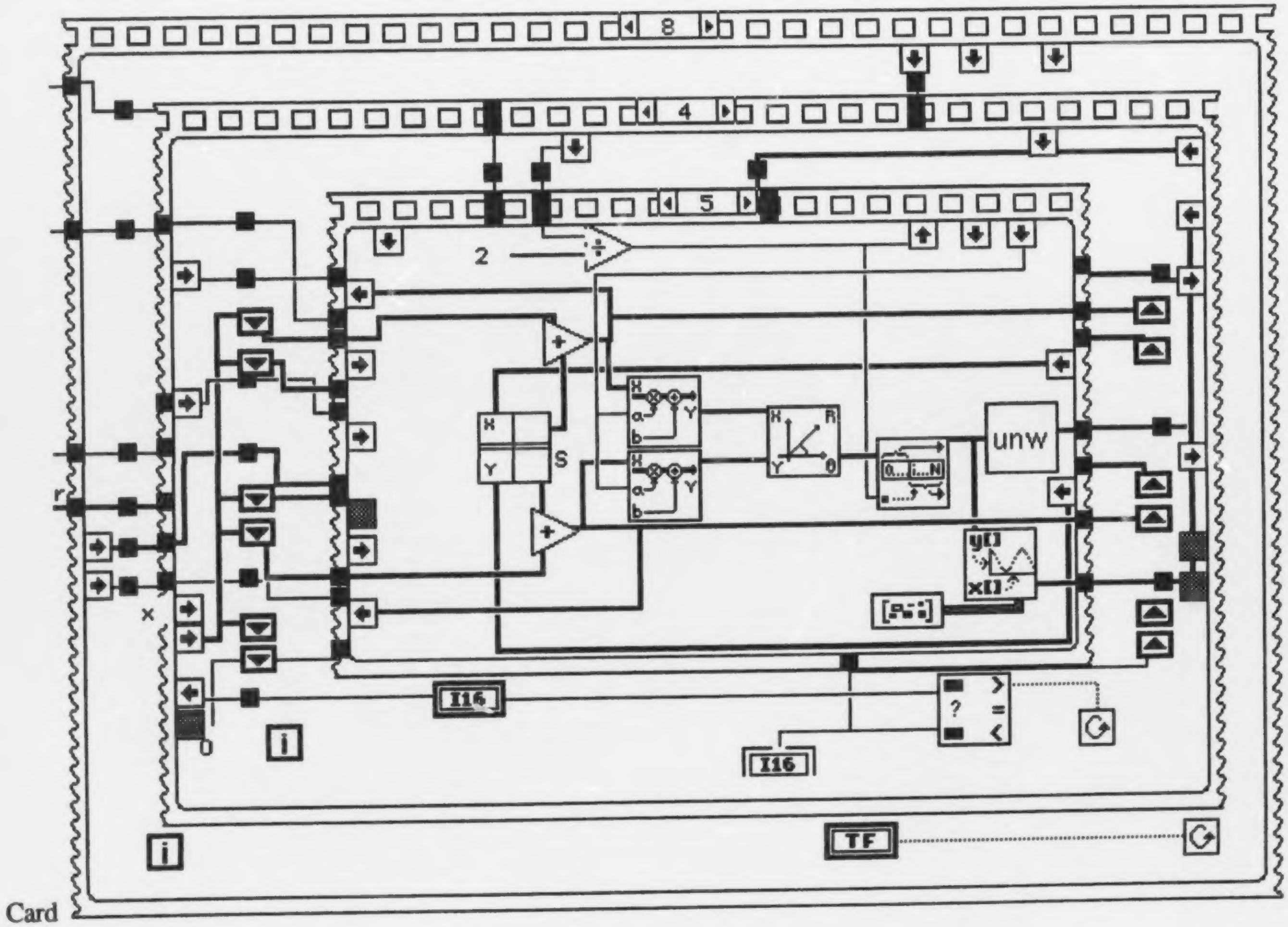
8
4
5
2
S
unw
I16
I16
TF
r
x
0
Card

Figure AI.19 Compute Phase of Cross-spectrum and unwrap.

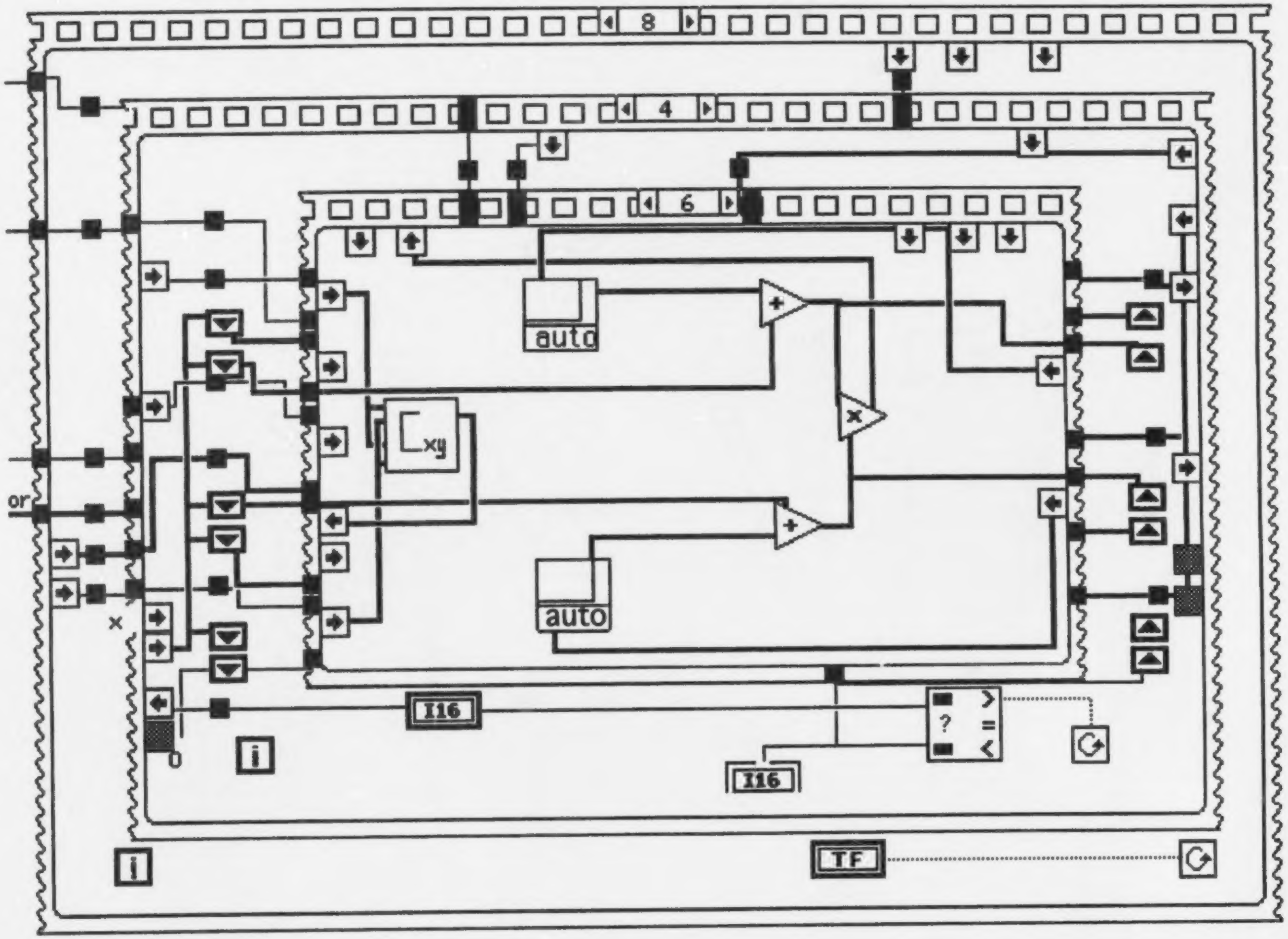
8
4
6
auto
auto
xy
or
×
I16
I16
?
TF
i
i
0

Figure AI.20 Calculate auto-power spectra.

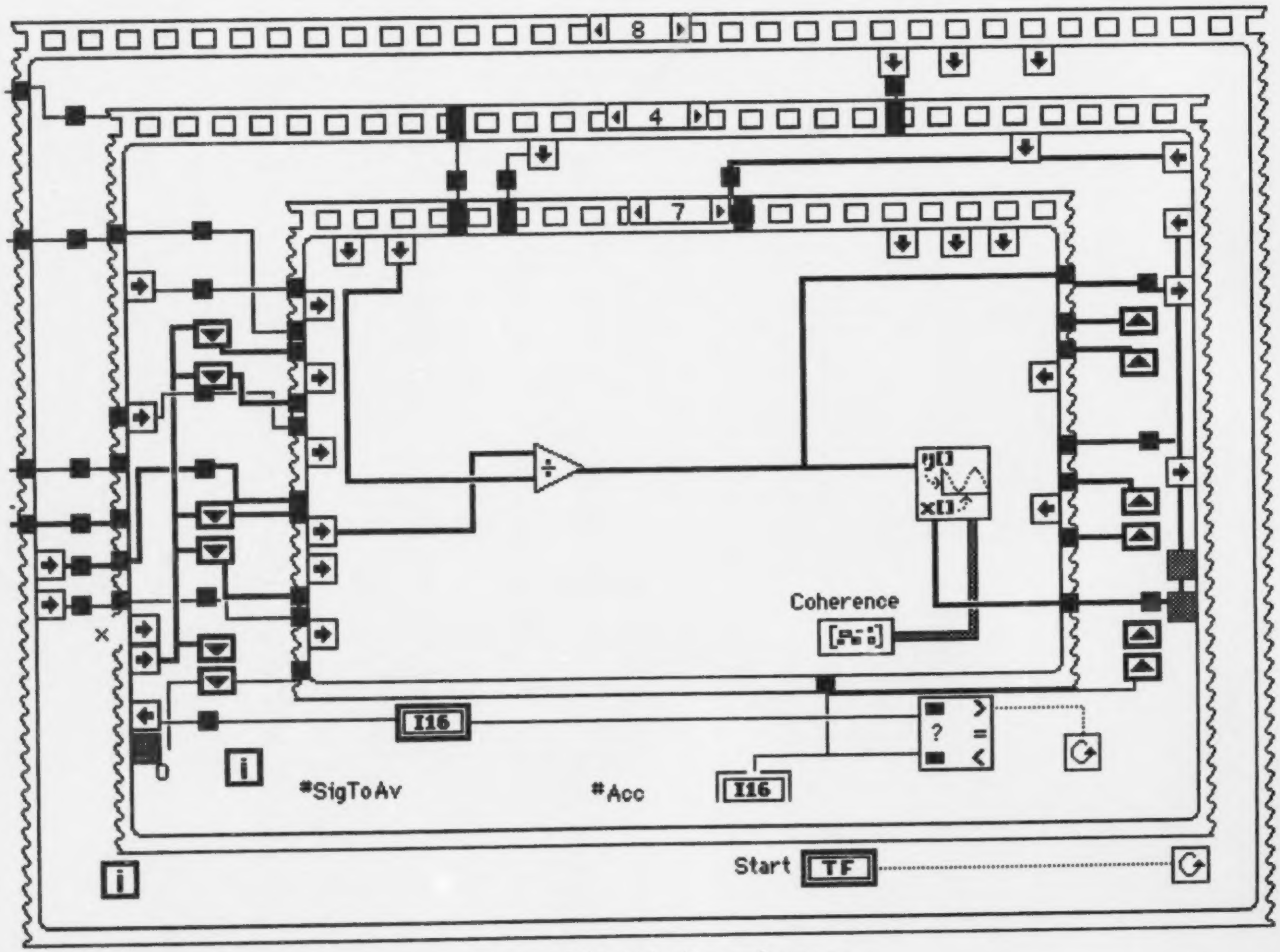
8
4
7
Coherence
I16
#SigToAv
#Acc
I16
Start
TF

Figure AI.21 Calculate coherence.

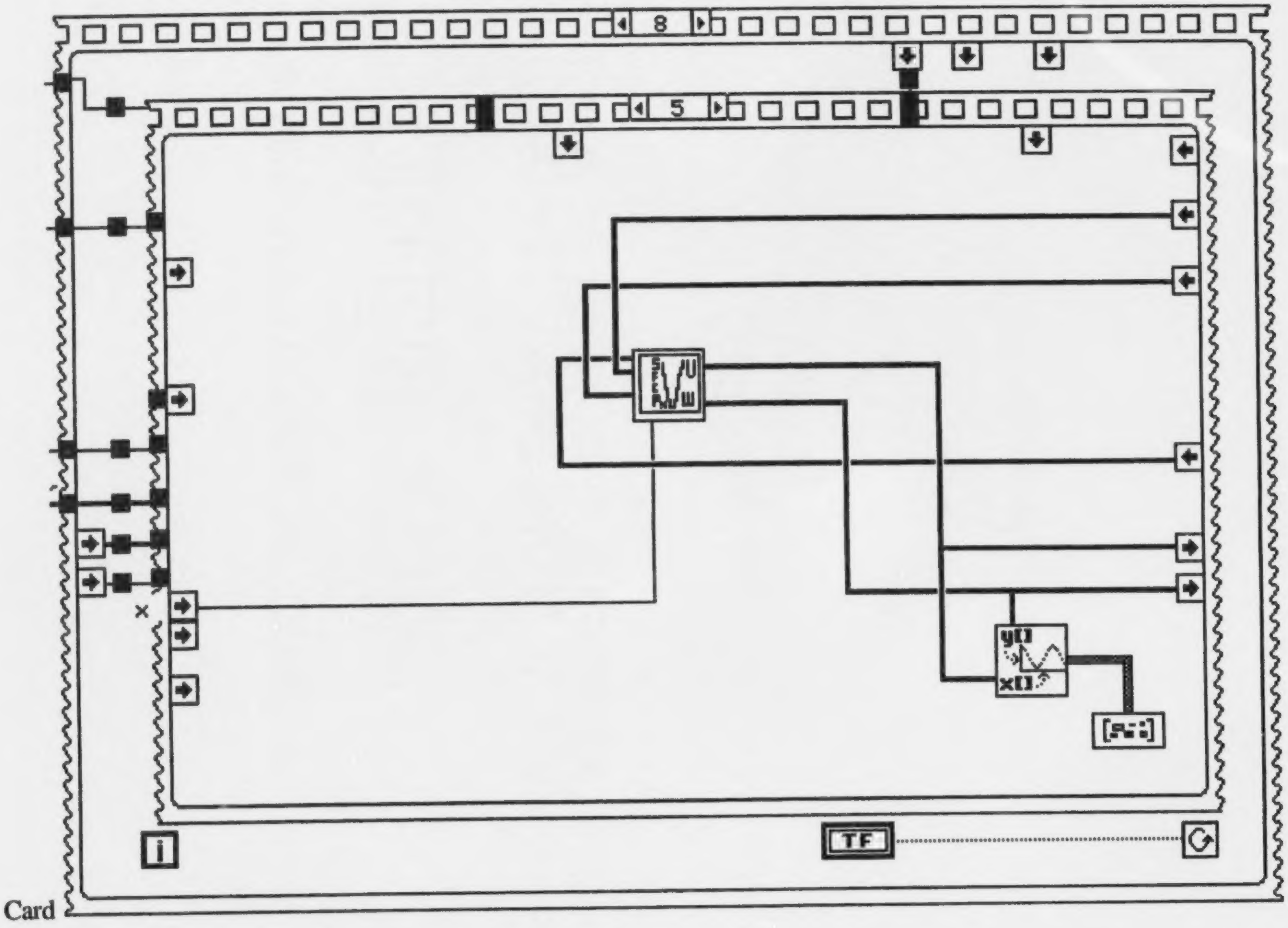
8
5
y[]
x[]
TF
i
×
Card

Figure AI.22 Computation of dispersion points at acceptable coherence.

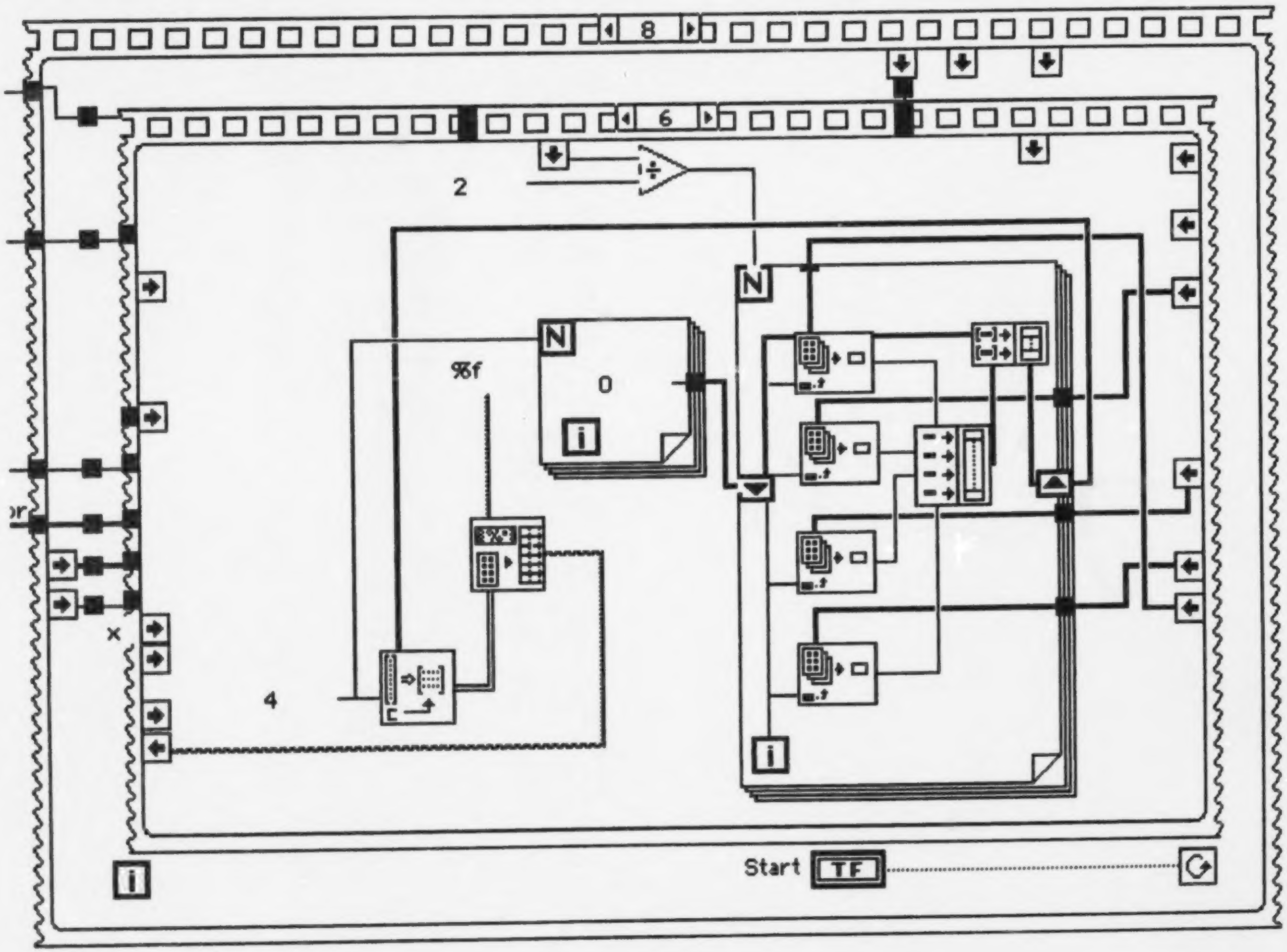
8
6
2
%f
0
4
x
Start
TF

Figure AI.23 Put acquired data in spreadsheet format.

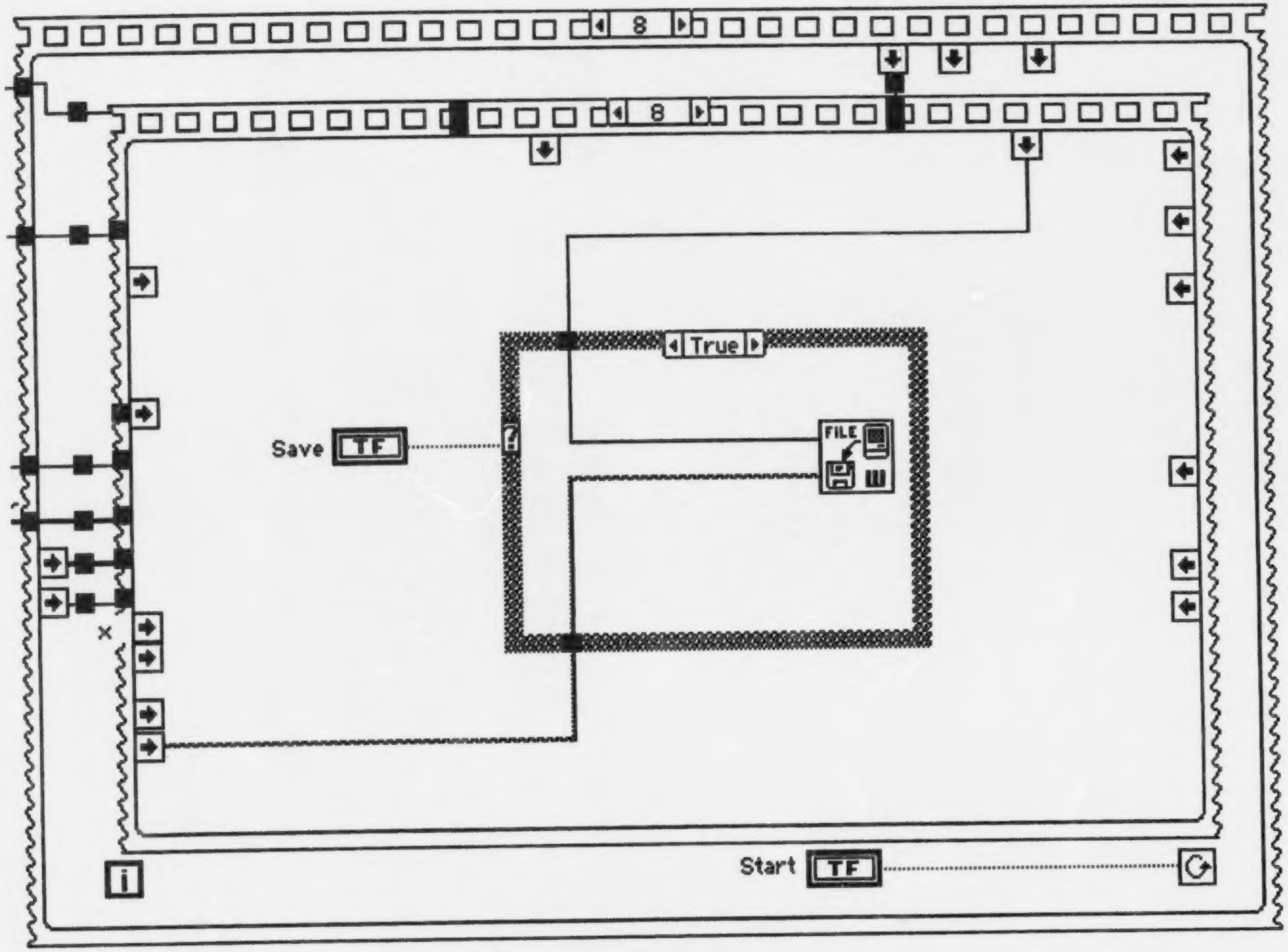
8
8
True
Save
TF
FILE
Start
TF
i

Figure AI.24 Write dispersion data to disk file.

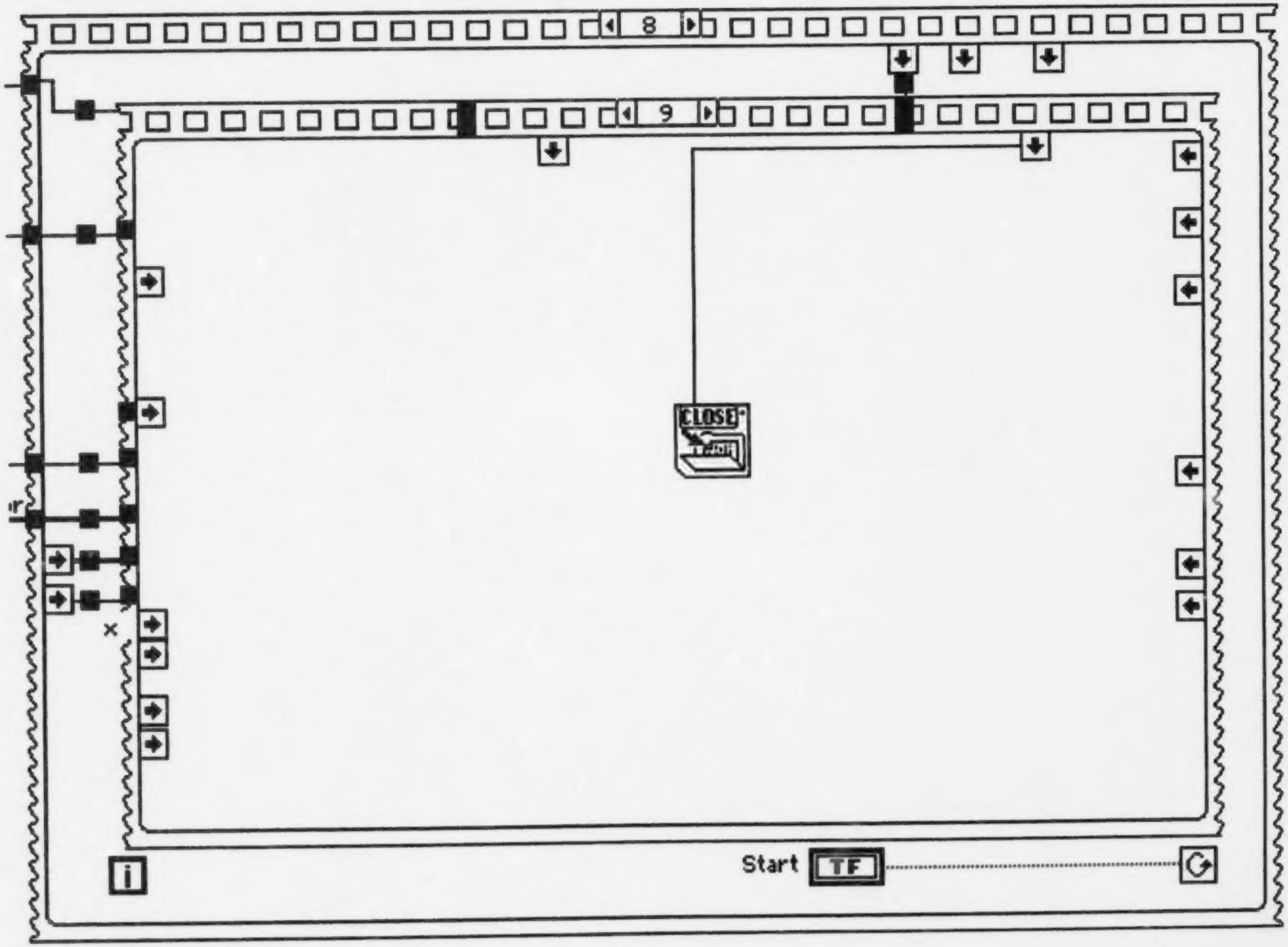
8
9
CLOSE
Start
TF
i
x

Figure AI.25 Close all open files and exit.

APPENDIX II.

SASW-FM

II.1 SAMPLE INPUT

```
RAYLEIGH 0.0
2 25 2 20
0.33 0.33 0.33 0.33 .33 .33 .33 .33 .33 .33 .33 .33 .33
1.  1.  1.  1.  1.  1.  1.  1.  1.  1.  1.  1.  1.
0.55 0.58 1.11 0.91 1.19 1.8 0.98 1.13 0.99 1.07 .97 .96 79.7 81.5 97.9 108. 131.9
154. 176.3 191.8 179.3 156.2 227. 221. 312.5
0.05 0.05 0.1 0.1 0.12 0.18 0.09 0.1 0.1 0.1 0.1 0.1 7.9 8.0 9.7 10.0 13.0 15.5 17.4
18.0 17.0 15.0 22.0 21.0 30.0
.001 .001 .001 .001 .001 .001 .001 .001 .001 .001 .001 .001 .001 .001 .001 .001 .001 .001
.001 .001 .001 .001 .001 .001 .001 .001
2932.0      70.41
2230.5      71.23
1508.0      72.45
1209.5      77.64
1005.3      80.13
858.70      82.77
762.96      85.41
683.30      87.66
628.32      90.04
578.05      92.91
345.58      110.39
278.55      133.78
260.75      166.81
251.33      200.35
240.86      230.10
220.81      246.11
202.63      258.00
185.00      265.00
172.79      275.37
158.79      278.66
```

II.2 SAMPLE OUTPUT

```
FILENAME :          Sample Site
WAVE TYPE:          Rayleigh
No. of Iterations   1177

Layer No.  Thickness(m)  S-wave Velocity (m/s)

1             0.92           83.91
2             2.37          125.82
3             2.95          108.28
4             2.59          140.31
5             1.34          165.17
6             1.47          147.11
7             1.58          156.16
8             0.96          173.03
9             1.29          194.41
10            1.04           63.11
Half-Space                  238.00

Wavelength (m)      Frequency (Hz)      Cfield (m/s)        Ccalc (m/s)


    0.10            1129.93             113.12              113.18
    0.20            569.96              114.45              117.12
    0.30            383.32              115.67              116.82
    0.40            289.98              116.20              116.54
    0.50            233.99              117.04              117.00
    0.70            168.57              118.39              118.80
    1.00            18.99               119.85              119.58
    2.00            60.00               120.00              120.44
    2.70            46.29               125.67              124.73
    3.50            40.00               140.45              141.00
    4.00            36.25               145.14              146.19
    4.50            33.33               150.09              151.52
    5.00            31.40               157.33              155.61
    6.00            27.50               165.12              164.66
    7.00            24.86               174.88              172.28
    8.00            22.50               180.70              180.82
    9.00            20.89               188.45              187.57
   10.00            19.50               195.37              194.01
   11.00            18.18               200.00              200.69
   12.00            17.17               206.42              206.21
   13.00            16.15               210.98              211.92
   14.00            15.50               217.48              215.62
   15.00            14.67               220.11              220.31
   16.00            14.00               224.23              224.06
   17.00            13.41               228.51              227.42
   18.00            12.78               230.36              231.20
   19.00            12.26               233.40              234.37
   20.00            11.90               238.05              236.52
STANDARD DEVIATION     =  1.17
STANDARD ERROR         =  0.44
```

II.3. BENCHMARK SOLUTIONS

This section describes the comparison of results from program SASW-FM for three synthetic profiles and their corresponding dispersion curves. The profiles are presented later in this appendix as Cases 1, 2 and 3.

For each case, the dispersion curve for each given profile was calculated using SASW-FM. These theoretical dispersion curves are presented in Figures AII.3.1(a), AII.3.2(a), and AII.3.3(a). The second stage of the evaluation consisted of determining the shear wave velocity profiles associated with the given dispersion curves using SASW-FM. The latter results are presented in Figures AII.3.1(b), AII.3.2(b), and AII.3.3(b).

Case 1 consists of a single layer over a stiffer half-space. Dispersion computations for such a simple case are straightforward and required only a few iterations. SASW-FM gave results that are essentially the same as the original 2- and 3-D solutions provided by Professor Stokoe.

Case 2 consists of asingle layer over a softer half-space. SASW-FM reproduced the original soultions with some difficulty at the layer interface. However, there is tendency to converge on the original solution

Case 3 consists of a stiffer layer sandwiched between a softer overlying layer and a softer half-space. SASW-FM produced results that slightly oscillate around the original solution.

From the three results just discussed, the overall indication is that SASW-FM gives results similar to an independent forward modelling program. Improvements are, however, required in the speed of convergence for cases where a stiff layer adjoins much softer layers. A second area requiring further improvement is the refinement of shear wave velocity magnitudes at such layer boundaries.

CASE 1: Single Layer over Stiffer Half-Space.

Layer Thickness		S-Wave Velocity		Poissons's Ratio	Mass Density	
(ft)	(m)	(ft/s)	(m/s)		(pcf)	(kg/m^3)
10	3.05	500	152.4	0.3	115	1842
Half-Space		1000	304.8	0.3	120	1922

CASE 2: Single Layer over Softer Half-Space.

Layer Thickness		S-Wave Velocity		Poissons's Ratio	Mass Density	
(ft)	(m)	(ft/s)	(m/s)		(pcf)	(kg/m^3)
10	3.05	1000	304.8	0.3	120	1922
Half-Space		500	152.4	0.3	115	1842

CASE 3: Layer sandwiched between softer upper layer and half-space.

Layer Thickness		S-Wave Velocity		Poissons's Ratio	Mass Density	
(ft)	(m)	(ft/s)	(m/s)		(pcf)	(kg/m^3)
10	3.05	500	152.4	0.3	115	1842
10	3.05	1000	304.8	0.3	120	1922
Half-Space		500	152.4	0.3	115	1842

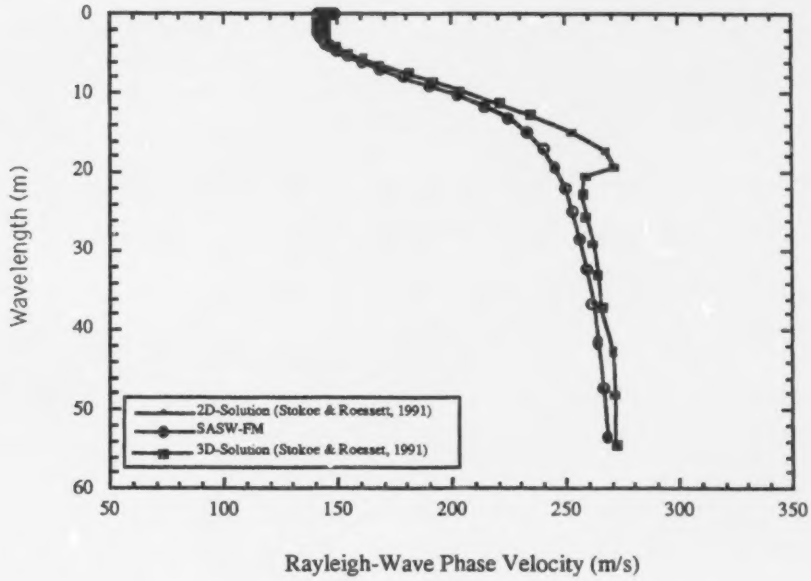

a) Dispersion Curves.

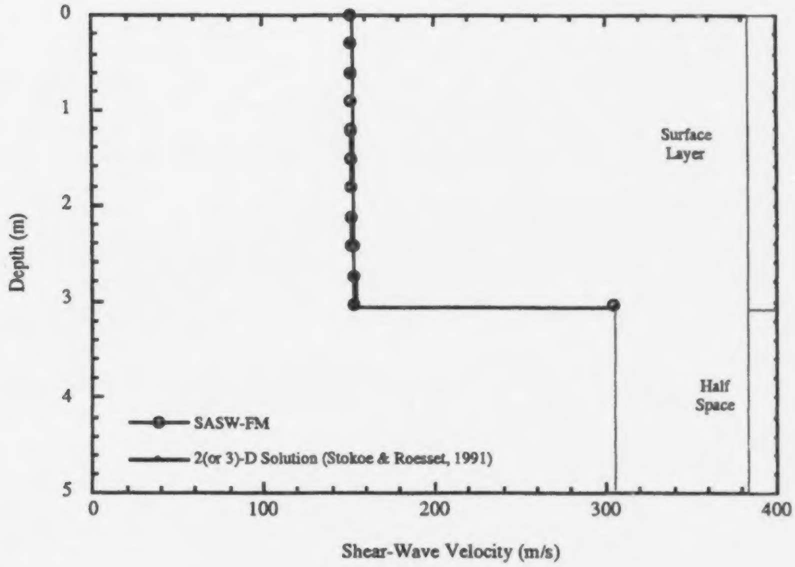

b) Shear-Wave Velocity Profiles

Figure AII.3.1 Verification of SASW-FM for Case 1.

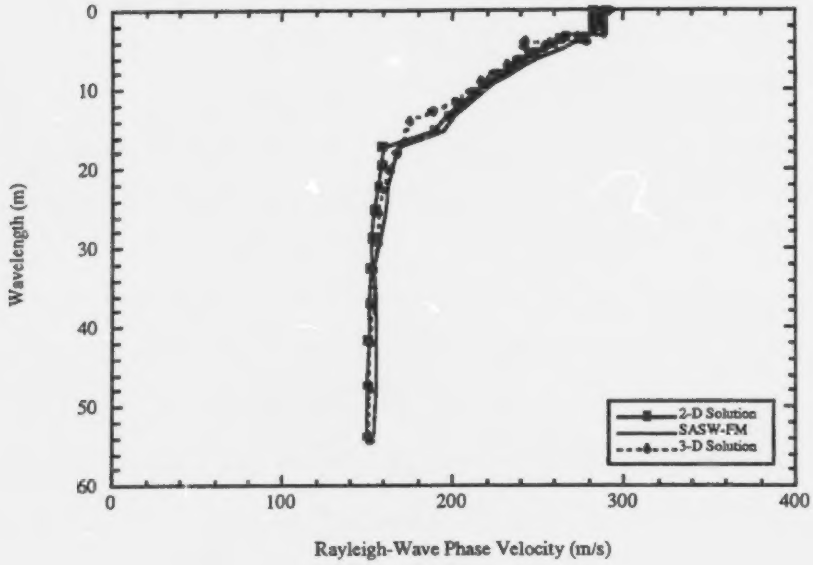

(a) Dispersion Curves.

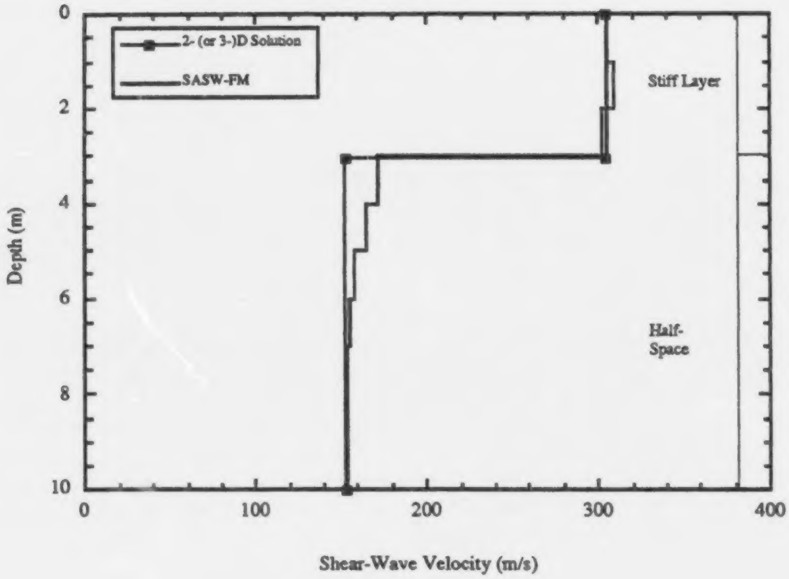

b). Shear-Wave Velocity Profiles.

Figure AII.3.2 Verification of SASW-FM for Case 2.

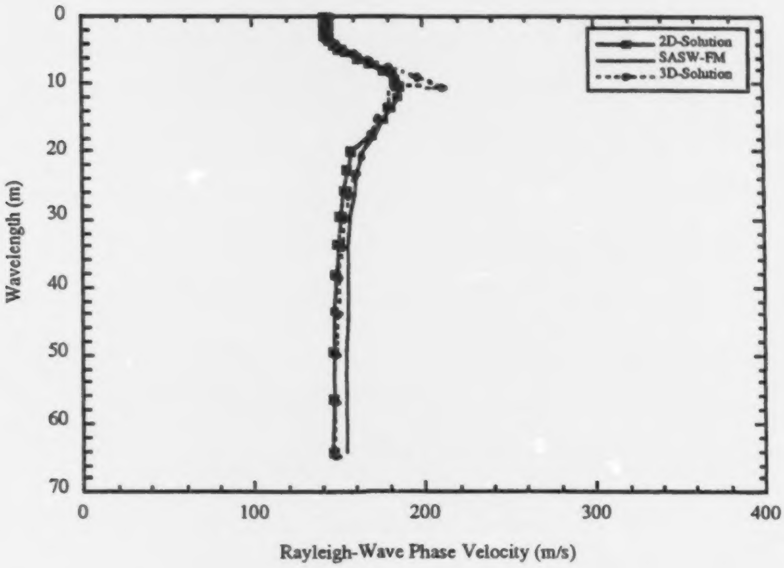

(a) Dispersion Curves

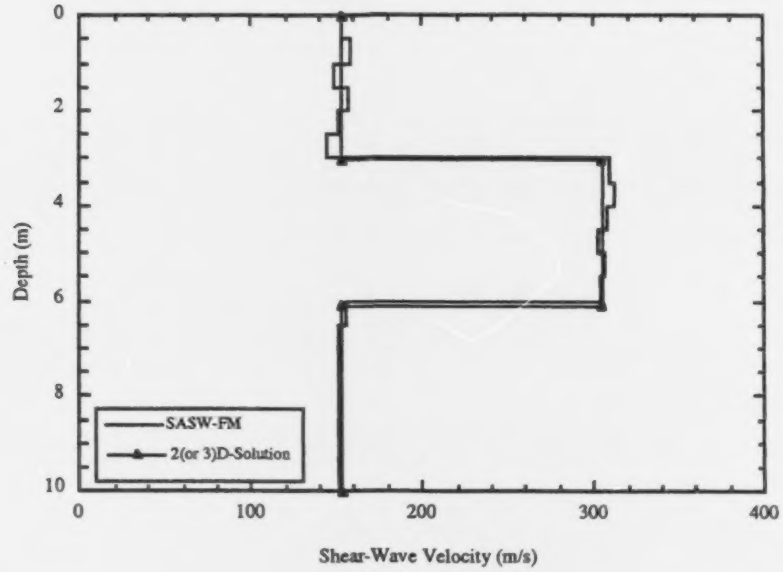

(b) Shear-Wave Velocity Profiles

Figure AII.3.3 Verification of SASW-FM for Case 3.

APENDIX III

III. CPT Results at University LRT Station

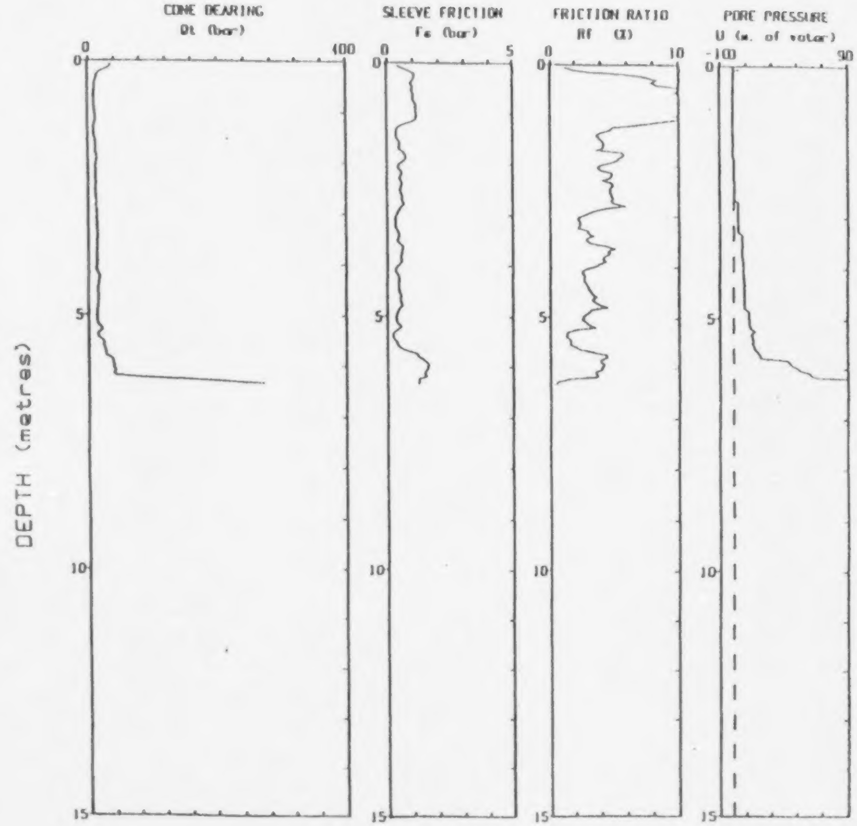

Figure A-III.1 Results of CPT-1 at University LRT Station.

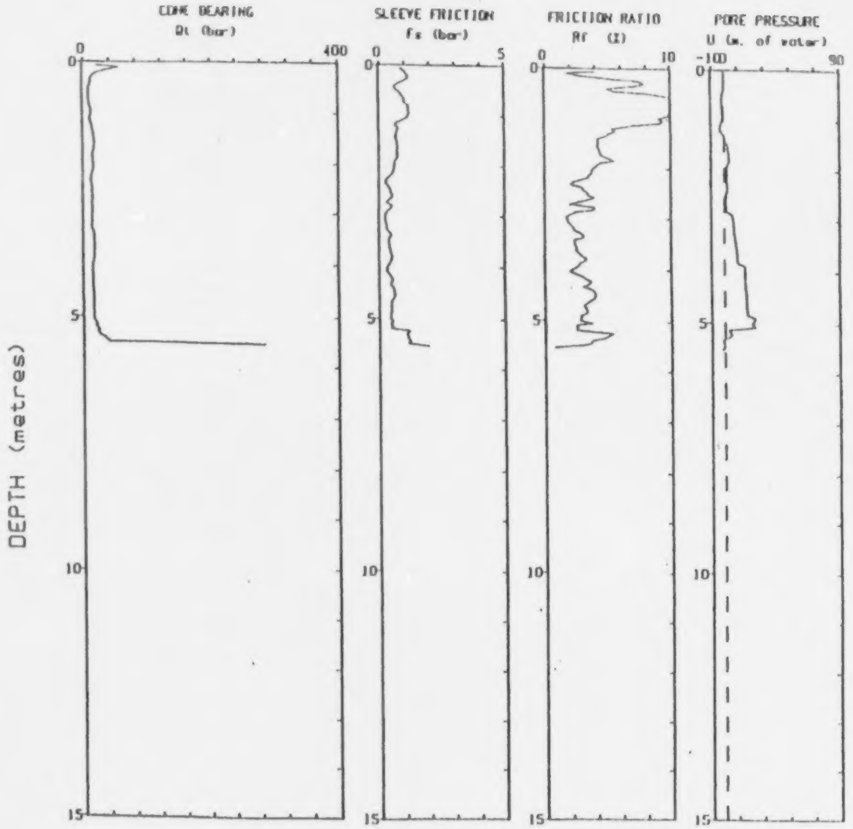

Figure A-III.2 Results of CPT-2 at University LRT Station.

APPENDIX IV

IV. CPT Results at NAIT Experimental Site

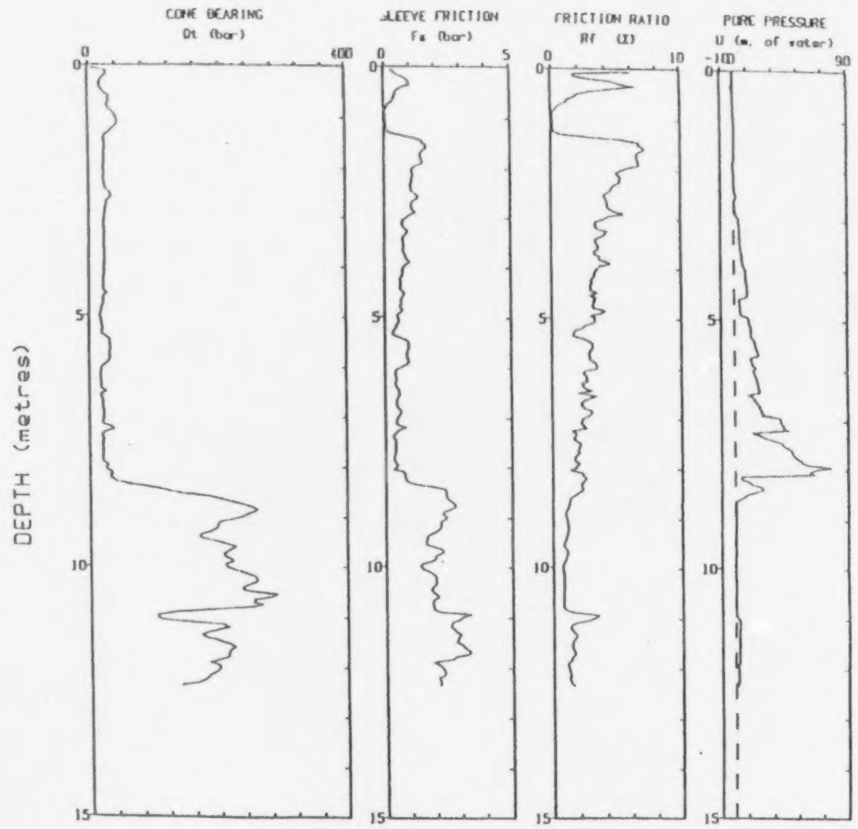

Figure A-IV.1 Results of CPT-1 at NAIT Experimental Site.

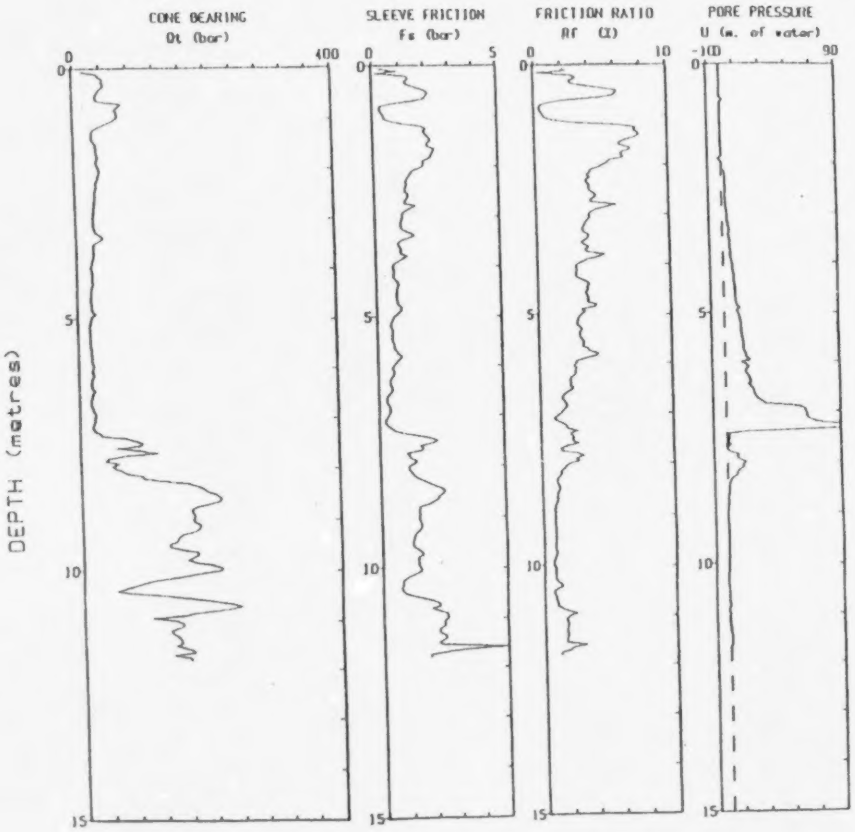

Figure A-IV.2 Results of CPT-2 at NAIT Experimental Site.

APPENDIX V

V. CPT Results at Richmond Dykes (Blundell Road)

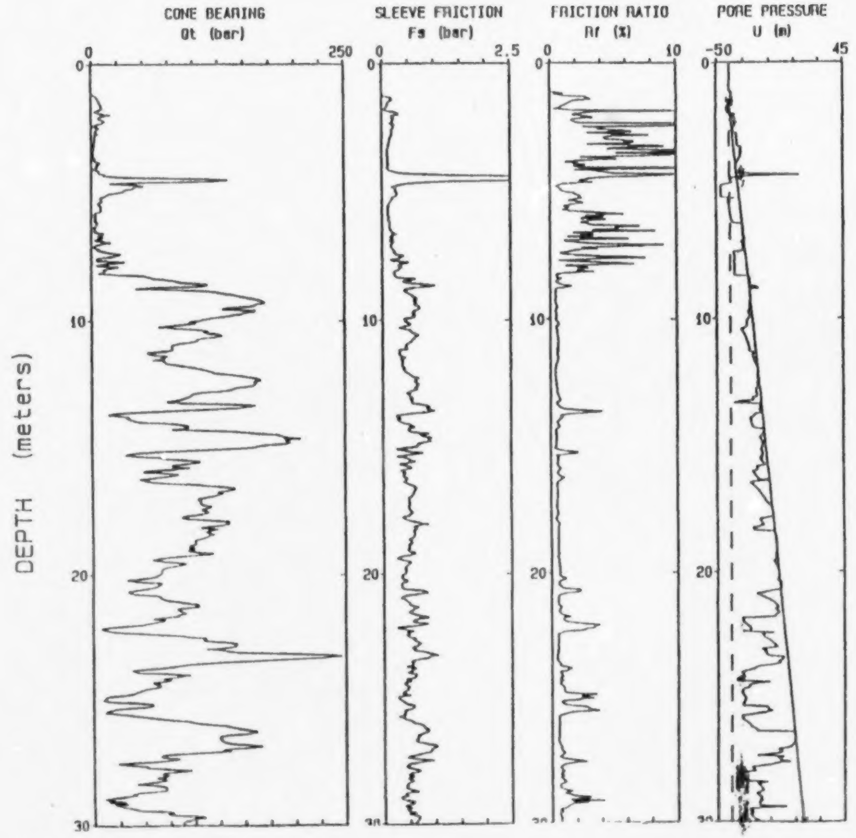

Figure A-V.1 Results of CPT-1 at Richmond Dykes (Blundell Road).

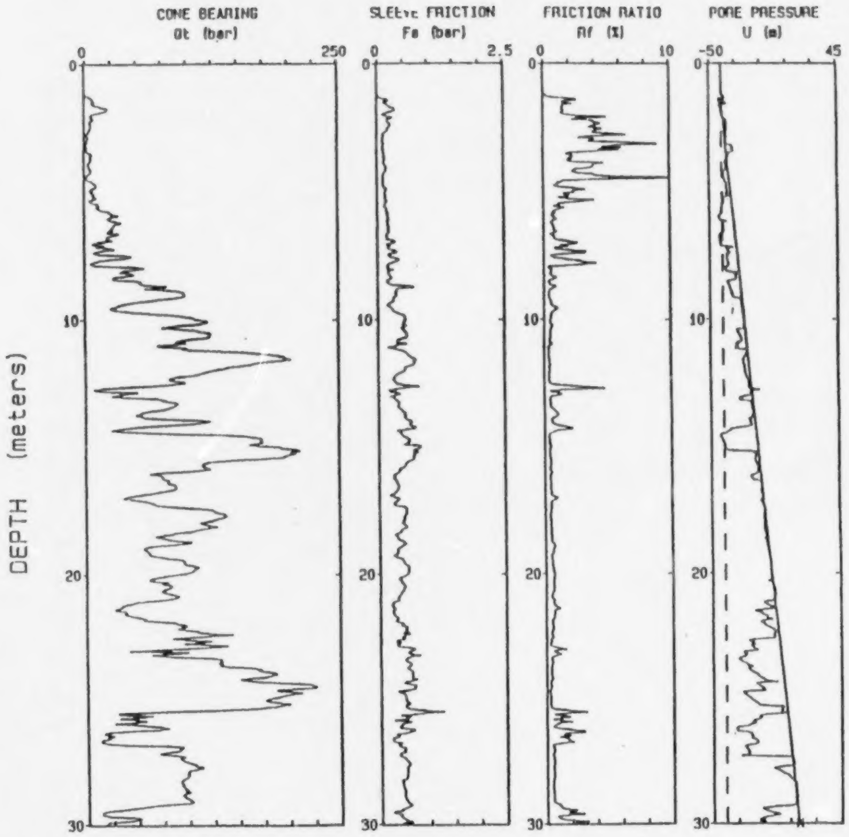

Figure A-V.2 Results of CPT-2 at Richmond Dykes (Blundell Road).

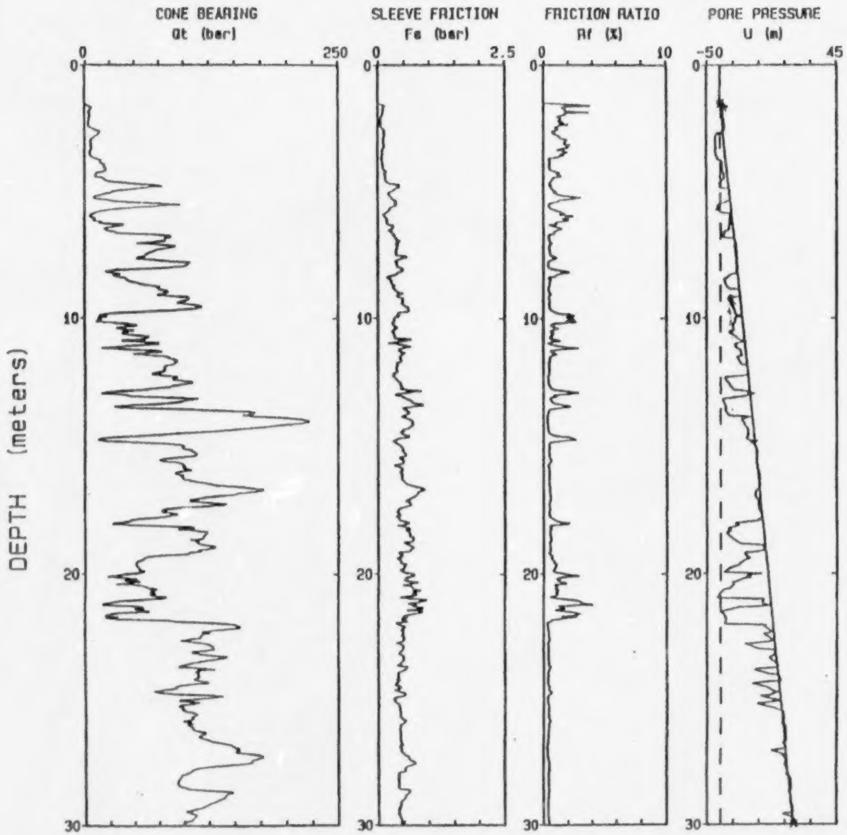

Figure A-V.3 Results of CPT-3 at Richmond Dykes (Blundell Road).

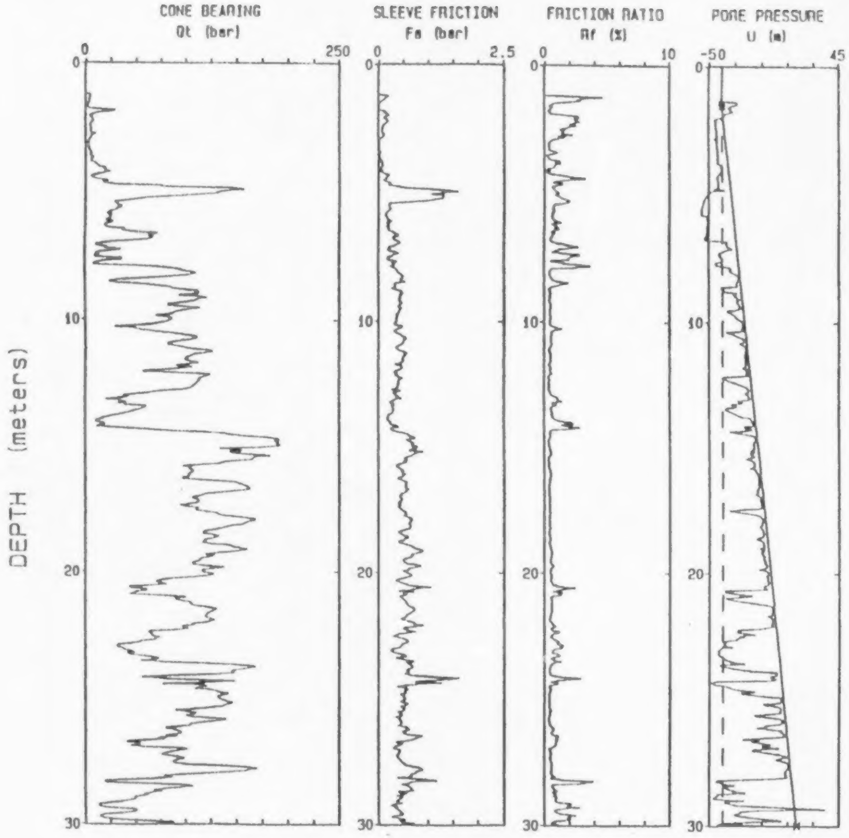

Figure A-V.4 Results of CPT-4 at Richmond Dykes (Blundell Road).

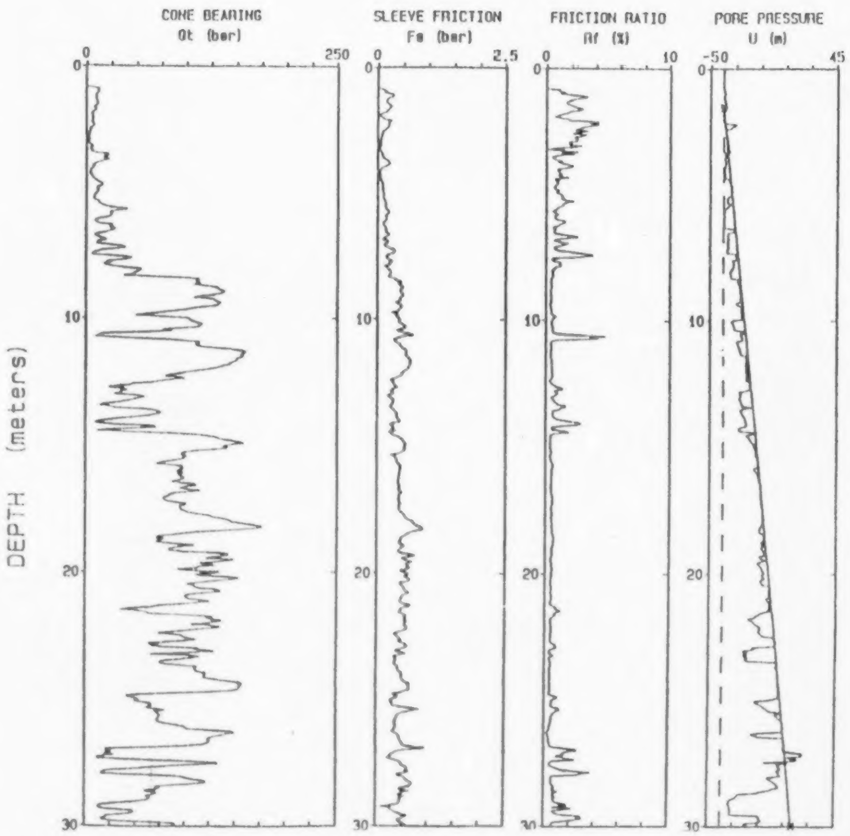

Figure A-V.5 Results of CPT-5 at Richmond Dykes (Blundell Road).

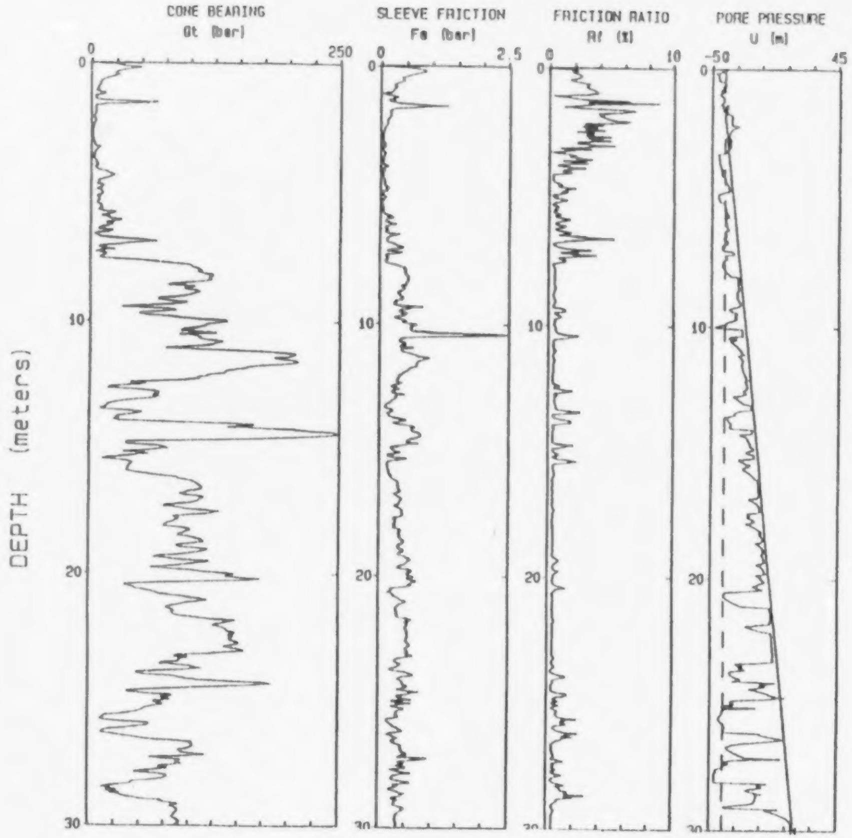

Figure A-V.6 Results of CPT-6 at Richmond Dykes (Blundell Road).

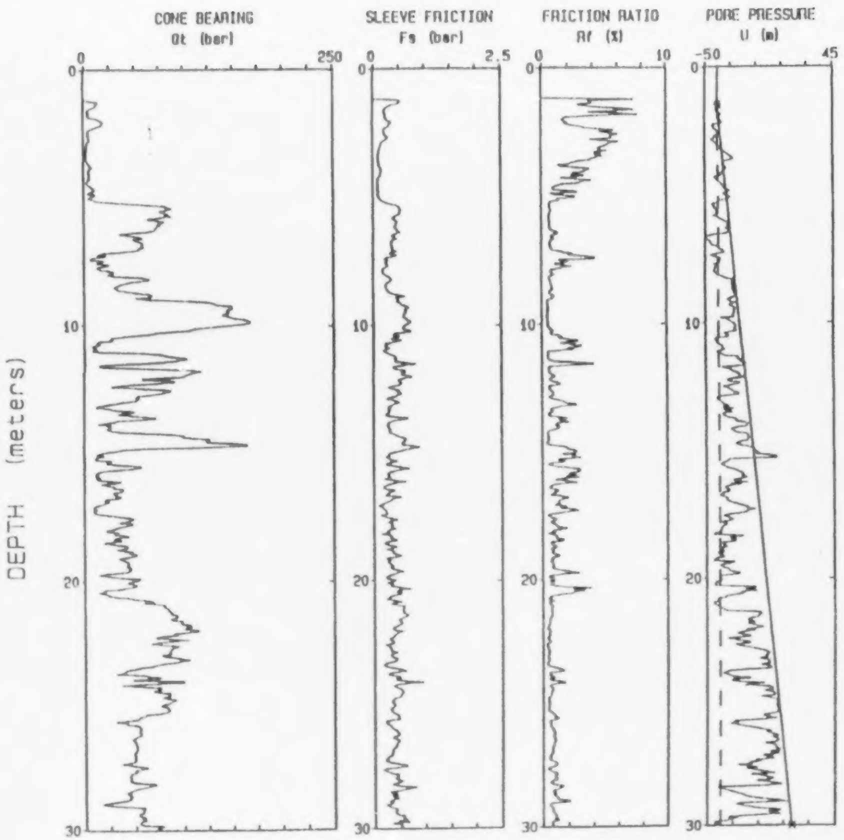

Figure A-V.7 Results of CPT-7 at Richmond Dykes (Blundell Road).

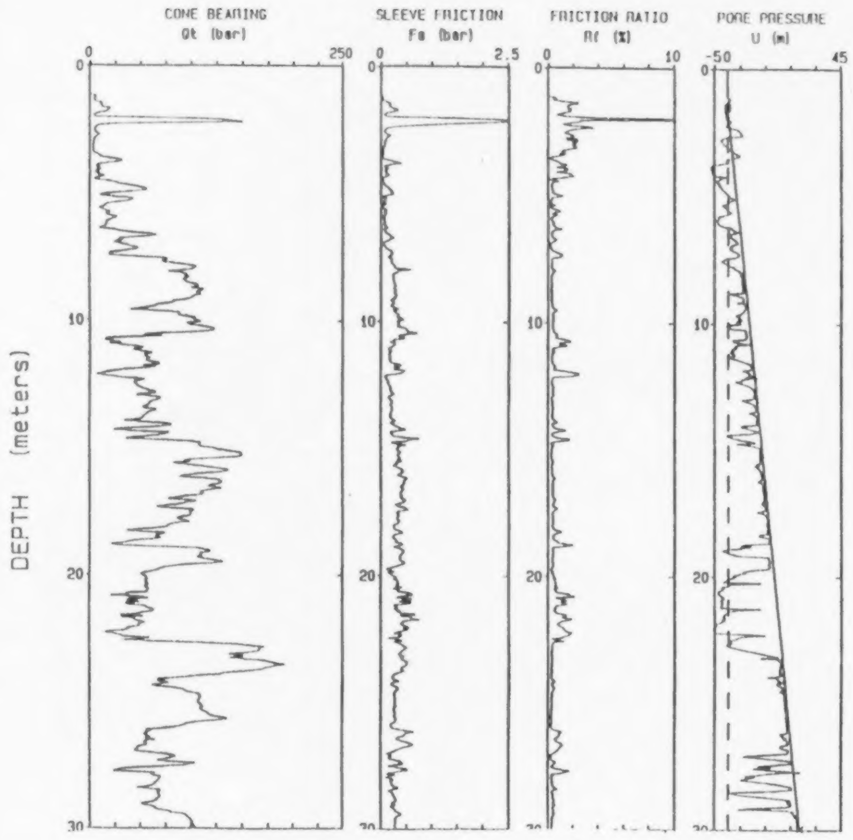

Figure A-V.8 Results of CPT-8 at Richmond Dykes (Blundell Road).

APPENDIX VI

VI. CPT Results at Richmond Dykes (Francis Road).

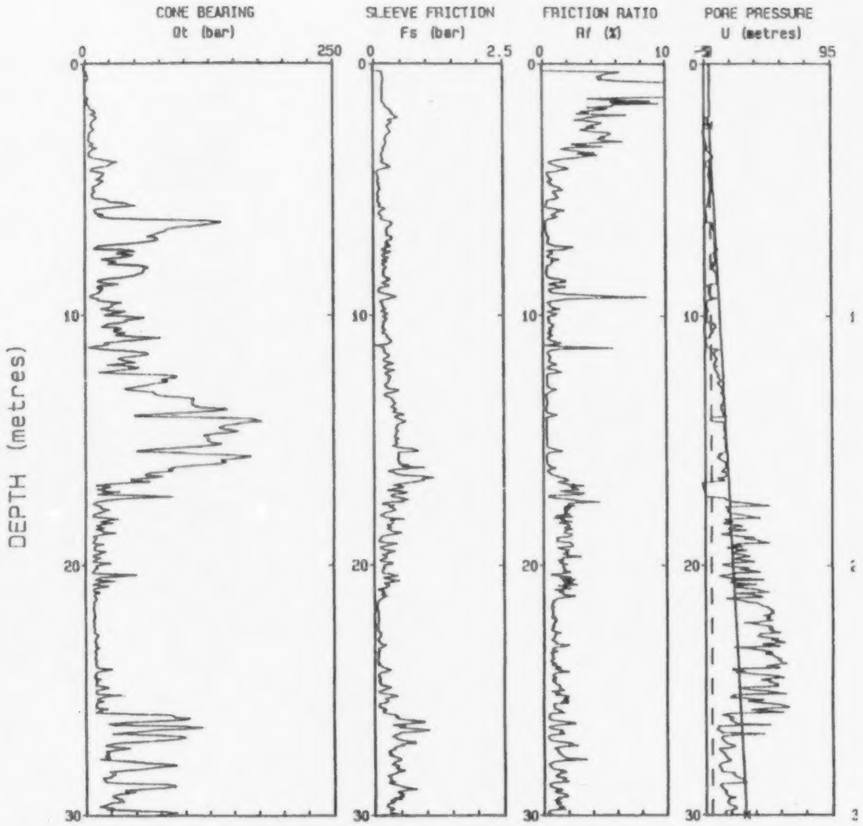

Figure A-VI.1 Results of CPT-1 at Richmond Dykes (Francis Road).

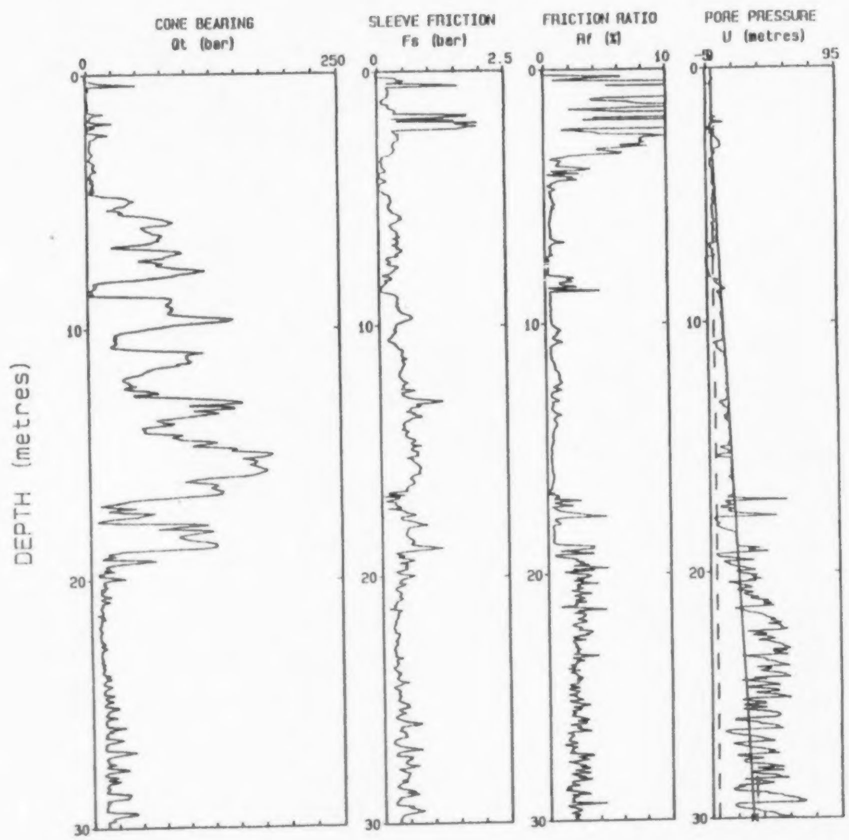

Figure A-VI.2 Results of CPT-2 at Richmond Dykes (Francis Road).

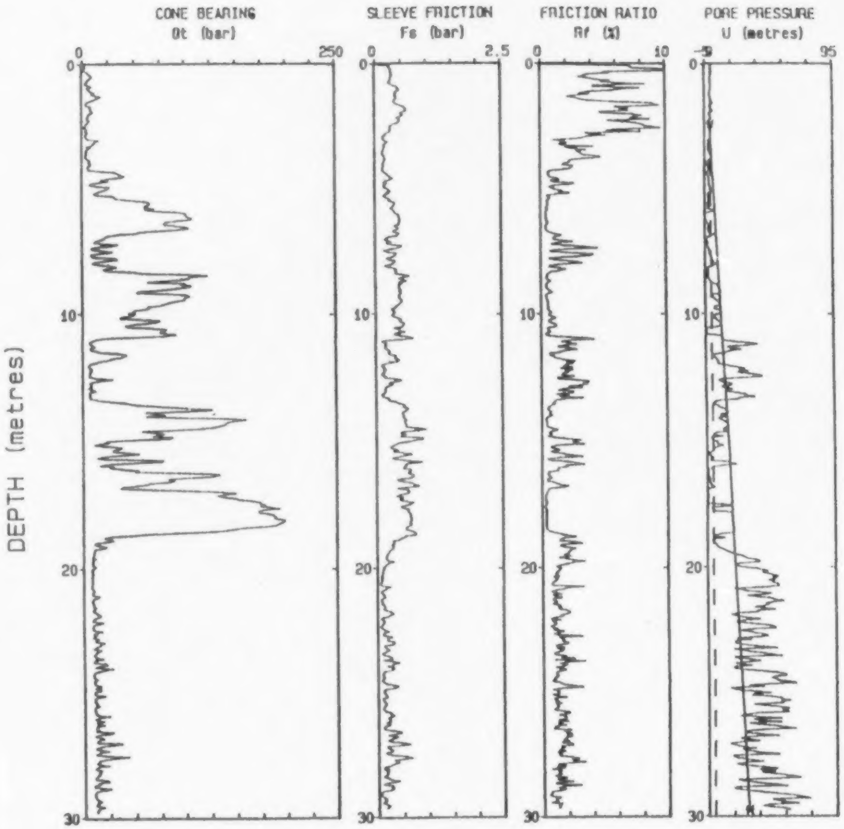

Figure A-VI.3 Results of CPT-3 at Richmond Dykes (Francis Road).

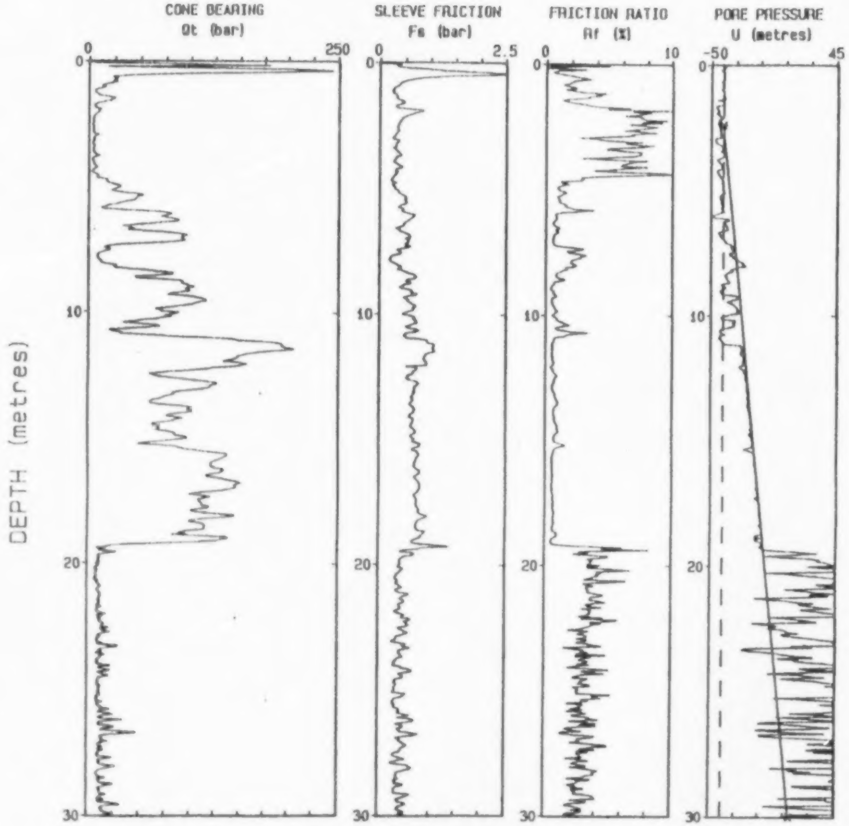

Figure A-VI.4 Results of CPT-4 at Richmond Dykes (Francis Road).

APPENDIX VII

VII. CPT Results at Richmond Dykes (Chatham Road)

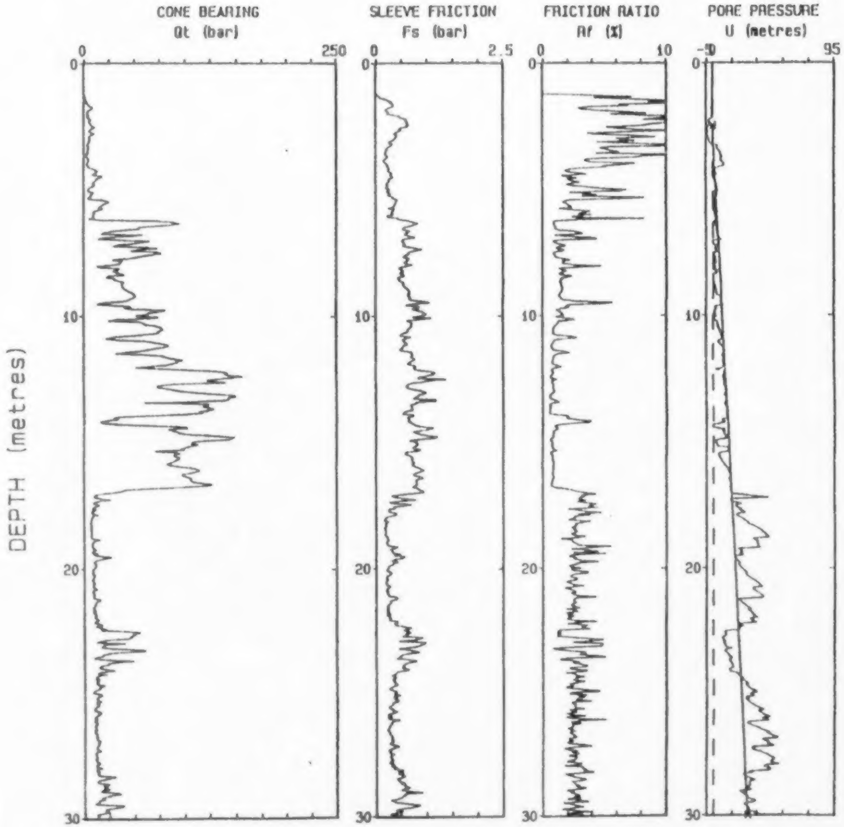

Figure A-VII.1 Results of CPT-1 at Richmond Dykes (Chatham Road).

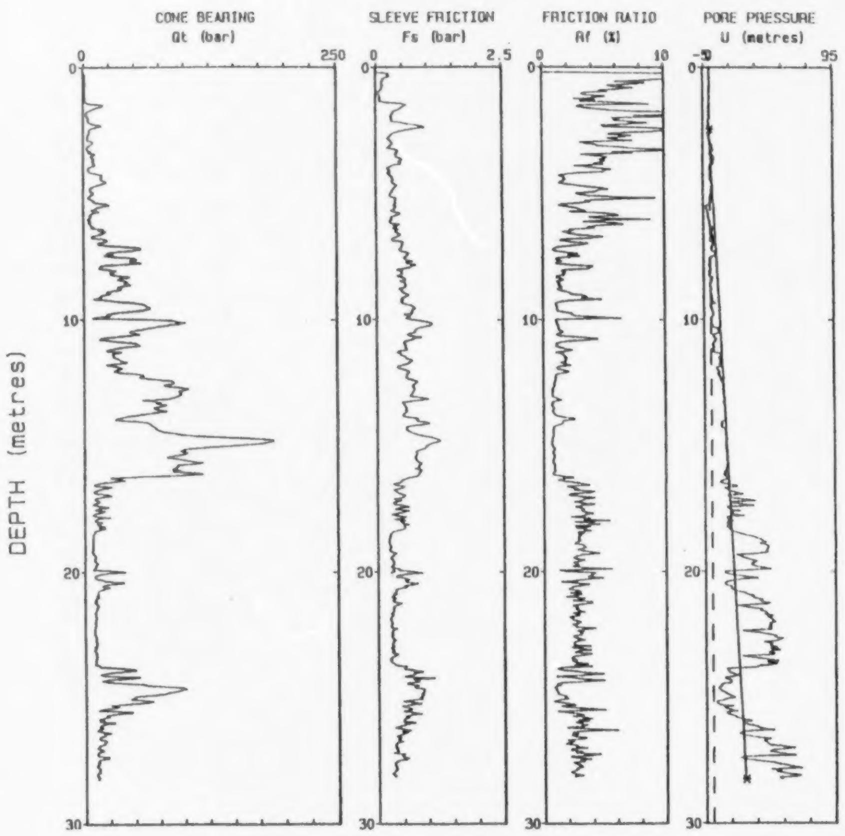

Figure A-VII.2 Results of CPT-2 at Richmond Dykes (Chatham Road).

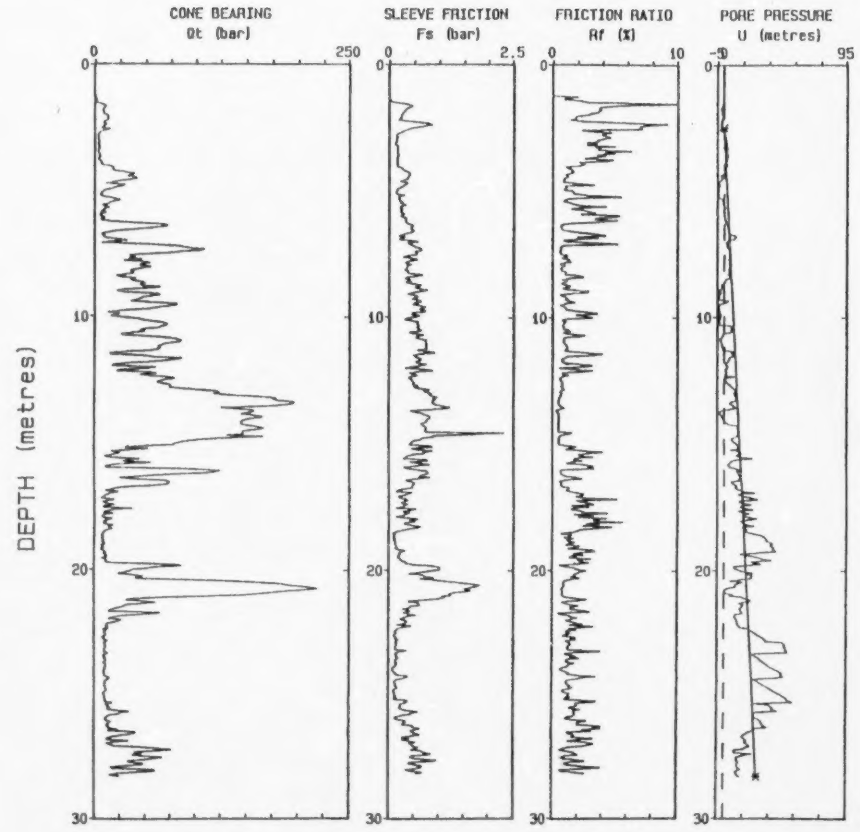

Figure A-VII.3 Results of CPT-3 at Richmond Dykes (Chatham Road).

APPENDIX VIII

VIII. CPT Results at Sea Island Site

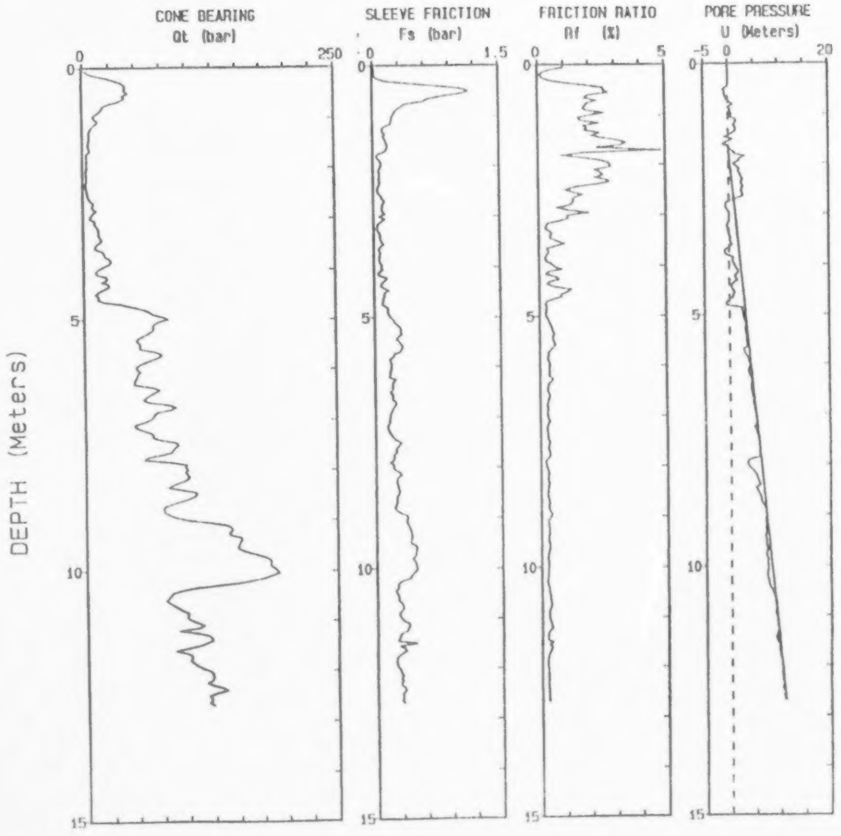

Figure A-VIII.1 Results of CPT-1 at Sea Island Site.

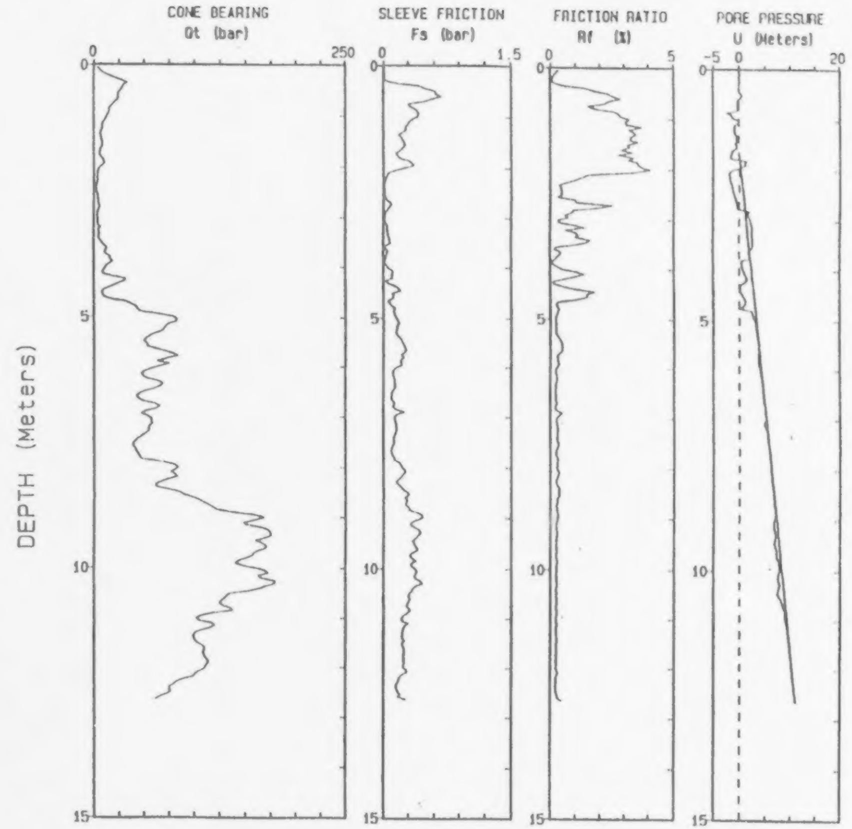

Figure A-VIII.2 Results of CPT-2 at Sea Island Site.

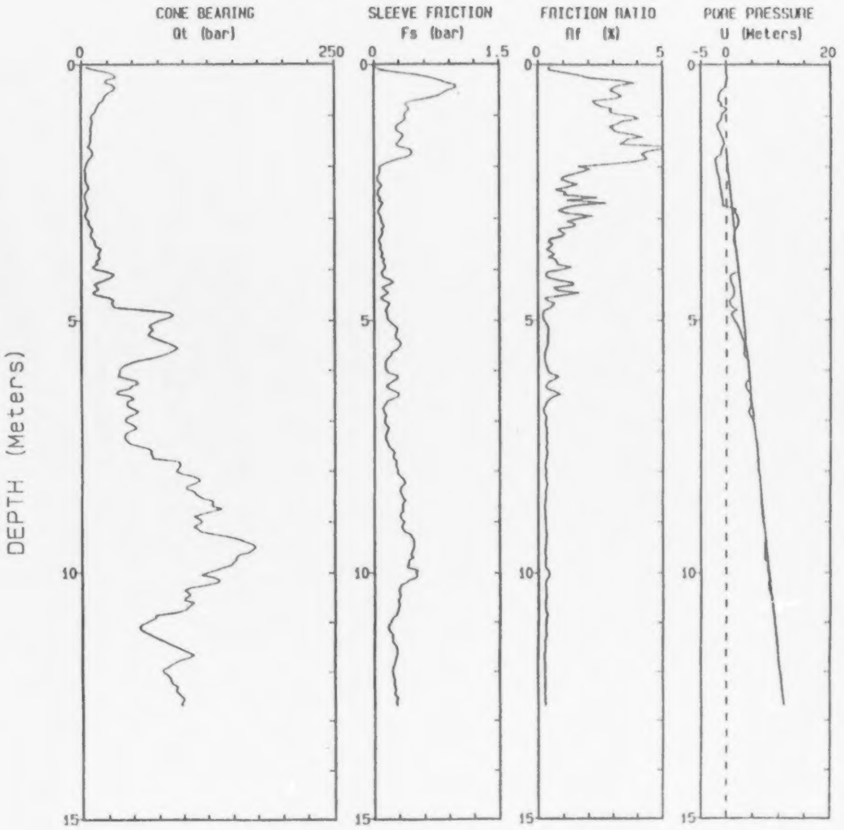

Figure A-VIII.3 Results of CPT-3 at Sea Island Site.

APPENDIX IX

IX. CPT Results at Burnaby Site

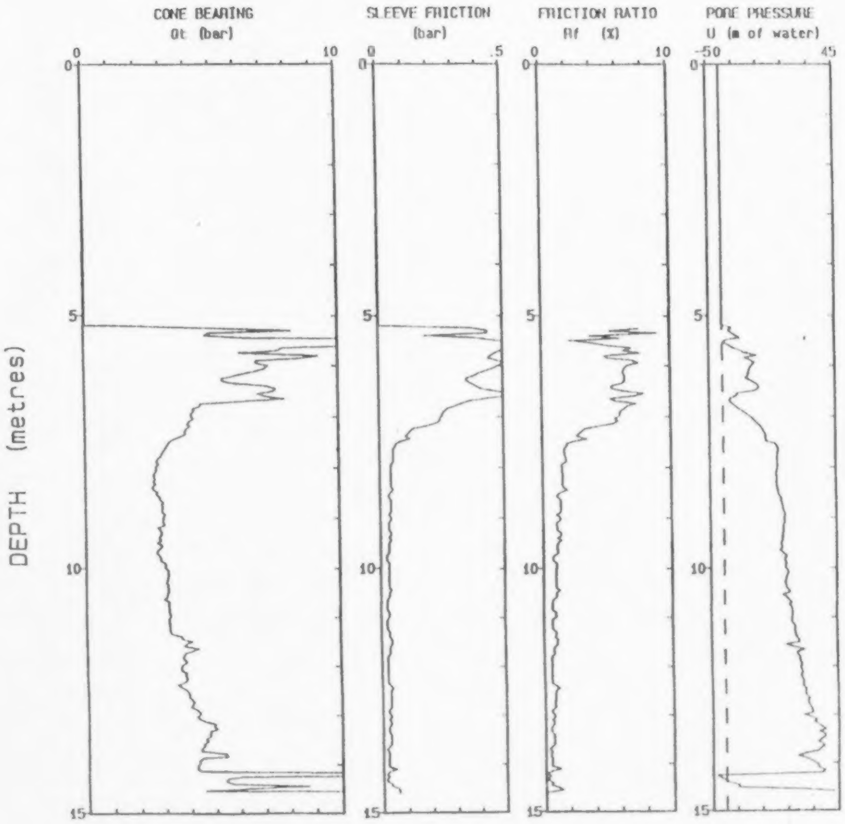

Figure A-IX.1 Results of CPT-1 at Burnaby Site.

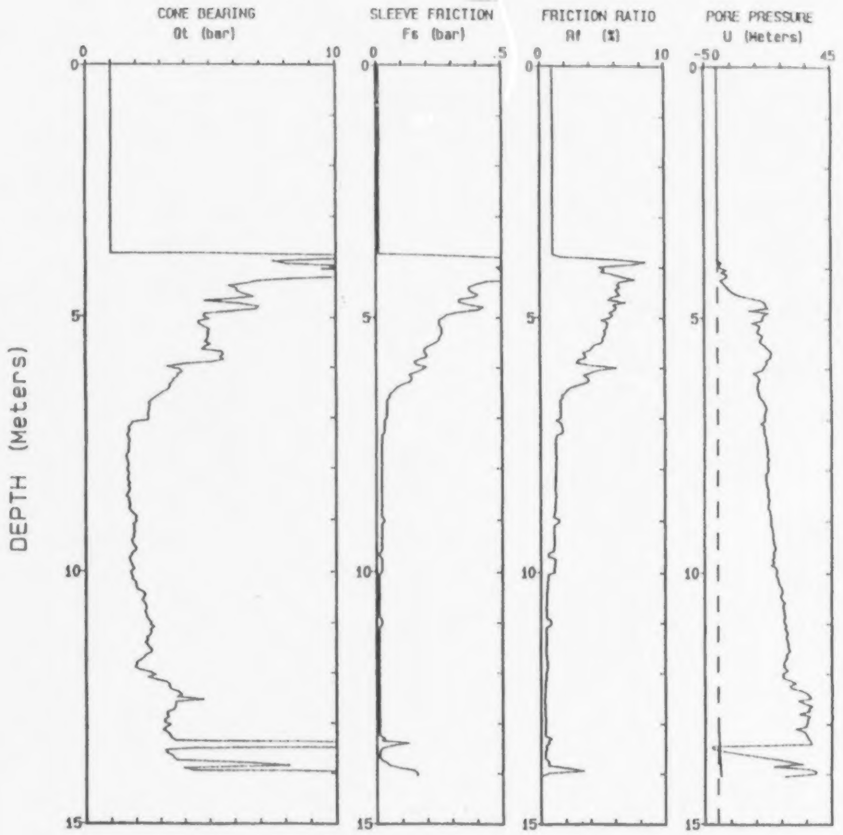

Figure A-IX.2 Results of CPT-2 at Burnaby Site.

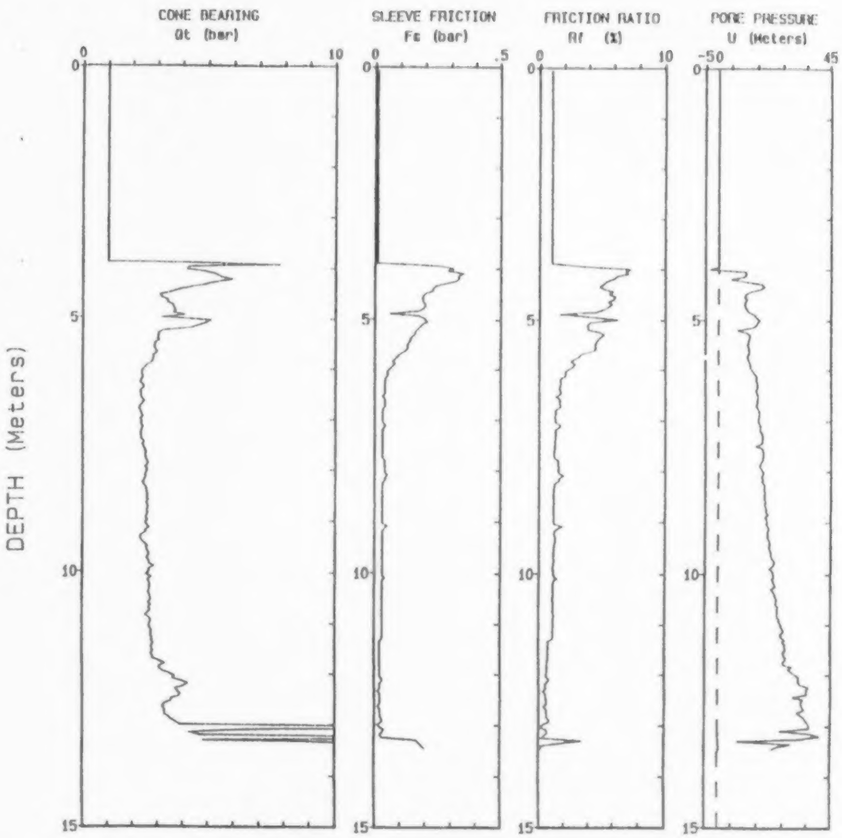

Figure A-IX.3 Results of CPT-3 at Burnaby Site.

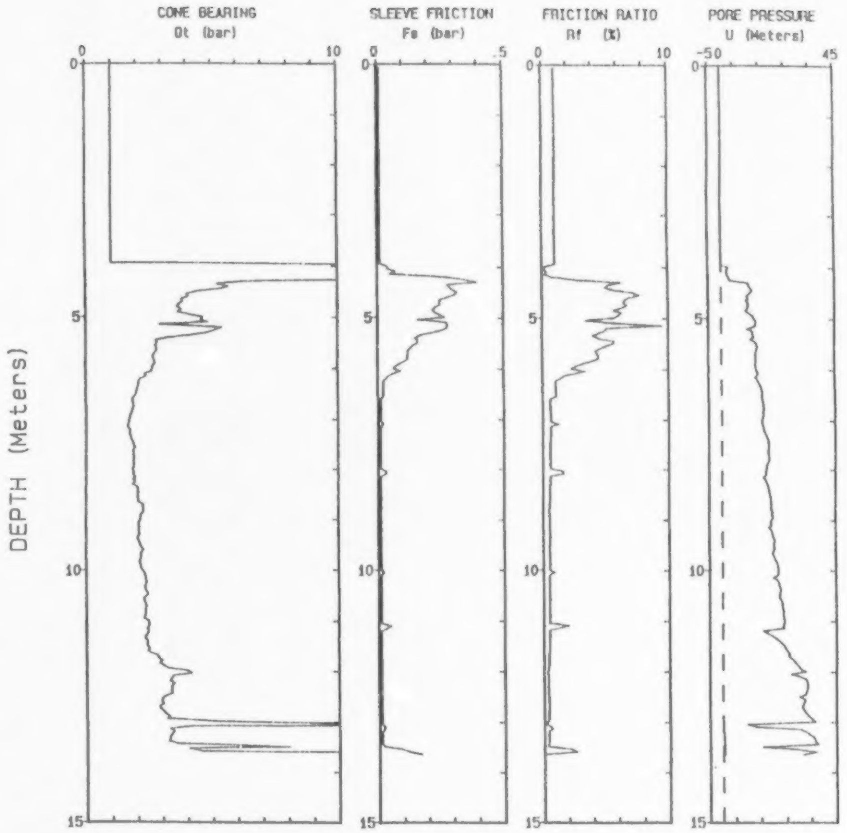

Figure A-IX.4 Results of CPT-4 at Burnaby Site.

APPENDIX X

X. CPT Results at Annacis Site

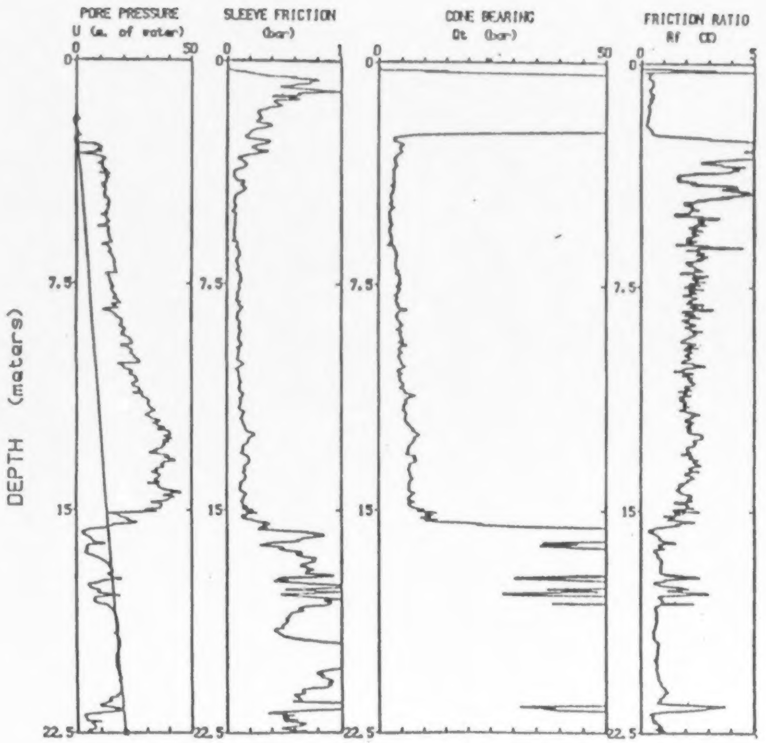

Figure A-IX.1 Results of Annacis Island Site.

APPENDIX XI

XI. CPT Results at Delta Site

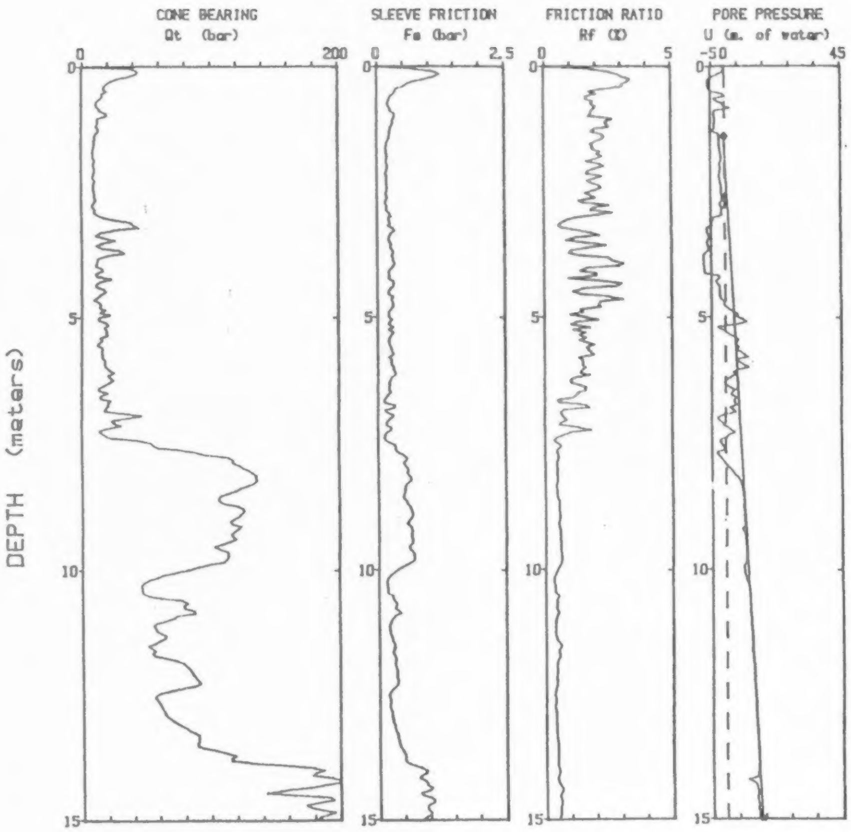

Figure A-X.1 Results of CPT-1 at Delta Site.

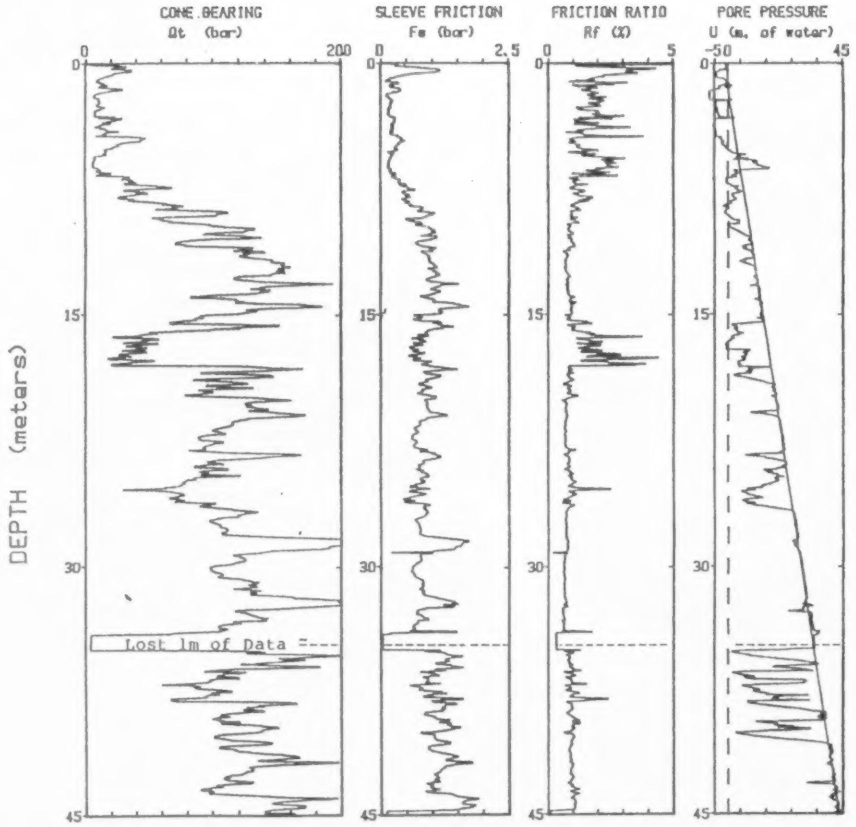

Figure A-X.2 Results of CPT-2 at Delta Site.

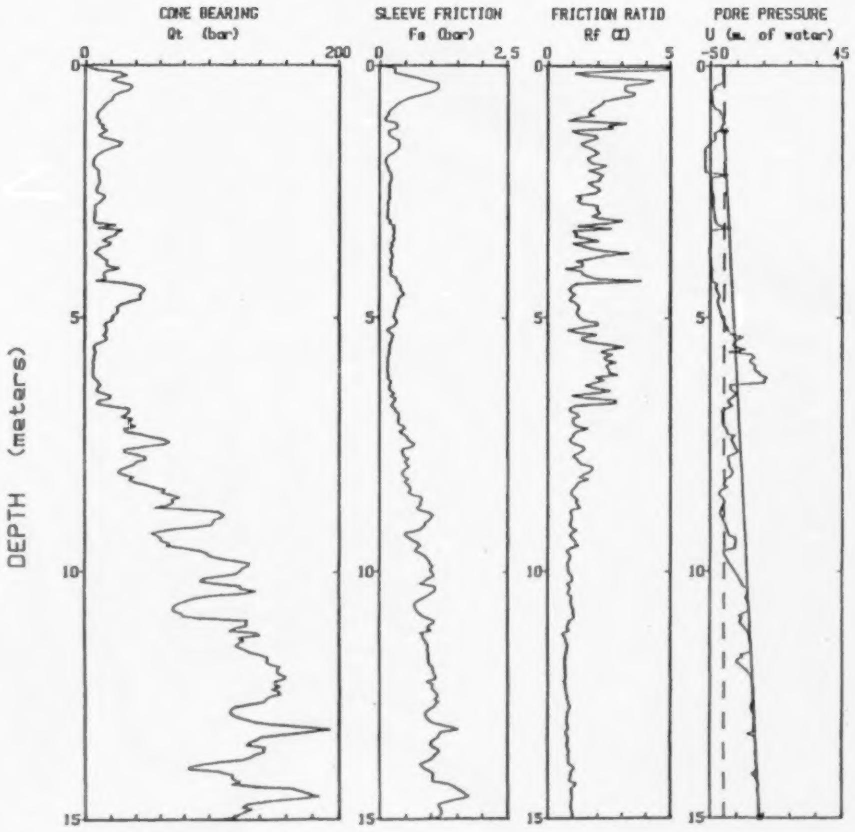

Figure A-X.3 Results of CPT-3 at Delta Site.

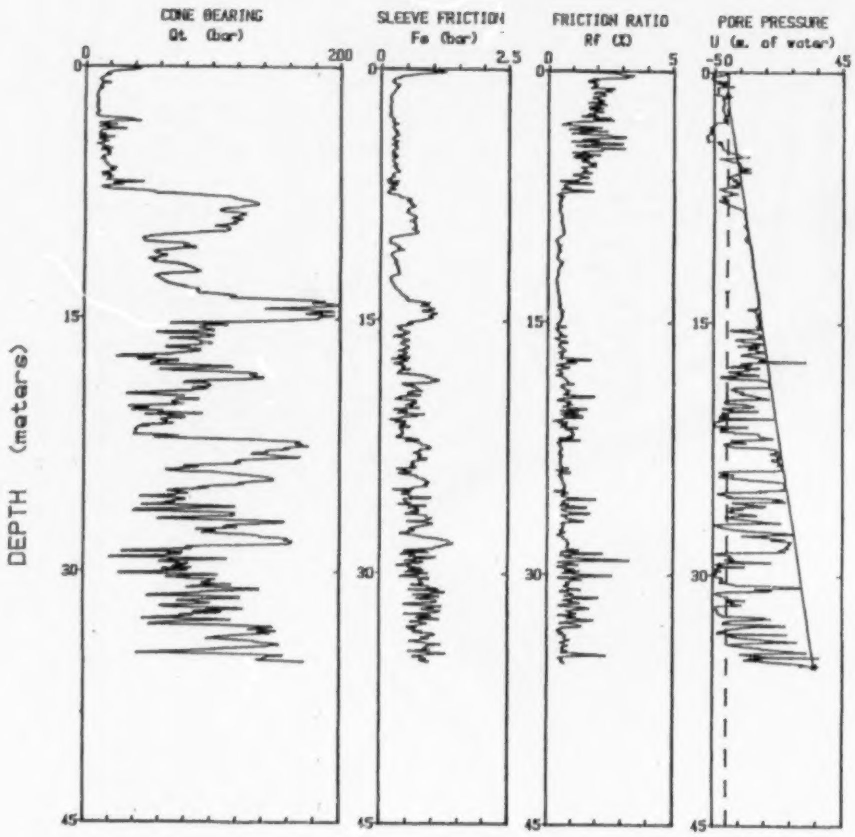

Figure A-X.4 Results of CPT-4 at Delta Site.

APPENDIX XII

XII. Becker Hammer Results at Matsqui Site

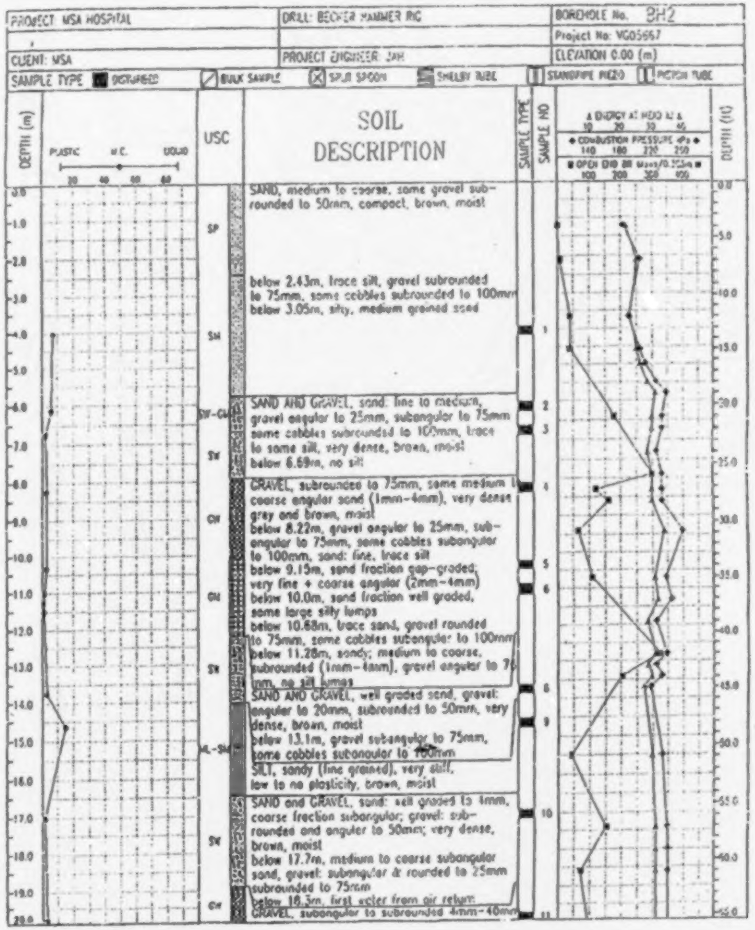

SAND, medium to coarse, some gravel subrounded to 50mm, compact, brown, moist

below 2.43m, trace silt, gravel subrounded to 75mm, some cobbles subrounded to 100mm
below 3.05m, silty, medium grained sand

SAND AND GRAVEL, sand: fine to medium, gravel angular to 25mm, subangular to 75mm some cobbles subrounded to 100mm, trace to some silt, very dense, brown, moist
below 6.69m, no silt

GRAVEL, subrounded to 75mm, some medium to coarse angular sand (1mm–4mm), very dense grey and brown, moist
below 8.22m, gravel angular to 25mm, subangular to 75mm, some cobbles subangular to 100mm, sand: fine, trace silt
below 9.15m, sand fraction gap-graded; very fine + coarse angular (2mm–4mm)
below 10.0m, sand fraction well graded, some large silty lumps
below 10.68m, trace sand, gravel rounded to 75mm, some cobbles subangular to 100mm
below 11.28m, sandy; medium to coarse, subrounded (1mm–4mm), gravel angular to 75mm, no silt lumps

SAND AND GRAVEL, well graded sand, gravel: angular to 20mm, subrounded to 50mm, very dense, brown, moist
below 13.1m, gravel subangular to 75mm, some cobbles subangular to 100mm

SILT, sandy (fine grained), very stiff, low to no plasticity, brown, moist

SAND and GRAVEL, sand: well graded to 4mm, coarse fraction subangular; gravel: subrounded and angular to 50mm; very dense, brown, moist
below 17.7m, medium to coarse subangular sand, gravel: subangular & rounded to 25mm subrounded to 75mm
below 18.3m, first water from air return

GRAVEL, subangular to subrounded 4mm–40mm

Figure A-XI.1 Becker Hammer Test Results at Matsqui Site.